Modulation of cerebellar Purkinje cell discharge by subthreshold granule cell inputs

Anais Grangeray-Vilmint

UNIVERSITÉ DE STRASBOURG

ÉCOLE DOCTORALE SCIENCES DE LA VIE ET DE LA SANTÉ

THÈSE

présentée par : **Anaïs GRANGERAY-VILMINT**

Soutenue le : **2 Juin 2016**

Pour obtenir le grade de : **Docteur de l'université de Strasbourg**

Spécialité : SCIENCES DE LA VIE – Mention NEUROSCIENCES

Modulation of cerebellar Purkinje cell discharge by subthreshold granule cell inputs

Modulation de la décharge des cellules de Purkinje du cervelet par des entrées sous-seuils des cellules des grains

THÈSE dirigée par :
Dr. Philippe ISOPE — INCI, Université de Strasbourg

RAPPORTEURS :
Prof. Ann LOHOF — Université Pierre et Marie Curie
Prof. Richard APPS — University of Bristol

AUTRE MEMBRE DU JURY :
Prof. Rémy SCHLICHTER — INCI, Université de Strasbourg
Examinateur

Preamble

The brain, center of the nervous system, is able to process sensory and motor information from the external world leading to adapted behavior.

It is composed of billions of neurons communicating with one another by means of axons, which carry trains of action potentials – the spikes - and convey the information to other parts of the brain. This allows the control of other parts of the body, by, for example, stimulating a group of muscles or causing hormone release. This centralized control allows fast and coordinated responses to a changing environment.

Understanding how information is processed in neurons and neural networks- 'cracking the neural code'- is a fundamental challenge for the modern neuroscience. It has been investigated with encoding and decoding approaches. The neural encoding concerns the way mapping or representation is made from the outside world (input stimulus) and transferred to the inside (spike output) in terms of activity patterns in the brain. In other terms, how precisely the output response of a neuron can be predicted, knowing the features of the incoming information (for example the modality, location or intensity). The neural decoding approach is based on the reverse mapping from the response to the stimulus, exploring how much information is carried in the spike output, and how well that would represent the stimulus information. Information content of a sequence of spikes may be read out using different coding paradigms by other neurons. It can be based on spiking rate, on its modulation, or their timing. It may also be read at the population level depending, for example, on spike synchrony between neurons.

During my PhD, I became interested in the specific question of how incoming inputs from a group of cerebellar GCs might change the output of one postsynaptic Purkinje cell (PC) and what features of the GC to PC connection influence the outcome of the

*input-output transformation performed by PCs. In order to describe my scientific investigation I will start with a brief overview of the cerebellum, presenting its gross anatomy and its roles (**Part I**). Understanding how the information is processed through the GC to PC connection requires to know the structure and the connectivity of the network it is integrated in. Therefore, I will thoroughly describe the anatomical structure of the cerebellar cortex, as well as relevant morphological characteristics of its neuronal components (**Part II**). Then, I will introduce the way information travels in the cerebellar network and how it is regulated (**Part III**). Lastly, I will present the firing properties of PCs and the way it can be modulated, trying to keep in mind its physiological relevance/implications for function (**Part IV**).*

*The main work of my PhD thesis has been the demonstration of differences in information processing in the GC to PC connection. In collaboration with Dr Arvind Kumar (KTH Royal Institute of Technology, Stockholm, Sweden), we also showed that short-term dynamics play a key role in determining the modulation of PC spiking activity (**Results**).*

*The results I obtained during my PhD support the idea that the organization of local microcircuits and temporal organization of GC inputs together control the cerebellar cortex output (**Discussion**).*

I hope it will "spike" your interest!

TABLE OF CONTENTS

List of abbreviations

-A-

AMPA	Acid alpha-amino-3-hydroxy-5-méthyl-4-isoxazolepropionic
ATP	Adenosine triphosphate

-B-

BC	Basket cell

-C-

CF	Climbing fiber
ChR2	Channelrhodopsin 2
CV 2	Coefficient of variation between two adjacent interspike intervals

-D-

DAPI	4',6-diamidino-2-phenylindole
DCN	Deep cerebellar nuclei
DSE	Depolarization-induced suppression of excitation

-E-

EAAT4	Excitatory amino acid transporter
E/I	Excitation inhibition
EPSC	Excitatory postsynaptic current
EPSP	Excitatory postsynaptic synaptic potential

-F-

FFI	Feedforward inhibition

-G-

GABA	γ-aminobutyric acid
GC	Granule cell

-H-

HSP25	Heat shock protein 25

-I-

IPSC	Inhibitory postsynaptic current
ISI	Interspike intervals

-K-

KCa	Calcium activated potassium channels
KCC2	Potassium chloride co-transporter 2

-L-

LED	Light emitting diode
LTD	Long term depression
LVr	Local variation with refractory period

-M-

mGluRs	metabotropic Glutamate receptor
MF	Mossy fiber
MLI	Molecular layer interneuron

-N-

NBQX	2,3-dihydroxy-6-nitro-7-v sulfamoyl-benzo[f]quinoxaline-2,3-dione
NMDA	N-methyl-D-aspartate

-P-

PC	Purkinje cell
PCA	Principal component analysis
PF	Parallel fiber
PPR	Paired-pulse ratio
PSTH	Peristimulus time histogram

-S-

SC	Stellate cell
SSE	Synaptically-evoked suppression of excitation
STD	Short-term dynamics

-T-

TTX	Tetrodotoxin

-U-

UBC	Unipolar brush cell

-V-

VGLUT	Vesicular glutamate transporter

-Y-

YFP	Yellow Fluorescent Protein

LIST OF FIGURES - INTRODUCTION

LIST OF FIGURES - RESULTS

INTRODUCTION

1. *A bit of history*

Insights about the role of the cerebellum already appeared during the 2nd century with Galen, who compared the medial part of the cerebellum (vermis) to a valve that would control the flow of animal spirit. Galen suggested that the cerebellum is the source of cranial nerves and the spinal cord (Clarke and O'Malley, 1996).

Early functional hypothesis arose at the 19th century with the work of Luigi Rolando (1809) showing that cerebellar lesions led to motor dysfunctions with no evident defects in vital or intellectual functions. A few years later, between 1814 and 1822, Pierre Flourens performed partial or total ablation of different sections of the brain on birds and observed the effect on their behavior. Cerebellar sections did not evoke pain or convulsions. Graded ablations of the cerebellum induced a gradual loss of the animal's ability to walk or run in a regular manner. Based on his observations, Pierre Flourens proposed a clear distinction between the function of the cerebrum (which he considered as the organ of intelligence) and of the cerebellum (organ for motor coordination). Animal experimentations performed by Luigi Luciani (1891) and clinical observations made by Gordon Holmes (1917, 1922) from soldiers wounded during the First World War and from patients with cerebellar tumors allowed a precise description of the symptoms attributed to cerebellar alterations. They could notice involuntary muscle movements (*diskinesia*), a reduction in muscle strength (*asthenia*), loss of muscle tone (*atonia*), defects in muscle contraction stability (*astasia*), or tremors during voluntary movements.

Back at that time, cerebellar functions were attributed to the whole cerebellum as the "unitary theory of cerebellar function". Because Luigi Luciani did not observe any focal symptoms in his ablation experiments, he denied the presence of a functional organization that would control different parts of the body (Manni and Petrosini, 2004). This view was reinforced by the description by Santiago Ramón y Cajal,

(1852-1934) of the crystalline structure of the cerebellar cortical network and the morphology of most of its cell types.

However, in parallel, the anatomists Lodewijk Bolk (1866-1930), Olof Larsell (1886-1964) and Alf Brodal (1910-1988) precisely compared the anatomy of the cerebellum of more than sixty different mammalian species and provided evidence for cerebellar functional localization. For example, according to Lodewijk Bolk, the anterior lobe of the cerebellum was dedicated to the coordination of muscles from the head like the eyes or the tongue.

This pioneering works regarding a structure-function relationship of the cerebellar cortex, along with the study of its connections (Voogd, 1967, 1969), the development of anatomical tracing (Taber et al., 2005) and electrophysiological investigations (Oscarsson, 1979; Manni and Petrosini, 2004), together challenged the previous unitary theory and rather shed light on the functional somatotopy of modular information processing in the cerebellar cortex.

Although Santiago Ramón y Cajal made some hypotheses on the operational principles of the cerebellar circuit and even made hypotheses about information pathways, it is only in the late sixties that theories about information processing came about. This new era in cerebellar physiology started with the influential work of Eccles, Ito and Szentágothai (1967) who described the cerebellar wiring. By using electrophysiological studies, combined with morphological analyses, they identified the excitatory and inhibitory nature of each cell providing the functional architecture of the cerebellar cortex. Masao Ito showed that projection Purkinje neurons are inhibitory, dismantling the dogma that inhibitory neurons are local connections in the network. Two years later, David Marr (1969) developed the first theoretical model for cerebellar function presented in “A theory of cerebellar cortex”, this model was expanded by James Albus (1971), functionally proved by Masao Ito (Ito and Kano, 1982) and is still today a reference framework for the computation performed by the cerebellum (see Dean et al., 2010).

Now, in 2016, there is an increasing body of evidence for regional variations in the connectivity and biochemical markers of the cerebellum that could account for different functional units serving different behaviors (Cerminara et al., 2010, 2015).

2. *The role of the cerebellum in motor control described in recent decades*

As part of the vertebrate motor system, the cerebellum - Latin for “little brain”- has a key role in postural and gait control as well as in the coordination and learning of skilled movements (Thach et al., 1992; Bastian, 2006). It can modulate both motor reflexes and the course of voluntary movements as the movement unfolds. Moreover, studies from subjects with cerebellar damage suggest that the cerebellum plays a primary role in predictive motor control (Bastian, 2006). Indeed, the cerebellum receives a copy of the motor command sent to the spinal cord by the primary motor cortex and predicts the expected sensory feedback triggered by the command based on body coordinates. The prediction is then compared with the actual feedback from sensory inputs including tactile, visual, vestibular, and auditory information. The result of the comparison (prediction error) is sent back to the motor cortex, adapting the motor program from one movement to the next (Bastian, 2006). Such an error-dependent learning process is believed to optimize complex movement behaviors in order to respond to specific contexts in a rapid, stereotypic and eventually automatic manner. Recent evidence has also demonstrated the key role of the cerebellar cortex in the precise timing of individual components of the motor program and in the synchronization of cerebello-thalamo-cortical oscillations observed during motor tasks (Spencer, 2003; Schnitzler and Gross, 2005; D’Angelo and De Zeeuw, 2009). The tapping finger ability of a pianist or the coordinated eye movements of a reader rely on an exceptional degree of such motor skills.

Although the fundamental function of the cerebellum in motor control is well acknowledged, information processing leading to the optimization and learning of complex movements remains poorly understood.

3. *Macroscopic divisions of the cerebellum*

A. *Gross anatomical segmentation*

The cerebellum is divided into two hemispheres united in the midline by a region called the vermis (**Figure I1.A**). They vary in size depending on the species, with the vermis being the biggest region in lower mammals while hemispheres are more developed in primates. All three consist of a highly folded outer layer – the cerebellar cortex – and inner tree-shape white matter (**Figure I1.B**). The two hemispheres can be further divided into an intermediate part called the paravermis and a lateral hemisphere (**Figure I1.A**).

Two deep transverse fissures split the cerebellar cortex in the anteroposterior axis into three lobes (**Figure I1.A**). The primary fissure divides the anterior and posterior lobes while the posterolateral fissure separates the floculonodular lobe from the posterior lobe. Superficial fissures further divide these regions into 10 lobules (Larsell, 1952) each composed of shallow folds, the folia (**Figure I1.B**), which can differ between species; for example, in mice, lobule VI is split into VIa and VIb-c.

The whiter matter contains three pairs of subcortical nuclei (deep cerebellar nuclei (DCN)) named in rodents the medial, interposed (anterior and posterior part) and lateral nuclei (**Figure I1.B**). They form, in combination with the vestibular nuclei, the output of the cerebellum. The white matter is essentially composed of the cerebellar afferences/efferences from/to the rest of the nervous system that I will briefly describe in the next section.

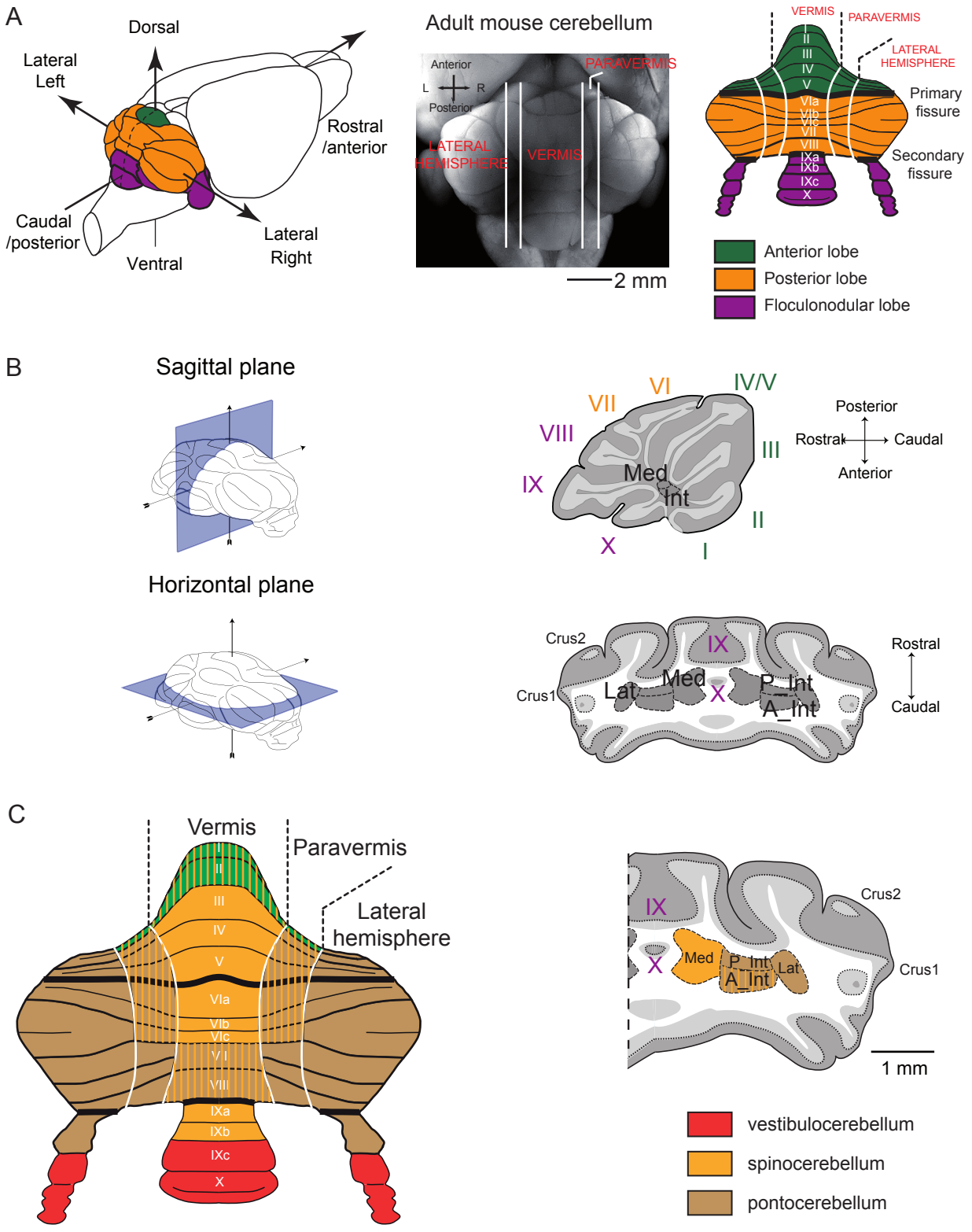

Figure I1. Macroscopic divisions of the cerebellum.

A: Gross anatomical segmentation. Representation of the mouse cerebellum (colored). Right panel: unfolded view of the cerebellar cortex showing hidden lobules, from I to X according to the nomenclature of Larsell (Larsell, 1952). Deep fissures are highlighted in bold and superficial fissures with regular lines. Note the three longitudinal compartments: the vermis, paravermis and hemispheres. **B:** The three pairs of deep cerebellar nuclei are displayed in the sagittal and horizontal sections of the cerebellum. Abbreviations: Int: interposed nucleus; A_Int and P_Int: anterior and posterior interposed nucleus. Lat: lateral cerebellar nucleus; Med: medial cerebellar nucleus. **C:** Functional divisions of the cerebellum (left) and their projections onto deep cerebellar nuclei (right). Hashed zones correspond to regions receiving a mixture of inputs.

B. *Phylogenetic and functional divisions*

The cerebellum has also been divided based on both its phylogeny and afferent and efferent connectivity, segmenting it into three main parts (Kandel et al., 2000; Jansen and Brodal, 1940) named vestibulocerebellum, spinocerebellum and pontocerebellum (**Figure I1.C**). Although this terminology can be confusing, as the "spinocerebellum" for instance does not receive inputs solely from the spinal cord as I will describe them in the following section.

The most primitive part, the vestibulocerebellum (or archicerebellum) appeared first in fish; it is composed of the flocculo-nodular lobe (lobule X) as well as lobule IX (**Figure I1.C**). It receives direct inputs from the vestibular nerve as well as proprioceptive inputs. It projects directly out of the cerebellum to the lateral vestibular nuclei, without any relay in the deep cerebellar nuclei. The vestibulocerebellum role is mainly limited to the control of balance and eye movements.

The second part receives its main inputs from the spinal cord and is thus called the spinocerebellum (or paleocerebellum). It consists of the vermal and paravermal regions (**Figure I1.C**). The vermis also receives visual and auditory inputs, as well as vestibular and somato-sensory information from the head and proximal limbs. Conversely, the paravermis receives inputs from areas related to distal limbs. The spino-cerebellum makes efferent connections to the vestibular nuclei, the spinal cord, the brainstem nuclei and cortical areas via the medial nuclei (for the vermis) and the interposed nuclei (for the paravermis). This part is thought to be mainly associated with posture and gaze control as well as coordination of the limbs.

The third part, phylogenetically most recent is contacted exclusively by the cerebral cortex via the pontine nuclei; hence it was named the pontocerebellum (or

neocerebellum) (**Figure I1.C**). It receives inputs from motor, sensory and associative cortices and sends projections back to these cortices through the thalamus and the dentate nuclei. This part is involved in planning of motor actions.

PART II: ANATOMO-FUNCTIONAL AND HISTOCHEMICAL ORGANIZATION OF THE CEREBELLAR CORTEX

1. *Cytoarchitecture and connectivity of the cerebellar cortex*

The discovery of the black reaction in 1873 by the Italian scientist Camillo Golgi opened the road towards the understanding of the cellular organization of the cerebellum. This is nowadays referred to as the Golgi method, which randomly stains few cells in a tissue allowing the visualization of the precise structure and interconnections between cells under light microscopy, although axons are not well stained. Ramón y Cajal (1852–1934) extensively applied this technique and thoroughly investigated the organization of the cortical layers of the cerebellar cortex (**Figure I2.A**) completing the early description of Camillo Golgi.

A. *Cerebellar cortical layers and cell types*

The cerebellar cortex is divided into three cortical layers and contains seven main neuronal types as well as astrocytes and oligodendrocytes (**Figure I2.B**).

The granular layer lies the deepest, directly on the white matter and is composed of a large number of densely packed GCs, some Golgi cells, Lugaro cells and unipolar brush cells (UBC). Its volume was estimated to be 41 % (28 ± 0.015 µl) of the total cerebellar volume in mice (Harvey and Napper, 1991).

The intermediate **PC layer** is the thinnest and consists of a one-cell-thick layer of PC somas. PCs send their axons through the granular layer and their dendrites are parasagittaly oriented in the more superficial molecular layer.

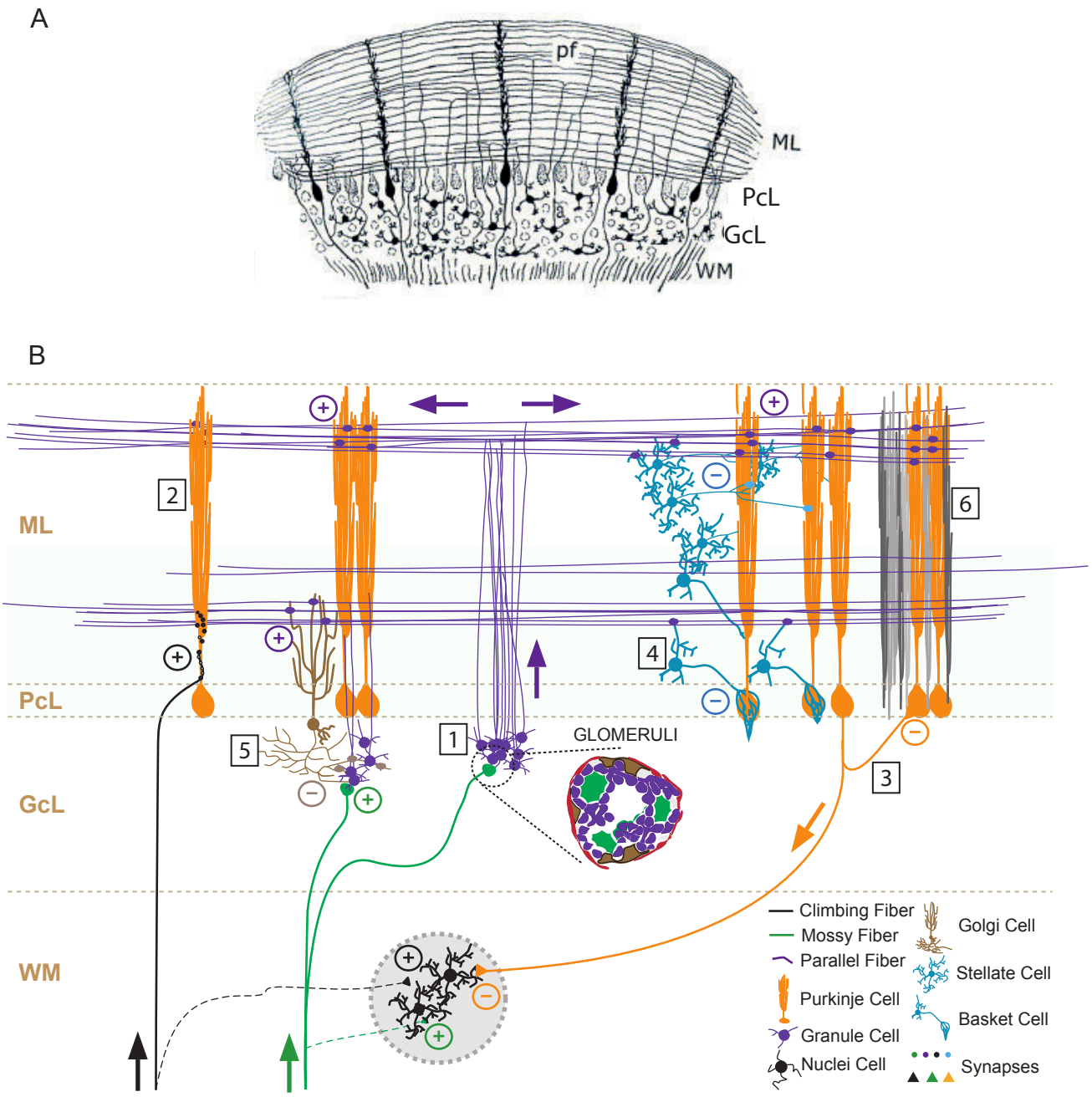

Figure I2. The cerebellar cortex: cytoarchitecture, connectivity and basic flow of information.

A: Drawing by Ramón y Cajal of a transverse section of the three-layer cerebellar cortex stained using the Golgi method. ML: molecular layer; PcL: PC layer; GcL: granular layer; WM: white matter. Adapted from Voogd and Glickstein, 1998. **B:** Diagram of the cerebellar cortical connectivity. Information flow is indicated with the arrows. +/- indicates excitatory/inhibitory connections. The cerebellar cortex receives two main excitatory inputs, the climbing (in black) and the mossy (in green) fibers. MF relay on GCs (in purple) that send a long bifurcating axon, the PF, contacting molecular interneurons (in blue), Golgi cells (in brown) and PCs (in orange). Numbers refer to the pictures displayed in C (on the right page).

C

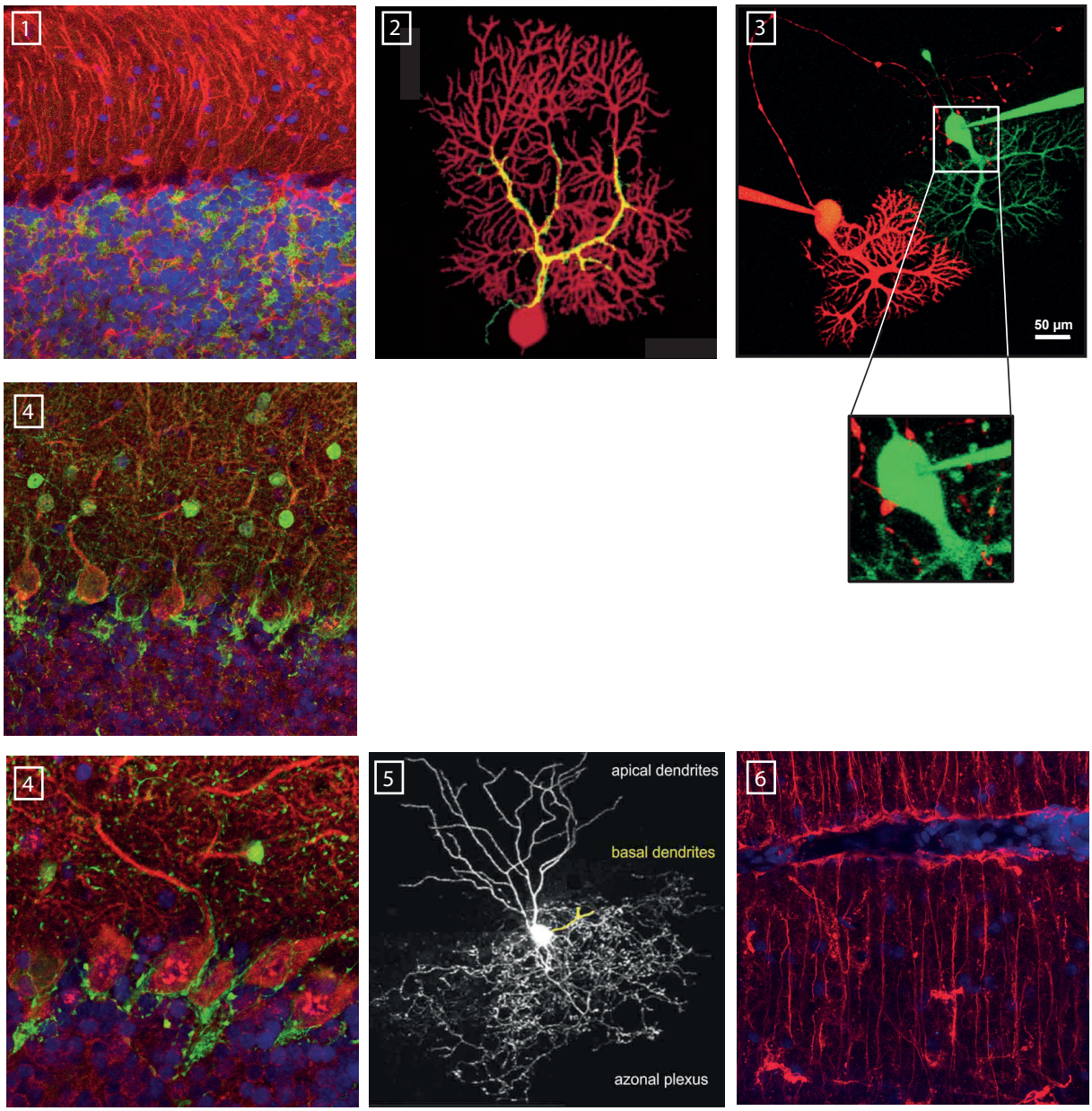

Figure I2 (follow up): The cerebellar cortex: cytoarchitecture, connectivity and basic flow of information.

C1: GCs are packed in the GC layer Nucleus are stained with DAPI, blue fluorescence. From Jean-Luc Dupont. **C2:** The PC (red) and its CF (yellow) were loaded using dextran-conjugated indicators. Adapted from Brenowitz and Regehr, 2012. **C3:** PC recurrent axon collateral (red fluorescence, Atto-594) contacting a neighboring PC (green, Atto-488). Adapted from Bornschein et al., 2013. **C4:** MLIs are immunostained with parvalbumin (green fluorescence). Note the basket and pinceau specializations of the BC surrounding the PC soma (caveolin, red). SCs are visible (green) in the molecular layer. From Jean-Luc Dupont. **C5:** Golgi cell. Adapted from D'Angelo et al., 2013. **C6:** Bergmann glia: immunostained using glial fibrillary acidic protein, displayed as red fluorescence. Nucleus: marked with DAPI, blue fluorescence. From Jean-Luc Dupont.

The molecular layer is bound on its external part by the pia mater and contains few neuronal cell bodies - the molecular layer interneurons (MLI) - but a very high density of axons from GCs known as parallel fibres (PF) and also probably from Lugaro cells. This layer has a volume of 12.0 ± 0.041 µl in mice (41% of total cerebellar volume; Harvey and Napper, 1991). It also contains dendrites of Golgi cells and PCs; both are perpendicularly intersected by PFs running in a mediolateral direction.

B. *Basic flow of information in the cerebellar cortex*

There are two major entries whereby information can reach the cerebellum: the mossy fibers (MFs) and the climbing fibers (CFs) (**Figure I2.B**). The cerebellar glutamatergic MFs carry sensorimotor information from several precerebellar nuclei of the brainstem. MFs make an excitatory contact onto GCs and also provide feedforward inhibition (FFI) via the MF-Golgi cell connection. GCs send their axon into the molecular layer and make excitatory synapses onto several targets including PCs, and MLI (stellate cells (SCs) and basket cells (BCs)) (Eccles et al., 1967b; Ito, 1984) that inhibit PCs in a feedforward fashion and Golgi cells (**Figure I2.B**). Golgi cells generate a feedback inhibition on GCs. PCs are the sole output neuron of the cerebellar cortex and inhibit DCN neurons. Additionally, each PC receives a strong excitatory input from one cerebellar CF (Eccles et al., 1967b; Ito, 1984). Both MFs and CFs also send collaterals to DCN (**Figure I2.B**).

I will now provide detailed morphological and anatomical information important for understanding the computation performed at the GC to PC connection in the adult cerebellum.

C. *Granule cells (Figure I2.C1)*

As for GCs in other brain structures like the hippocampus or olfactory bulb, cerebellar GCs are the smallest neurons of the cerebellum, with a soma of around 5 µm in rats (Harvey and Napper, 1991). They have on average 3.1 (± 1.1) dendritic stems (Sultan and Bower, 1998). Each dendrite is embedded into a different spherical structure (of about 110-200 µm3 in the rat) called a glomerulus that contains dendrites from many GCs, MF terminal and Golgi cell axons (Jakab and Hámori, 1988). GCs receive and integrate excitatory inputs from MFs and UBC, and inhibitory inputs from Golgi cells. The initial part of GC axons run vertically in the molecular layer and is called the *ascending axon*, before splitting into two bifurcating branches called *PFs*. PFs can run up to 4.7 mm in the mediolateral axis of the folium in rats and were found to be thicker and shorter in deeper parts of the molecular layer than those at the surface (Pichitpornchai et al., 1994). It cannot be excluded though that the observed differences arise from a misclassification of PFs with Lugaro cell axons which are also located in the molecular layer and partially myelinated. GCs release glutamate, and hence exert excitatory effects on their proximal and distal targets.

Parallel fiber and ascending axon synapses

Ramón y Cajal already described PF organization but the concept of synapses was not yet defined. PFs are a highly conserved structure from birds to mammals. They are unmyelinated in rats (Shepherd et al., 2002) but can be myelinated in some species (cat, marmoset, and macaque: see Gatzeva-topalova et al., 2011). They are organized as bundles of fibers referred to as “beam” in the literature and cross perpendicularly the dendritic tree of hundreds of on beam PCs with one PF making *en passant* synapse with one out of two dendritic trees it crosses (Napper and Harvey, 1988a). PF to PC synapses are enwrapped by astrocytic processes of Bergmann glia cells (Palay and Chan-Palay, 1974). Biocytin injections in the granular layer show that synapses from the ascending axon are regularly spaced out by about 4 µm

distance as well as in the first part of the PFs, while the distance gradually increases up to 7 µm in the most distal part (Pichitpornchai et al., 1994).

PFs also make excitatory synaptic contacts on MLI and apical dendrites of Golgi cells. PF to Golgi cell connection leads to feedback inhibiton onto GCs (**Part III.1.E**).

D. *Purkinje cells (Figure I2.C2)*

Camillo Golgi first illustrated the PC cytoarchitecture and already hypothesized a motor role for this cell after identifying its projection out of the cerebellum. PC was then precisely described by Ramón y Cajal. The rat cerebellum is composed of about $3.38x10^5$ PCs (Napper and Harvey, 1988a). PCs have pear-like somas arranged in a single layer all over the cerebellar cortex. Each PC has a gigantic fan-shape dendritic tree of about 200 x 20 µm in rats (Palay and Chan-Palay, 1974) that extends in a parasagittal plane and is surrounded by on average eight Bergmann glia astrocytes which prolong on the entire molecular layer (Reichenbach et al., 1995). Dendritic arbors have one, sometimes two, main smooth primary dendrites which are subdivided into secondary smooth branches and tertiary thin spiny branchlets. Smooth dendrites are contacted by the climbing fibres while spiny branchlets (Fox and Barnard, 1957) are contacted by the PFs. The massive number of spines dramatically increases the surface of the PC and allows a large number of contacts by the PFs, around 175 000 (Harvey and Napper, 1991). Each spine receives one PF synapse (Palay and Chan-Palay, 1974), sometimes two (Napper and Harvey, 1988b). Each PF makes around 600 synapses onto PCs (Harvey and Napper, 1988). In the adult cerebellum, each PC is innervated by a single CF (while multi-innervations occur during development), that makes around 300 synaptic connections exclusively on the larger primary smooth dendrites in the deepest part of the molecular layer. CF to PC synapses are ensheathed by astrocytic processes (Palay and Chan-Palay, 1974). Inhibitory MLI make contact mostly on the dendritic shaft and on the soma of PCs.

Output connectivity and collaterals (**Figure I2.C3**)

The myelinated axon of PC runs through the white matter without branching until it gets near deep cerebellar nuclei. The terminals of each axon target specific area in the DCN and their shape and size vary from elongated, wide to compact morphologies depending on the localization of the PC and the nuclei targeted (Sugihara et al., 2009). For example, PCs from the vermis showed more widely spread axonal terminals as compared to those arising from the hemispheres (Sugihara et al., 2009).

PC axon can also branch and form collaterals onto other targets, as evidenced by electron microscopy studies showing collaterals making synaptic contacts onto neighboring and distant PCs, sometimes in other lobules (Cajal, 1911; Palay and Chan-Palay, 1974; Orduz and Llano, 2007; Bornschein et al., 2013). Collaterals can also contact Golgi cells (Cajal, 1911; Palay and Chan-Palay, 1974), Lugaro cells (Larramendi and Lemkey-Johnston, 1970; Hawkes and Leclerc, 1989) and MLI (Palay and Chan-Palay, 1974) (King and Bishop, 1982; O'Donoghue et al., 1989). PC to PC synapse have the particular characteristic that their synaptic cleft is wide, twice larger as other synapses (Chan-Palay, 1971).

Quantitative electron microscopy studies in rats that compared the total number of PC axonal boutons with the number of DCN neurons suggested that each PC targets around 35 DCN neurons (Palkovits et al., 1977). Conversely, the degree of PC to DCN convergence, which has been controversial (see: (Person and Raman, 2012a) has been estimated to be from tens to hundreds (Palkovits et al., 1977; Sugihara et al., 2009). Therefore, there is a high degree of both convergence and divergence of PC output onto DCN (Person and Raman, 2012b).

E. *Molecular layer interneurons (Figure I2.4)*

MLI are inhibitory GABAergic interneurons and receive several hundreds of excitatory inputs from GCs (Palay and Chan-Palay, 1974) and between one and twenty inhibitory inputs from other MLI (Lemkey-Johnston and Larramendi, 1968; Llano and Gerschenfeld, 1993; Häusser and Clark, 1997). They might also receive inputs from PC axon collaterals, especially the BCs (Palay and Chan-Palay, 1974; O'Donoghue et al., 1989).

Divergence estimates are variable from one interneuron contacting 50 PCs (Eccles et al., 1967b; Hubbard et al., 1967) to fewer than 5 (Bishop, 1993). Each PC is contacted by 6 to 10 interneurons in the rat (Palay and Chan-Palay, 1974; Korbo et al., 1993; Häusser and Clark, 1997), and 30 to 50 interneurons in the cat (Palkovits et al., 1971; Ito, 2006).

As for PC dendrites, MLI have their dendrites and axons oriented in the parasagittal plane, occupying the space between two PC dendritic trees (Cajal, 1911). Although Ramón y Cajal described a wide range of morphologies including BCs, large SCs, small outer SCs or dwarf cells, the classical view distinguished only two subtypes of MLI : the basket and SCs (Palkovits et al., 1971; Palay and Chan-Palay, 1974), and many studies consider them as one population, using the term MLI. The studies in which a distinction was made separated the BCs from the SCs based on the location of their soma. The BCs are assumed to be located in the lower two-third of the molecular layer while SC somas are considered to be positioned in the upper part. However, the only quantitative study based on principal component analysis of forty morphological variables of MLI in the rat (Sultan and Bower, 1998) revealed that axonal plexus morphology is another important parameter in the distinction which does not necessarily follow the soma-position-based criterion. The authors concluded that there is a morphological continuum between basket and SCs forming a single population.

The classical BC axonal plexus forms a basket containing chemical synapses around the soma of one PC in close vicinity and extend further into the first 20µm of the granular layer surrounding the initial segments of the PC axon with an elaborate axonal specialization called the pinceau, devoided of any chemical and electrical synapses (Iwakura et al., 2012). Each pinceau is composed of around 50 collaterals from BCs (Palkovits et al., 1971) and has an average volume of 1020 µm3 for a surface of 479µm2 (Chiu et al., 2002). Every BC participates in the formation of five to ten pinceaux (Palay and Chan-Palay, 1974). This somatic and axonal inhibition regulates the timing of action potential from the PC. In addition, it has been demonstrated recently that the BC pinceau release positive charges in the extracellular field around the PC axon leading to an extremely fast inhibition of PCs mediated by an ephaptic interaction (Blot and Barbour, 2014).

SC have short and thin dendrites (Sultan and Bower, 1998), and their axons are more local than BCs, although variable in length. They contact the dendritic tree of PC contributing to synaptic integration.

Interneuron-interneuron connectivity

MLI are interconnected by inhibitory chemical synapses (Häusser and Clark, 1997) and electrical synapses (Mann-Metzer and Yarom, 1999; Alcami and Marty, 2013) having different functional roles in information processing (**Part III.2.B**). A recent study showed that they are not randomly connected (at least when considering more than two interneurons), but instead chemical and electrical interneuron networks are strictly restricted to the sagittal plane with some overlap between the two networks (Rieubland et al., 2014). In addition, chemical connectivity depends on the position in the molecular layer; connections are preferentially oriented towards the inner part of the molecular layer due to MLI dendritic morphologies that become gradually longer when located deeper in the molecular layer (Rieubland et al., 2014).

F. *Golgi cells (Figure I2.5)*

Golgi cells are inhibitory interneurons of the GC layer and provide feedback and FFI onto GCs. Golgi cells are either mixed GABAergic-glycinergic (80%), purely GABAergic (15%) or purely glycinergic (5%) (Simat et al., 2007). Furthermore, Golgi cells have been classified into five subtypes according to their morphology and two additional neurochemical markers: the metabotropic glutamate receptor 2 (mGluR2) and neurogranin (Simat et al., 2007). The first subgroup (65 %) is composed of mixed GABAergic-glycinergic Golgi cells that express both mGluR2 and neurogranin. The second and third subgroups (5 to 10 % each) which differ in the size of their soma and their position in the GC layer are also mixed Golgi cells but express solely mGluR2. The fourth group (15%) is purely GABAergic and only shows neurogranin expression. Lastly, the fifth group (5 %) is purely glycinergic and devoid of both mGluR2 and neurogranin.

Golgi cells have basolateral dendrites in the granular layer (Palay and Chan-Palay, 1974) and apical dendrites extending into the molecular layer, preferentially oriented parasagittaly (Barmack and Yakhnitsa, 2008a; Sillitoe et al., 2008). Basolateral dendrites are locally and directly contacted by MFs making “en passant” synapses and by GC ascending axons forming about 400 functional synapses (Cesana et al., 2013). Basolateral dendrites of the Golgi cells are also contacted by a disynaptic MF-GC-Golgi cell pathway where GCs can innervate both basolateral or apical dendrites. Golgi cells apical dendrites also receive inputs from distal GCs through PF activity and from Lugaro cells (see next section).

Functionally, the MF-GC-Golgi cell pathway is involved in feedback inhibition of GCs via the local GC synapses (Cesana et al., 2013) while direct MF inputs onto Golgi cells are thought to control FFI of GCs.

Lastly, Golgi cells make inhibitory GABAergic synapses onto other Golgi cells (Hull and Regehr, 2012) and are densely interconnected via their gap-junction proteins connexin36 on apical dendrites (Dugué et al., 2009; Vervaeke et al., 2010) where each Golgi cell was estimated to be electrically coupled to ten other Golgi cells (Vervaeke et al., 2010).

G. *Lugaro cells*

Lugaro cells are mixed GABAergic-glycinergic inhibitory interneurons (Dumoulin et al., 2001), located just underneath the PC layer (Palay and Chan-Palay, 1974). They are activated by serotonergic fibers (Dieudonné and Dumoulin, 2000) most probably through volume transmission (Dieudonne, 2001), and by recurrent PC axons. Their thick dendrites can extend up to 200 µm parasagittaly (Dieudonné and Dumoulin, 2000). Two axonal plexus extends from their fusiform cell body, one has a local parasagittal projection into the molecular layer targeting basket and SCs (Lainé and Axelrad, 1998) while the other axonal plexus follows the mediolateral axis going through the GC layer and ascends back towards the molecular layer. The long projection axon can reach more distant targets including the apical dendrites of Golgi cells (Dieudonné and Dumoulin, 2000) and PCs (Dean et al., 2003). A subtype of Lugaro cell with a globular shape soma has also been reported (Lainé and Axelrad, 1998). Lugaro and globular cells populations each represent 15% of the interneurons in the granular layer (Simat et al., 2007). It has been estimated that one Lugaro cell targets more than a hundred Golgi cells with around 10 Lugaro axons making synaptic contact on each Golgi cell (Dieudonné and Dumoulin, 2000). And there is around one Lugaro cell for 15 PCs in the rat (Dieudonné and Dumoulin, 2000) and for 30 PCs in the cat (Sahin and Hockfield, 1990).

H. *Bergmann glial cells (Figure I2.6)*

Bergmann glia are specialized astrocytes specific to the cerebellum; their soma forms a monolayer located in the PC layer. There are around eight Bergmann glia cells for one PC (Korbo et al., 1993; Reichenbach et al., 1995). Each Bergmann glia cell has up to five processes named the radial fibers that branch in the parasagittal plane and extend over the whole depth of the molecular layer. Their processes ensheath the soma, dendrites and dendritic spines of PCs. In addition, radial fibers form small microdomains that envelop excitatory and inhibitory synapses onto PCs (Palay and Chan-Palay, 1974). Radial fibers interact with neighboring Bergmann glia processes forming a lattice that likely maintains the structural geometrical organization of the molecular layer (De Zeeuw and Hoogland, 2015). Bergmann glia are electrically coupled together (Müller et al., 1996) and with PCs (Pakhotin and Verkhratsky, 2005).

Importantly, Bergmann glia participate in glutamate uptake through the high number of glutamate transporters they express (Bergles et al., 1997). Similarly, it has been proposed that they would also respond to GABA release since their processes are enriched in GABAA receptors in the vicinity of GABAergic synapses onto PCs (Riquelme et al., 2002). Lastly, Bergmann glia tonically release GABA (Lee et al., 2010; Yoon et al., 2011, 2014). Altogether, these suggest they could locally regulate synaptic transmission.

2. *Modular organization of the cerebellar cortex*

I will now present the two glutamatergic afferent fiber systems innervating the cerebellar cortex, the CFs and the MFs, which both play a major role in carrying

sensorimotor information that will be integrated and processed by the cerebellum. Other afferents also project to the cerebellar cortex including noradrenergic, dopamiergic, cholinergic and serotonergic fibers (Schweighofer et al., 2004; Oostland and van Hooft, 2013).

Although the focus of my project is on the MF-GC-PC pathway, I will here also detail the organization of the CFsystem which is of major importance. First, CFs define the microzonal organization of the cerebellar cortex. Second, CFs select the inputs received by PCs by controlling the direction of plasticity at multiple synapses of the GC to PC connection (Jörntell and Hansel, 2006), either via its direct connection onto PC dendritic tree but also indirectly through spillover to MLI (Szapiro and Barbour, 2007).

A. *Organization of climbing fiber afferents in the cerebellar cortex*

Many structures send information to the inferior olive, the source of the CF afferents to the cerebellum: the mesodiencephalic junction, the spinal cord, the cerebral cortex, the thalamus, the hindbrain e.g. dorsal column nuclei, (superior colliculus and red nucleus) and the cerebellum via its collaterals from the DCN and vestibular nuclei. All the CFs arise from one of the three main nuclei of the inferior olive (the principal olive, the medial and dorsal accessory olive) and reach the cerebellum via the contralateral inferior cerebellar peduncle (Sugihara et al., 1999, 2001).

a. Cortical longitudinal zones and olivo-cortico-nuclear loops

The olivo-cerebellar projections forming the CFs are topographically organized, targeting specific zones of the cerebellar cortex. This was first observed in the 1940s in rats in degeneration studies of the inferior olive (Jansen and Brodal, 1940). Since then, many tracing studies have confirmed the existence of rostrocaudally oriented longitudinal zones of projection of 1 to 2-mm-wide in the cerebellar cortex, that extend perpendicularly to the lobules. Using ferret and later cat cerebellar sections stained with the Häggqvist technique (staining axons and myelin sheaths of individual fiber in blue and red respectively) Jan Voogd could delineate white matter compartments based on differences in myelin sheath diameters and divided the cerebellar cortex into seven longitudinal zones (**Figure I3.A**) (Voogd, 1967, 1969), later observed in rats (Azizi and Woodward, 1987; Jörntell et al., 2000) and mice (Schonewille et al., 2006). New subdivisions have been added afterwards defining the following twelve longitudinal zones from the medial to the lateral plane: A, AX, X, B and A2 zones in the vermis; C1, CX, C2 and C3 in the paravermis; D1, D0 and D2 in the hemisphere (**Figure I3.B**) (Apps, 1990; Buisseret-Delmas and Angaut, 1993; Atkins and Apps, 1997; Jörntell et al., 2000; Voogd et al., 2003; Sugihara et al., 2004; Voogd and Ruigrok, 2004). A zonal organization of the focculus and nodulus has also been identified (Ruigrok et al., 1992; Tan et al., 1995). Electrophysiological studies provided functional evidence for the existence of such longitudinal zones/for the organization of olivocerebellar and corticonuclear projections (Oscarsson, 1968; Larson et al., 1969; Armstrong et al., 1974; Trott and Armstrong, 1987) that, except for zone D2/d2, matched with the anatomically defined zones (Ekerot and Larson, 1982). CFs from adjacent olivary neurons originating from a given nucleus of the inferior olive target in most cases one longitudinal zone of the cerebellar cortex (Ekerot and Larson, 1979; Garwicz et al., 1992; Sugihara et al., 2001; Apps and Hawkes, 2009). However, they sometimes project mediolaterally to two longitudinal zones, as observed in the X, C1 and C3 zones (Voogd et al., 2003, Apps et al; 1997, Apps & Garwicz; 2000).

Each longitudinal zone of the cerebellar cortex receives CF afferents from a specific olivary subnucleus (Voogd and Glickstein, 1998; Sugihara et al., 2004) and sends Purkinje projections to a specific zone of the deep cerebellar or vestibular nuclei (**Figure I3.B**). DCN which are also compartmentalized (Chung et al., 2009; Sugihara et al., 2009) send an inhibitory feedback to the same subnucleus of the inferior olive defining olivo-cortico-nuclear closed loops (Pijpers et al., 2005). In addition, CFs provide collaterals to the deep cerebellar or vestibular nuclear target of the PCs

located in these longitudinal zones (Beitz, 1976; Buisseret-Delmas and Angaut, 1993; Sugihara et al., 1996, 1999; Ruigrok and Voogd, 2000). This arrangement in loops enforces a modular organization of the olivo-cortico-nuclear network.

b. Olivary climbing fiber projections

Injections of biotinylated dextran amine into the inferior olive allowed the visualization and reconstruction of individual olivocerebellar axons (Sugihara et al., 1999) and revealed their ramification into thick branches, the CFs, innervating roughly 10 to 15 PCs in the cerebellar cortex as well as thin collaterals that end in one given nucleus of the DCN and occasionally in the GC layer (Sugihara et al., 1999). Thick branches are most of the time parasagittally, rarely mediolaterally, oriented. Each PC is innervated by a single CF in adult mammals (Sugihara et al., 1999, 2001) following the regression of its developmental multi-innervations that takes place during the three first postnatal weeks (Crepel and Mariani, 1976; Watanabe and Kano, 2011).

The axon of a single olivary neuron gives rise to two to seventeen CFs in the rat, seven on average, targeting one or several lobules (**Figure I3.C**) (Sugihara et al., 2001). Estimates for other species can be deduced from studies where the total number of olivary neurons and PCs have been counted, giving around 9 to 11 CFs per axon in the cat (Escobar et al., 1968) and 15 for humans (Escobar et al., 1968). CF activation generates a strong excitatory response in PC, named the complex spike which will be detailed in **Part IV.1.D**.

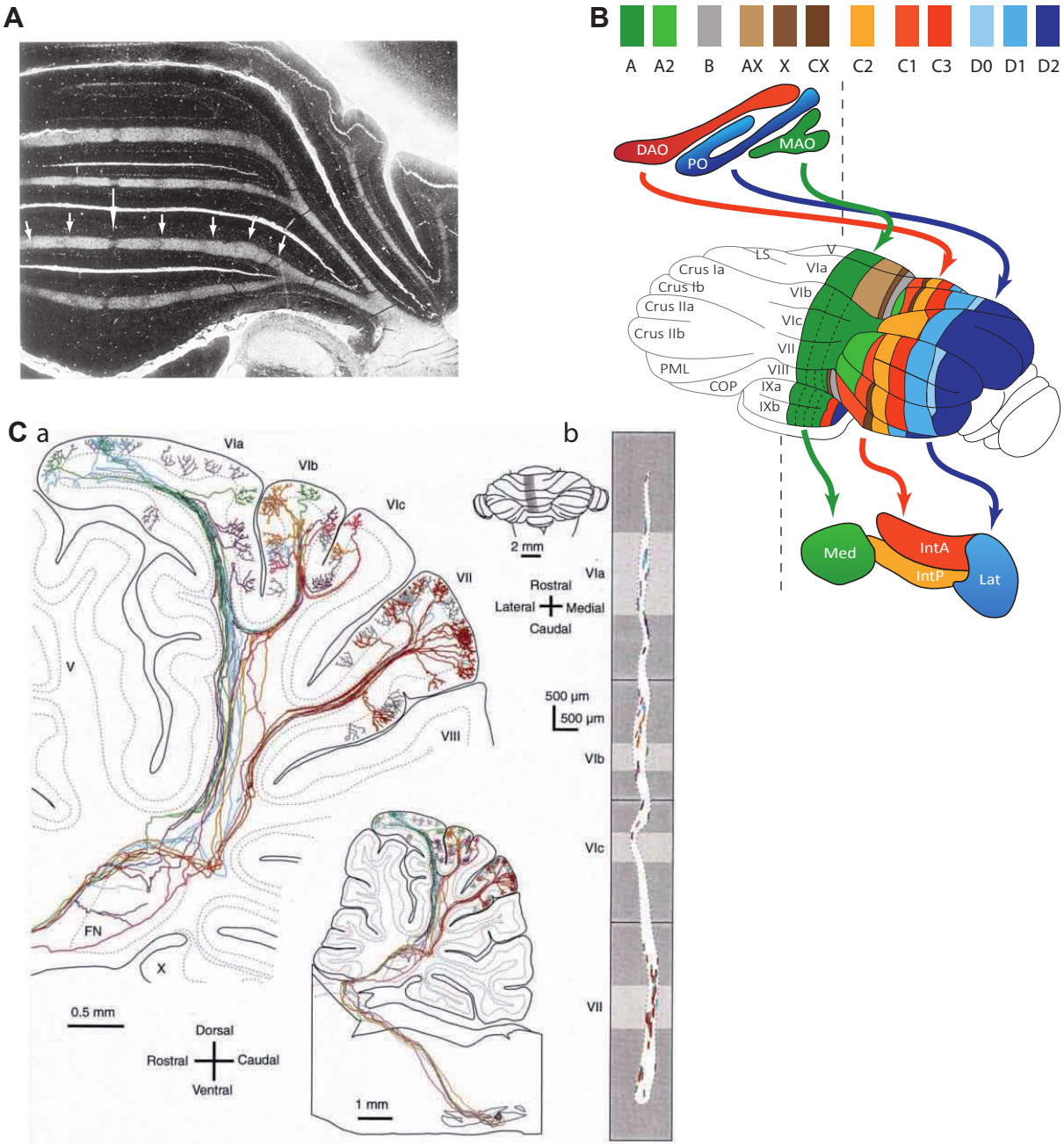

Figure I3. Organization of climbing fiber afferences in the cerebellar cortex.

A: The longitudinal subdivision of the white matter uncovered by the Häggqvist technique which differently stains axon and myelin sheaths, puts forward a compartmentation of input and/or output connectivity of the cerebellar cortex into seven longitudinal zones (indicated with arrows). Picture of a ferret cerebellar section from the anterior lobe, adapted from Voogd, 1967. **B:** Cerebellar cortical longitudinal zones and simplified view of the olivo-cortico-nuclear loops. The cerebellar cortex is now divided into twelve rostro-caudally oriented longitudinal zones: A, A2, B, AX, X, CX, C1, C2, C3, D0, D1, D2 of 1 to 2 mm wide. Each zone is defined by its CF inputs arising from a specific subzone of the contralateral inferior olive, and its corticonuclear projections to a specific part of the ipsilateral deep cerebellar or vestibular nuclei. Vestibular nuclei are not represented here. Adapted from Apps and Hawkes, 2009. Abbreviations: COP: copula pyramidis, DAO: dorsal accessory olive, IntA: anterior interposed nucleus, IntP: posterior interposed nucleus, Lat: lateral cerebellar nucleus, LS: lobule simplex, MAO: medial accessory olive, Med: medial cerebellar nucleus, PML: paramedian lobule, PO: principal olive. **C:** Anatomical microzonal organization of the cerebellar cortex. Reconstruction of six olivocerebellar axons (a, colored) and their projections on the unfolded view of the vermal cerebellar cortex (b) shows narrow longitudinal bands of CF projections, which are smaller than the longitudinal zones. From Sugihara et al., 2001.

c. Cortical microzones as the functional units of the cerebellar cortex?

Electrophysiological mapping studies from the group of Oscarsson revealed that CFs with similar receptive fields, i.e. activated by the same peripheral inputs, terminate within 0.1 to 0.3 mm wide regions of the cerebellar cortex (Andersson and Oscarsson, 1978; Oscarsson, 1979), further dividing longitudinal zones of 1 to 2 mm wide into smaller microzones, composed of hundreds of PCs and possibly covering several lobules. The microzone has been proposed to be the minimal functional unit of the cerebellar cortex (Oscarsson, 1979; Sugihara and Shinoda, 2004) controlling one motor element (possibly one muscle fiber, or an entire muscle, or a set of muscles).The CF afferences would carry information about features of the movements involving this motor element. Furthermore, Sugihara et al., (2001) showed that all the CFs of single olivary neurons target localized areas of 200-300µm wide in the rat cerebellar cortex, that may be the anatomical substrate of the microzones (**Figure I3.C**).

In addition, based on electrophysiological (Garwicz and Ekerot, 1994) and anatomical works (Garwicz et al., 1996; Apps and Garwicz, 2000), the cerebellar paravermis was proposed to be organized as “multizonal microcomplexes” composed of functionally related microzones sharing common CF receptive fields. These microzones are sometimes located in different longitudinal zones, for instance in C1 and C3 zones (Apps and Garwicz, 2000), and converge to the same output DCN. In support of this “multizonal microcomplexes” arrangement, four microzones related to eyeblink were found on one side of the paravermis in decerebrate cats (Hesslow, 1994). Together, the combined divergence of the olivocerebellar information onto the paravermis with the convergence of corticonuclear information onto one nucleus of the DCN illustrate parallel information processing in the cerebellar cortex (Apps and Garwicz, 2005).

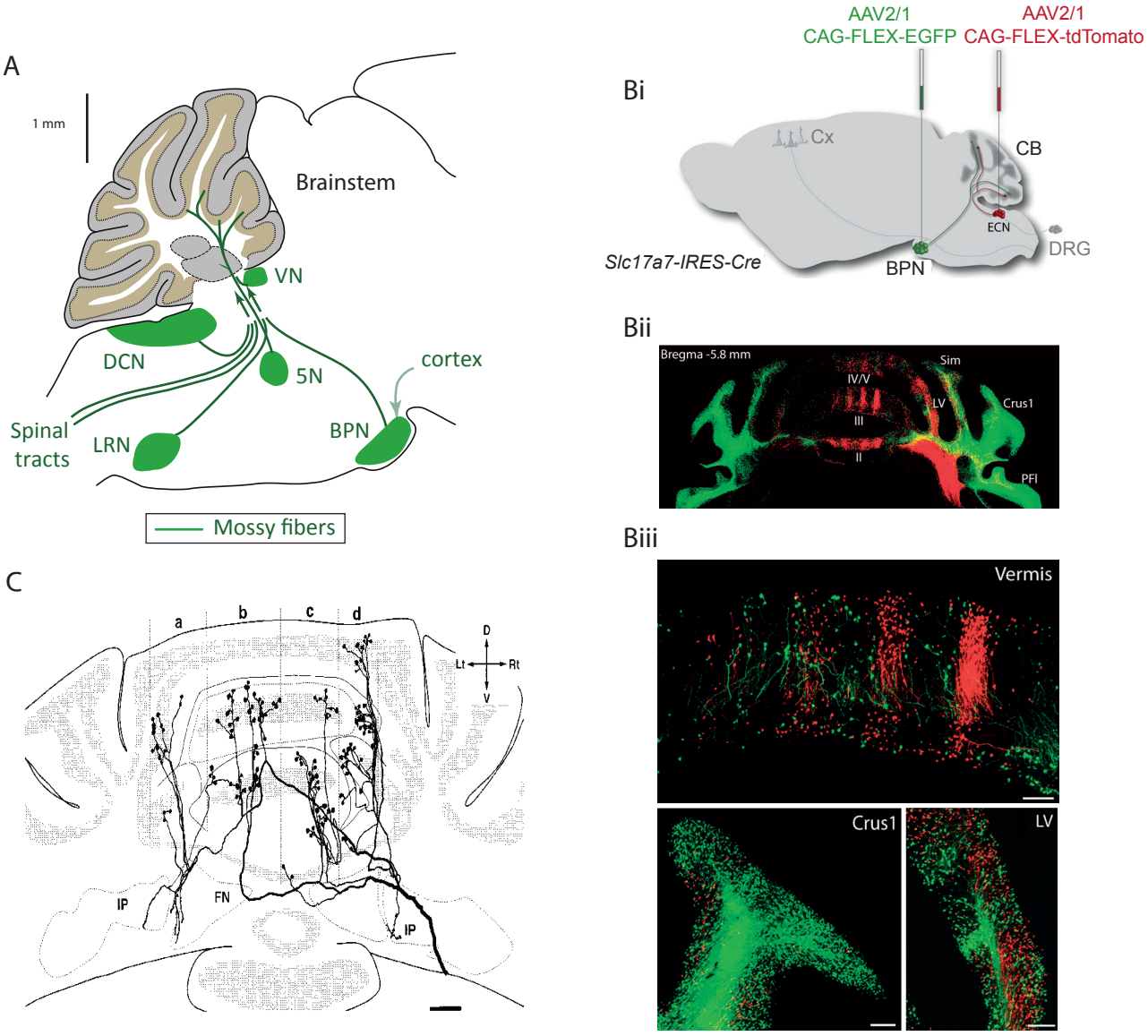

Figure I4. Anatomical organization of mossy fiber afferences.

A: Diversity of MF origins – MF arise from spinocerebellar tracts and many precerebellar nuclei. MF project onto the granular layer of the cerebellar cortex, sometimes making collaterals onto deep cerebellar nuclei neurons. Abbreviations: 5N: motor trigeminal nuclei; DCN: dorsal column nuclei including the external cuneate nucleus (ECN); LRN: lateral reticular nuclei; BPN: basilar pontine nuclei carrying integrated information from the cerebral cortex; VN: vestibular nuclei.
B: MF of different origins show distinct distribution termination patterns in the cerebellar cortex but can overlap. **Bi:** Specific labeling of MF from the ECN and BPN using adeno-associated virus injections. **Bii:** BPN MF projections mainly innervate the lateral hemispheres and the paravermis of the cerebellar cortex while MF arising from the ECN exhibit clear bands of projection mostly into the ipsilateral vermis. **Biii:** Magnified view displaying zones of both overlapping and segregated co-termination patterns of BPN and ECN MF. Adapted from Huang et al., 2013.
C: Extensive bifurcations and divergence of single MF projections. Trajectory of a single reconstructed MF axon originating from the LRN projecting bilaterally to the cerebellar cortex and deep cerebellar nuclei. Its collaterals form longitudinal cortical bands of projection along the mediolateral axis as for MF originating from ECN. From Wu et al., 1999.

Additionally, recent high spatial resolution imaging experiments revealed small parasagittal zones of complex spike synchrony, that can be activated spontaneously or by sensorimotor inputs. They match with the electrophysiologically defined microzones (Mukamel et al., 2009; Ozden et al., 2009; Schultz et al., 2009; Tsutsumi et al., 2015). PC synchronization highlight the topographical organization of olivo-cerebellar CFs (Sugihara et al., 2001) within a microzone and the electrical coupling of inferior olivary neurons (Lang, 2001; Blenkinsop and Lang, 2006). Indeed, adjacent olivary neurons are electrotonically coupled by dendritic gap junctions (Llinas et al., 1974) synchronizing nearby olivary neurons (Devor and Yarom, 2002; Leznik et al., 2002; Leznik and Llinás, 2005), further supporting the idea that the microzone forms the functional unit of the cerebellar cortex. Lastly, as the CFs control long term plasticity at both PF-PC and MLI-PC synapses (Jörntell and Ekerot, 2002), connectivity within a microzone might be to some extent stereotyped, suggesting microzone-specific information processing rules.

B. *Organization of mossy fiber afferences in the cerebellar cortex*

a. Bands of mossy fiber projections

MFs arise directly from the spinocerebellar tractus (Alisky and Tolbert, 1997) and from precerebellar nuclei of multiple origins including the lateral and paramedian reticular nuclei, the basilar pontine nuclei (Serapide et al., 2001; Odeh, 2005), dorsal column nuclei, trigeminal nuclei (Yatim et al., 1996) and vestibular nuclei (**Figure I4.A**). These nuclei carry sensori motor information about the body state to the cerebellar cortex such as limb position, movement velocity or more integrated information from the cerebral cortex via the pontine nuclei.

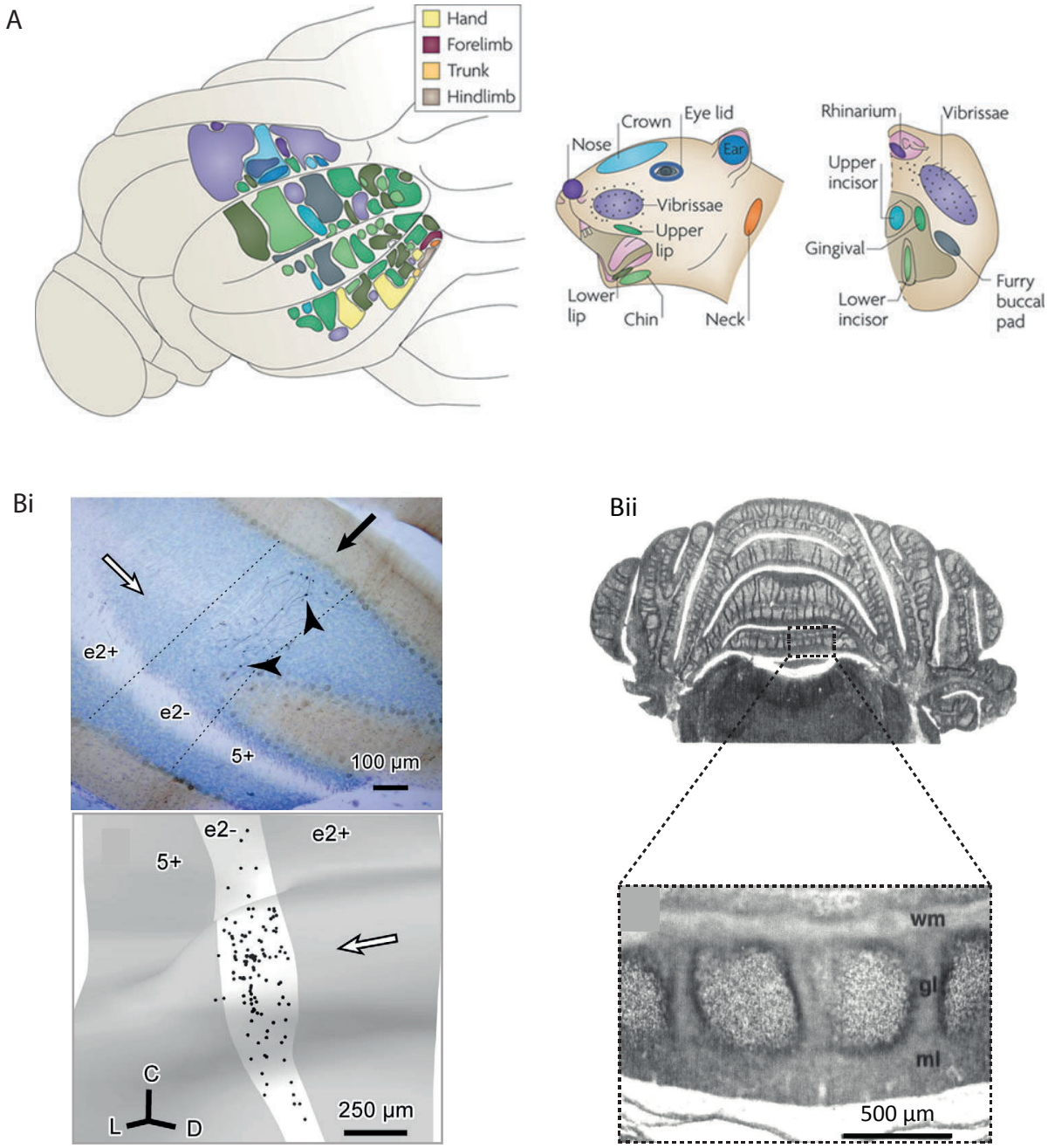

Figure I5. Functional organization of mossy fibers afferences and anatomical equivalent.

A: Functional organization of MF afferences. «Fractured somatotopical map» displaying non-overlapping patches of MF receptive fields in the granular layer of the cerebellar cortex (left) in response to the tactile stimulation of the corresponding colored zones of the rat face (right). Patches of MF activation are of variable size and multiple representation of the same face part appears. From Apps and Hawkes, 2009.
B: Anatomical correlation of functional MF patches. **Bi:** clustered terminals of a single MF originating from the cuneate nucleus show patch-like projections to e2- compartment of the copula pyramidis. Fom Quy et al., 2011. **Bii:** “Blebs” following dehydratation of the granular layer have similar size as MF patches. From Hawkes et al., 1997.

MF projections in the cerebellar cortex have been extensively studied. Jan Voogd showed that spinocerebellar fibers end in a number of distributed MF terminals forming parasagittal bands in the granular layer (Voogd, 1967, 1969). Similar distributions were found for the other MF systems (**Figure I4.C**). (Matsushita and Wang, 1987; Ji and Hawkes, 1994; Wu et al., 1999; Serapide et al., 2001; Quy et al., 2011). While CF target one or two longitudinal zones of the cerebellar cortex, MF from a common origin (Ruigrok, 2003) and individual MF (Wu et al., 1999; Sultan, 2001) show extensive transverse bifurcations and innervate several longitudinal zones mediolaterally, providing redundant information to different modules/microzones/multizonal microcomplexes. The wide divergence of MFs is further amplified by the PF system (see above).

b. Functional patches of mossy fiber activation

Precise micromappings of tactile MF inputs have been obtained giving rise to cerebellar somatosensory maps. More specifically, these were revealed by performing systematic mechanical or electrical stimulation of relatively small cutaneous receptive fields while recording evoked potentials in the GC layer in the caudal vermis (Joseph et al., 1978) or hemispheres (Shambes et al., 1978a, 1978b; Bower et al., 1981) of anesthetized rats, later confirmed in decerebrate cats (Kassel et al., 1984; Garwicz et al., 1998; Ekerot and Jörntell, 2001). Cerebellar tactile maps displayed circumscribed activation of GCs at multiple locations of the cerebellar cortex forming non-overlapping “patches” of receptive fields of variable shape and size (up to 1.5mm^2) from different parts of the body surface (**Figure I5.A**).

Surprisingly, some very distant receptive fields therefore from distant zones of the body can display neighboring patches of activation in the cerebellar cortex and reciprocally, which has led to the notion of a “fractured somatotopy” specific to the cerebellum. This topographical organization is conserved between animals (Bower and Kassel, 1990; Bower, 2011). To my knowledge, the anterior part of the vermis where I have been performing my experiments have not been mapped so far.

c. *Mossy fiber organization as bands or patches?*

One way to interpret the discrepancy between the observed anatomical MF projection bands and the recorded physiological patches may arise from the different levels of resolution of the corresponding techniques used. Bands may actually be functionally divided into an assembly of patches and/or microzone(s). In support to this hypothesis, results from individual MF tracing studies showed afferent terminals that may correspond to the functional patches (**Figure I5.Bi**) (Shinoda et al., 2000; Quy et al., 2011).

Interestingly, the anatomical equivalent of the receptive field patches may have been already found in early studies. Indeed, when cerebellar sections were rehydrated after fixation with ethanol and embedded into paraffin, Richard Hawkes and collaborators systematically observed, in the vermis and hemispheres, shrunken zones in the granular layer of about the size of patches at reproducible locations (**Figure I5.Bii**). Those zones, named by the authors 'blebs' are conserved between mice (Hawkes, 1997; Hawkes et al., 1999) and aligned with PC zebrin bands (see above).

C. *Histochemical compartmentation of the cerebellar cortex*

In addition to the anatomo-functional organization defined by input-output connectivity, the cerebellar cortex also shows a molecular topography with spatially restricted expression of neurochemical markers. Several proteins are expressed by subsets of PCs. The best characterized were named zebrins by Richard Hawkes and colleagues (Hawkes et al., 1985) because of their pattern of expression as alternating parasagittally oriented bands of zebrin-positive or zebrin-negative PCs along the medio lateral axis (Sillitoe and Hawkes, 2002; Sugihara and Quy, 2007; Apps and Hawkes, 2009). Each band contains hundreds of PCs. The most studied is

the expression pattern of the brain-specific glycolytic enzyme zebrinII/aldolase C (first showed in rat and fish (Brochu et al., 1990), which has a key role in ATP biosynthesis. Importantly, its expression pattern is reproducible between animals and its band organization is a common feature in every mammal and bird species studied so far (more than 20 species), at least for the anterior zone of the vermis (Sillitoe et al., 2004) and the posterior lobe (Marzban and Hawkes, 2011). Some zebrins share the same pattern as Zebrin II including EAAT4 (Dehnes et al., 1998), GABAB receptor 2 (Chung et al., 2008) or phospholipase C β3 (Sarna et al., 2006); others show opposite patterns of expression such as for mGluR1β (Mateos et al., 2001) or PLCβ4 (Sarna et al., 2006), or a different pattern, for instance the small heat shock protein (HSP25) (Reeber et al., 2014).

The GC layer is also histochemically compartmentalized into zones, bands or patches, although less thoroughly investigated. Differences in molecular expression have been observed between MF systems. For example, the type 2 vesicular glutamate transporter (VGLUT) is expressed in spinocerebellar MFs while dorsal column nuclei MFs strongly express VGLUT1 and weakly VGLUT2 (Gebre et al., 2012).

In addition, the expression of acetylcholinesterase in MF (Boegman et al., 1988), NR2C subunit of N-methyl-D-aspartate (NMDA) receptor in GCs (Karavanova et al., 2007), calretinin and mGluR1alpha in UBCs (Nunzi et al., 2002) and NPY and HSP25 in Bergmann glia (Reeber et al., 2014) show all a patterned expression in the cerebellar cortex.

This histochemical compartmentation of the cerebellar cortex has functional implications (for a review, see: Cerminara et al., 2015; see next section).

D. *Climbing fiber and mossy fiber afferents coincide with Purkinje cell stripes: implications for the functioning of a microzone*

Zebrin II boundaries were found to match with MF afferents in the anterior part of the vermis (Ji and Hawkes, 1994) and in the hemispheres (Voogd et al., 2003) as well as with CFafferent projection zones (Sugihara and Shinoda, 2004).

Importantly, more recently, when organization of both climbing and MF afferents were studied together in the same experiment, they were found to be aligned forming ----- oriented columns in the cerebellar cortex that matches with PC zebrin stripes (Voogd et al., 2003; Pijpers et al., 2006).

Interestingly, by using a transgenic mouse line that allowed the visualization of zebrin stripes (aldolase C here) *in vivo*, a very recent work demonstrated for the first time with a high spatial (single-cell) resolution a clear relationship between the zebrin band patterning and the microzones (zones of complex spike synchrony) in response to sensory stimulation in anesthetized animals (Tsutsumi et al., 2015).

Together, these results are likely to have physiological implications at the microzone scale. Indeed, there is an increasing body of evidence that the zebrin phenotype identifies different functional cerebellar local circuits. Differences in the spiking behavior of PCs were for example reported between zebrin II bands. These include differences in simple spike discharge frequency, irregularity and complex spike-mediated pause in simple spike (Xiao et al., 2014; Zhou et al., 2014, 2015).
In addition, differences in synaptic plasticity at PF-PC synapses were documented (for review: (Hawkes, 2014); for example depending on zebrin EAAT4 (Wadiche and Jahr, 2005) and mGluR1 (Wang et al., 2011).

Therefore the cerebellar cortex might be organized in functional units with specific information processing that will accordingly shape PC spike output.

E. *Other heterogeneities of the cerebellar cortex*

The cerebellar cortex display regional and local variations in its cytoarchitecture, first highlighted in anatomical and histological studies in the 1970s-80s. Differences in cell size, cell density, morphology or ultrastructure were revealed (reviewed in: Cerminara et al., 2015). PCs, GCs and Golgi cells were for instance found to be larger in the vermis than in the hemispheres (Lange, 1982) although a misclassification of Golgi cells which have similar size and location as UBC or Lugaro cells cannot be excluded. More detailed study using specific markers of the different cell types would be necessary to test this possibility.

Differences in fiber diameter of the PCs axons between distinct longitudinal zones in the same region were also reported: fibers were for example larger in vermal C1 and C3 zones than in C2 zone; and in D2 zone of the hemisphere than in D1 zone (see Voogd, 2011).

Many regional variations discriminate the posterior cerebellum from the rest of the cerebellum, especially lobule IX and X, where there is a larger number of UBC and Golgi cells as well as higher levels of expression of dopamine signaling molecules (Kim et al., 2009) which may support the specific functions of the vestibulocerebellum.

Conclusions Part II:

Underneath the simple architecture of the cerebellar cortex, the regular connectivity of its cell types repeated throughout the entire cerebellum and the topography of its afferences and efferences, it appears a complex functional organization of longitudinal zones, microzones, stripes and patches exists that process specific inputs. Which one(s) of the latter(s) is the unit for information processing? A zone of ten thousands PCs, a patch of tens PCs? This remains to be elucidated.

Regional and local heterogeneities of the cerebellar cortex add one more level of complexity where functional units are likely to have specific information processing rules depending on lobules/their location and neurochemical identities.

PART III: INFORMATION PROCESSING AT THE MOSSY FIBER-GRANULE CELL-PURKINJE CELL PATHWAY

I will now describe how sensorimotor inputs carried by the MFs will be processed in a cerebellar microzone.

1. *Activity/Information processing in the granular layer*

A. *Diversity of mossy fiber discharge*

As previously described in **Part II.2.B.a**, MFs arise from a multitude of precerebellar nuclei and therefore convey various types of information including vestibular (Arenz et al., 2008), somatosensory (Chadderton et al., 2004; Jörntell and Ekerot, 2006), tactile (Jörntell and Ekerot, 2006; Bengtsson and Jörntell, 2009), proprioceptive (Bengtsson and Jörntell, 2009; Sawtell, 2010) or locomotion-related information (Powell et al., 2015). *In vivo,* MF discharge can range from a few Hz (proprioceptive stimuli) up to 1 kHz (tactile stimuli) (Bengtsson and Jörntell, 2009).

Recordings of MF discharge in monkeys while they perform multiple sets of goal directed movements, which involved different and specific joints, revealed a wide range of MF discharge from purely tonic (18 %) to phasic responses (20 %). The most common pattern of discharge was a mixture of brief tonic and sustained phasic activities (63 %) (van Kan et al., 1993). In addition, the MF high frequency tonic discharge was shown to encode for the direction of the movement while the slow phasic rate-coded modulation was correlated with the movement velocity (van Kan et al., 1993), as observed more recently in the case of vestibular stimuli (Arenz et al., 2008). Similarly, the rate of MF discharge was found to increase during locomotion in relation to the step cycle of the walking mouse (Powell et al., 2015).

B. *Transmission at mossy fiber to granule cell synapses*

MF-GC synapses are embedded within the glomerulus structure also containing Golgi cell axons closely interacting with these synapses. The glomerulus is isolated by glial processes, which promote neurotransmitter spillover between neighboring synapses for both glutamate (Mitchell and Silver, 2000; DiGregorio et al., 2002) and GABA (Rossi and Hamann, 1998). MF-GC transmission is mediated by alpha-amino-3-hydroxy-5-methyl-4-isoxazolepropionic acid (AMPA) receptors activated by glutamate spillover that favor reliable transmission (DiGregorio et al., 2002) but also by NMDAR activation, especially in the case of sustained low frequency MF discharge (Silver et al., 1992; Schwartz et al., 2012). Although connections between MFs and GCs show strong initial presynaptic depression due to AMPAR desensitization (Xu-Friedman and Regehr, 2003), they can sustain high frequency transmission thanks to their large pool of available vesicles (around 300 per site) and their quick reloading at each release site (Saviane and Silver, 2006).

Altogether, the wide range of MF discharge from slow firing modulation to high frequency tonic discharge can be faithfully transmitted to GCs (Rancz et al., 2007; Schwartz et al., 2012). It should be mentioned that inputs from a single MF were found to be sufficient to trigger a spike in its postsynaptic GC (Rancz et al., 2007).

Lastly, recent evidence (Chabrol et al., 2015) suggest input-specific properties at the MF-GCs synapses, in terms of both strength and short-term dynamics. Indeed, by selectively electrically stimulating distinct groups of tagged MFs in mouse acute slices the authors recorded depressing synapses with strong synaptic strength from primary vestibular input pathway while synapses from visual pathway were facilitating with smaller synaptic weight. The authors confirmed this specificity *in vivo* by performing whole-cell patch-clamp recordings from GCs in anesthetized mice while either stimulating vestibular pathways by passive whole-body rotation of the mouse or the visual pathways by moving gratings in a given direction. Together, this suggests a diversity of filtering properties of MF-GC synapses.

C. *Multimodal inputs onto granule cells*

It has long been debated in the field whether MF inputs from multiple origins make synapse onto the same GC which would promote multimodal integration properties, in line with the pattern discrimination operation of the GC layer proposed by Marr and Albus theory for cerebellar function (Marr, 1969; Albus, 1971). GCs receive on average four inputs (Eccles et al., 1967b; Palkovits et al., 1971; Jakab and Hámori, 1988) and experiment performed *in vitro* showed the requirement of at least two of the four MF-GC synapses to trigger a spike in the GC (D'Angelo et al., 1995).

The proposed multimodal integration of GCs was recently challenged by studies from the group of Henrik Jörntell showing that MFs innervating a common GC share the same receptive field in the C3 zone of decerebrated cats (Jörntell and Ekerot, 2006; Bengtsson and Jörntell, 2009).The authors then proposed that GCs could act as a noise filter for this unimodal GC arrangement. However, these findings of a functional convergence of MFs inputs might be specific to cutaneous inputs.

By contrast, there is an increasing body of evidence for multimodal inputs on GCs in more recent studies. The first evidence came from an *in vivo* study of cerebellum-like structure in electric fish (Sawtell, 2010) and was confirmed in the rodent cerebellum (Huang et al., 2013; Chabrol et al., 2015). Huang et al., (2013) anatomically demonstrated multimodal convergence of MFs from the external cuneate nucleus carrying proprioceptive inputs (sensory feedback signal from the forelimb and upper-trunk) and from the basilar pontine nucleus signaling motor-command related information onto common GCs. Those individual GCs combining inputs from different MF origins were not uniformly distributed and define patches throughout the cerebellum. Of the GCs receiving external cuneate nucleus inputs 40% also receive also inputs from basilar pontine nucleus.

Lastly, the first physiological demonstration of multisensory inputs integrating onto single GCs was elegantly provided recently (Chabrol et al., 2015). The authors revealed that distinct groups of MFs conveying primary vestibular, secondary

vestibular or visual inputs can innervate the same GC. They next investigated how GCs process different MF input sources that have distinct synaptic properties (**Part III.1.B**). Interestingly, it appears that they shape GC spike output with a temporal signature: the first spike latency to the onset of stimulation encodes the different MF combinations (Chabrol et al., 2015). Computational modeling suggests that such diversity in the delay of GC firing improves the capacity of PC to discriminate among the different MF input patterns. It remains to be explored how such GC spike latency differences are read out/decoded by the PC. It would be also interesting to explore if the different MF input combinations are genetically determined, if they are set by activity-dependent mechanisms or randomly organized.

D. *Wide range of granule cells discharge*

GC discharge has been technically difficult to record *in vivo*. Several attempts for *in vivo* extracellular recordings failed to give good spike clustering due to the extremely high packing density of GCs (Hartmann and Bower, 2001; Gao et al., 2012a). However, it was made possible to study activity of individual GCs by the development of *in vivo* patch clamp recording methods (Chadderton et al., 2004). Somatosensory air puff stimulation of the whiskers or perioral regions in the anaesthetized rat evokes short bursts of excitatory postsynaptic currents (EPSCs) in GCs. In current clamp mode, excitatory postsynaptic synaptic potential (EPSP) summation is required to elicit an action potential. Since then, studies showed that GCs can discharge over a wide range of frequencies up to 1 kHz (Chadderton et al., 2004; Jörntell and Ekerot, 2006; Rancz et al., 2007; Arenz et al., 2008).

Remarkably, GC activity in behaving animals could be very recently obtained by the groups of Ian Duguid and Michael Häusser (Powell et al., 2015).They whole-cell recorded single GC activity in vermal lobule V in the awake mouse while the mouse was stepping on a spherical treadmill. They found an increased frequency of

EPSCs in GCs during locomotion as well as sparse high frequency bursts (bursts of 12 spikes at 100 Hz on average), each burst occurring at around 2 Hz. Interestingly, GC EPSCs and spiking were modulated according to the step cycle of the walking mouse. By using computational modeling, the authors went further and claim that they could predict step patterns during locomotion solely based on the MF discharge and GC spike output (Powell et al., 2015).

E. *Inhibition mediated by Golgi cells defines the time window and the input gain of granule cell activity*

GCs have low firing rates at rest due to their tonic inhibition mediated by Golgi cell activity. Golgi cells are spontaneously active with an average frequency of ~ 20 Hz in non anesthetized rats (Jirenhed et al., 2013) and their discharge is regulated by sensory inputs *in vivo* (Holtzman et al., 2006; Barmack and Yakhnitsa, 2008b). As described in Part II, Golgi cell dendrites are constrained to parasagittal modules (Sillitoe et al., 2008; Apps and Hawkes, 2009) receiving both local inputs from MFs and GC ascending axons and distal inputs from other modules (Holtzman et al., 2006, but see: Valera et al., 2016) through PF activity, the latter of which may provide lateral inhibition between cerebellar modules.

MF inputs onto Golgi cells trigger FFI of GCs. Such feedforward Golgi cell inhibition restricts the duration of GC bursts in response to MF inputs providing a unique time window in which the information can be transferred from the GC layer to the molecular layer. Of importance, it has to be reminded that Golgi cells contact a huge number of GCs along with the MFs in the glomerulus; therefore by setting a time window for MF integration by GCs, Golgi cells can synchronize a large population of GCs. Also, Golgi cells are synchronized by electrical coupling through gap junctions (Dugué et al., 2009) imposing a rhythmic inhibition onto GCs. However, the Golgi cell network can be transiently and locally desynchronized by MF inputs

which is likely to influence GC layer activity (Vervaeke et al., 2010). This phenomenon is triggered by MF-induced Golgi cell excitation that in turn electrically inhibits local Golgi cells via their gap junctions.

Electrical inhibition is differentially spread in the network depending on the number and strength of electrical synapses. Golgi cells having the strongest coupling will fire first while those having the weakest will fire last thereby resulting in various delays of subsequent spikes (up to 100ms) which transiently desynchronize the local Golgi cell network (Vervaeke et al., 2010).

GCs, when they receive MF inputs, generate via their ascending axon a direct excitation of Golgi cells with fast kinetics (Cesana et al., 2013), which in turn provides feedback inhibition onto those local GCs. It timely regulates the gain of the system (Mitchell and Silver, 2003) by controlling the amount of MF inputs that can be transferred to the molecular layer. In addition, this configuration allows only the strongest activated GCs to spike thereby increasing the contrast between small and strong inputs to the GC layer and controlling the number of patterns received by PCs.

2. *Activity/Information processing in the molecular layer*

A. *Granule cell ascending axon and parallel fibers: a long controversy?*

As described so far, the diversity of sensori motor information carried by the different MF systems is topographically conveyed to the input layer of the cerebellar cortex - the granular layer- where patches of activated GCs (**Part II.2.B.b**) transfer the information to PCs and modulate its discharge (**Part IV.2.B**).

Considering that PFs run mediolaterally and cross hundreds of PCs across several microzones (**Part II.2.A.c**), it possibly means that every "on beam" PC can be modulated by all the different MFs targeting the granular layer underlying the given PF beam. The "beam hypothesis" corresponding to a beam-like excitation of PC in response to MF activation of GCs was first proposed by Valentino Braitenberg and Roger Atwood (Braitenberg and Atwood, 1958; Braitenberg, 1961). In support of this hypothesis, *in vivo* mapping of intracortical field potentials in the anterior lobe of anesthetized cats (C3 and D zones) revealed spread responses to MF inputs in the molecular layer up to 1.5 mm away from the MF termination area suggesting a propagated activity along the PFs (Garwicz and Andersson, 1992). Similarly, *in vivo* multiple single-unit recordings of distant PCs in crus 1 and crus 2 in the transverse plane demonstrated that simple spike activity can be correlated in response to single-whisker stimulation, suggesting that the same beam of PFs activates both PCs (Bosman et al.,2010).

However, this view has been challenged by several studies showing that PCs are activated only by local GCs located in the same cortical column (i.e. just below the PCs) (Bower and Woolston, 1983; Cohen and Yarom, 1998; Brown and Bower, 2001; Rokni et al., 2007). Also correlations in simple spike synchrony (**Part IV.3**) assessed either by *in vivo* paired recordings or double juxtacellular recordings were found only in neighboring PCs (located fewer than 100 µm apart; (Ebner and Bloedel, 1981; De Zeeuw et al., 1997a; Shin and De Schutter, 2006; Heck et al., 2007; Wise et al., 2010). Together, these studies support local GCs as the main excitatory drive to PCs which is referred to as the "radial hypothesis" stating that it is the ascending axon, and not the PFs that provide the major input to PCs.

In vitro and *in vivo* experiments have shown that most of the GC-PC synapses are silent (Ekerot and Jörntell, 2001; Isope and Barbour, 2002). Indeed, on beam PCs are not uniformly activated when stimulating cutaneous receptive fields *in vivo* (Ekerot and Jörntell, 2001) and paired recordings of connected GCs and PCs in acute slices revealed a low functional connectivity (0.1) for distant GCs located more than 30 µm away from the recorded PC (Isope and Barbour, 2002). Silent synapses could

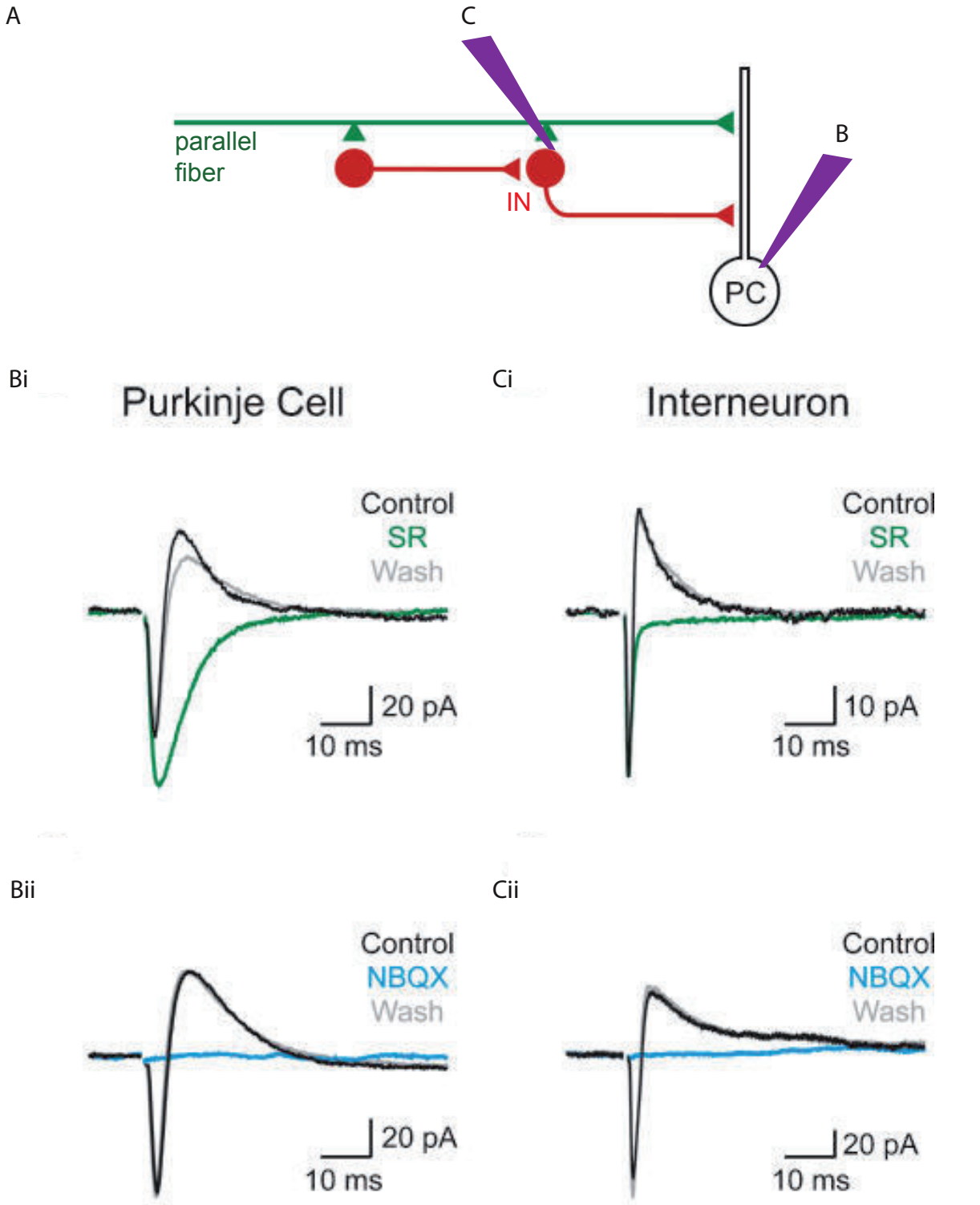

Figure I6. Molecular layer interneuron-mediated feed-forward inhibition onto Purkinje cells and other molecular layer interneurons.

A: Feed-forward inhibitory circuit onto PC (B) and onto MLI (C).
B: Feed forward inhibition onto PCs. **Bi:** Electrical stimulation of the PF elicited EPSCs in the PC followed by disynaptic IPSCs with a rapid onset (1.4 ± 0.2 ms on average). Disynaptic IPSCs were blocked by bath application of the GABAA antagonist SR95531 (10 μM). **Bii:** Both EPSCs and IPSCs were fully blocked following bath application of NBQX (6 μm), an AMPA receptor antagonist. **C:** Feed forward inhibition onto MLI. The same as in B is observed with a similar fast onset of IPSC (1.4 ± 0.1 ms on average). AMPA; EPSCs; GABA; IPSCs; NBQX.

be mute – presynaptically inactive – or deaf – lacking postsynaptic receptors. Several lines of evidence support the deaf hypothesis, potentially following the induction of a long term depression (LTD) during specific conjunctive activation of CFs and GCs (Ito, 2006). However, when GC and PC somas are close to each other, suggesting that they belong to the same microzone, the probability of connection increases several fold (up to 0.5) (Isope and Barbour, 2002). Also, the Ekerot group (Jörntell and Ekerot, 2002, 2011) has demonstrated *in vivo* that the number of active GC-PC synapses on a given PC of a specific microzone can be sustainably enhanced when stimulating at high frequency either tactile receptive fields or PFs, suggesting that long term depression (LTD) could be reversed by a long term potentiating mechanism. These findings indicate that synaptic weights between GCs and PCs are the result of a selection process that correlates with the remodeling of PCs receptive fields. Interestingly, the high amount of inactive synapses would allow an optimized number of information to be stored (Brunel et al., 2004) and appear to play a role in motor learning.

Finally, the controversial results opposing a local GC control versus a parallel beam control of PCs can be reconciled by findings showing that specific groups of both local and distant GCs have been selected by PCs (Valera et al, 2016). Therefore, activity dependent processes or specific topography of MF inputs might functionally control whether individual PCs are activated by local or distant GCs or both.

B. *MLI-mediated feedforward inhibition gates granule cell inputs onto PC and MLI*

MF-GC inputs can be transferred either directly to PCs or through disynaptic pathway onto PC (**Figure I6.A**) as evidenced in uncaging experiments *in vitro* where GC activation triggers both excitation and inhibition of PCs (Dizon and and Khodakhah, 2011). Properties of the FFI circuit onto PC spike output have been dissected by Mittmann and colleagues in acute slices (Mittmann et al., 2005; Mittmann and Häusser, 2007). The authors explored the temporal interaction of excitatory and

inhibitory inputs onto MLI and PCs during electrical stimulation of PF and showed that evoked PC EPSPs were followed by disynaptic IPSPs (**Figure I6.B**) (Mittmann et al., 2005) with a rapid onset of inhibition (Eccles et al., 1967a; Brunel et al., 2004; Mittmann et al., 2005). FFI resulted in a decrease in the number of PC output spikes (Mittmann et al., 2005) and enhanced spike timing accuracy by imposing a short time window for EPSP summation (Mittmann and Häusser, 2007). In addition, *in vivo* studies have suggested MLI-mediated FFI as a key player in spatially restricting the beam activation of PFs and therefore the propagation of MF-GC inputs (Jaeger and Bower, 1994; Santamaria et al., 2002, 2007; Cramer et al., 2013).
This FFI activity can be amplified by network mechanisms, including CF firing, synchronizing local MLIs that innervate the same PC within a microzone (Mathews et al., 2012). Also, it appears that reciprocal inhibition seems restricted to functionally-related MLI of a microzone (Jörntell et al., 2010). Indeed, MLI IPSPs are evoked *in vivo* by tactile stimulation only when the stimulated receptive field is the same as the one that triggers MLI EPSPs (Ekerot and Jörntell, 2003). A contribution from Lugaro cell-mediated inhibition onto MLI cannot be totally excluded. Also, the local MLI action in a microzone is also supported by their morphology and parasagittal orientation (**Part II.1.E**).

Nevertheless, *in vivo,* PCs and MLI do not share the same cutaneous receptive fields (very distant) (Ekerot and Jörntell, 2001). It is thereby unlikely that PCs and their connected MLI could be activated by the same PFs. Yet, direct stimulation of beams of PFs (Mittmann et al., 2005; Mittmann and Häusser, 2007) undoubtedly targets a combination of some PFs activating interneurons and some others activating PCs, which would explain the discrepancy between experiments using receptive field activation and those using electrical stimulation.

Therefore, it remains to be elucidated if a real FFI exists *in vivo. O*ne argument in favor for it is the irregularity of PC firing (**Part IV**) recorded *in vivo*, that is controlled by MLI (Wulff et al., 2009). The authors also demonstrated that MLI-mediated inhibition plays a role in the consolidation of motor learning (Wulff et al., 2009), supported by *in vitro* findings showing that feed-forward inhibition can be promoted or

conversely lowered via the interplay of long-term plasticity mechanisms: long-term potentiation (LTP) or LTD at the three compound synapses of the GC to PC connection.

C. *Properties of the granule cell to Purkinje cell pathway*

I will here describe the synaptic properties and short-term dynamics of the three synapses of the GC-PC pathway, namely PF-PC, PF-MLI and MLI-PC synapses.

a. Synaptic properties

i. Fast and reliable synaptic transmission at the GC- PC synapses

GC ascending axon to PC synapses and PF to PC synapses are glutamatergic. Neurotransmission is mediated by non-NMDA glutamate postsynaptic receptors (Perkel et al., 1990), including AMPA receptors (Konnerth et al., 1990) and perisynaptic metabotropic glutamate receptors (mGluRs) (Batchelor et al., 1994).

Unitary PF-PC synaptic responses are small (8.4 ± 7.1 pA on average) and variable (Isope and Barbour, 2002). Importantly, few tens of simultaneously active GCs are enough to excite one given PC (Barbour, 1993; Isope and Barbour, 2002).

On the presynaptic side, PF-PC synapses were first found to have a low initial release probability (~ 0.05) at physiological calcium concentration (Dittman et al., 2000; Foster, 2005) which was challenged by more recent data revealing a higher release probability (Isope and Barbour, 2002; Sims and Hartell, 2005; Valera et al., 2012; Schmidt et al., 2013). There are 7 to 8 docked vesicles on average

(Xu-Friedman et al., 2001). Interestingly, ascending axon synapses have a higher release probability than PF synapses (Sims and Hartell, 2005) meaning that local GCs are more likely to generate EPSCs than distal GCs (Isope and Barbour, 2002). Importantly, the probability of synaptic failure, i.e. the probability of not releasing any synaptic vesicles, was low (~ 0.1; Isope and Barbour, 2002), supporting a reliable transmission at excitatory GC-PC synapses.

ii. Synaptic properties at the GC-MLI synapses

A single stimulation of PFs evokes a fast AMPAR-mediated EPSC in MLI (Atluri and Regehr, 1998; Clark and Cull-Candy, 2002) with a fast decay due to AMPAR deactivation (Barbour, 1994).

In contrast, trains of PF stimulation (5 or 10 pulses at 100Hz) result in prolonged EPSCs in MLI mediated by AMPAR and extrasynaptic NMDAR (Carter and Regehr, 2000) that can last for hundreds of milliseconds. This sustained response could be explained by asynchronous/delayed release (Atluri and Regehr, 1998; Nahir and Jahr, 2013), glutamate spillover from neighboring sites, known to activate AMPA and NMDA receptors in MLI (Carter and Regehr, 2000) or presynaptic facilitation (Atluri and Regehr, 1996) and the fast replenishment of vesicular release sites (Crowley et al., 2007). Recently, activation of extrasynaptic NMDAR were observed at unitary PF-MLI synapses (Nahir and Jahr, 2013). Also, a single GC and even a single quantum can elicit an action potential in a connected MLI (Barbour, 1993; Carter and Regehr, 2002) in acute slices.

iii. Synaptic properties at inhibitory synapses onto PC discharge

PCs are mostly inhibited by MLI from the same microzone (Ekerot and Jörntell, 2001, 2003; Jörntell and Ekerot, 2002; Jörntell et al., 2010). One PC receives inputs from 9 MLI on average (Häusser and Clark, 1997). Inhibition is mediated by $GABA_A$ and GABAB receptors (Batchelor and Garthwaite, 1992). Inhibitory postsynaptic currents

(IPSCs) recorded in PCs are highly variable in amplitude (Vincent and Marty, 1996; Häusser and Clark, 1997), particularly for BCs, and are developmentally regulated. MLI starts inhibiting PC from postnatal day 10 (P10) (Crepel, 1974; Batchelor and Garthwaite, 1992) with large IPSCs (Vincent and Marty, 1996) that later decrease in amplitude more than ten times between P11-15 and P26-31 (Pouzat and Hestrin, 1997). Also, inhibitory strength is seven fold higher at BC to PC synapses (1.73 ± 0.55 nA) than at SC-PC synapses (0.24 ± 0.04 nA) in P16-28 mice (Bao et al., 2010). A difference was also reported in younger rats (P9-P15) (Vincent and Marty, 1996).

MLIs produce an irregular discharge pattern in PCs and other MLI (Häusser and Clark, 1997). Interestingly, activation of a single MLI is sufficient to cause a delay in PC firing in acute slices (Häusser and Clark, 1997) but not *in vivo*. Indeed, dual loose patch recordings of MLIs (more likely BCs) and PC separated by less than 10 µm distance in decerebrated cats show rather small or no effect of single MLI onto PC firing (Bengtsson et al., 2013). This could arise from the weak synaptic strength of the unitary inhibitory synaptic connection (Häusser and Clark, 1997). In addition, *in vivo* higher levels of network activity tend to decrease the neuronal membrane resistance which would attenuate any influence on PC spiking.

iv. Reciprocal synaptic inhibition between MLIs

As introduced in **Part II.1.E**, MLIs perform reciprocal inhibition through chemical and electrical synapses. Chemical synapses alter the timing and reliability of spike in its postsynaptic targets (Häusser and Clark, 1997; Mittmann et al., 2005) while electrical synapses can favor synchrony in local MLI networks (Mann-Metzer and Yarom, 1999).

b. Short-term synaptic plasticity

Many forms of synaptic plasticity have been demonstrated at specific cerebellar synapses, and at different time scales. My focus here will be on short-term plasticity referring to short-lasting modification of synaptic strength from milliseconds to tens of seconds at the different synapses of the GC to PC pathway. Depending on the recent

activity of the presynaptic neuron, of the postsynaptic neuron or both, two forms of plasticity – short-term facilitation and short-term depression - can be induced, respectively leading to an increase and a decrease in synaptic efficacy.

Short-term plasticity is a crucial dynamical process that strongly influences the impact of a presynaptic neuron onto the discharge of its postsynaptic targets. Importantly to my study, the combination of different short-term plasticities at the PF-PC, PF-MLI and MLI-PC synapses could possibly modulate the balance between excitation and inhibition.

i. Short-term synaptic plasticity at PF-PC synapses

When electrical paired-pulse stimulation is applied to PFs with a short interval duration of less than 500 ms, the ratio of amplitudes of the second to the first evoked PF-PC EPSCs (the paired-pulse ratio, PPR) is increased (Atluri and Regehr, 1996). This short duration potentiation of synaptic transmission is homosynaptically induced and referred to as paired-pulse facilitation.

The PF connections have modest paired pulse facilitation at 40 milliseconds interval (Isope and Barbour, 2002). However, PPR estimates vary widely in the literature, possibly due to different stimulation and recording conditions including the age of animals, external calcium concentration, stimulation location, and temperature of recordings (Atluri and Regehr, 1996; Isope and Barbour, 2002; Valera et al., 2012). At PF-PC synapses, PPR value was 2.5 (Atluri and Regehr, 1996) when recorded at 24°C in young rats using 2 mM external calcium and stimulating in the molecular layer. However, in adult rats at 32°C, using the same stimulation protocol and calcium conditions the PPR was 1.7 (Isope and Barbour, 2002). An even lower facilitation (1.36-1.37) was found when stimulating in the GC layer or in the case of unitary GC-PC connections (Isope and Barbour, 2002). It should be emphasized that stimulation in the molecular layer activates dense bundles of PFs targeting a localized area of the PC dendritic tree, which is unlikely to be physiological. Such protocols recruit a high number of synapses locally, resulting in excessive transmitter release and increased PPR proposed to be mediated by glutamate spillover onto

extrasynaptic receptors from the large number of adjacent active synapses (Marcaggi and Attwell, 2005, 2007; Sims and Hartell, 2005). PPR is frequency-dependent and does not seem to depend on the synaptic location on the dendritic tree across the molecular layer and on synaptic weight (Valera et al., 2012). PF-PC synapse facilitates during short bursts of stimulation and sustain neurotransmission at high frequencies (Valera et al., 2012).

Short-term facilitation has a presynaptic origin; when an action potential goes through a PF *en passant* synapse, the induced membrane depolarization leads to the opening of P/Q-type (Cav2.1) and N-type (Cav2.2) voltage-gated calcium channels. The resulting calcium influx triggers a rapid release of synaptic vesicles. The presynaptic residual free calcium after an action potential leads to an accumulation of calcium in the presynaptic terminal during repetitive stimulation thereby increasing neurotransmitter release and the amplitude of subsequent postsynaptic EPSC amplitudes (Katz and Miledi, 1968; Mintz et al., 1995; Brenowitz and Regehr, 2007). This mechanism can confer high pass filtering properties to these synapses. One study investigated the short-term potentiation at PF-PC synapses (Goto et al., 2006) when induced by short periodic bursts (90 sets of 5 stimulations at 50 Hz every second). This potentiation of PC EPSP is mediated by presynaptic mechanisms and lasts up to 20 minutes.

Interestingly, short-term plasticity can be modulated. For example, activation of mGluR4 receptors lead to short-term depression of excitatory synaptic transmission at PF-PC synapses by inhibiting presynaptic calcium influx through a signaling cascade involving the activation of phospholipase C and protein kinase C (Abitbol et al., 2008). mGluR4 interacts with proteins of the SNARE complex, possibly syntaxin, SNAP-25, or α-synuclein, that mediate docking of synaptic vesicles to the presynaptic membrane (Abitbol et al., 2008; Ramos et al., 2012).

In the case of intense activity of PFs (and CFs), PCs are subjected to another form of short-term plasticity called depolarization-induced suppression of excitation (DSE) that last seconds (Kreitzer and Regehr, 2001). DSE is induced by postsynaptic depolarization resulting in a transient reduction of presynaptic vesicular release. It is

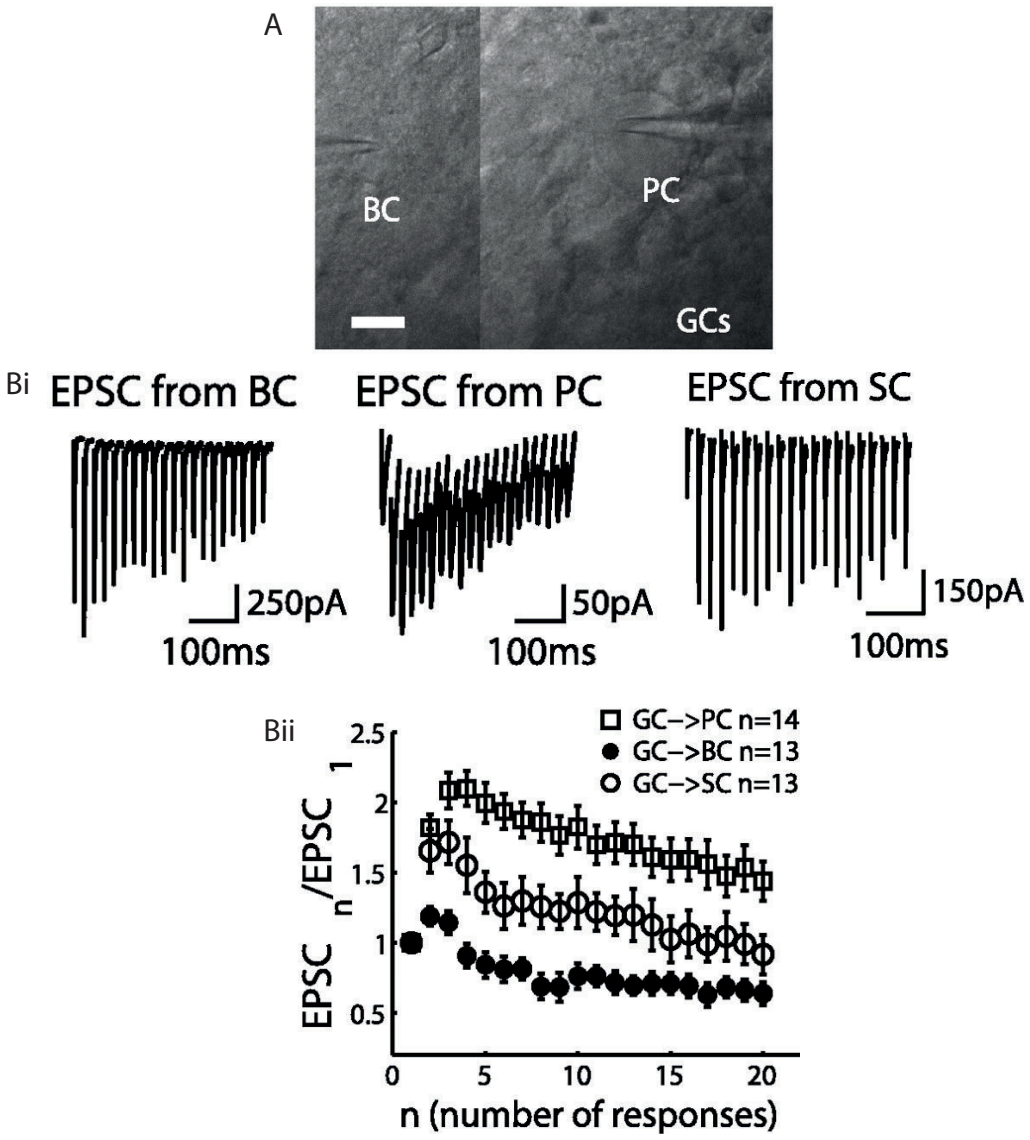

Figure I7. Short-term synaptic plasticity at the parallel fiber to molecular layer interneuron synapses.

A: GCs were electrically stimulated at 50 Hz and PC or MLI were whole-cell patch clamped at – 65 mV. **Bi:** Elicited EPSCs in representative cells: a BC, a PC and a SC Scale bar: 10 µm. **Bii:** Group data showing the strong facilitation of GC-PC and GC-SC synapses while GC-BC synapses exhibited no change, or a slight depression. Modified from Bao et al., 2010.

mediated by the calcium dependent release of endocannabinoids synthesized from membranous lipidic precursors which diffuse across the postsynaptic neuron membrane and on presynaptic boutons. The synaptic efficacy is reduced by a smaller presynaptic calcium entry and decreased neurotransmitter release at each action potential possibly due to inhibition of presynaptic N-type and P/Q-type voltage-dependent calcium channels, or from the upregulation of presynaptic potassium channels shortening action potential. Total inhibition of presynaptic firing is likely to be mediated by upregulation of the G protein-coupled inwardly-rectifying potassium type of potassium channel (Kreitzer et al., 2002) increasing the threshold for spike generation. Therefore, endocannabinoids act as a retrograde messenger activating presynaptic type 1 cannabinoid receptors that reduce synaptic efficacy. (Egertová and Elphick, 2000). In addition, DSE displays a late component of depression of presynaptic PF inputs, involving VGLUT3-mediated vesicular release of glutamate from the PC (Crepel et al., 2011) and soluble N-ethylmaleimide-sensitive factor attachment protein receptor (SNARE)-dependent mechanisms (Duguid and Smart, 2004; Duguid et al., 2007). Retrogradely released glutamate binds to kainate receptors on PFs (Crepel, 2007; Crepel and Daniel, 2007).

In most of these studies, induction protocols for short-term plasticities were performed via direct stimulation in the molecular layer and not by stimulating GC layer, therefore the physiological relevance of DSE remains to be elucidated. If this is confirmed, it is tempting to predict that DSE would have a neuroprotective role by locally regulating the activity of a neural circuit and preventing it from being overexcited.

ii. Short-term synaptic plasticity at PF-MLI synapses

Very interestingly, Bao and colleagues (Bao et al., 2010) showed that PF-MLI synapses have different short-term dynamics depending on the target cell whether it is a SC or BC (**Figure I7**), a phenomenon called target-dependent short-term plasticity (for review: Blackman et al., 2013). PF synapses onto SCs facilitate in response to 50Hz train of stimuli while those onto BCs show no change or a

minor depression (**Figure I7**) (Bao et al., 2010). Target-dependent short-term plasticity has also been observed in the hippocampus (Pouille and Scanziani, 2004) and neocortex (Buchanan et al., 2012).

These results are of importance for information processing considering that synapses subjected to short-term depression are more prone to transmit efficiently low frequency information while those endowing facilitation would optimally transfer high frequency information (Fuhrmann et al., 2002). In other words, it means that the same GC input will be filtered differently by basket and SCs thereby conveying different aspects of the same information to its specific target compartment in the PC - the soma and the dendritic tree respectively. In support of this hypothesis, spiking probability of BCs were demonstrated to decrease up to 50% during 50 Hz GC stimulation while SCs, which have a low initial probability of release, increase their spike probability during the train of stimulation (Bao et al., 2010). These different output spike patterns to the same high frequency train of stimulation produce a transient early onset somatic inhibition onto PC followed by a persistent late onset dendritic inhibition.

DSE was also demonstrated in both stellate and BCs, but was found to be weaker than in PC, possibly due to a lower release of endocannabinoid from MLI (Beierlein and Regehr, 2006). Interestingly, the authors also investigated this phenomenon in more physiological conditions: instead of depolarizing the MLI membrane as for DSE, they generated brief PF bursts (trains of 10 pulses at 50 Hz) and observed short-term depression now referred to as synaptically evoked suppression of excitation (SSE). This evokes endocannabinoids release (2-AG) from basket and SCs that transiently suppress the ability of PF synapses to elicit action potentials in MLI, thereby reducing FFI onto PC. SSE involves either or both NMDAR and mGluR1 receptor activation leading to an increased postsynaptic intracellular calcium concentration in MLI and activation of diacylglycerol lipase required for endocannabinoids release.

iii. Short-term synaptic plasticity at MLI-PC synapses

MLI to PC synapses show strong paired-pulse depression in P11-P15 rats (0.62 ± 0.16 at 33,3Hz, (Pouzat and Hestrin, 1997)) and P16-P28 mice (Bao et al., 2010) but facilitate in more mature rats at P26-P31 (1.77 ± 0.23 at 33,3Hz, (Pouzat and Hestrin, 1997)). The calcium binding protein parvalbumin was shown to play a role in the paired-pulse depression (Caillard et al., 2000).

As for DSE, a short depolarization of PC can induce depolarization-induced suppression of inhibition (DSI; (Llano et al., 1991; Vincent et al., 1992)). Paired recordings between MLI and PCs showed that the firing frequency of presynaptic interneurons (Kreitzer et al., 2002), the amplitude of evoked IPSCs and the frequency of miniature IPSCs are decreased during DSI (Diana et al., 2002). DSI could lead to a 90 % decrease in synaptic transmission and like DSE is mediated by activation of presynaptic CB1 receptors (Diana et al., 2002) and relies on increased postsynaptic intracellular calcium (Glitsch et al., 2000).

High frequency activation of CF (trains of more than 10 pulses at 50 Hz) is also able to induce DSI (5-10 seconds) at BC-PC synapses via the activation of presynaptic AMPAR (Satake et al., 2000). Glutamate spillover from CF to PC synapses that are in close vicinity to BCs axons contributes to AMPAR activation (Satake et al., 2000). However, AMPA-receptor–mediated DSI might be expressed only in young animals (P13-P20) (Liu, 2007).

DSI can decrease MLI excitability through the opening of potassium channels (Kreitzer et al., 2002) thereby reducing synaptic transmission with postsynaptic PCs and other MLI.

DSI can be followed by a short-lived large increase in the frequency of miniature IPSCs (Duguid and Smart, 2004) that the authors called depolarization-induced potentiation of inhibition (DPI) and was also observed when repeatedly activating CF with low frequency stimulation (2 Hz for 5 seconds). PC depolarization or CFactivation opens postsynaptic voltage gated calcium channels leading to calcium entry and somatodendritic release of glutamate by the PC (Duguid et al., 2007). Released glutamate binds to presynaptic NMDAR expressed onto MLI terminals (Duguid and Smart, 2004). However, this precise localization of NMDAR expression

has to be considered with caution since the studies were performed in culture and not in acute slices. Furthermore, it remains to be explored how the release of glutamate can activate presynaptic NMDAR considering that glutamate is uptaken by transporters expressed at postsynaptic PC and surrounding Bergmann glia membranes. Pugh and Jahr (2011) did not find any evidence for functional NMDAR on BC varicosities.

A complementary mechanism was recently suggested (Duguid et al., 2007), involving PC autocrine activation of postsynaptic mGluR1 leading to an increased endocannabinoids release and consequently short-term depression of inhibitory inputs onto PC.

c. Long-term plasticity

A wealth of studies have explored in detail long term plasticity at the GC-PC. Postsynaptic and presynaptic LTP and LTD have been demonstrated at the PF-PC and PF-MLI synapses regulating synaptic efficacy at individual contacts (for review: Ito, 2001; Jörntell and Hansel, 2006; Gao et al., 2012b). These mechanisms influence the balance between excitation and inhibition in PCs. However, my work started after the establishment of these plasticities during the life of the animal. Because I mostly studied the role of the short-term dynamics on the PC discharge, I decided to focus my introduction on these specific mechanisms and considered that a detailed description of long term plasticity might be beyond the scope of this manuscript.

As the sole output of the cerebellar cortex, PC has a key role in cerebellar function. Its discharge integrates and encodes all the information that is transmitted to the downstream layer, the DCN neurons.

A key step for the understanding of cerebellar information processing is to describe how context-specific or modality-specific MF inputs are processed in the GC to PC pathway, i.e. how a group of activated GCs following a given MF input will impact PC discharge; and how short-term plasticity or the level of activity of the local network (background activity, activity from neighboring PCs) will be translated into PC spike output.

1. *Purkinje cell discharge*

PC have a unique electrophysiological signature since they can generate two different types of action potentials. Simple spikes occur either spontaneously or in response to the activation of the MF-GC-PC pathway. Complex spikes are triggered by inferior olivary neurons via the CFpathway.

A. *Spontaneous activity of Purkinje cells and simple spikes*

Interestingly, PCs discharge spontaneously in the absence of synaptic inputs with a firing frequency typically ranging from 20 to 60Hz which can reach a maximum of 250Hz. It was observed in different preparations including cultured PCs (Gruol and

Franklin, 1987), cerebellar acute slices (Hounsgaard, 1979; Llinás and Sugimori, 1980; Häusser and Clark, 1997) and even in isolated somas of PCs (Nam and Hockberger, 1997; Raman and Bean, 1997).

This pacemaker activity is not specific to PCs though – it is also found in cerebellar interneurons (Häusser and Clark, 1997), DCN neurons (Jahnsen, 1986; Aizenman and Linden, 1999) and among other neurons of the central nervous system, notably in interneurons of the hippocampus (Alger and Nicoll, 1980), in thalamic neurons (McCormick and Pape, 1990) and in the suprachiasmatic nucleus (Pennartz et al., 1997).

PCs pacemaker activity is driven by a combination of low threshold voltage dependent conductances notably tetrodotoxin (TTX) sensitive Na-current and a large tetraethylammonium sensitive K-current (Nam and Hockberger, 1997; Raman and Bean, 1999). Involvement of hyperpolarization-activated *current* Ih maintain the membrane potential within a range where the inward Na-current responsible for the generation of spontaneous firing can be activated (Williams et al., 2002). Inhibition of Ih current leads to quiescent periods. Several channels modulate the spontaneous discharge of PCs. Apamin sensitive small conductance K^+ channels (SK), located both in PC dendrites and at the soma (Womack and Khodakhah, 2003), control the pacemaker firing frequency (Edgerton and Reinhart, 2003). Low voltage activated T-type calcium channels, mainly expressed in dendrites (Mouginot et al., 1997; Watanabe et al., 1998) and spines (Isope and Murphy, 2005) also seem to be involved in frequency regulation since their blockade leads to a 30 % reduction in the PC spontaneous firing rate (Raman and Bean, 1999). By their opening upon small depolarizations (between – 40 mV and – 60 mV), T-type calcium channels may contribute to increase the membrane depolarization up to the level required for Na channel opening and subsequent spike generation. Large conductance potassium channels (BK) along with SK channels control the temporal precision of PC discharge (Edgerton and Reinhart, 2003). Both are activated by the calcium influx entering through P/Q type voltage-gated Ca^{2+} channels, highly expressed in PCs (‘P’ channel

refers to “Purkinje”). Besides, mutations of P/Q channels cause cerebellar dysfunctions.

Recent evidence indicates that simple spike firing rate may vary depending on the location in the cerebellar cortex. Indeed, a higher PC firing frequency was recorded in zebrin negative bands as compared to zebrin positive bands (Xiao et al., 2014; Zhou et al., 2014). In addition, PC intrinsic membrane properties were found to differ in lobules receiving different sensorimotor information, such as lobule III to V of the spinocerebellum as compared to lobule X of the vestibulocerebellum (Witter and De Zeeuw, 2015).

This can contribute to differences in signal processing (Kim et al., 2012). In awake animals, firing frequency also depends on the behavioral task performed.

B. *Simple spike activity is correlated with motor control*

A short, transient and synchronized optogenetic suppression of spontaneous spiking in PCs of the paravermis is sufficient to trigger several orofacial movements in mice (Heiney et al., 2014) suggesting a causal link between PC discharge and movement. Indeed, timing and kinematic properties of the movements can be modulated depending on how much and how long PC discharge is suppressed. This occurs through a graded disinhibition of DCN neurons.

In addition, encoding of movement parameters in the simple spike discharge has also been observed across a wide range of motor behaviors. For example, simple spike activity was correlated with movement direction during passive forelimb movement in anesthetized cats (Valle et al., 2000) and rats (Giaquinta et al., 2000). Similarly, during active arm movement, limb position, direction and velocity were signaled in the simple spike activity of awake monkeys (Roitman, 2005). A recent study in awake

mice demonstrated a linear encoding of whisker position by PC discharge (Chen et al., 2016).

Some authors have proposed that PC simple spikes encode the motor command including the muscles strength required to perform voluntary movements (Holdefer and Miller, 2009). Interestingly, simple spike discharge in individual PCs encodes prediction and feedback error performance (by changing the sign of its modulation) (Popa et al., 2012), suggesting that the cerebellum might store internal models of the motor apparatus as proposed by theoretical models (Wolpert et al., 1998).

C. *Bistability and trimodal patterns*

PCs have bistable membrane properties, allowing them to alternate between a hyperpolarized stable membrane potential (down-state) and a more depolarized state (up state). With regard to PC spike output, bistability is expressed as intermittent pauses followed by tonic simple spike firing.

Experimental and modeling studies have given insights into the underlying ionic mechanisms for bistability. Blocking TTX-sensitive sodium current reduces bistability (Williams et al., 2002) by disrupting the plateau of depolarization of the up state (Llinás and Sugimori, 1980). Calcium activated potassium channels (KCa) were found to be involved in the transitions from the up state to down state (Williams et al., 2002; McKay et al., 2007; Rokni and Yarom, 2009). Calcium current required to activate these KCa channels might be provided by low voltage activated channels, since bistability is not suppressed when blocking high voltage-activated calcium channels using Cd^{2+}. Cav3.2 low voltage activated T-type calcium channel is a candidate, since recent evidence demonstrated its physical proximity to intermediate conductance KCa (KCa3.1), in PC dendrites (Engbers et al., 2012). Although not

clear, hyperpolarization-activated current Ih does not seem involved either in the generation or in the transition between up and down states, but rather has a regulatory role (Williams et al., 2002; Oldfield et al., 2010).

In vitro, the switch from up and down states - *"toggling"*- were reported to occur either spontaneously , following current pulse injections or by synaptic inputs (Jacobson et al., 2008). CF (McKay et al., 2007), PF and MLI (Rokni et al., 2009; Oldfield et al., 2010) can induce these transitions and Bergmann glia controls the duration of up states by dynamically regulating extracellular K^+ via Ca^{2+}-dependent mechanisms (Wang et al., 2012).

Sensory-evoked CF inputs, using air puff stimulation of the vibrissae in anesthetized animals, induce toggling (Loewenstein et al., 2005; Kitamura and Hausser, 2011) and the authors suggested a role in short-term processing and storage of sensorimotor information (Loewenstein et al., 2005). However, whether bistability occurs in physiological conditions is still a matter of debate in the cerebellar community. Recordings were obtained from different animal species (mice, cats, rats, ferrets, guinea pigs) and, depending on the preparation (awake, anesthetized), the cerebellar location, and the type of anesthesia (ketamine/xylazine, isoflurane), results are conflicting. This controversy was further pointed out by the work of Schonewille and colleagues (Schonewille et al., 2006), showing that the long pauses in PC simple spike activity recorded in animals under isoflurane anesthesia were suppressed when removing anesthesia and in the awake animal. Moreover, ketamine and isoflurane anesthetics block potassium and sodium channels (Zhou and Zhao, 2000; Schnoebel et al., 2005) raising the possibility of a direct effect on PC ion channels.
Only half of the recorded PCs in awake cats displayed tonic firing and pauses (Yartsev et al., 2009). Therefore bistability may not be observed in all PCs or PC may operate both modes. This is further supported by the serotonin-induced conversion of PC tonic firing into bistable mode (Williams et al., 2002). A cell-to-cell differential FFI cannot be excluded though, as it is based on extracellular recordings only, as for all

of the so-far available data in awake animals.

Another debated firing pattern - the trimodal pattern- has been recorded in PCs corresponding to a regular switch between tonic firing, repetitive calcium spikes, and an hyperpolarized quiescent state. Trimodal patterns occur when CF input is removed and absent when restored (Cerminara et al., 2004), or during postnatal maturation (P12-P18) of the PC dendritic tree (Womack and Khodakhah, 2002; McKay and Turner, 2005). Based on my personal observations and on the literature, I consider that it is most likely due to an unhealthy state of the cells, rather than a physiological signature; therefore I discarded them from my study.

D. *Complex spikes*

Complex spikes are composed of one sodium spike and subsequent smaller spikelets. They occur at low frequency, around 1 Hz, following CF activation. The strong depolarization induced by the CF input recruits AMPA receptors leading to the activation of voltage-dependent sodium channels, and T-types and P-types calcium channels (Cavelier et al., 2008) which generate a depolarization plateau in PC dendrites. Spikelets can potentially also be transmitted as action potential in the axon (Davie et al., 2008). The waveform of a complex spike is controlled through activity-dependent long-term depression mechanisms (Schmolesky et al., 2002) and its duration depends on PC firing frequency (Warnaar et al., 2015). Both are non-uniformly expressed through the cerebellar cortex (Zhou et al., 2014, 2015), which may explain the tendency for regional differences in complex spike waveforms *in vitro*, although not yet confirmed *in vivo*. Complex spikes are longer during upstate (Tal et al., 2008).

Because CF triggers a massive dendritic calcium signal involved in the induction of plasticity mechanisms at the PF-PC synapse, complex spikes are often considered as a teacher in learning or as a motor error signal (Marr, 1969; Albus, 1971; Jörntell and Hansel, 2006).

E. *Purkinje cell discharge regularity*

a. In vivo neuronal discharge irregularity

By irregularity I here refer to the degree to which spikes occur repeatedly at variable time intervals. PCs recorded *in vivo* display irregular spiking behaviors (Goossens et al., 2001) as opposed to very regular firing in the *in vitro* slice preparation (Häusser and Clark, 1997) suggesting that PC discharge irregularity is controlled by excitatory and inhibitory synaptic inputs (Llinás and Sugimori, 1980; Raman and Bean, 1999).

In vivo neuronal discharge irregularity has been extensively studied in cortical areas including the primary visual cortex (Rieke et al., 1999). The detailed comparison of neuronal discharge from fifteen different cortical areas (one thousand neurons were analyzed) reveal differences depending on the structure: neurons fire highly irregularly in the visual and prefrontal cortex but more regularly in higher order motor areas (Shinomoto et al., 2009).

The level of irregularity is typically assessed by the standard deviation of the distribution of inter-spike intervals (ISI) or their coefficient of variation (Feng and Brown, 1999). A perfect regularity, corresponding to a periodic series of action potentials, is reflected by a coefficient of variation of zero while at the extreme opposite, a Poisson process has a coefficient of variation of 1.

Spatial variation of PC regularity was found based on these two metrics; PCs localized into the Zebrin negative bands have more regular and higher rate of

discharge than those located in Zebrin positive bands (Xiao et al., 2014). However, due to the refractory period of action potentials, high frequency bursts of spikes are more regular than low frequency spike trains (Shin et al., 2007). To overcome this limitation, local metrics, less sensitive to the discharge frequency, have been developed including the two that I choose to use in my study, namely the coefficient of variation for a sequence of two ISIs (CV2) (Holt et al., 1996; Taube, 2010) and the local variation with refractory period (LVr) (Shinomoto et al., 2009).

Using the CV2 parameter, it has been demonstrated that PCs recorded in anesthetized or awake mice are not that irregular locally, but instead composed of regular spike patterns (of 2 to 21 ISIs) separated by long ISIs (Shin et al., 2007). More than half of the ISIs are part of regular patterns and the number of regular patterns expands during tactile stimulation in anesthetized rats, which is therefore likely to encode behaviorally relevant information as a rate coding strategy.

b. Irregular firing results from intense synaptic background activity in vivo

The difference in regularity between the *in vitro* and *in vivo* conditions arises from the reduced synaptic connectivity in acute slices and lower temperature used in most *in vitro* studies that lead to a decrease in background synaptic activity (Paré et al., 1998).

The intense barrage of excitatory and inhibitory inputs received by neurons in intact networks *in vivo* -often referred to in the literature as 'synaptic bombardment' – results in the opening of many synaptic receptors and voltage-dependent-gated channels. Consequently, membrane potential is depolarized and continuously fluctuates, time constants are shortened (Destexhe et al., 2003) and input resistance decreases (Paré et al., 1998) putting the cell in a "high conductance state" (Woody et al., 1978). The level of synaptic background modulates the gain of neuronal

responses (Chance et al., 2002). In addition, experimental and theoretical studies have demonstrated that these phenomena significantly affect synaptic integration by shunting distal synaptic inputs and decreasing the reliability of spike initiation, which would account for the irregular spike trains produced in spontaneously active neurons.

c. Alteration of Purkinje cell discharge in cerebellar pathologies

A reduced firing frequency of PC discharge is commonly reported in several mouse models for example of spinocerebellar ataxia type 2 (Hansen et al., 2013), type 3 (Shakkottai et al., 2011), type 27 (Shakkottai and Paulson, 2009) or human episodic ataxia type-2 that is caused by a mutation in the CACNA1A gene coding for P/Q type channels. *In vitro* recordings of PC firing from P/Q type channel KO mice, a model of ataxia, showed impaired pacemaking activity (Walter et al., 2006). Application of a positive modulator of SK channels, thought to augment the affinity of calcium for the channel (Pedarzani et al., 2001) recovered the regularity of PC firing *in vitro*. Moreover, by performing *in vivo* microperfusion of the SK modulator into the cerebellum of this ataxic mice, Walter and collaborators (Walter et al., 2006) reported improved cerebellar – dependent motor performance, providing evidence for a causal link between alteration of the temporal structure of PC discharge and cerebellar motor dysfunction.

Similarly, in another ataxic strain of mice - *tottering*- also carrying a mutation in P/Q-type voltage-gated calcium channels, application of regular electrical stimulation patterns mimicking a normal simple spike activity rescued motor impairment (Hoebeek et al., 2005) hence supporting the importance of regularity for motor control.

2. *Modulation of Purkinje cell discharge*

Importantly, because PCs are spontaneously active, their discharge allows a bidirectional encoding of information. In addition, weak inputs can potentially influence PC discharge, since their membrane potential is close to the threshold for sodium channels.

Both simple and complex spikes can be modulated by synaptic inputs and synaptic plasticity. This can be reflected as a modification of their timing, their occurrence, or, in the case of the complex spikes, by the modulation of their amplitude or the number of spikelets they contain. Modulation of complex spike activity itself is out of my scope. However, they were found to possibly regulate simple spike occurrence. Therefore, I will dedicate a short section to the question of simple spike-complex spike interactions.

A. *Complex spike – simple spike interaction*

Complex spikes modulate simple spike activity by inducing a pause (Granit and Phillips, 1956; Bloedel and Roberts, 1971; Ebner and Bloedel, 1981) via an afterhyperpolarization mediated by calcium-dependent BK and SK channels (McKay et al., 2007) or through activation of local MLI via glutamate spillover from the CF to PC synapse (Szapiro and Barbour, 2007). Differential levels of expression of the perisynaptic EAAT4 transporter, known to regulate glutamate spillover at this synapse, may explain regional differences between post complex spike pause duration (Xiao et al., 2014). Also, post complex spike pause and shape are regulated through the level of expression of potassium channels (Veys et al., 2013) and by dendritic spiking (Davie et al., 2008) respectively.

B. *Simple spike modulation by synaptic inputs*

Simple spike discharge is modulated by the intrinsic activity of PCs, but also by excitatory synaptic inputs from PFs and inhibitory inputs from MLI.

a. In vivo evidence

Wada and collaborators (Wada et al., 2007) could reversibly block/unblock GC neurotransmission in awake mice by expressing the tetanus toxin specifically into GCs that can be activated/deactivated by pharmacological agent. Stopping GC activity decreased PC simple spike frequency near zero (not complex spikes) in a reversible manner. Similarly, a blockade of synaptic inhibition by ionophoretic application of bicuculline - a $GABA_A$ receptor antagonist - to PC in the floculus increased their firing frequency during head rotation in awake rabbits (Miyashita and Nagao, 1984).

b. In vitro - Impact of excitatory inputs on PC discharge

Blocking inhibition pharmacologically in acute slices, increased the number of simple spikes in response to PF stimulation (Walter and Khodakhah, 2006). Both the number of additional spikes and the maximum simple spike frequency following the PF inputs linearly increased with stimulation intensity, which led the authors to propose a linear input-output transformation in PCs.

Steuber et al. (Steuber et al., 2007) performed a similar experiment (inhibition blocked with SR95531) and observed a silent period in PC discharge following the evoked bursts of simple spikes. The pause lasts several tens of milliseconds and its duration increases with the strength of PF EPSPs as they are measured by whole-

cell recordings right after the cell-attached mode. The pause could be explained by the experimental design in which a bundle of PFs was stimulated leading to a focal input on the PC dendritic tree. Such strong inputs could activate dendritic voltage-gated calcium channels leading to calcium dependant potassium channel activation and hyperpolarization of the membrane. Indeed, Walter and Khodakkah (2006) performed exactly the same experiments but stimulated GCs in the granular layer. Although the strength of excitatory GC inputs was still linearly encoded in the PC discharge, no pause was observed, supporting a role of afterhyperpolarization in the generated pause.

In this manuscript, I will refer to subthreshold stimulation for inputs having a low probability of triggering directly an action potential in the PC. Therefore, subthreshold PF inputs modulate PC simple spike activity (Mittmann and Häusser, 2007) either by accelerating the occurrence of the next action potential or adding one spike.

c. In vitro - Impact of feedforward inhibition on PC discharge

Most *in vitro* investigations have been performed by blocking inhibitory transmission. However, activation of PFs under physiological conditions can involve a feedforward inhibitory microcircuit (**Part III.2.B**) shortening PF EPSPs in PCs and thus generating a very precise temporal sequence of excitation and inhibition (Brunel et al., 2004; Mittmann et al., 2005). Whether and how it is converted into temporal patterns of PC simple spikes remains to be clearly elucidated.

It is very likely that different patterns of PF activity, thus of GCs, will modify the balance between excitation and inhibition (E/I ratio). However, there is currently no data available on the physiological range of the E/I inputs ratio received by PCs *in vivo*. Predictions from dynamic clamp studies (Mittmann and Häusser, 2007) suggest different outcomes of PC output discharge depending on the E/I ratio. Additional spikes triggered by EPSP (3 mV) are predicted to be followed by a pause when FFI is

added, in line with the strong influence of inhibitory inputs alone on PC discharge output (Midtgaard, 1992; Häusser and Clark, 1997), as confirmed by Walter and Khodakkah (Walter and Khodakhah, 2006) who reported a 50 to 300 ms pause in firing rate induced by FFI, without affecting the linear encoding of GC input strength in the PC output. In accordance, FFI can regulate the number of spikes triggered by subthreshold PF inputs, lowering it on average from 2.5 extra spikes (when blocking inhibition) to 1 (Mittmann et al., 2005). Interestingly, the number of action potential, their precise timing, the jitter in spike occurrence between trials and the pause duration following inputs reflect the strength of both excitatory and inhibitory inputs (Mittmann and Häusser, 2007). By limiting the temporal window for GCs/PF inputs, FFI also controls precisely the timing of the evoked spikes in the PC (Mittmann et al., 2005): for a fixed value of excitation its accuracy increases with the level of inhibition (Mittmann and Häusser, 2007). The restricted time window for EPSP summation limits the efficacy of imprecisely timed subsequent inputs. It further supports the fact that weak inputs that do not directly trigger action potential, could still modulate the PC discharge by either reducing the impact of forthcoming inputs or by preventing spontaneous activity of PCs (Mittmann and Häusser, 2007).

One would then hypothesize that FFI would select only the relevant inputs by shutting down the multiple asynchronous ones, which would be in agreement with a role for the cerebellum in precisely coordinating movements in the millisecond to seconds range. That would be a way to increase the signal to noise ratio.

d. Other potential regulatory inputs

FFI between MLIs themselves might possibly regulate PC output as well, but no studies are available so far. We should also keep in mind that Golgi cells also indirectly modulate PC simple spike discharge through their feedback inhibition of GCs.

C. *Simple spike modulation by synaptic plasticity*

PC discharge integrates the results of plasticity occurring in the cerebellar cortex and transmits it to their downstream targets. As they are spontaneously active, they are well suited to encode the strength of both excitatory and inhibitory synapses.

The relationship between synaptic strength and PC discharge has been studied by Mittmann and colleagues (2007). Their findings are crucial for my study; therefore, I will report details regarding the effect of LTD on excitatory inputs, on inhibitory inputs and the impact when they are combined together in the feedforward circuit.

Pairing PF EPSPs with CF inputs leads to LTD of about 25 % of the PF EPSPs reflected in PC spike output by a reduction of about 70 % of additional spikes, which, when considering the spontaneous activity of PCs can also be viewed as an increased latency of the following spike. Synaptic plasticity also alters the precision of the timing of evoked action potentials (63.8 % less time-locked). The number of additional spikes seems to be correlated to the level of plasticity (Mittmann and Häusser, 2007). Surprisingly, inhibitory synaptic inputs received by PCs are subject to the same level of LTD when CF is coactivated, resulting in the exact opposite modulation of PC discharge. This balanced plasticity might maintain the relative strength of excitatory and inhibitory synaptic inputs in the circuit, an important feature in controlling the pattern of spikes (Higley and Contreras, 2006) and reducing variations in computation in neural networks (Mariño et al., 2005).

Steuber et al. (Steuber et al., 2007) simulated learning by PF LTD in a PC computational model and compared several features of the PC discharge when presenting learned input patterns to novel ones. Pause duration is the most discriminative criterion, which was shorter in response to learned input patterns, independently of the FFI, spontaneous firing frequency or background noise. In addition, electrophysiological recordings of PCs in awake behaving mice displayed an increased duration of long inter-spike intervals when LTD is impaired (LTD-deficient), the range of the difference in pause duration with wild-type littermates

matches with model predictions and *in vitro* study (Steuber et al., 2007), and difference increases during optokinetic simulation suggesting a behavioral relevance.

Modeling predictions were also confirmed in cerebellar acute slices through dynamic clamp studies (Mittmann and Häusser, 2007) where a balanced LTD (20 %) of excitatory and inhibitory inputs shortens the duration of the subsequent pause for all simulated E/I ratio. Balanced LTD also reduces the number of additional/accelerated spikes by 10 %. Interestingly, predictions from dynamic clamp suggest a different effect of LTD on the net spike output depending on the balance between excitation and inhibition (Mittmann and Häusser, 2007). Net spike output is reduced by LTD for relatively high E/I ratio while it is increased for low E/I ratio. Synaptic plasticity does not modulate the net spike output for intermediate E/I ratio. Similarly, accuracy of the triggered additional/accelerated spikes was reduced by LTD in the case of purely excitatory inputs.

Altogether, it seems that the outcome of synaptic plasticity on the spike output of the cerebellar cortex depends on the excitatory and inhibitory activities at the GC to PC connection.

What is a pause in Purkinje cell discharge?

There is confusion in the literature regarding the definition of the pause in PC activity, notably there is no consensus about its minimum duration. In addition, because the PC is spontaneously active, no distinction can be made between an omitted action potential and a delayed spike which brings about even more ambiguities. Because each PC fires at a different firing frequency, the pause might be cell specific. This led authors to use the term “longer ISIs” rather than an absolute minimum duration. If we go further, we could also maybe define a local pause based on a short-term increase in ISI duration as compared to a few precedent ones. The diversity of mechanisms responsible for the generation of a pause in PC discharge adds another level of

complexity. Some authors consider the downstate as a pause (Schonewille et al., 2006; Yartsev et al., 2009), sometimes different from a quiescent state. A pause can also be the consequence of after hyperpolarization induced by a strong depolarization of the PC membrane in response to strong PF inputs, or following CF mediated complex spikes. FFI is also able to trigger a pause in PC discharge, depending on the EI ratio.

3. *Purkinje cell synchrony*

PC synchrony of both simple spikes and complex spikes increases during cerebellar-dependent movement or sensory stimulation in a time-locked manner which might therefore encode information to downstream DCN with a high temporal resolution. Complex spike synchrony occurs in the parasagittal plane forming microzonal bands of synchronized responses (Ozden et al., 2009), most likely resulting from the innervation of several PCs by the same CF. In addition, the strong electrical coupling of inferior olivary neurons mediated through their gap junctions (Blenkinsop and Lang, 2006) may synchronize neighboring CFs controlling the spatial extent of complex spike synchrony.

The study of (Bell and Grimm, 1969) was one of the first demonstrations of simple spike *synchrony in vivo*, where neighboring PCs tended to fire simultaneously in anesthetized cats. Since then, simple spike synchrony was observed in many preparations (mouse, rat, guinea pigs) and conditions (several types of anesthesia or behavior-related tasks). However, how the synchrony of simple spikes is spatially organized in the cerebellar cortex, meaning which PCs are synchronized together and which components of the PC discharge are synchronized remains to be clearly elucidated.

PC simple spike synchrony was reported to be widespread, organized in parasagittal zones throughout the floculus (De Zeeuw et al., 1997a, 1997b), vermis and paravermis (Wise et al., 2010). Interestingly, these zones correlate with zones of complex spike synchrony, and thus seem likely to involve the post complex spike pause, which can also be synchronized (Kitazawa and Wolpert, 2005), although their duration is very variable (from tens to more than a hundred fifty milliseconds; (Steuber et al., 2007).

In contrast, multielectrode recordings of on-beam and off-beam PCs in the paramedian lobe of behaving rats showed a transversally oriented synchronization of simple spikes, specifically restricted to on-beam PCs (Heck et al., 2007) suggesting parallel- fiber mediated excitation as a trigger for synchrony and not CFs.

PC simple spike synchrony was also reported to be more local. Paired recordings of PCs separated by less than 100 µm along the transverse axis in anesthetized rats show a strong synchronization in their simple spike activity, supporting an organization as patches (Shin and De Schutter, 2006) in line with other previous studies (Bell and Grimm, 1969; Ebner and Bloedel, 1981). The synchronization observed was caused by spikes associated with pauses independent from CF activity, likely due to local inhibition and possibly via PC recurrent collateral inhibition of neighboring PCs (de Solages et al., 2008), or through gap junction-mediated electrical coupling between MLI and PCs (Middleton et al., 2008).

Together, several mechanisms might act in combination to drive PC synchrony, or might be differently activated depending on the behavioral task.

Context

As described in the introduction, cerebellar PCs are the sole output neurons of the cerebellar cortex inhibiting DCN neurons, the output of the cerebellum. This anatomical organization suggests the structure of PC discharge is a key determinant for the motor output, which is altered in mice displaying problems with motor coordination. PCs are spontaneously active and their discharge is modulated *in vivo* by sensorimotor inputs. Consequently, integration of information processed in the cerebellar cortex seems to be reflected by the modulation of PC firing patterns. PCs receive inputs from GCs, one of the two afferent pathways to the cerebellar cortex. GCs also provide a FFI on PCs through activation of MLIs. Since PCs are spontaneously active, the GC input pathway can influence PC discharge either by increasing firing rate through a direct connection or by delaying the discharge through MLIs activation.

Aims of my PhD project:

With this as a frame of reference, the aim of my PhD project is to study the modulation of PC discharge by bursts of a patch of connected GCs in a given microzone.

Specific questions of my PhD project

- **Are subthreshold synaptic granule cell inputs able to modify Purkinje cell discharge thereby directly influencing cerebellar cortical output?**
- **How different patterns of granule cell inputs modulate Purkinje cell spiking?**
- **What is the influence of the feedforward inhibition mediated by molecular layer interneurons?**
- **How the excitation-inhibition balance and short-term plasticity at granule cell - Purkinje cell pathways influence PC spike output?**

MATERIALS AND METHODS

1. *Animal experimentation*

A. *Ethics in animal experimentation*

All procedures were in accordance with national (council directive 87/848, October 1987) and European community guidelines (2010/63/EU). Animal experiments were approved in advance by the local French Ethics Committee of Strasbourg (C.R.E.M.E.A.S.; CEEA35; agreement number/reference protocol: A67-2018-38).

B. *Mice*

Mice were bred and housed in our animal facility (Chronobiotron, UMS 3415, CNRS, Strasbourg) with a 12 hours light/dark cycle and free access to standard laboratory rodent food and water. Ovarian estrogens are known to impact on cerebellar glutamatergic neurotransmission (for a detailed review: see Hedges et al., 2012), therefore only males were used.

Three to eight weeks old heterozygous CD1 L7-ChR2(H134R)-eYFP (YFP for yellow fluorescent protein, Chaumont et al., 2013) and C57/bl6 or CD1 Thy1-ChR2-eYFP mice of the founder line 18 (Wang et al., 2007) were used for my PhD project. For the collaboration with Dr Puccio (IGBMC): three and eight months old Adck3 KO mice were used. Wild-type littermates served as controls.

2. *Genotyping*

Mice were genotyped by PCR of genomic DNA from tail biopsies.

A. *DNA extraction*

- L7-ChR2-eYFP mouse line: tails were digested at 98°C in (per tail) 100 µL of 25 mM hydroxyde sodium during 1 hour. 40 mM Tris-HCl was then added to stop the digestion and samples were centrifuged during 10 minutes at room temperature.

- Thy1-ChR2-eYFP mouse line: each tail was digested in 10 µL of extraction buffer, 2 µL of enzyme completed with 88 µL water from Sigma at 75°C for 10 minutes. Digestion was stopped by incubating the samples at 95°C for 5 minutes and centrifuged for 1 minute.

B. *Amplification of the sequence of interest*

- L7-ChR2-eYFP mouse line: PCR mix for one tail (23 µL) was composed of 2.5 µL of 10X Buffer, 0.5 µL of 100 mM dNTP, 0.5 µL of forward and reverse primers, 1.5 µL of 50 mM MgCl2, 0.2µL Taq DNA polymerase (GoTaqR Flexi DNA Polymeras Kit, Promega) and 3 µL of DNA sample, completed with 17.3 µL of water from Sigma. The PCR protocol runs this sequence of temperatures: 5 minutes at 94°C, 30 times the following: 30 seconds at 94°C, 30 seconds at 60°C, seconds at 72°C, and lastly 10 minutes at 72°C.

- Thy1-ChR2-eYFP mouse line: PCR mix for one tail (25 µL) contained: 12.5 µL of Green PCR Master Mix (KAPA mouse genotyping kit; KAPA Biosystem), 0.5 µL of both primers at 10 µM, 1 µL of DNA extract, completed with 10.5 µL of water from Sigma. The same PCR protocol as above was used.

C. *Primers and expected product size for PCR*

- L7-ChR2-eYFP mouse: Primer F: 5'-GAAATCAGTGCGTTCGAACGCTAGA-3'. Primer R: 5'-TGATGGACATGTTCAGGGATC-3'. Expected size: 500bp.
- Thy1-ChR2-eYFP mouse: Primer F: 5'-AAAAATGTGTTCGCGCCATA-3'.
Primer R: 5'-GCTTCTTCAACCTGCTGACC -3'. Expected size: 800bp.

Electrophoresis gel and migration 1% agarose (InVitrogen) electrophoresis gels were prepared in 1X TAE buffer, and melted in a microwave. When cooled down 0.01 % of thermosensitive GelRed DNA Stain was added (InVitrogen S33102). Loading buffer and 3 to 6 µL of PCR samples were loaded in each well; a 2-Log DNA ladder

(1µL / well) from New England BioLab was used. 75 V was applied through the gel during 15 to 30 minutes, before being revealed under ultraviolet lights.

3. *Electrophysiology*

I will purposely detail some of the precautions taken through the experimental procedures to preserve at best cerebellar network integrity in submerged acute slices and perform experiments in conditions as physiological as possible.

A. *Acute cerebellar slices preparation*

Mice were decapitated under isoflurane anesthesia (Belamont, France). Cerebellum was dissected out and quickly placed in a 4 °C artificial cerebrospinal fluid bubbled with carbogen (95% O_2, 5% CO_2). artificial cerebrospinal fluid was composed of -in mM- : 120 NaCl, 3 KCl, 26 $NaHCO_3$, 1.25 NaH_2PO_4, 2 $CaCl_2$, 1 $MgCl_2$, 20 glucose, 0.00005 minocyclin, where minocyclin was used to limit microglial activation.

Sagittal or transverse 300 µm-thick slices were then prepared (Microm HM 650V, Microm) in ice-cold potassium-based medium containing in mM: K-gluconate 130; KCl 14.6; EGTA 2; Hepes 20; glucose 25; minocyclin 0.00005, and 1 kynurenic acid. This composition is similar to intracellular medium to prevent cell depolarization and calcium influx into cut neurons and dendrites. As an antagonist of AMPA, NMDA and kainite receptors, the kynurenic acid was used to minimize excitotoxicity. To allow metabolic reactivation of the cells, slices were soaked in a sucrose- based medium at 34 °C, containing in mM: sucrose 230; KCl 2.5; $NaHCO_3$ 26; NaH_2PO_4 1.25; glucose 25; $CaCl_2$ 0.8; $MgCl_2$ 8; minocyclin 0.00005; and D-APV 0.05 before being transferred and maintained in artificial cerebrospinal fluid medium at least one hour prior to electrophysiological recordings.

B. *Electrophysiological recordings*

Slices were transferred to a submerged recording chamber under the microscope and perfused with oxygenated ACSF (**see slice preparation**). To ensure oxygen and glucose availability, the volume of the submerged chamber was set as low as possible and perfusion flow was optimally set to its highest rate yet avoiding slice mechanical instability which is critical for the long-lasting recordings that were performed. Flow rate was kept fixed throughout the experiment since it may influence spontaneous neuronal activity, as observed in hippocampal interneurons (Hajos and Mody, 2009). All recordings were located in the anterior part of the vermis (lobule III to VI) and performed at physiological temperature (32 ± 0.5°C). Recorded PCs were visually identified under infrared light.

- **Extracellular recordings of Purkinje cells**

PC spiking discharge was monitored with the noninvasive extracellular recording technique using 15 – 30 MΩ pipettes filled with 0.5 M NaCl. Extracellular recording pipettes were made from borosilicate glass electrodes (Harvard Apparatus) pulled on a horizontal puller (P-97 Sutter Instruments, USA). For the experiments in which the modulation of PC discharge by GC input was investigated, recorded PCs were located 50-75 µm beneath brain slice surface to ensure that FFI is best preserved.

- **Whole-cell recordings of Purkinje cells**

Whole-cell voltage clamp recordings of PCs were performed using 3–4 MΩ pipettes made from borosilicate glass electrodes (Harvard Apparatus) that were pulled on a vertical puller (Narishige, Japan) in two steps. Tips were coated with dental wax to limit pipette capacitance.

Currents were recorded at - 60 mV using the following pipette internal solution (in mM): 135 KMeSO4, 6 NaCl, 10 HEPES, 4 MgATP, and 0.4 Na2GTP, 1 MgCl2 with pH adjusted to 7.3 with KOH (osmolarity to 300 mOsm).

Experiments in which both EPSCs and IPSCs were recorded were performed using the following pipette internal solution (in mM): 135 $CsMeSO_4$, 6 NaCl, 10 HEPES, 4 MgATP, 1 EGTA, 0.4 Na_2GTP, 1 $MgCl_2$, $6H_2O$ and 5 Qx-314. pH was adjusted to 7.3

with CsOH and osmolarity was set to 290 mOsm. Qx-314 was used to block voltage dependent sodium channels.
In E/I ratios experiments (**Results Part III**), PCs were voltage-clamped at - 60 mV and then 0 mV to measure EPSCs and IPSCs, respectively.

Series resistance was monitored and compensated (80% typically) in all experiments. Voltages were not corrected for the liquid junction potential, which was calculated to be 9 mV; therefore the real membrane potential was 9 mV more hyperpolarized than reported. We accepted recordings for which the inward current at – 60 mV did not exceed 1 nA.

All the data were recorded using an Axopatch 200A or a multiclamp 700B (Molecular Devices, USA) and acquired using WinWCP 4.5.4 freeware (John Dempster, University of Strathclyde, UK). Recordings were filtered at 2 kHz and sampled at 50 kHz.

C. *Optical stimulation used to reproduce in vivo Purkinje cell discharge irregularity in acute slices*

- **L7-ChR2-eYFP**

This strain of mice specifically expresses ChR2 in PCs (Chaumont et al., 2013). PCs were photo-stimulated either using wide field 470-nm light emitting diode (LED)-based illumination (collimated LED M470L2-C1 powered by a T-cube LEDD1B driver from Thorlabs) through the objective (40 ×) of the microscope (BX61WI Olympus).

Alternatively, ultrafast laser scan (Fluoview, FV300, Olympus) spanning the whole PC dendritic tree was performed using a 473-nm diode-pumped solid state (DPSS) laser (CrystaLaser). This configuration ensures that ChR2 current was elicited randomly all over the dendritic tree, mimicking a barrage of excitatory synaptic inputs (**Results Part I**). Speed of the laser scan was improved by using a spatial resolution

of 256 x 256 pixels and by collecting only one pixel out of four. Laser power was set to values below 1 mW/cm^2 to keep ChR2 conductance subthreshold.

- **Thy1-ChR2-eYFP**

This strain of mice expresses ChR2 in MFs (**see Results Part I**). MFs were photo-stimulated using 470-nm LED-based illumination (collimated LED M470L2-C1 powered by a T-cube LEDD1B driver from Thorlabs) through the objective (40 ×) of the microscope (BX61WI Olympus). Waveforms used to drive illumination were generated using custom macros written in Igor Pro v6.32A (Wavemetrics, Oregon) and contained high frequency bursts mimicking MF input patterns.

Illumination intensities were calibrated to result in an increased irregularity of PC discharge (see data analysis section of the material and methods).

D. *Electrical stimulation*

GC firing patterns were reproduced in acute cerebellar slices using extracellular electrical stimulation of GC somas with a glass pipette filled with HEPES-buffered saline connected to an electrical stimulator (ISO-STIM 01D, NPI Electronic, Germany). HEPES-buffered saline contained in mM: NaCl 120; KCl 3; HEPES 10; NaH_2PO_4, H2O 1.25; $CaCl_2$ 2; $MgCl_2$ 1; Glucose 10. The stimulation of GCs somas and not PFs was chosen to mimic the activation of a “patch” of GCs as *in vivo*.

Stimulated GCs were located at a lateral distance of 100-300 µm from the recorded PC to avoid direct stimulation of local interneurons and CFs and to prevent from antidromic activation of the PC.

For PC discharge modulation experiments, stimulation intensity (70 µA - 1 mA, 20 µs) was adjusted to alter moderately the probability of discharge of the PC ($P < 0.8$) following a single stimulus, which we defined as a subthreshold stimulation. Subthreshold level of the stimulation was systematically checked offline (see data

analysis). Bursts of 1, 3 and 7 stimuli at 200 Hz were repetitively performed every 30 seconds.

For PPR experiments, stimulation intensity was calibrated to evoke an initial EPSC of ~ 100 pA and a seven-step protocol in which sequences of one to seven stimuli were applied was performed.

E. *Pharmacology*

In order to take advantage of the fingerprint of cerebellar learning that occurred through the animal life and not interact with it when studying GC to PC connection, we blocked NMDA, adenosine, CB_1, $GABA_B$ and $mGluR_1$ receptors by adding the following antagonists respectively (in mM): 0.05 D-AP_5, 0.0005 DPCPX (8-cyclopentyl-1,3-dipropylxanthine), 0.001 AM251 (*N*-(Piperidin-1-yl)-5-(4-iodophenyl)-1-(2,4-dichlorophenyl)-4-methyl-1*H*-pyrazole-3-carboxamide), 0.001 CGP52432 (3-[[(3,4-dichlorophenyl)-methyl]amino]propyl] (diethoxymethyl)phosphinic acid) and 0.002 JNJ16259685 (3,4-dihydro-2*H*-pyrano[2,3]β-quinolin-7-yl)(*cis*-4-methoxycyclohexyl) methanone).

In subsets of experiments:

- GCs activity was increased by applying 100 µM of furosemide, a GC-specific α6-subunit-containing $GABA_A$ receptor blocker.
- existence of direct photocurrent in PCs was checked by blocking neurotransmission with 100 µM of TTX.
- inhibitory transmission was blocked using the $GABA_A$ receptor antagonist picrotoxin at 100 µM.

Except for picrotoxin (Sigma, USA), all drugs were supplied by Tocris (UK).

4. *Data analysis*

➢ Data extraction

Spikes were detected using open source software OpenElectrophy (http://neuralensemble.org/OpenElectrophy/; Garcia and Fourcaud-Trocmé, 2009). Appropriate absolute threshold was set for spike detection and verified manually through careful inspection of all spike trains.

Because spikes from more than one PC could be recorded at the same site location, the waveform of every single spike was extracted and a principal component analysis was performed on them. Cluster(s) of spikes generated by different cell(s) were obtained, allowing us to focus our analysis on one cell. The train of spikes was determined by the time of occurrence of each spike recorded. Data were stored in SQL databases.

Spike trains were analyzed using Python software written in-house (SynaptiQs developed by Antoine Valera) and custom based routines that I designed for each type of analysis.

➢ Analysis of Purkinje cell discharge irregularity

PC discharge irregularity was assessed using the CV2 (Holt et al., 1996) which is calculated as follows: CV2 = 2|ISIn+1-ISIn|/(ISIn+1+ISIn) where ISI_n is the ISI containing the stimulation and ISI_{n+1} is the ISI following the ISI_n. A low CV2 value reflects short-term regularity of consecutive ISIs.

As PCs are spontaneously active with displaying a wide range of firing frequency, irregularity was also determined using the frequency-independent local variation of ISIs with refractory period (LvR; Shinomoto et al., 2009) a more discriminative parameter (Kumbhare et al., 2015).

- **Control for subthreshold stimulation**

Peri-stimulus time histogram (PSTH) of PC responses to a single stimulation of GCs was systematically computed to check for the subthreshold level of the stimulation. 1ms bin width PSTH were constructed by aligning consecutive repeated trials ($n > 50$) on the stimulus onset and calculating the spike probability in each bin. Stimulation was considered subthreshold if no single peak response of high spike occurrence probability (> 0.8) was observed in the first bins following the stimulation.

- **Analysis of Purkinje cell discharge modulation**

The net effect and time-course of PC discharge modulation were respectively extracted from the mean and the cumulative sum of the number of spikes after GCs stimulation normalized to the baseline firing rate. Trapezoidal method for integration was chosen to avoid specific sample parity requirements of other integration techniques. Spontaneous firing was calculated as the mean ISI on the 500 ms baseline of the PC discharge before GC stimulation.

- **Excitation-inhibition balance and short-term dynamics analyses**

All measurements were made after averaging at least 20 traces. E/I was calculated as the ratio of EPSCs and IPSCs amplitude (or charge) in response to a single stimulation of GCs. Bi-exponential fits to average EPSCs and IPSCs were performed to measure mean synaptic charge transfer. EPSC–IPSC delay was determined between the stimulation and 10% of EPSC/IPSC amplitude.

For PPR analysis, amplitudes of evoked EPSC and IPSC resulting from the n^{th} stimulus were defined as E_n and I_n. PPR was calculated as follows:

PPR $E_{n+1} = \frac{mean\ En+1}{mean\ E1}$;

PPR $I_{n+1} = \frac{mean\ In+1}{mean\ I1}$

Because high-frequency stimulation was used, residual amplitude of the preceding current ($EPSC_{n-1}$ or $IPSC_{n-1}$) affected E_n or I_n. Therefore, decays of average $EPSC_{n-1}$ (and $IPSC_{n-1}$) responses were fitted with a mono-exponential function and E_n (or I_n) was determined after correction for the residual current of the preceding current.

- **Exploratory analysis - Principal Component Analysis (PCA) and Hierarchical Cluster Analysis (HCA)**

Both were performed using FactoMinR plug-in in R i386 3.2.2 software. The 12 variables injected into PCA analysis were obtained from the time course of PCs discharge modulation (**Results PartIV** and **Figure R.13.A**) and were the following: the number of additional spikes in response to 3 and 7 stimulations (Add3, Add7), numbers of omitted spikes (Om3, Om7), durations of acceleration (AddDur3, AddDur7), durations of delay (OmDur3, OmDur7), net effect (Net3, Net7), EPSC and IPSC. Variables were centered on their means and reduced. The E/I ratio was added as a supplementary variable. Extracted principal with higher variance are considered more important. Principal components with lower variances were discarded and the size of the dataset (dimensionality) reduced. The minimum number of principal components required to significantly explain the structure (and variance) was based on the significance 95% quantil value according to the following table.

Hierarchical classification was performed on the selected principal components of PCA analysis (Husson et al., 2009).

- **Statistical tests**

Statistical analysis was carried out using Sigmaplot software (version 12.0, Systat Software, Inc.). All data are presented as mean ± standard deviation (SD) in the text and standard error of mean (SEM) on plots. Performed statistical tests are specified in the text. A value of $P \leq 0.05$ was considered significant.

- **Other softwares**

Some data were plotted and fitted using Igor v6.12A (WaveMetrics, USA). Figures and illustrations were edited in Adobe Illustrator CS5 (Adobe systems Inc, USA).

5. *Simulation (next)*

Cerebellum circuit

Neuron model

$$C_m \frac{dV_m}{dt} = g_{leak}(V_m - E_{leak}) + I_{syn}^{exc}(t) + I_{syn}^{inh}(t) + I_{ext}(t) \tag{1}$$

where C_m is the membrane capacitance, g_{leak} is the leak conductance, E_{leak} is the resting potential of the neuron. I_{syn}^{exc} represents the total excitatory inputs arriving from the Granule cells and I_{syn}^{inh} represents the total inhibitory inputs arriving from the inhibitory interneurons.

In the absence of any specific stimulus Purkinje cells (PC) spike at about $\approx$30 Hz in a quasi-periodic manner ($CV_{isi} \approx 0.2$). To mimic this ongoing activity in our simple point neuron model of the PC we injected noisy excitatory current ($I_{ext}(t)$) corresponding to a spike train drawn from a sinusoidally modulated Γ-process (frequency =37 Hz; order = 4). The magnitude of the sinusoidal modulation was 10% of the average input rate which was set to 2000 spikes/sec to obtain 30 spikes/sec as the output firing rate in the model neuron. For each trial we used a different realization of the sinusoidally modulated Γ-process to generate the background activity in the PC.

Synapse model

Synapses were modelled as a conductance transients:

$$I_{syn}^{a}(t) = S_a(t)(V_m(t) - E_a^{rev}) \tag{2}$$

where $S_a(t)$ ($a \in \{\text{exc., inh.}\}$) is the synaptic transient, V_m is the membrane potential and, E_a^{rev} is the reversal potential of the synapse. See Table 1 for the parameters.

Each presynaptic spike induced an alpha function shaped conductance transient in the postsynaptic Purkinje neuron:

$$S_a(t) = J_a(t) \times \frac{t}{\tau_a} exp(-\frac{t}{\tau_a}) \tag{3}$$

where τ_a is the synaptic time constant and $J_a(t)$ is the amplitude of the synapse. When synapses are static $J_a(t)$ is constant and when synapses change according to the history of the previous presynaptic spikes, the temporal evolution of $J_a(t)$ is given by the eq. 8.

To model the short-term dynamics of the PSP amplitude we used a deterministic model proposed by Tsodyks et al. (1997).

$$\frac{dx_a}{dt} = \frac{z_a}{\tau_{\text{rec}}} - u_a x_a \delta(t - t^{\text{spike}}) \tag{4}$$

$$\frac{dy_a}{dt} = -\frac{y_a}{\tau_I} - u_a x_a \delta(t - t^{\text{spike}}) \tag{5}$$

$$\frac{dz_a}{dt} = \frac{y_a}{\tau_I} - \frac{z_a}{\tau_{\text{rec}}} \tag{6}$$

$$\frac{du_a}{dt} = \frac{u_a}{\tau_{facil}} - U_a(1 - u_a)\delta(t - t^{\text{spike}}) \tag{7}$$

where x_a, y_a, z_a ($a \in \{\text{exc., inh.}\}$) are the three state variables that describe the state dependent use of the synaptic resources in the recovered (x_a), active (y_a), and inactive (z_a) states, respectively. t_{spike} is the timing of the previous spike. τ_I is the decay time constant of the postsynaptic current, τ_{rec} is the time it takes the synaptic resources to recover from their inactive state. The variable $u_a(t)$ keeps track of the use of the synaptic resources at a synapse. To model synaptic facilitation the variable u_a is instantaneously increased by a small amount U_a at the time of spike and then returns to the baseline value with a time constant τ_{facil} (eq. 7).

The effective synaptic weight was given by

$$J_a(t) = A_a \times y_a(t) \tag{8}$$

To systematically change the nature of the synapses from facilitatory to depressing, we changed the variable U_a while keeping all other variable unchanged. Because we kept all the time constants unchanged in the model, going from facilitation to depression did not affect the frequency dependence of the synapses and we observed on the effect of the change in the short-term dynamics. The parameter A_a was changed to increase the amplitude of the postsynaptic potential independent of the short-term dynamics. The values of these various parameters are provided in the Table 1 and corresponding facilitation and depression of synaptic strength is shown in the Fig. 1

Patterned stimulation

The activity of the granule cells was modeled as a train of 3 or 7 spikes (inter-spike-interval = 5 ms). The feedforward inhibition created by the inhibitory interneurons was also modelled as a train of 3 or 7 spikes (inter-spike-interval = 5 ms). Both spike trains were identical in each trial. The inhibitory spikes arrived at the PC 1.5 ms after the arrival of the excitatory spikes. The excitatory and inhibitory synapses exhibited short-term dynamics.

Neuron Parameters	
Membrane Capacitance (C_m)	250 pF
Membrane time constance (τ_m)	20.0 ms
Resting membrane potential (V_{rest})	-70 mV
Refractory time (τ_{ref})	2 ms
Spike threshold (V_{th})	-55.0 mV
Excitatory Synapse Properties	
Excitatory reversal potential	0 mV
Excitatory time constant	1.0 ms
Static unitary exc. postsynaptic potential	0.5 – 4.0 mV @-70 mV
Synaptic delay (Δ_{exc})	1.0 ms
Short-term dynamics of excitatory synapses	
Synaptic decay time constant (τ_{psc}^{exc})	1.5 ms
Recovery time constant (τ_{rec}^{exc})	30.0 ms
Facilitation time constant (τ_{fac}^{exc})	500.0 ms
Fraction of opened Ca+ channels (U^{exc})	0.02 – 0.5
Synaptic amplitude scaling (A^{exc})	1.5 – 337.5
	(EPSP range: 0.5–4.0 mV)
Inhibitory Synapse Properties	
Inhibitory reversal potential	-80.0 mV
Inhibitory time constant	5.0 ms
Static unitary inh. postsynaptic potential	0.3 – 1.4 mV @-70 mV
Synaptic delay (Δ_{inh})	2.5 ms
Short-term dynamics of inhibitory synapses	
Synaptic decay time constant (τ_{psc}^{inh})	1.5 ms
Recovery time constant (τ_{rec}^{inh})	100.0 ms
Facilitation time constant (τ_{facil}^{inh}	800.0 ms
Fraction of opened Ca+ channels (U^{inh})	0.03 – 0.6
Synaptic amplitude scaling (A^{inh})	-1.667 – -150.0
	(IPSP range: -0.3 -1.4 mV)

RESULTS

PART I: STRATEGIES TO MIMIC IN VIVO CONDITIONS IN ACUTE CEREBELLAR SLICES

The reduced synaptic connectivity in acute slices leads to a decrease in synaptic background bombardment (Paré et al., 1998). As a consequence, the effect of synaptic inputs might be overestimated and the reliability of the threshold for spike initiation falsely increased, which is, in the PC, reflected as a more regular spontaneous firing (Häusser and Clark, 1997) as compared to *in vivo* (Goossens et al., 2001).

To mimic *in vivo* synaptic bombardment in PCs, we first took advantage of the L7-ChR2(H134R)-eYFP transgenic mouse line developed in our laboratory, in which the light activated ion channel Channelrhodopsin 2 (ChR2) is specifically expressed in PCs and all along their dendritic tree (**Figures R1.A** and **R1.B**) (Chaumont et al., 2013).

We first checked that ChR2-mediated current could mimic synaptic inputs in L7-ChR2(H134R)-eYFP mice. Sagittal cutting orientation was chosen to preserve the parasagittally oriented PC dendritic tree. PCs were recorded in whole-cell voltage clamp configuration at – 60 mV and brief pulses of light (one millisecond) were delivered onto the slice using wide-field light-emitting diode (LED) illumination (470 nm) (**Figure R1.C**). Cationic ChR2-mediated photocurrent could be recorded (**Figure R1.C**) whose kinetics mimic compound EPSCs evoked by extracellular stimulation in the GC layer (Isope and Barbour, 2002). By performing ultrafast laser scan illumination (473 nm) across the whole dendritic tree, we could systematically mimic a barrage of excitatory synaptic inputs, as shown in whole-cell voltage clamp recordings (**Figure R1.D**). Using extracellular recordings of PC discharge, we checked that laser power was calibrated to keep ChR2 conductance subthreshold and avoid depolarization block. Using extracellular recordings of PCs (**Figure R2.Ai**), we then showed that our photostimulation strategy increased variability and induced irregularities in PC discharge (n = 6). To quantify PC firing variability due to simulated synaptic inputs, CV2 was calculated over more than 500 interspike intervals (ISIs)

per cell (**see material and methods**). Our measurements were compared with in vivo data obtained from juxtacellular recordings performed in wild-type littermates without photostimulation (n = 6, data recorded by Joseph Chaumont).
Significantly increased CV2 values were found (mean CV2 photostimulation: 0.202 ± 0.055; control: 0.136 ± 0.054, Wilcoxon paired test, $p < 0.05$) and were close to those obtained *in vivo* (mean CV2: 0.215 ± 0.110, Wilcoxon unpaired test, $p > 0.05$) (**Figure R2.Aii**).

Photostimulation-triggered change in PCs conductance state was assessed in whole-cell voltage clamp recordings by measuring the modification of PC current in response to a – 10 mV step depolarization (**Figure R2.Bi**). Our photostimulation approach significantly increased current in PCs (averaged current, photostimulation: 495 ± 1.25 pA; control: 379 ± 0.05 pA, Wilcoxon paired test, $p < 0.05$, n = 6; **Figure R2.Bii**) and thereby their conductance state (0.012 µS increase).

Overall, our findings demonstrate that photostimulation of PC dendrites in L7-ChR2(H134R)-eYFP positive mice can reproduce a high conductance state close to *in vivo* conditions. A clear correlation between the conductance state of PCs and CV2 value of their discharge was found. A summary of the differences between the high and low conductance states is displayed in **Figures R3.Ai** and **R3.Aii**. As a consequence, CV2 was systematically used as a parameter to validate our method in the following sets of experiments. However, the described approach simulates only excitatory barrage onto PCs but does not include inhibitory inputs also impinging onto PC dendrites *in vivo*.

To generate both, excitatory and inhibitory barrage onto PCs, one possibility is to increase the activity of the GC to PC pathway. We tried a pharmacological approach using furosemide, known to prevent GCs tonic inhibition by blocking GC-specific α6-subunit-containing $GABA_A$ receptor (Wall, 2002). The CV2 of PC discharge was increased as *in vivo* (data not shown). However, because furosemide also blocks potassium chloride co-transporter 2 (KCC2) ((Zhu et al., 2005), intracellular concentration of chloride in PCs is likely to be modified. Since we aimed at investigating the impact of inhibition on the modulation of PC discharge, this strategy was discarded. GCs are known to burst when NMDA receptors are unblocked (Schwartz et al., 2012), therefore removing applied antagonist (D-APV) from our

preparation could have been another possibility. However, because NMDA receptors are involved in plasticity mechanisms at the GC to PC pathway, this approach was not considered.

Finally, we took advantage of Thy1-ChR2-eYFP transgenic mice (line 18), known to express ChR2-eYFP in cerebellar MFs (Wang et al., 2007). ChR2-eYFP expression was assessed in transverse slices of fixed Thy1-ChR2-eYFP adult mice (**Figure R4.Ai**) using confocal microscopy. ChR2-eYFP was strongly expressed in rosettes, the MF terminals in the GC layer (**Figures R4.Aii** and **R4.Aiv**). Additional weak fluorescence was observed around PC somas and in the molecular layer (**Figure R4.Aiii**) indicating that ChR2 might also be expressed in some PCs. Therefore, we tested if this weak expression was sufficient to induce direct ChR2-mediated excitatory current in PCs. Transverse slice orientation was chosen to preserve MFs (and FFI). PC responses to wide-field LED illumination (470 nm) were recorded in whole-cell voltage clamp configuration at - 60 mV (**Figure R4.Bi**). Small EPSCs were elicited with a mean amplitude of 38 ± 2.7 pA (n = 6 cells). Those excitatory responses were fully blocked by bath application of TTX (100 µM, **Figure R4.Bii**) indicating that they were not due to direct illumination onto PCs. Therefore, this model can be used to increase excitatory and inhibitory synaptic noise on PCs.

To mimic MF input patterns, waveforms containing high frequency bursts were generated and used to drive illumination applied onto the slice (**Figure R5.A**). A barrage of excitatory and inhibitory synaptic inputs was then induced, the amplitude of which could be modulated by illumination intensity (**Figure R5.B**).

To confirm that this strategy could be used to reproduce *in vivo* conditions, extracellular recordings of PCs were then performed before and during optogenetic illumination (**Figure R5.Ci**) and CV2 and LvR parameters were calculated. For both, higher values were significantly obtained during illumination conditions as compared to controls (**Figures R5.Cii** and **R5.Ciii**, mean CV2, illumination: 0.202 ± 0.09; control: 0.152 ± 0.09, signed rank test, $P = 0.001$, $n = 32$; mean LvR, illumination: 0.086 ± 0.084; control: 0.050 ± 0.077, signed rank test, $P \leq 0.001$, $n = 32$), validating the use of the implemented *in vivo*-like model.

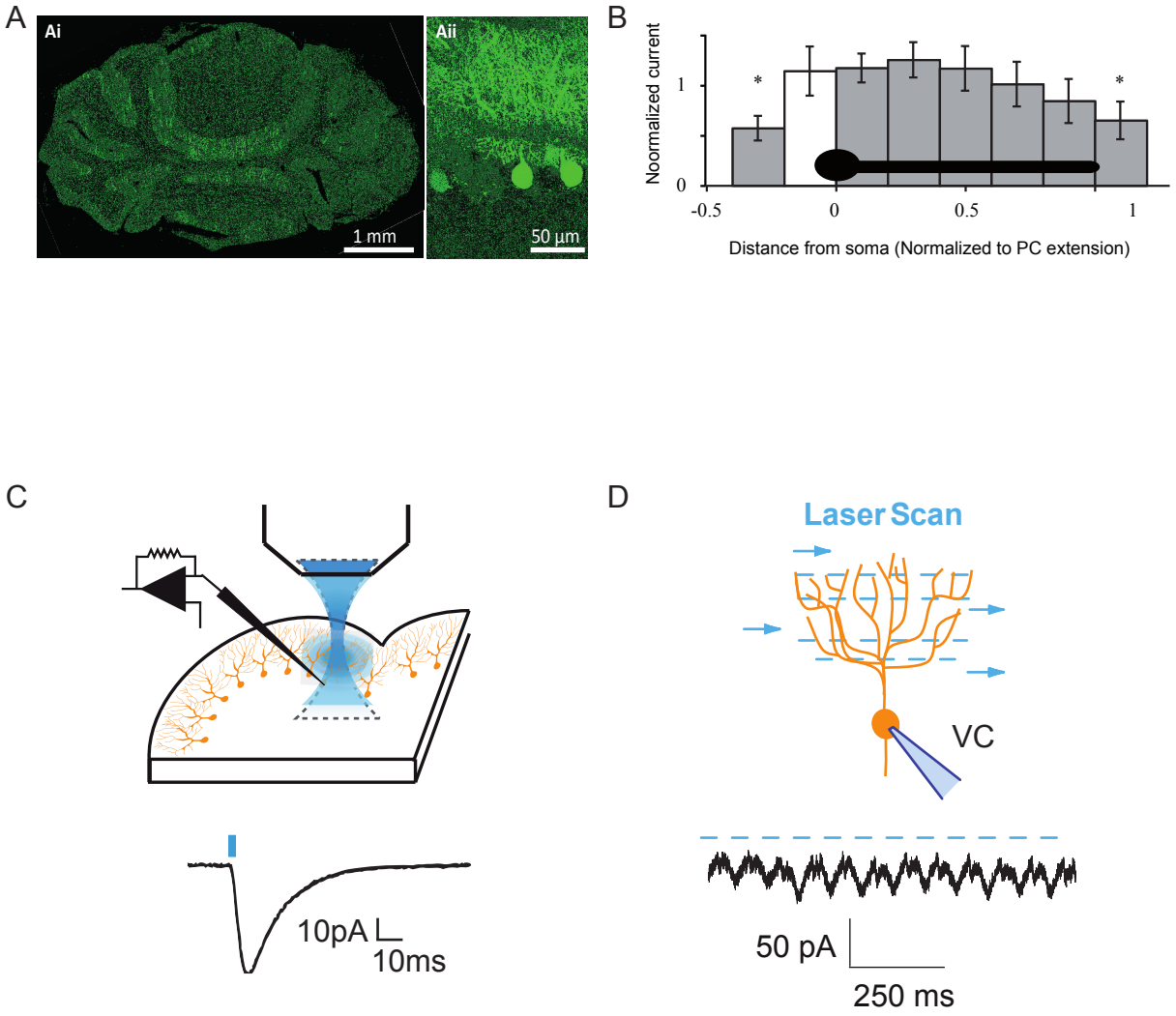

Figure R1. First strategy to mimic in vivo conditions in cerebellar acute slices.

A: Dendritic expression of ChR2-eYFP in PC of L7-ChR2(H134R)-eYFP mice. **Ai:** Coronal cerebellar slice (80 µm) showing YFP fluorescence in PCs in the whole cerebellar cortex. **Aii:** Sagittal slice (80 µm) displaying YFP fluorescence the entire PCs, including their dendritic tree. **B:** ChR2-mediated current can be elicited all along the Purkinje-cell dendritic tree with photostimulation. Current is normalized (± SEM) (adapted from Chaumont et al., 2013). **C:** Synaptic input can be simulated in PCs following 1 ms wide-field 470 nm LED illumination (sagittal plane). **D:** A barrage of excitatory synaptic inputs can be mimicked in PCs by random blue laser point-scan photostimulation spanning the whole dendritic tree.

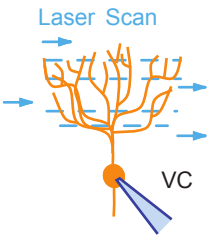

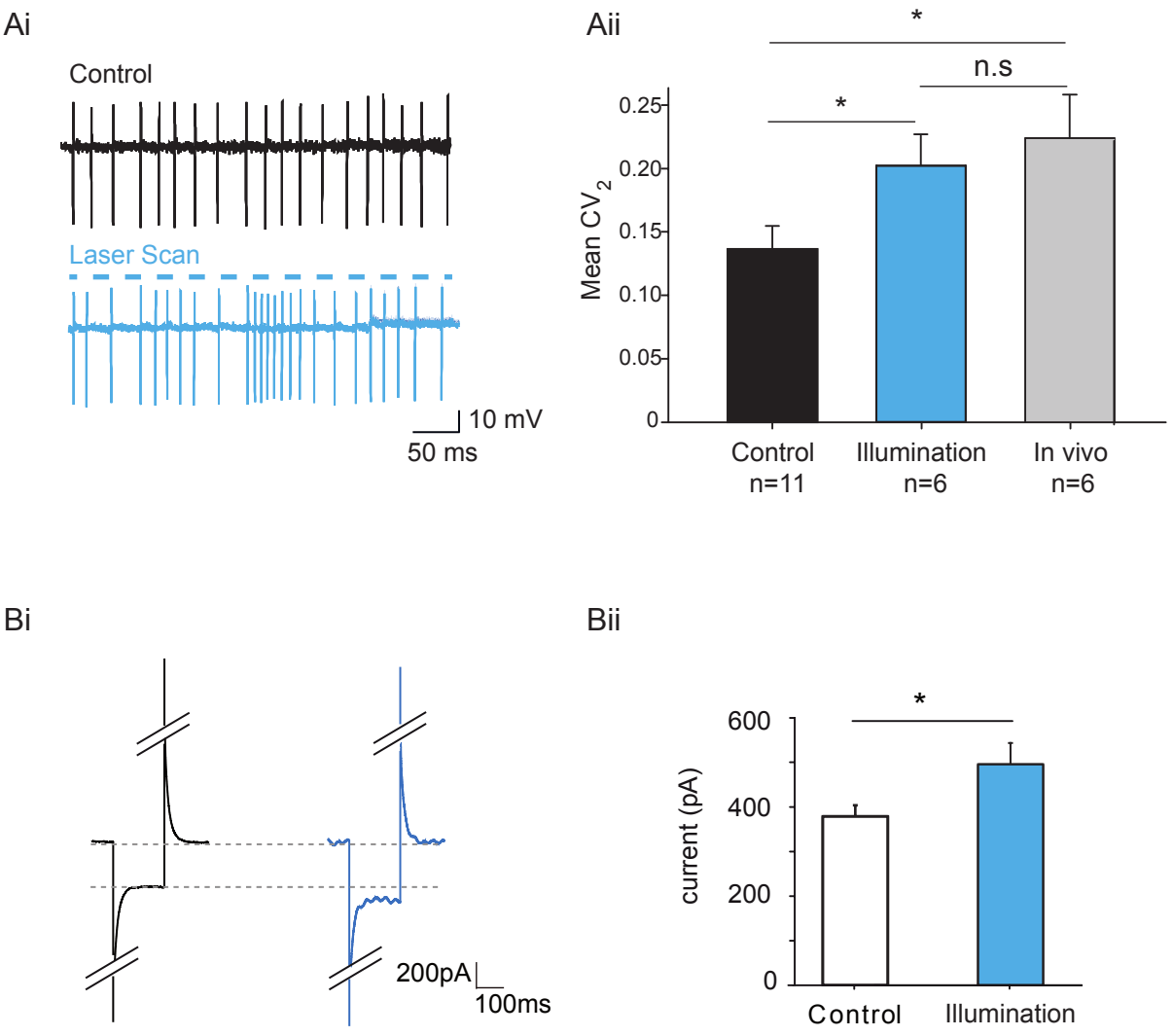

Figure R2. Our first strategy reproduces a high conductance state in Purkinje cells in acute cerebellar slices.

Ai: Example of extracellular recordings of one PC in L7-ChR2(H134R)-eYFP mouse before (control, black trace) and during 1 ms pulses random point-scan photostimulation (blue trace). PC firing irregularities can be elicited by the photostimulation strategy. **Aii:** Quantitative analysis of PC discharge assessed by the CV2, coefficient of variation between two adjacent ISI in control (n = 11 cells) and during photostimulation (n = 6). CV2 value was increased when the regularity of spike pattern was decreased. The optogenetic photostimulation strategy reproduces in vivo PC firing irregularities (Wilcoxon unpaired test, n = 6 cells, $p > 0.05$). In vivo CV2 was quantified from juxtacellular recordings in wild-type littermates provided by Joseph Chaumont. **Bi:** Example of whole cell (current average of 30) during a depolarizing voltage step (- 10 mV) recorded in PC before (black trace) and during 1ms pulses random point-scan photostimulation (blue trace). **Bii:** The photostimulation strategy increased the conductance (g) of PCs assessed by the higher elicited current (I) in response to a – 10 mV voltage step (ΔV) during photostimulation as compared to before (control), $I = \Delta V * g$.

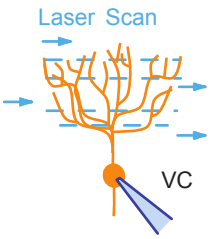

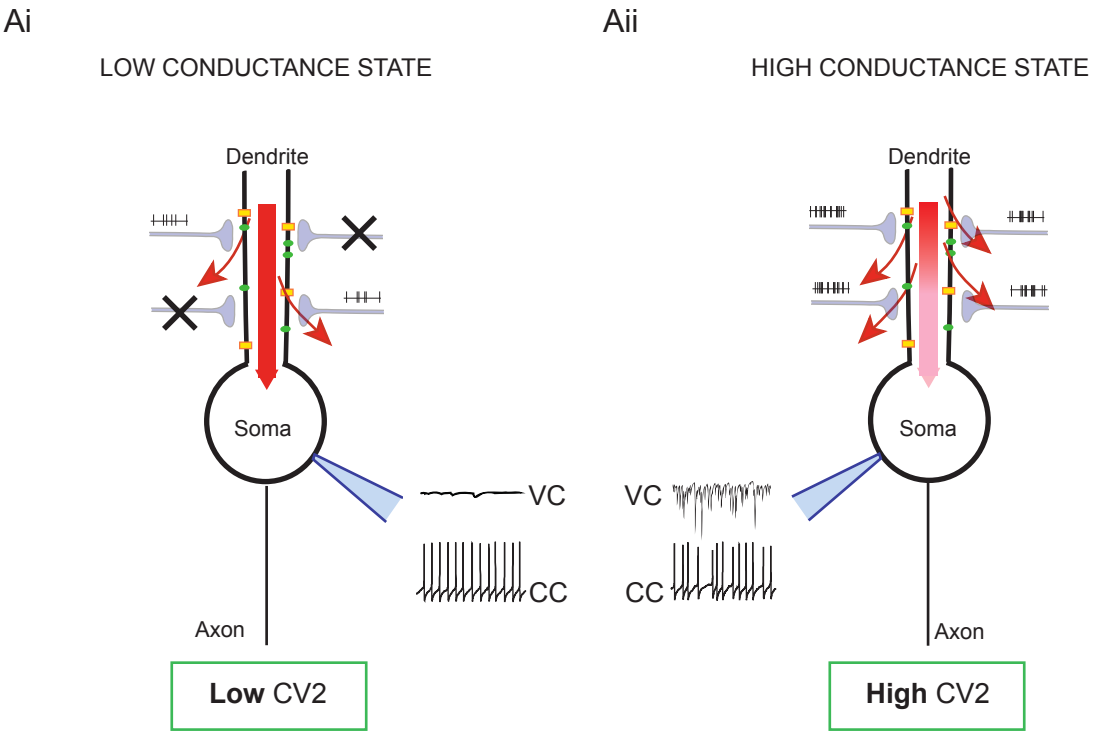

Figure R3. Schematics summarizing the high and low conductance state in the Purkinje cell.

Ai: Low conductance state in classical acute slices. Only one dendrite is represented. Cut axons in slice reduce the number of synaptic contacts on target cells thereby largely decreasing the number of dendritic inputs as shown in the voltage clamp (VC) recording. As a result, only a few synaptic receptors (green) and voltage-dependent gated channels (yellow) are opened decreasing the membrane conductance of the cell. Thereby, PC spontaneous discharge is regular (low CV2) as displayed in current clamp (CC) recordings. **Aii:** In vivo like higher conductance state is reproduced in slices using photostimulation. Only one dendrite is represented. Numerous synaptic inputs generated by high network activity in vivo trigger the opening of many channels and receptors. The resulting membrane leak can shunt distal inputs and reduce the reliability of spike initiation, leading to irregular spontaneous PC discharge (high CV2).

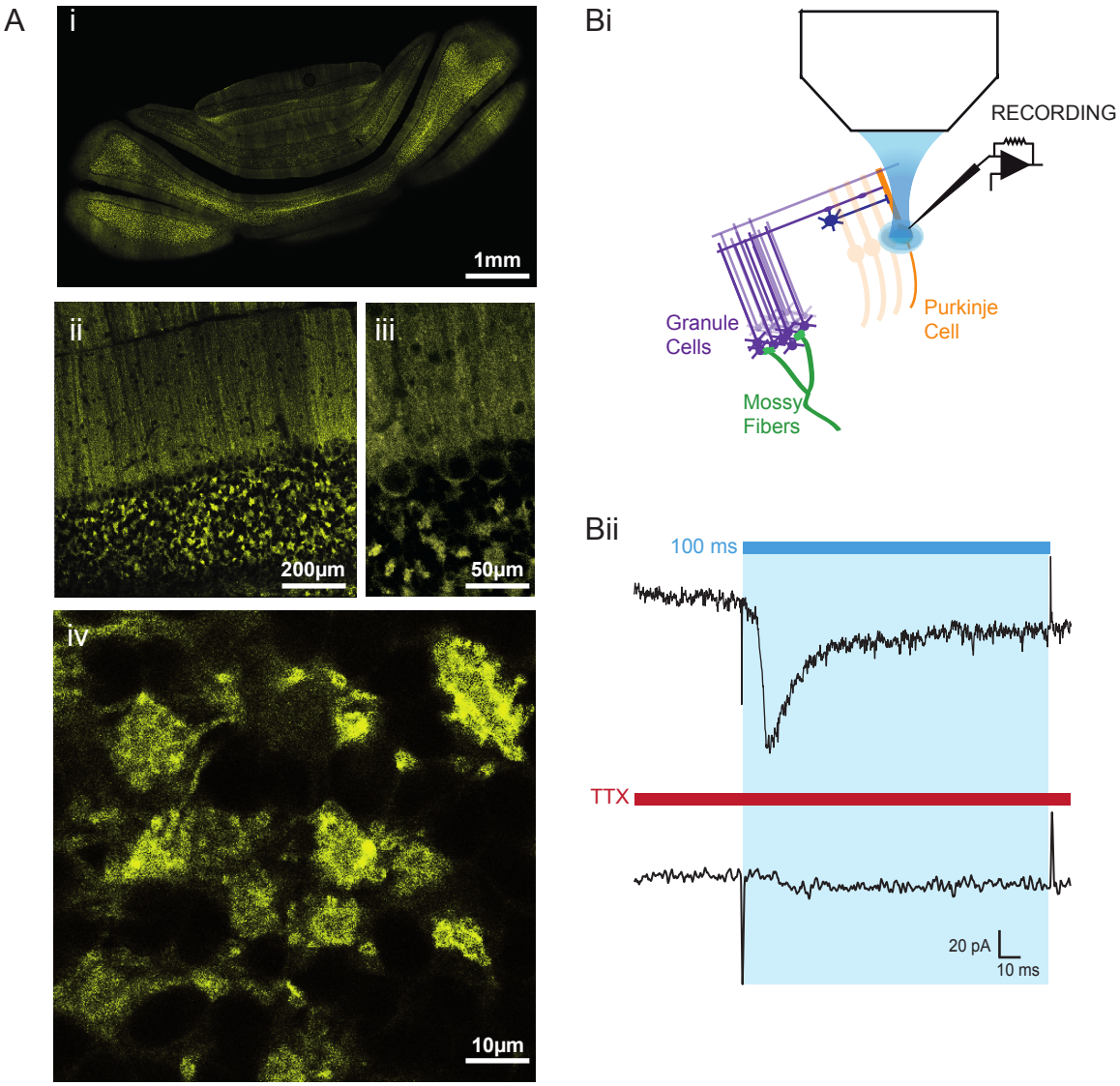

Figure R4. Final strategy to mimic in vivo conditions in cerebellar acute slices – calibrations.

A: ChR2-eYFP transgene expression monitored by YFP fluorescence in transverse cerebellar sections from adult Thy1-ChR2-eYFP mice using confocal microscopy.
Ai, Aii: A strong expression can be observed in the granular layer and more specifically at the MF terminal rosettes for which a zoom is displayed in Aiv. Aiii: weak fluorescence is observed around PC somas and in the molecular layer.
B: There is no direct effect of the illumination onto Thy1-ChR2-eYFP PCs.
Bi: PC responses to 470 nm wide-field LED illumination were recorded in whole-cell voltage clamp configuration at - 60 mV.
Bii: Elicited EPSCs were fully blocked by bath application of TTX.

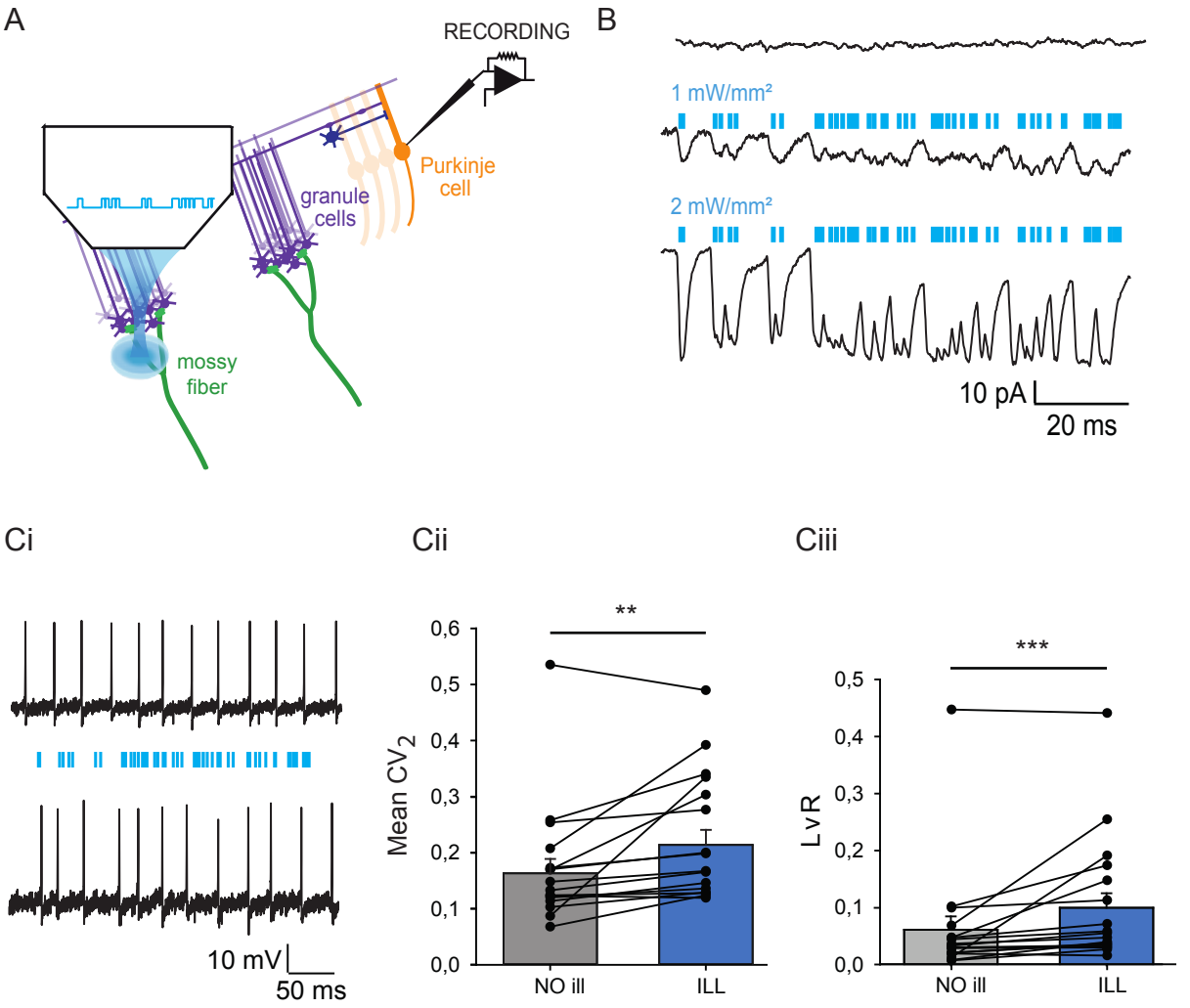

Figure R5. Illumination of Thy1-ChR2-eYFP reproduces in vivo conditions in cerebellar acute slices.

A: Effect of the photostimulation of MF in Thy1-ChR2-eYFP mice was assessed by recording PC before (NO ill) and during the photostimulation (ILL) either using whole cell voltage-clamp recordings (**B**) or extracellular recordings (**C**).
B: Excitatory and inhibitory synaptic barrages in the absence of photostimulation (top) and during the photostimulation (middle and bottom)
C: Photostimulation-induced irregularities in the PC discharge. **Ci**: Example of extracellular recordings before (top) and during the photostimulation (bottom).
Cii, **Ciii**: Quantitative analyses of PC discharge irregularities assessed by the CV2, CV2and the frequency-independent parameter LvR. In control conditions (NO ill, grey) and during photostimulation (ILL, blue).

PART II: DIVERSITY OF PURKINJE CELL DISCHARGE MODULATION IN RESPONSE TO GRANULE CELL STIMULATION

In this chapter, we will show how we studied and described the influence of subthreshold GC stimulations onto the discharge of PCs. It should be noted that all experiments were performed without blocking inhibitory transmission and using Thy1-ChR2-eYFP mice in cerebellar acute slices (**see Results Part I**).

1. *Experimental approach*

In vivo, GCs can fire high frequency bursts when receiving sensorimotor inputs carried by MFs (see introduction). GC firing patterns were reproduced in acute cerebellar slices using extracellular electrical stimulation of GC somas while PCs were recorded using extracellular configuration (**Figure R6.Ai**).The recording pipette was positioned close to Purkinje neuron initial segment (**Figure R6.Aii**). To avoid stimulation of the CFand direct stimulation of local interneurons (Golgi and Lugaro cells), the stimulation electrode was positioned at a lateral distance of 100-300 µm from the recorded PC. At least fifty trials per condition were tested to determine the spike train statistics of PC response. The high conductance state was achieved by illuminating MFs (see above). Illumination waveform and intensity were calibrated for each GC to PC pathway to increase CV2 values of PC discharge (**see Results Part I**) and kept constant throughout the experiment. In order to describe the functional synaptic organization established during the life of the mice, long-term plasticity mechanisms were blocked pharmacologically (**see material and methods**).

In our study we defined GC stimulation as subthreshold if it does not systematically elicit a time locked action potential in the PC. To confirm that stimulation intensity was subthreshold, average responses of the PC to a single stimulation of GCs was systematically checked by constructing PSTH (**see material and methods**). If GC

stimulation was suprathreshold, a time-locked spike to the stimulus pulse would be evoked in the PC discharge which would appear as a single sharp peak in the PSTH (**Figure R6.Bi**). It is interesting to note that these strong excitatory synaptic inputs could reset PC pacemaker, displayed as the remaining time locked spiking behavior (**Figure R6.Bi**). Conversely, a flat PSTH would reflect no increase in average spike probability indicating that GC inputs did not modulate the PC discharge. For these reasons, only broad peak(s) in the PSTH to a single stimulation of GCs were considered as subthreshold GC inputs (**Figure R6.Bii**). Effects of high frequency short and long bursts (1, 3 spikes and 7 spikes at 200 Hz respectively) of GC inputs onto PC discharge were investigated. To prevent failures in spike propagation, input frequency was limited to 200 Hz. To exclude synaptic fatigue and allow trial-to-trial independency, stimulation trials were interspersed with a thirty second interval.

2. *Modulation of Purkinje cell discharge – quantification*

We found that subthreshold GCs inputs, including single GCs spike, could modulate PC discharge in many different ways, from an acceleration of the spontaneous firing rate that elicited additional spike(s) (**Figures R7.Ai** and **R7.Bi**, n = 42) to a strong delay in the spontaneous firing rate leading to missed spike(s) (**Figures R7.Aii** and **R7Bii**, n = 9). These effects are observed in the PSTH as an increase or a decrease in spike probability.

We then set out to quantify the different modulations observed. One difficulty was to discriminate between spontaneous, additional or missed spikes. Therefore, I developed a method of analysis to systematically assess the net impact of GC synaptic inputs onto PC discharge, also allowing comparisons between cells and conditions (**Figure R8**). The averaged spike probability was integrated and corrected for the mean spontaneous firing rate calculated during baseline. The net number of additional or omitted spike(s) caused by GCs stimulation could then be obtained and

will be referred to as the “net effect”. Our first approach was to analyze the variation of averaged instantaneous firing frequency during the time window of GC inputs and compare it to baseline spontaneous firing. However, this quantification underestimates short-term modulations and introduces a bias for modulations lasting longer than the input duration.

Interestingly, the net spike outputs were highly diverse between GC groups in response to each stimulation condition (**Figure R9.A**). When performing a single stimulation of GCs, a modification of PC discharge could be observed, which varied from a net spike output of - 3.09 to 0.53 (3.09 missed spikes to 0.53 additional spikes). Overall, 53% of the pathways showed a negative modulation (n = 27 cells) while 41% displayed an increased total spike number (n = 21 cells). Three cells did not show any net change in response to a single spike. Overall, the population of GCs to PC pathways (n = 51) was negatively modulated with an average of - 0.29 ± 0.09 missing spikes.

The dynamic range of PC discharge modulation increased in response to a burst of 3 stimulations, from a net effect of 4.87 missed spikes to 2.32 additional spikes. Every PC was modulated in this condition. 28 of the cells (54.9%) showed a negative net effect while 23 cells (45.1%) were positively modulated. Overall, an average of - 0.34 ± 0.21 missed spikes was found at the population level.

Strikingly, for a longer burst of stimulation (7 spikes), the mean modulation of all GC to PC pathways was significantly shifted to a positive value of 1.05 ± 0.43 additional spikes (Kruskal-Wallis test by ranks, $p \leq 0.001$, n = 51). Dynamic range of PC responses expanded both towards negative and positive modulations. Diversity of responses to 7 input spikes greatly increased as compared to responses to both 1 and 3 input spikes (Kruskal-Wallis test by ranks, $p \leq 0.001$, n = 51), going from 10.40 omitted spikes to 8.58 additional spikes.

These results suggest that the feedforward inhibitory pathway is combined with the GC-PC synapses to expand the diversity of PC responses to GC inputs. Indeed, when considering the three conditions (1, 3 and 7 stimulations) for a given pathway, three types of net responses could be identified (**Figure R9.B**). One group of PCs showed a decrease in the net spike output when adding stimuli (**Figure R9.Bi**) which

will be considered as the “delay” group. Another group displayed a (slight) decrease followed by an increase in the net effect (**Figure R9.Bii**) that will be referred to as the “shift” group. Lastly, some PCs exhibited an increase in the net spike output when augmenting the number of stimulus (**Figure R9.Biii**), named the “acceleration” group.

Altogether, the diversity observed in PC response to a given input pattern demonstrates an heterogeneity among GCs to PC pathways, suggesting the existence of GC-specific differences in information processing. In addition, the differential distribution of responses of the same pathways to different GCs input patterns indicates input-specific coding strategy.

3. *Conclusions*

Overall, our findings showed that subthreshold GCs inputs can modulate PC discharge with a wide diversity of outcomes. This could potentially arise from differences in local network properties and whether or not the feedforward inhibitory circuit is recruited. GC to PC synapses are selected during motor learning via long-term plasticity mechanisms, those of which also affects MLIs to PC synapses in the opposite direction. Therefore, these could putatively promote either excitation or inhibition onto PCs, and possibly generate diverse balance between excitation and inhibition among the different GCs to PC pathways.

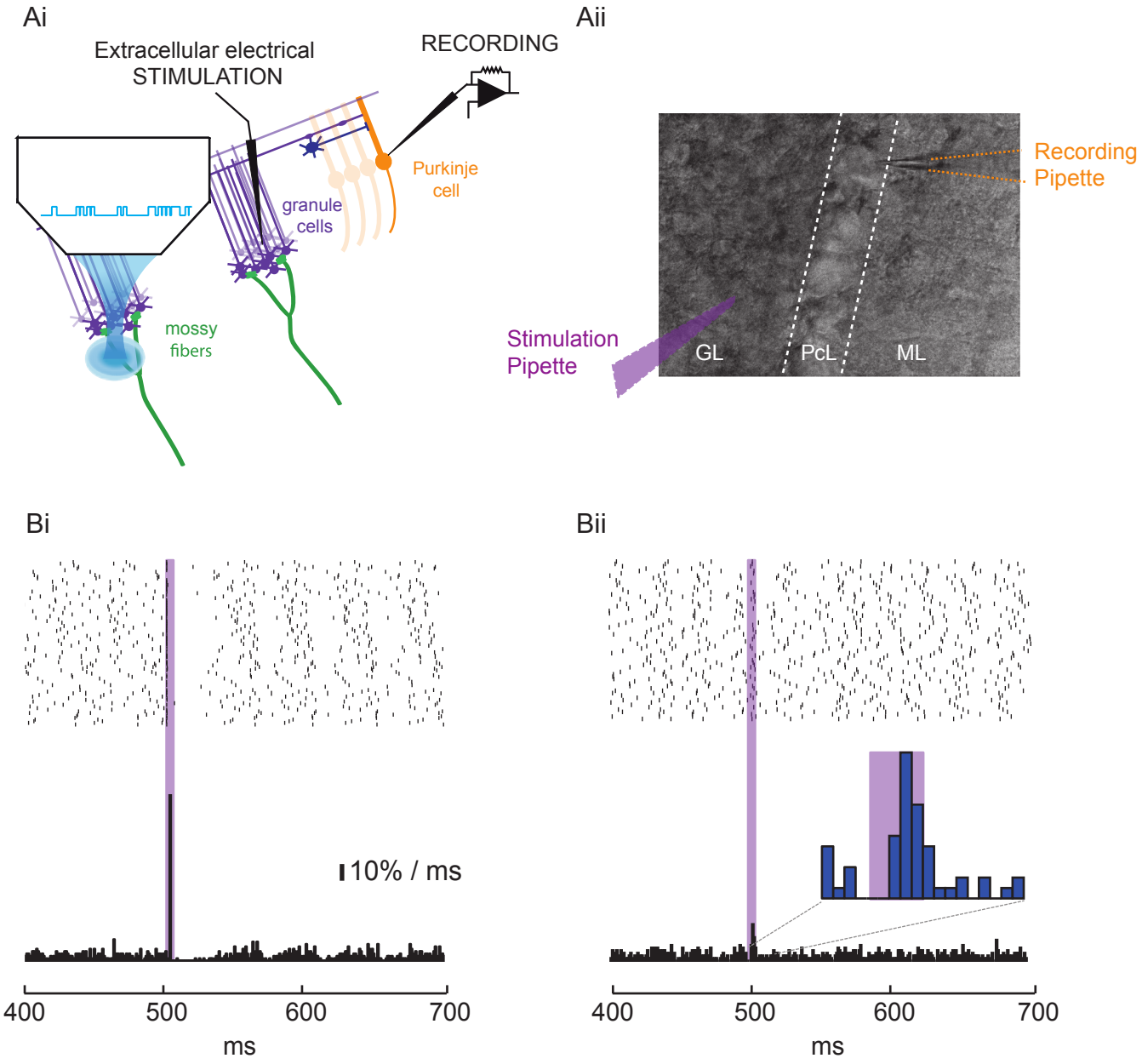

Figure R6. Experimental approach to study the modulation of the Purkinje cell discharge in response to subthreshold granule cells inputs.

Ai: A single PC was recorded using extracellular configuration. A group of connected GCs located 100-300 µm laterally from the recorded PC was electrically stimulated. Protocols of 1, 3 or 7 stimuli at 200 Hz were used. High frequency optogenetic illumination was simultaneously applied onto distant MF. **Aii:** View of the acute cerebellar slice under the microscope. Deep GCs were stimulated. Recording pipette was positioned close to PC soma.

Bi, Bii: Top: Aligned successive spike trains of the PC discharge. Each line is one trial, each vertical bar represents a spike. Bottom: corresponding PSTH illustrating the probability of occurrence of spikes. GCs stimulation period is shown in purple. **Bi:** Suprathreshold GCs stimulation assessed as a time-locked increase in PC spiking to the stimulus pulse (purple). Note the pacemaker rhythm resetting following the stimulation. Bii: Subthreshold GCs stimulation illustrated by a moderate increase in spike probability after the stimulation.

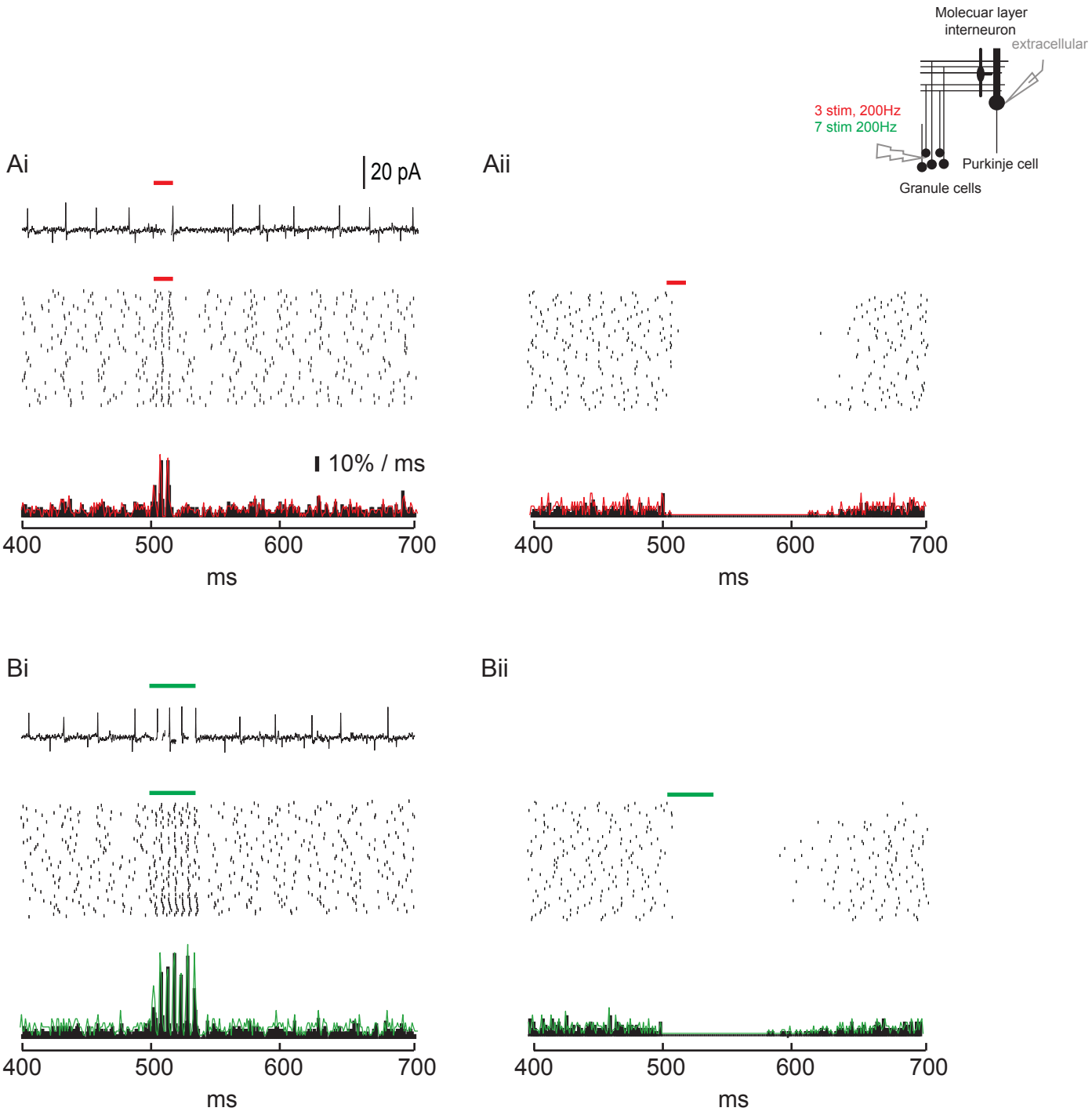

Figure R7. Modulation of the Purkinje cell discharge.

Top: Example traces of PC extracellular recording. Stimulation artefacts have been removed. Middle: Spike rasters of 50 trials Bottom: Mean PSTH (colored, PSTH) displayed on top of the PSTH.

A: Modulation of the PC discharge in response to 3 stimulations of GCs at 200 Hz. Two illustrative examples of opposite modulations: **Ai:** acceleration of spontaneous firing eliciting additional spikes. **Aii:** delay of spontaneous firing corresponding to an omission of spikes.

B: Modulation of the PC discharge in response to 7 stimulations of GCs at 200 Hz. **Bi**: same as Ai. Bii: same as Aii.

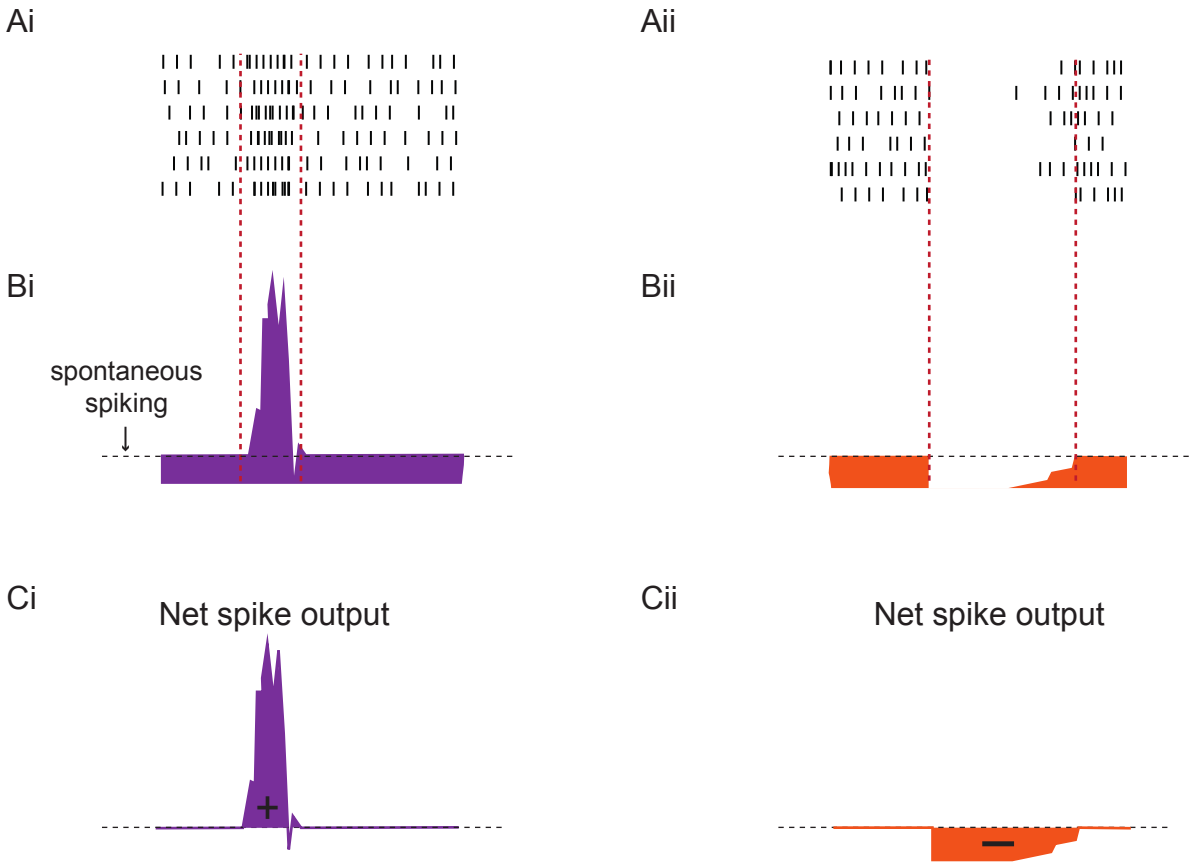

Figure R8. Quantification of the net modulation of the Purkinje cell discharge.

Ai, **Bi**, **Ci**: Schematics representing an acceleration of the PC discharge (as observed in figure R7Ai).

Aii, **Bii**, **Cii** : Delay in PC discharge (as in figure R7 Aii).

A: Raster plot.
B: Mean peristimulus time PSTH of the raster plot.
C: The net number of additional (**Ci**) or omitted spikes (**Cii**) is determined by computing the cumulative integral of the mean PSTH.

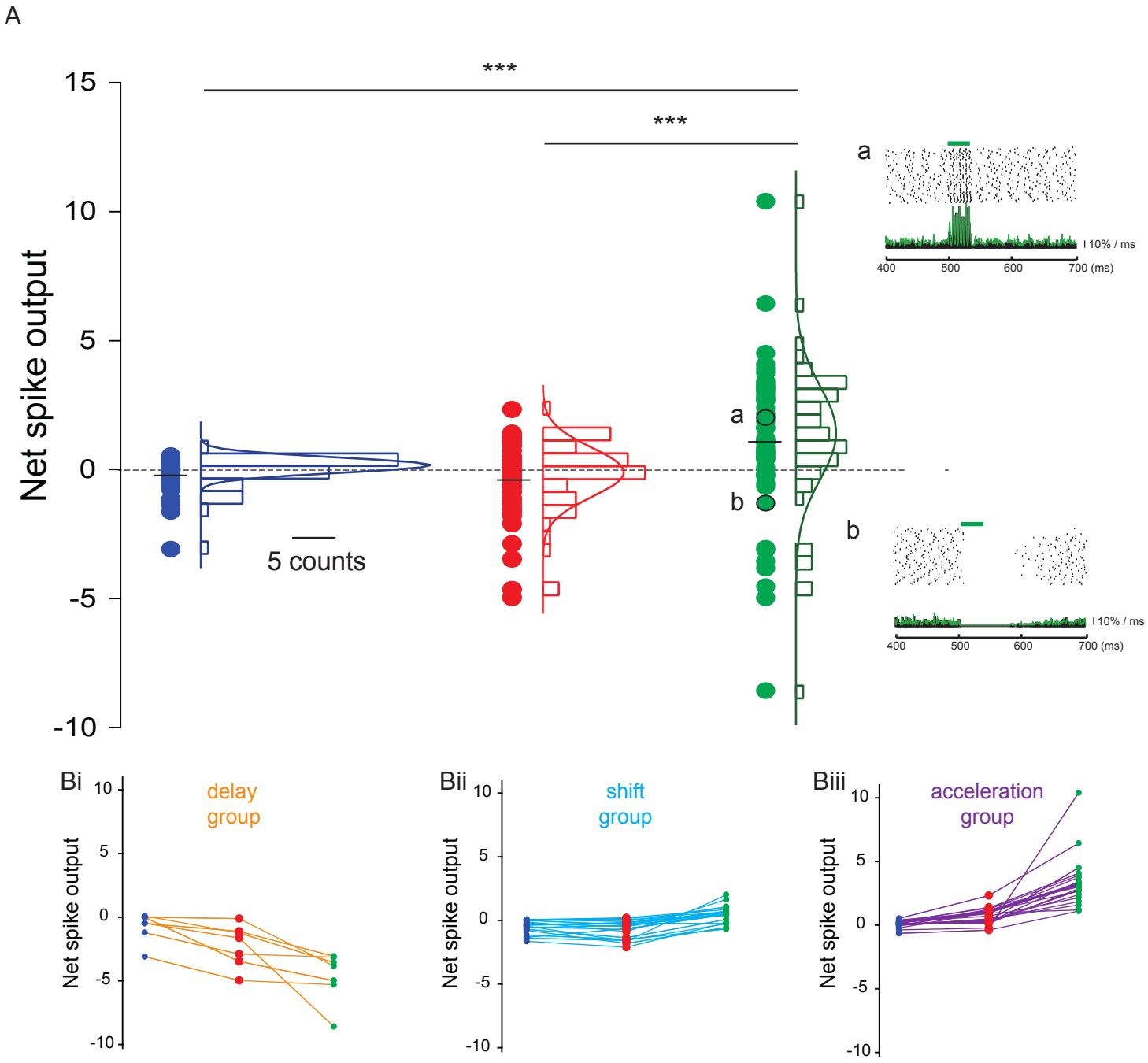

Figure R9. Wide diversity of Purkinje cell net spike output in response to subthreshold granule cells stimulation.

A: Net spike output in PCs (n = 51) in response to 1.3. and 7 stimulations of GCs: one (blue), three (red) or seven (green) stimulations at 200 Hz. Black horizontal lines indicate the mean value for each condition of stimulation. Statistical test used: Kruskal-Wallis one way analysis of variance on ranks, P ≤ 0,001. a, b: Illustrative examples of two PCs displaying a positive (a) and negative (b) net spike outputs in response to seven stimulations of GCs. Insets: top: raster plots, middle: Mean PSTH (green) displayed on top of the PSTH, bottom: Cumulative integral of the mean PSTH.
B: Same data as shown in A showing the three conditions of GC stimulations (1, 3 and 7) for each GC-PC pathway displayed as straight lines. Three groups of net spike output responses were observed: a decrease (delay group, **Bi**), a decrease followed by an increase (shift group, **Bii**) or an increase (acceleration group, **Biii**) in PC net spike output.

PART III: FEED-FORWARD INHIBITION CONTROLS PURKINJE CELL SPIKE OUTPUT

We first addressed whether the net negative modulation and delays in the PC discharge resulted from MLI-mediated FFI onto PCs as previously reported (Mittmann et al., 2005). After a first set of extracellular recordings of PCs in response to 1, 3 and 7 stimuli in the GC layer, inhibitory neurotransmission was blocked using the $GABA_A$ antagonist picrotoxin. Delays in PC discharge that were elicited by GC inputs before bath application of picrotoxin were totally suppressed (**Figure R10**), net effects increased (n = 6) and could be reversed (n = 4/6). I should mention that blocking FFI in some cases increased spontaneous firing frequency. However, this did not affect the measured net effect change (to zero or positive value) since our analytical method corrected it. It is interesting to note that sometimes delays caused a time locking of subsequent spikes, putatively as a result of strong inhibitory inputs resetting PC pacemaker activity. Overall, our findings demonstrate the involvement of FFI in controlling PC spike output.

The wide diversity of modulations observed could therefore potentially arise from differential balance between excitation and inhibition (E/I) in the GC to PC pathways. To test this hypothesis, in one set of experiments, PCs (n = 17 cells, N = 15 animals) were whole-cell patch clamped after extracellular recordings and both EPSCs and IPSCs were measured in the same PC by holding its membrane potential at - 60 mV and 0 mV respectively (**Figure R11.A**). E/I was calculated as the ratio of averaged EPSCs and IPSCs amplitude or charge in response to a single stimulation of GCs (**Figure R11.B**). The measured latency between excitation and feed-forward inhibition was in the range of 0.94 - 3.23 ms, as previously reported (Mittmann et al., 2005). Interestingly, a wide range of synaptic weights and charge could be observed at GCs to PC pathways. Excitatory synaptic weights varied from 18 pA to 617 pA with an average of 228 ± 190 pA (n = 17 cells). Inhibitory synaptic strengths varied from 0 pA to 3188 pA with an average of 1178 ± 1040 pA. We finally observed a wide diversity of E/I ratios between pathways, going from 0.055 to the infinity (0 pA inhibition).

Synaptic charge transfers in response to a single stimulation of GCs were also very different from pathways to pathways with respective minimal and maximal measured values of 141 pC and 6744 pC for excitatory GC to PC synapses, and of 0 pC and 12028 pC for GCs to inhibitory MLI to PC pathways. Mean synaptic charge transfers of 2080 ± 2158 pC and 4352 ± 2869 pC (n = 17 cells) were obtained for excitatory and inhibitory pathways respectively.

These experiments in which extracellular recordings were followed by patch clamp recordings of the same PC were technically challenging. As explained in the previous section (**see Results Part II**), long recordings lasting at least one hour and a half were required to obtain PC discharge data. These included calibration of illumination, searching for connected GCs to the recorded PC, calibration of the stimulation to be subthreshold and testing the effects of three different conditions of GC stimulations onto the PC discharge with a sufficient signal-to-noise ratio. To keep PC integrity at its best in such long lasting experiments, extracellular recording configuration was chosen over cell attached recordings. Therefore, the pipette had to be changed between extracellular and patch clamp recordings which introduced some difficulties in identifying which cell had been extracellularly recorded. Sometimes, in cases where PCs were localized deep into the slice, the recorded PC could not be visualized afterwards. Patch clamp experiments were not performed if any doubt regarding PC identity.

The second difficulty was the low success rate of keeping the patch stable and long enough to acquire paired data at both - 60 mV and 0 mV, which was necessary to determine the E/I ratio. Lastly, when the patch was successful, we unexpectedly, often observed an absence of excitatory synaptic currents, likely arising from the subthreshold level of stimulation (weak GCs inputs). Since it was not possible to assess if there were no elicited excitatory synaptic currents or if they were too small to be detected and measured, those data were excluded. Alternatively, we checked for a possible rundown effect of GCs activity with time and did not find any evidence for it. This limitation was overcome and our success rate was increased by increasing stimulation settings while keeping GCs inputs subthreshold.

In 17 cells, we could then obtain combined extracellular and patch clamp data at both holding potentials that met all criteria: increased CV2 value (**see Results Part I**), subthreshold stimulation and effect onto the PC discharge. Net effects were determined in response to stimulation of 1 spike: - 3.09 to 0.24; 3 spikes: - 4.97 to 1.41; and 7 spikes: - 4.98 to 3.34 with mean net effects of - 0.55 ± 0.13; - 0.96 ± 0.23 and 0.15 ± 0.036 in response to 1, 3 and 7 stimulations respectively. These results match with data obtained in the previous set of experiment (**see Results Part II**).

Next, net spike outputs were plotted as a function of E/I ratios of amplitude or charge, for each stimulation condition. Since no significant differences have been observed between the two graphs, I will present only data from E/I ratios of amplitude (**Figure R11.C**). Higher E/I ratios (weaker inhibition) displayed higher net spike outputs in response to 1 (and to less extent) 3 and 7 stimulations, indicating that the E/I balance influences the modulation of PC discharge. However, a clear discrepancy between lower and higher E/I ratios appeared: there is an extremely wide dynamic range of net spike outputs for the lower E/I ratios, in all stimulation conditions. Therefore, GCs to PC pathways with stronger inhibition showed a great variability in net modulation of the PC discharge providing further evidence in support to the influence of E/I ratios and demonstrating a key role of FFI in coding diversity/expanding coding possibilities (**see discussion**). But different and even sometimes opposite net modulations could be observed for GCs to PC pathways having close E/I balance, revealing that E/I ratio alone did not determine PC net spike output.

Overall, we found that MLI-mediated FFI causes spike suppression in PC firing. We also showed that E/I balance influences but does not predict the modulation of PC discharge in response to GC inputs. Therefore we attempted to identify other synaptic parameters that could underlie the wide distribution of GC influence of PC discharge.

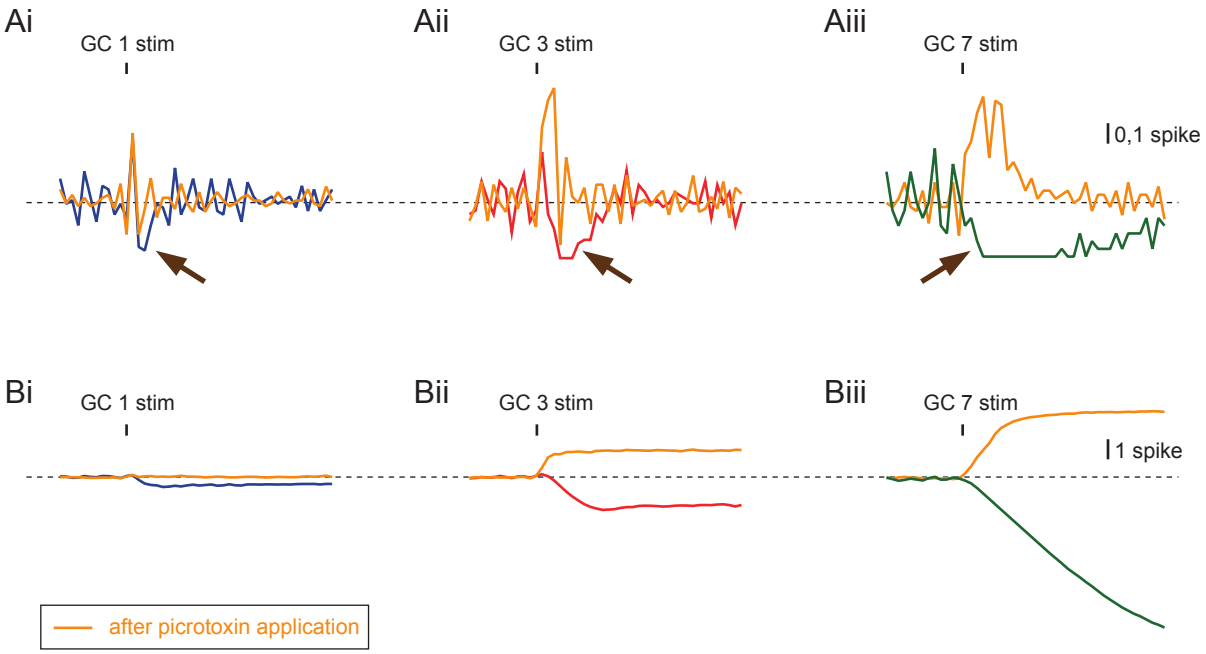

Figure R10. Delays in the Purkinje cell discharge are mediated by molecular layer interneuron-mediated feed-forward inhibition.

A: Mean PSTH corrected for the baseline firing (dashed line) in response to 1, 3 or 7 stimulations (blue, red, green lines respectively) of GCs (**Ai**, **Aii**, **Aiii**) in control conditions and after application of picrotoxin,a GABAA antagonist picrotoxin (in orange). Delays were suppressed indicating that they were mediated by FFI.
B: Cumulative integral of data displayed in A showing the net number of additional (above the dashed line) or omitted (below the dashed line) spikes. Blocking MLI mediated FFI increased the net spike output in all GC stimulation conditions and shifted the net effect from a negative to a positive value (see **Bi** and **Bii**).

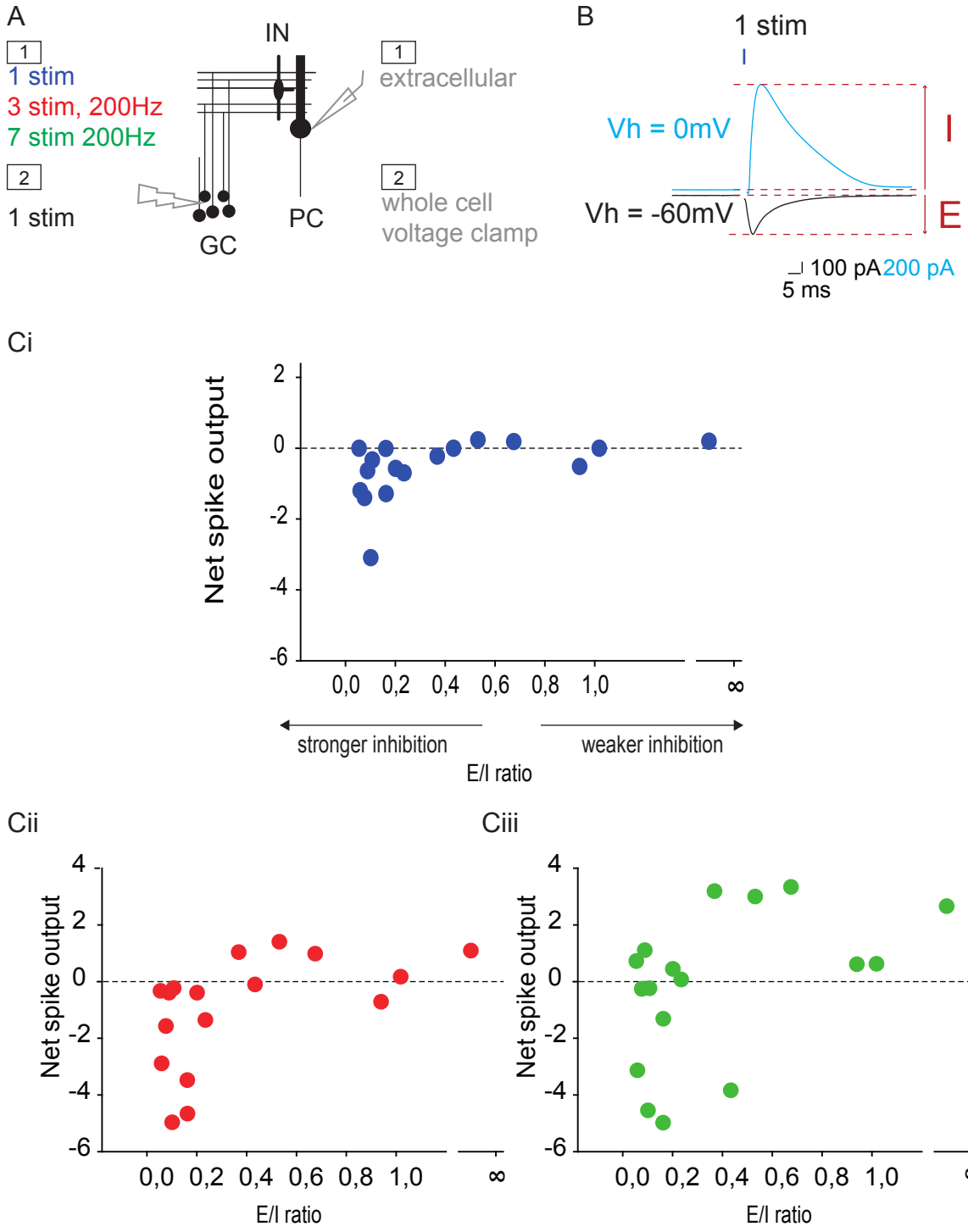

Figure R11. Influence of the excitation-inhibition balance on the net Purkinje cell spike output.

A: Diagram of the experimental protocol: PC spike responses to 1, 3 and 7 stimulations of GCs at 200Hz were extracellularly recorded. The same PC was then whole-cell patch clamped and EPSCs and IPSCs were recorded at - 60mV and 0 mV respectively.
B: Excitation-inhibition balance (E/I ratios) were calculated as the ratio of EPSC and IPSC amplitudes following 1 stimulation.
C: PC net spike output as a function of E/I ratios in response to 1 (**Ci**), 3 (**Cii**), and 7 (**Ciii**) stimulations of GCs at 200 Hz. Higher E/I ratios (weaker inhibition) show greater PC net spike outputs than lower E/I ratios. Lower E/I ratios display a strong diversity of modulations of the PC discharge.

PART IV: THE TIME COURSE OF PURKINJE CELL MODULATION BY GRANULE CELL INPUTS IDENTIFIES THREE GROUPS OF BEHAVIOR IN THE GRANULE CELL TO PURKINJE CELL PATHWAY

Quantitative analyses of the net effect of a given group of GCs onto PC spike output gave an estimate of the overall modulation of PCs. However, this parameter does not consider a more complex influence of PC discharge (**Figure R12.Aii**) displayed as biphasic spike responses and which can lead to both positive or negative net spike outputs depending on their relative predominance. To discriminate between these, we set out to study the time course of the PC discharge by computing the cumulative average of spike responses corrected for the mean spontaneous firing for each PC and each stimulation condition (**Figure R12.B**). We independently quantified the periods of acceleration (additional spikes) and delay (omitted spikes) by calculating the average numbers of additional and omitted spikes, as well as the average durations of acceleration and delay (**Figure R13.A**). A wide diversity in the shapes and durations of the cumulative responses were observed in every condition (**Figure R13.B**). It is interesting to mention that some responses (n = 4/51) did not show any acceleration period in any of the three stimulation conditions, suggesting a possible pure inhibitory effect of GCs onto the PC (**see discussion**).

The durations of the whole modulation varied between GC to PC pathways and the number of stimuli (one-way ANOVA on ranks, $P \leq 0.001$, n = 51). In response to one stimulation, effects lasted up to 95.00 ms with an average of 30.59 ± 24.37 ms (n = 51) in response to 1 stimulation. Response durations to 3 stimuli ranged from 10.00 ms to 175.00 ms with an average of 57.35 ± 35.11 ms (n = 51) while they went from 30.00 ms to 235.00 ms with an average of 79.41 ± 47.93 ms (n = 51) for 7 stimuli. In addition, the variability increased for all the four parameters investigated with the number of stimuli of GCs (**Figure R14**), as observed for the net effect (**see Results Part II**). Notably, the acceleration displayed a greater significant increase between 1, 3 and 7 stimulation conditions for

both the number of additional spikes and acceleration duration (**Figures R14.A** and **R14.C**; for both: one-way ANOVA on ranks, $P \leq 0.001$, $n = 51$). Conversely, the delay period increased only between the 1 stimulation and 3 stimuli conditions (for detailed values: **Figures R14.B** and **R14.D**; for both: Wilcoxon paired test, $P \leq 0.001$, $n = 51$). Together, these findings suggest that long burst of stimulation favor acceleration (additional spikes) over delay (omission of spikes) to the benefit of a more positive net effect. This is confirmed by the shift in the trajectory of the net effect observed between 3 and 7 stimulations for the "shift" group of PCs (**Figure R14.E** modified from R9.Bii).

The time course of the modulation of the shift cells exhibited biphasic spike responses. Short burst of three stimulations led to omitted spikes while longer burst of seven stimulations switched the response to a net acceleration, as displayed in the illustrative example in **Figure R14.F**. Interestingly, no correlation have been observed between the E/I ratio and this switch in the shift cell group as revealed by very diverse balances ranging from 0.055 to 1.019 with a mean value of 0.34 ± 0.40 suggesting that other synaptic parameters such as short-term plasticity might underlie influence PC responses. Additionally, the shift cells exhibited relatively strong IPSCs and EPSCs (mean IPSCs 1566.0 ± 1054.4 pA; mean EPSCs: 252.8 ± 176 pA) as compared to the two other groups of cells that showed different trajectories in the net effect (mean IPSCs: 1120.8 ± 1047.7 pA and 474.2 ± 804.7 pA; mean EPSCs: 115.5 ± 44.5 pA and 318.7 ± 290.9).

To determine which parameter of our multi-parameter datasets drove most the variability of the PC responses observed, exploratory statistical tools were used. Specifically, principal component analysis (PCA) was performed on data from the 51 groups of GC to PC pathways in response to 3 and 7 stimuli.

The following twelve variables were used for descriptive correlations:

- average number of additional spikes in response to 3 and 7 stimuli (Add3, Add7)
- average numbers of omitted spikes (Om3, Om7)
- average durations of acceleration (AddDur3, AddDur7)
- average durations of delay(OmDur3, OmDur7)
- net effect (Net3, Net7)
- EPSC
- IPSC

As the E/I ratio is correlated with EPSC and IPSC variables, it was not considered for principal component calculations but added instead as a supplementary variable (Husson et al., 2009). It should be noted that the variables used did not have the same units; therefore variables were centered on their means and reduced to ensure standardization. Sets of independent principal components corresponding to linear combinations of the twelve variables were obtained from PCA analysis. Principal components with low variance (less than 1, **Figure R15.A**) were discarded leading to a reduction of the size of our dataset to the first two principal components. Dimensionality reduction to two expressed 67.85% of the total variance which significantly captured most of the variance of our dataset (95% quantil significance value of 45.5% when 12 variables and 51 samples are considered). Respective contribution of each of the twelve variables to the variance of the two principal components is illustrated in **Figure R15.B**. Importantly, delay durations elicited by long burst of GC inputs and the resulting number of omitted spikes appeared (without any assumptions) to contribute the most to the heterogeneity of PC responses observed (**Figure R15.B**), further validating the feedforward inhibitory circuit as an important source of diversity in the modulation of the PC discharge. In addition, the E/I ratio did not explain much of the variance (**Figure R15.B**), strengthening our previous conclusions that E/I ratios are not the key determinant for PC discharge modulation.

Three groups of PC spiking behavior could be objectively extracted by performing hierarchical clustering on the two first principal components of the PCA. Interestingly, these groups match with the delay, shift and acceleration groups observed earlier in **Results Part II**. Groups were computed so that the variance was maximal between them. Their projection onto the reduced plane (the two first principal components) is displayed in **Figure R15.Ci** and their more detailed characteristics (Add3, Add7, AddDur3, AddDur7, Om3, Om7, OmDur3, OmDur7, E/I, EPSC, IPSC) can be found in the annex section. Using this hierarchical clustering analysis, we also confirmed that the data from the E/I ratio set of experiments are representative of the whole population distribution (**Figure R15.Cii**). Additionally, the spiking behaviors and corresponding recorded successive EPSCs and IPSCs in response to 1, 3 and 7 stimuli for one representative cell of each of the three extracted groups are shown in **Figure R16.A**. Their value for EPSC, IPSC, E/I ratios, short-term synaptic plasticity of excitatory (PPR E) and of inhibitory synapses (PPR I) are displayed in the table **Figure R16.B**. It can be noted that the spiking behavior of the Purkinje cell cannot be predicted from the E/I ratio alone. The illustrative and representative shift cell displayed in **Figure R16.A** showed a low E/I ratio and therefore would be expected to be delayed in response to GCs stimulation. When measuring the dynamics of EPSCs and IPSCs during GC burst of stimulation, it appears that the inhibition was depressing in that case while it was facilitating in the delay group. In addition, the acceleration group showed strong EPSCs that were facilitating while inhibition was depressing. Altogether, these suggest that short-term dynamics could modulate the Purkinje cell discharge.

Conclusion

Combining all results: the time course of PC modulation for each GC group and condition, the excitatory and inhibitory synaptic weights, the E/I ratios, and the different groups of spiking behaviorsand combined PPR of the excitation and inhibition, brings into light the complexity of the determinants of PC discharge modulation. We described a cumulative effect of excitation while inhibition saturated when increasing the number of stimuli. This matched with the spiking behavior of the shift cells characterized by a shift in their net spike output towards more positive values. Together with our results from PCA and hierarchical clustering analyses, these strongly suggest that short-term dynamics of excitatory synapses might be a key determinant in the shifting spiking behavior observed, a hypothesis that we will test in the next part.

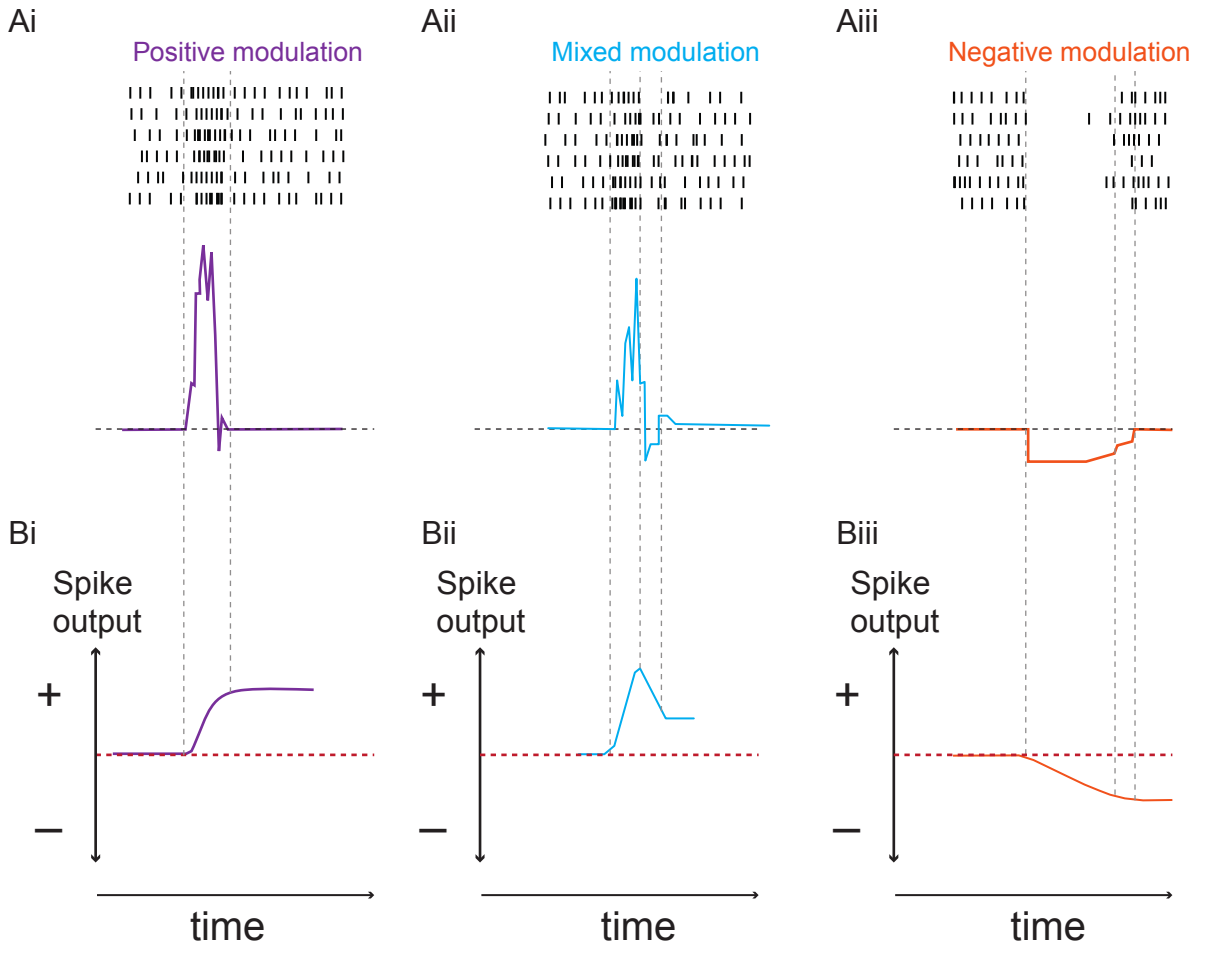

Figure R12. Discriminating biphasic Purkinje cell responses by studying the time course of the discharge.

A: Three types of modulation of the PC discharge (top) and their corresponding mean PSTH (bottom). **Ai**: Acceleration of spontaneous PC firing or induced additional spikes displayed as a positive monophasic mean PSTH; **Aii**: Acceleration followed by a delay in spontaneous PC firing exhibited as a biphasic mean PSTH response; Aiii: Delay in spontaneous PC firing or induced omitted spikes displayed as a negative monophasic mean PSTH.
B: The time course of the PC modulation is determined by computing the cumulative integral of the mean PSTH (displayed above).

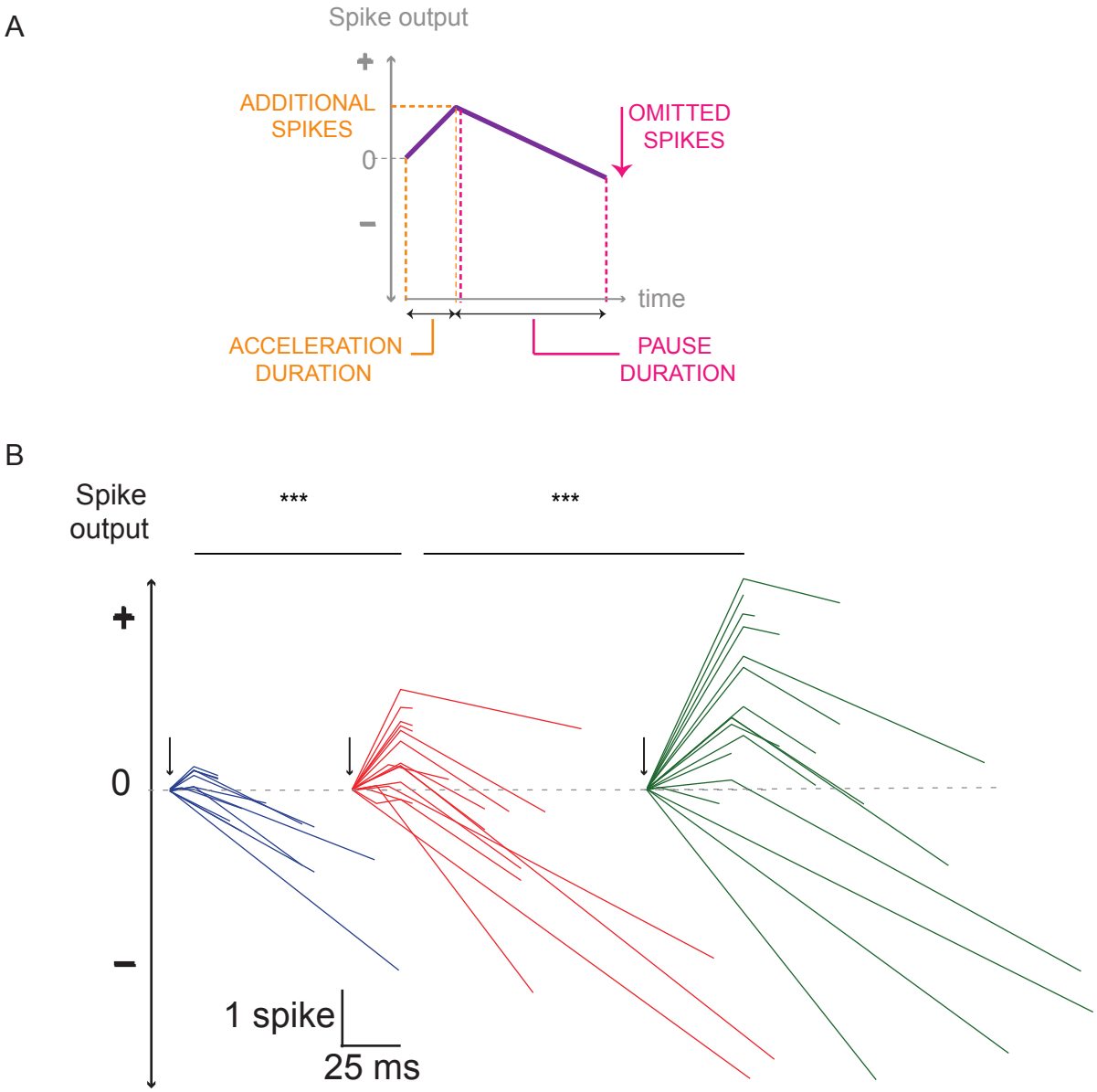

Figure R13. Wide diversity in the time courses of Purkinje cell modulation in response to subthreshold granule cells stimulation(s).

A: Four parameters were measured in the cumulative integral of the mean PSTH (see figure R12B) to assess the time course of the modulation: the number of additional or omitted spikes, and the duration of the acceleration or the pause.
B: For clarity of the illustration, only cumulative integrals of the mean PSTH of 17 PCs (from the E/I ratios set of experiments, figure R11) are displayed. Blue, red, green: time course for 1, 3, 7 GC stimulations. Arrows indicate the onset of the stimulation. Note the wide diversity of response for all the four parameters, in every stimulation condition. Statistical test used: one-way ANOVA on ranks, $P \leq 0.001$.

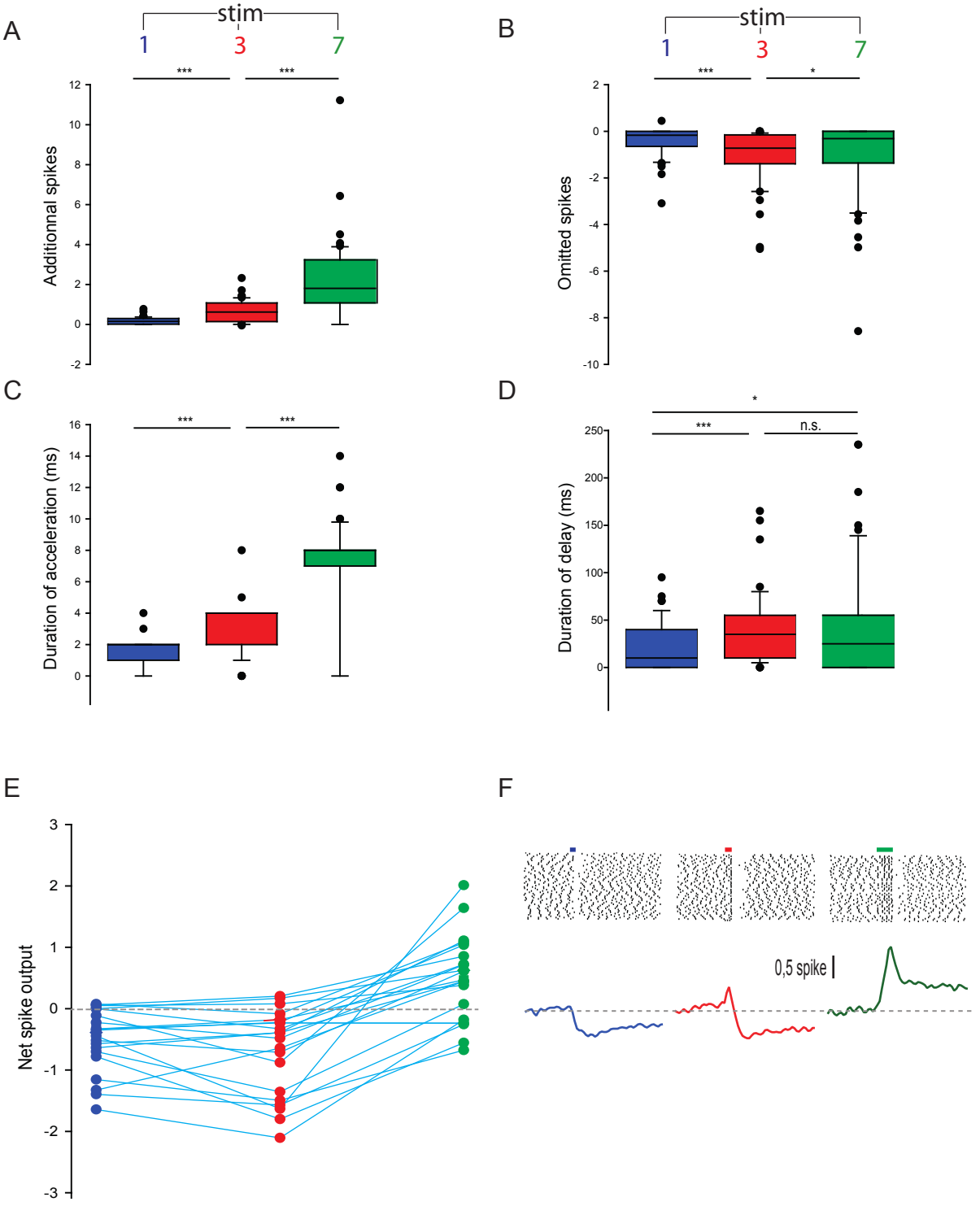

Figure R14. Quantification of the diversity in the time course of Purkinje cell modulation in response to subthreshold granule cells stimulation(s).

Group data (n =51) for the four measured parameters: the number of additional (*A*) and omitted (**B**) spikes, the duration of acceleration (**C**) and delay (**D**) in response to 1 (blue), 3 (red) and 7 (green) GCs stimulations. Statistical tests used: one-way ANOVA on ranks (**A**, **C**); Wilcoxon paired test (**B**, **D**). The four parameters show an increased variability when increasing the number of GC stimulations. While the number of additional spikes and the acceleration duration strongly increased when increasing stimulus number, few differences in the number of omitted spikes and the delay duration between 3 and 7 GC stimulations were observed. **E**: PC net spike output of the shift group. **F**: raster plots (top) and cumulative integral of the mean PSTH (bottom) of an example PC of the shift group. Note the increase in the acceleration duration and number of additional spikes along with a decrease in the pause duration and number of omitted spikes.

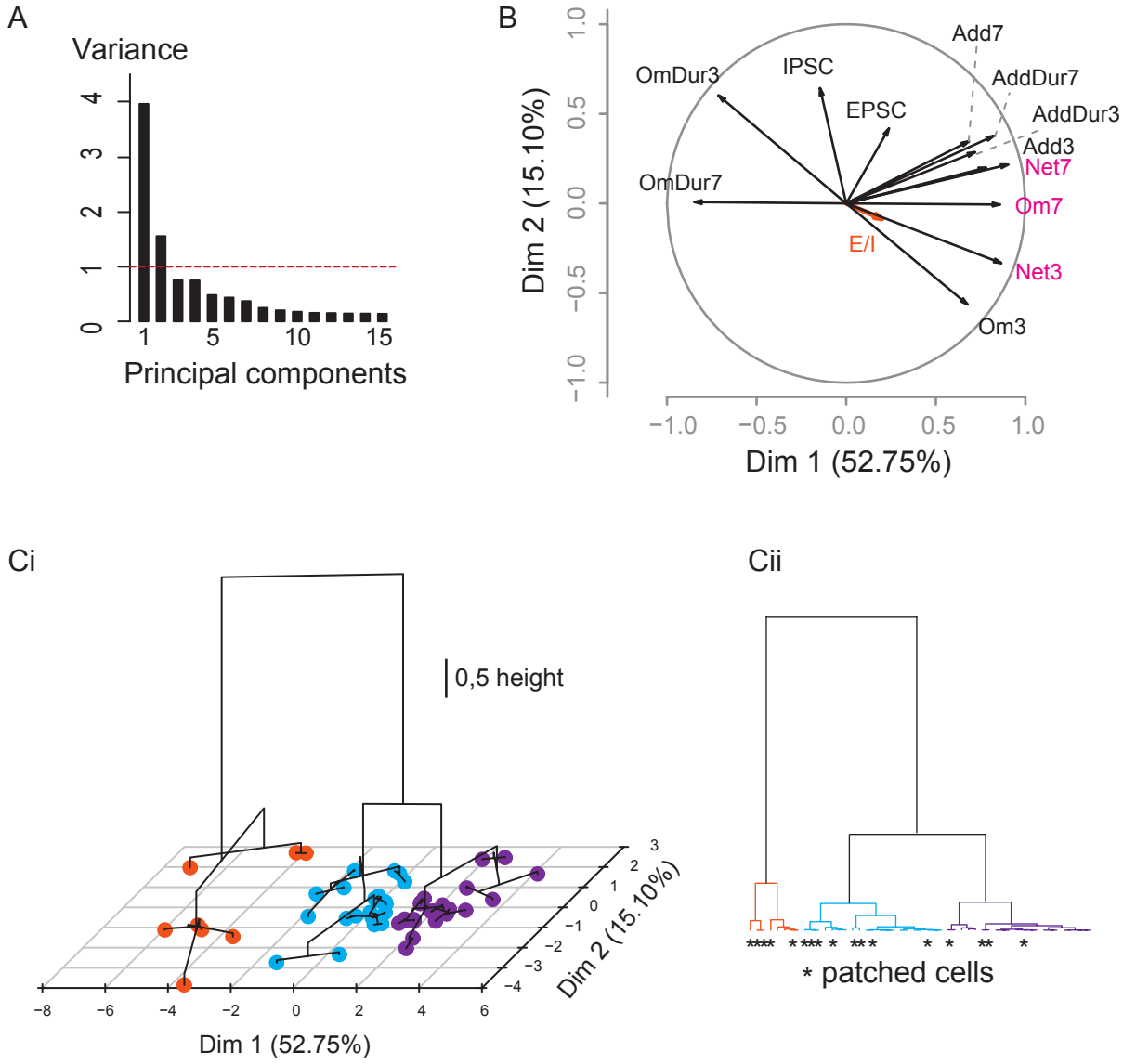

Figure R15. Heterogeneity of Purkinje cell responses explored using statistical tools.

Twelve parameters extracted from the time courses of the modulation of the PC discharge were considered: the average number of additional spikes in response to 3 and 7 GC stimulations (Add3, Add7), the average numbers of omitted spikes (Om3, Om7), the average durations of acceleration (AddDur3, AddDur7), the average durations of the delay (OmDur3, OmDur7), the net effects (Net3, Net7), EPSC and IPSC. The parameter(s) driving the most the heterogeneity of PC responses were determined by PCA from a group of 51 GC-PC pathways.

A: Variance is explained by the first 2 principal components (variance > 1).
B: Polar plot representing the respective contributions of each of the 12 parameters to the heterogeneity of PC responses. Net7, Om7 and Net3 contribute the most to the heterogeneity of PC responses while the contribution of the E/I balance is limited.
Ci: Projection of each of the PC time courses modulations on the two first dimensions. Dendrogram distance tree showing the clustering of PC responses into three groups of behavior that match with the delay (orange), shift (blue) and acceleration (purple) groups (figure R9B). **Cii:** The 17 PCs of the E/I ratios set of experiments (figure R11) are distributed in each of the three groups and therefore are representative of the whole population.
.

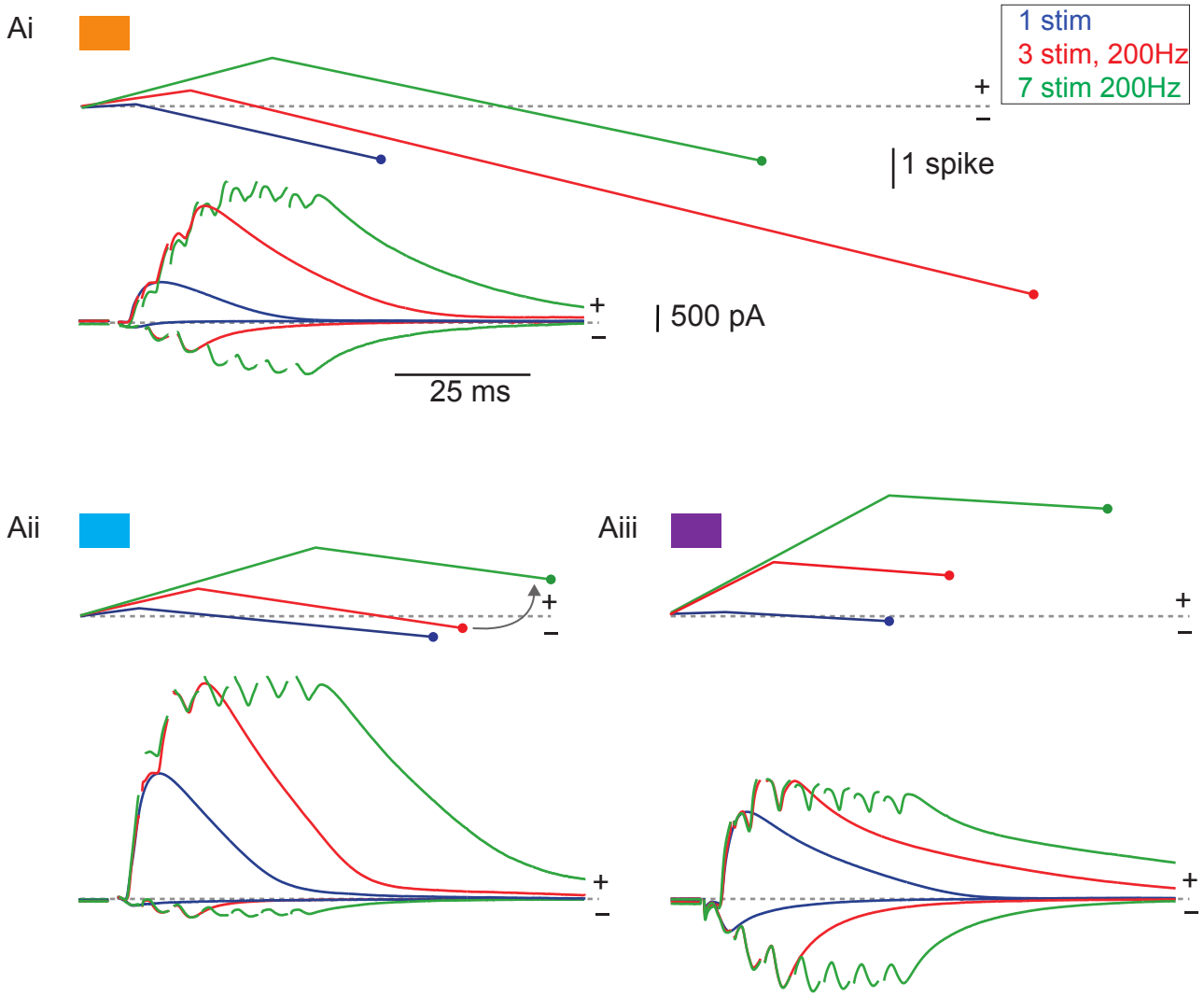

B

	EPSC (pA)	IPSC (pA)	E/I	PPRE	PPRI
Cell Ai	118	725	0.16	2.64	1.34
Cell Aii	210	2368	0.09	1.58	0.67
Cell Aiii	617	1675	0.37	1.57	0.41

Figure R16. Representative cells of the three groups of behavior identified in the GC-PC pathways

A: Time course of PC modulation (top) and recorded elicited EPSC and IPSC (bottom) are aligned at the onset of the stimulation and the same timescale is used to allow comparison.
B: Mean values of synaptic parameters.
Cell **Ai**: Representative cell of the delay group. The net spike output (dot) is negative in the 3 GC stimulation conditions although the excitation is strongly facilitating (PPR E = 2.64). EPSCs are relatively small and inhibition is facilitating (PPR I > 1). As a consequence, the inhibition predominates in response to all stimulation conditions. Note the extremely longer delay duration in response to 3 as compared to 1 stimulation.
Cell **Aii**: Representative cell of the shift group. The net spike output (dot) shifts towards positive values (indicated with the arrow) when increasing the number of stimulations. This can be explained by the strong inhibition that depresses while the excitation is facilitating. Excitation dominates over the inhibition only for long bursts of GCs stimulation.
Cell **Aiii:** Representative of the acceleration group. The net spike output (dot) is positive in the 3 GC stimulation conditions. EPSCs are strong and facilitates while inhibition depresses. Excitation predominates in response to all stimulation conditions.

PART V: THE COMBINATION OF SHORT-TERM PLASTICITY AND SYNAPTIC WEIGHTS CONTROL OUTPUT PATTERNS TRANSMITTED BY PURKINJE CELLS

Experimental approaches are limited and extracting the relative contribution of the excitation-inhibition (E/I) balance and short-term dynamics of synaptic connections to the diversity of PC output patterns is challenging. Therefore, we developed numerical simulation of the GC-PC pathways and initiated a collaboration with Dr Arvind Kumar (KTH Royal Institute of Technology, Sweden) who is specialist in computational neuroscience.

1. *Simulation of granule cell to Purkinje cell pathways*

Simulated GC-PC pathways was implemented in NEural Simulation Tool (NEST) software, a simulator for spiking neural network models that focuses on the dynamics, size and structure of neural systems. Short-term synaptic plasticity was simulated based on Tsodyks and Markram phenomenological model of frequency dependent synaptic transmission (Markram et al., 1998; Tsodyks et al., 1998), which assumes that a synapse is defined by a finite amount of resources and that synaptic responses to trains of presynaptic spikes are frequency dependent. Synaptic variables and parameters of Tsodyks and Markram model are the followings:

Our simulation of GC to PC pathways was based on five fixed parameters: the membrane time constants of EPSPs and IPSPs, recovery times of EPSPs and IPSPs, and EPSP-IPSP delay. The only free parameters of the numerical simulation were the E/I ratio - i.e. EPSP and IPSP - and short-term synaptic plasticity of excitatory and inhibitory synapses i.e. PPR E and PPR I. Because PPR is generally assumed to reflect the release probability, we used the probability of

release/recovered synaptic efficacy parameter (**U**) of Tsodyks and Markram model as a parameter for PPR allowing us to implement dynamic synapses.

2. *Determination of the short-term dynamics at the GC-PC pathways and calibrations of the simulation*

We first attempted to constrain the numerical simulation to physiological ranges in order to fit experimental data. We therefore calibrated EPSP, IPSP and EPSP-IPSP delay parameters to physiological values (**see material and methods**) and performed another set of experiments for PPR calibration/to choose acceptable PPR values matching our experimental conditions. Indeed, the only available data on short-term dynamics of excitatory GCs to PC synapses at 200 Hz were obtained from rats at 2.5 mM extracellular calcium concentration (Valera et al., 2012) while our recordings were performed in mice at 2 mM extracellular calcium concentration. Furthermore, no values of the resulting effect of combined short-term synaptic plasticities at the GCs-MLI- PC pathway have been reported so far.

Consequently, in transverse acute cerebellar slices, PCs where whole-cell patch clamped at - 60 mV and 0 mV to record elicited EPSCs and IPSCs respectively in response to sequential stimulations of GCs. Stimulations and recordings were performed exactly as for the E/I ratio set of experiments (**Figure R11** and **material and methods**). E_n and I_n were defined as the evoked EPSC and IPSC amplitudes resulting from the n^{th} stimulus (**Figure R17.A**). In all but one recorded cells, facilitation of excitatory neurotransmission was sustained during the train of seven stimuli. A modest PPR was observed at each stimulus number (**Figure R17.B**): PPR_{E2} = 2.19 ± 0.59 (n = 17), PPR_{E3} = 2.57 ± 1.41 (n = 7), PPR_{E4} = 3.16 ± 2.43 (n = 7); PPR_{E5} = 2.57 ± 1.79 (n = 7),PPR_{E6} = 1.98 ± 1.83 (n = 7), PPR_{E7} = 3.23 ± 1.83 (n = 7). These findings also illustrate the variability of PPR between GCs to PC pathways, which was at lowest between the 1^{st} and 2^{nd} pulses: PPR_{E2} ranged from 1.16 to 3.16. The highest variability in short-term plasticity was observed between the

4^{th} and the 5^{th} pulses: PPR_{E4} ranged from 1.00 to 7.31. This might contribute to the previously noted larger diversity of PC output in response to long GCs input bursts.

We observed a wide diversity in the short-term dynamics at the disynaptic GCs-MLI-PC pathway (**Figure R17.B**), as it could be expected by the fact that there are two synapses. A huge heterogeneity of PPR was observed following the 2^{nd} stimulation (**Figure R17.B**). PPR_{I2} ranged from 0.40 to 6.30 with a mean value of 1.49 ± 1.38 (n = 20). Recruitment of interneurons (and not only synaptic properties) is very likely to be involved in this facilitation. We measured the following mean PPR I: PPR_{I2} = 2.53 ± 0.63 (n = 16), PPR_{I3} = 0.96 ± 0.24 (n = 16), PPR_{I4} = 0.63 ± 0.18 (n = 13); PPR_{I5} = 0.34 ± 0.10 (n = 11), PPR_{I6} = 0.28 ± 0.09 (n = 9), PPR_{I7} = 0.23 ± 0.09 (n = 7). In many cases, separation of IPSCs was not possible at the end of the burst of stimulation, explaining the lower number of measures. Interestingly, we found a high variability, from facilitation to depression in response to the first four stimuli while depression systematically occurred from the 5^{th} spike of the burst (**Figure R17.B**), suggesting that short bursts might favor inhibition while long bursts would promote an excitation of the PC discharge. These findings support our hypothesis that short-term plasticities play a key role in the diversity of PC spike outputs.

Simulations were then implemented by reproducing PSTH responses of recorded PCs discharge by adjusting EPSP, IPSP, PPR E and PPR I. Simulations were run several times for each set of parameters and for each stimulation pulse. More importantly, we could reproduce experimentally observed modulations of the PCs discharge. Example of results obtained from the simulations corresponding to two experimentally recorded PCs (**Figure R7**) are shown in **Figure R18**. The simulated cell showing an increased spiking behavior (**Figures R18.Ai** and **R18.Bi**) was characterized by strong and facilitating EPSPs (3.0 mV at -70 mV) while IPSPs were small (-0.8 mV at -70 mV) and mildly depressing (**Figure R18.Ci**). Conversely, the simulated cell exhibiting a decreased spiking behavior (**Figures R18.Aii and R18.Bii**) was characterized by weak and strongly depressing EPSPs (1.2 mV at -70 mV) while IPSPs were strong (-1.2 mV at -70 mV) and mildly facilitating (**Figure R18.Cii**). Next, we evaluated PPR responses/sensitivity to variations in short-term dynamics in the simulation for both excitatory and inhibitory synapses (**Figure R19.A**). Synapses

progressively switched from a depression to a facilitation state when decreasing vesicle release parameter. More importantly, we could match simulated EPSP and IPSP short-term dynamics to the PPR of EPSC and IPSC observed experimentally (**Figure R19.B**).

Overall, the simulation allowed us to reproduce both PC spiking behaviors and short-term dynamics of the experimental recordings, validating our approach.

3. *Co-influence of E, I, PPRE and PPRI in Purkinje cell spike probability*

We then explored how the four parameters, E, I, PPR E and PPR I, influence PC discharge. 4536 simulations were performed using 8 different values of EPSP, 7 for IPSPs, 9 values for PPR I and 9 for PPR E (**Figure R20**). As expected, spike probability in PC discharge in response to the first two stimulations was the highest for strong EPSPs (see at 2.7 and 3.0 mV at -70 mV in **Figure R20.A**) providing that they are facilitating. Spike probability was the lowest when IPSPs were strong (see at -1.8 and -2.2 mV in **Figure R20A**), if not depressed. A null spike probability (white square in **Figure R20**) or even a pause in PC discharge (assessed by successive white squares in response to following stimulations) was observed from the 4th input spike when EPSPs were depressed, highlighting the importance of excitation for spike emission.

Importantly, a mosaic of colors is observed from the third stimulation response in which colors referred to spike probability, indicating that a wide range of spike probability can occur depending on the value of the four parameters (EPSP, IPSP, PPR E, PPR I) (**Figure R20**). This also means that any of these parameters can strongly influence PC spike output and thereby the contribution of the three other ones. Furthermore, these findings are in support of the wide diversity of modulation we demonstrated. This is particularly the case at the end of long bursts, in agreement

with the increased variability observed in chapter 2 between pathways in response to seven stimuli (**Figure R9.A**).

In addition, short-term dynamics directly influence spike probability. For fixed EPSP and IPSP sizes, therefore for a given E/I ratio, many outcomes could be obtained depending on PPR values (**Figures R20.Bi** and **R20.Bii**), which confirms our experimental results revealing that E/I alone does not determine PC spike output. Furthermore, this emphasizes the key role of PPR in shaping PC responses, which will be further discussed.

4. *Co-influence of E, I, PPR E and PPR I in Purkinje cell spike output patterns*

Spike probability investigations can be viewed as a multidimensional study of the time course of PC response, where average response is taken into account but not spike rank which could be different from trials to trials. Therefore, patterns of PC response to each trial were studied and the motifs were converted to “spike words” where response to each stimulation was weighted by 2^{n-1}, n being the stimulus number (**Figure R21.A**). Thus a response with 7 spikes elicited by the 7 stimuli will be converted to 127.

For one set of experiments, the occurrence of the first or second preferred word for different combinations of E, I, PPR E, PPR I and E/I were investigated for three and seven stimuli (not all data are shown). Interestingly, for mild facilitation of EPSPs (0.05 to 0.1) and mild to strong depression of IPSPs (0.2 to 0.5), small change in excitatory and inhibitory synaptic strengths massively modified PC output spike words (data not shown). Strong depression of EPSPs led to a null word (no spike) while strong depression of IPSPs allowed all stimulation to trigger a spike, thereby making information transfer independent of synaptic weights.

Importantly, changes in short-term synaptic plasticities dramatically affect the pattern of transmission in simulated GC-PC pathways (**Figure R21.B**). Interestingly, several combinations of parameters resulted in the same output spike words, which may have physiological implications.

We next explored the diversity of output spike words when modifying other parameters (not all data are shown). For a fixed set of short-term dynamics, a change in EPSP and IPSP weights could result in up to 40% increase in spike word diversity (**Figure R21.C**). For strong depression of EPSPs, change in synaptic weight had no impact on output words. However, when EPSPs were facilitating, changes in EPSP and IPSP weights had a strong effect in modifying the output. Importantly, this suggests that short-term dynamics are a key determinant of the PC output sensitivity for synaptic weights.

We also found that short-term dynamics can introduce diversity in output spike words. Indeed, for a fixed EPSP and IPSP combination, a change in short-term dynamics parameters increased the diversity at most by 20 % (data not shown) provided EPSPs were strong and IPSPs weak. Together, these findings revealed that in most cases, the short-term dynamics has a greater impact on the output spike word for stronger synapses.

5. *Purkinje cell output spike patterns are pathway specific*

Interestingly, in our experimental dataset, predominant pattern(s) of responses were observed in every analyzed cell (n = 38) (**Figure R22**). The first preferred word in

response to three stimuli occurred at least 26 % and up to 78 % of the trials (60 trials on average) with a mean of 47.6 ± 13.0 % while the second word occurred between 4.0 % and 15.0 % of the trials with an average of 27.3 ± 6.5 %. First and second word occurrences were on average lower in case of 7 stimuli: 29.3 ± 19.3 % and 15.8 ± 6.69 %, ranging from 9.0 % to 89.0 % and from 5.0 % to 40.0 %, respectively. This difference is very likely to arise from the increased word possibilities when expanding the number of stimulation. Indeed, the number of words per cell varied from 3 to 7 with a mean of 4.61 ± 0.97 in case of three stimuli while it ranged from 2 to 27 with 14.08 ± 5.83 in case of seven stimuli.

It should be pointed out that the number of spike words transmitted may be underestimated since a minimum of 256 trials would be required for each spike word to may have at least two opportunities of occurrence, hence to fairly approximate the "dictionary size" of the PC. This was not our aim, but could easily be investigated using our implemented simulation. In addition, a possible stochastic effect in PC spike output word is more likely to arise for short than for long input bursts. If we consider the number of possible ordered combinations: 8 and 128 permutations could be obtained in case of three and seven stimulations respectively. A five words diversity among eight possibilities would then correspond to 62.5 % of variability while 27 words among 128 combinations would represent 21.1 % of variability.

Together, these findings are particularly interesting when considering that long term plasticity mechanisms were pharmacologically blocked, therefore each recorded pathway had fixed PPR E and PPR I in addition to a fixed E/I ratio determined by the number of interneurons and GCs involved in the pathway as well as by the number and strength of active synapses defined by long-term plasticity mechanisms. These observations emphasized another potential level of pathway-specific coding strategy.

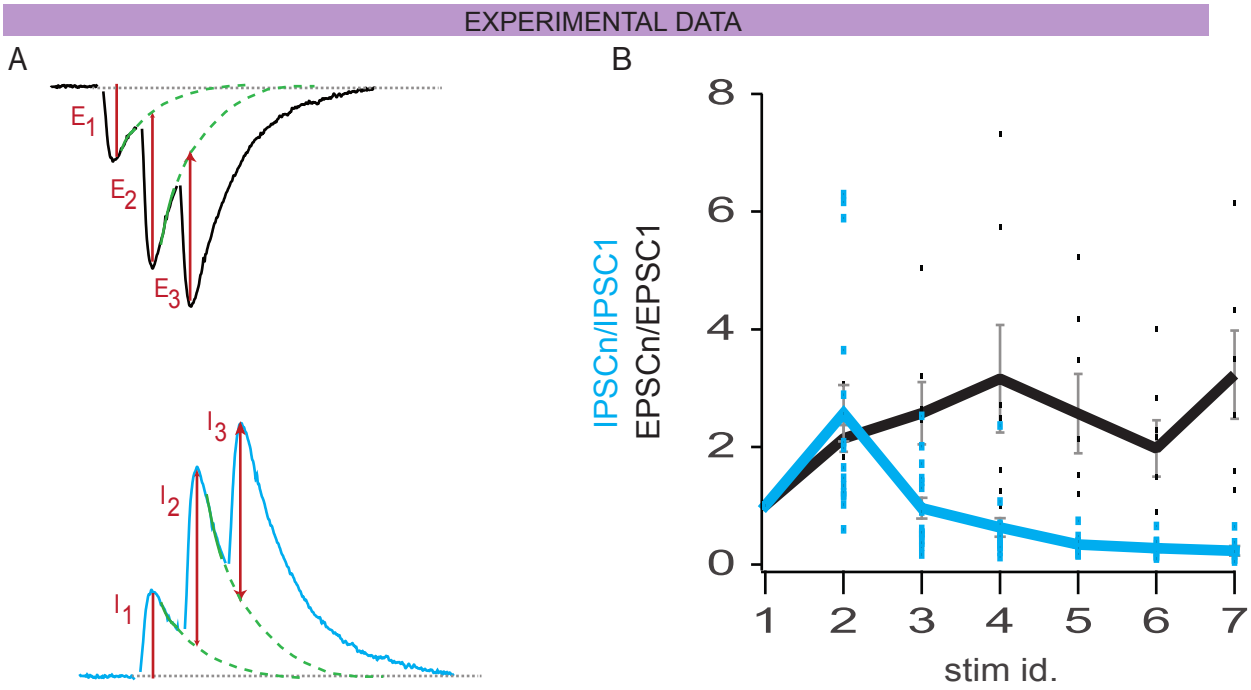

Figure R17: Short-term dynamics of excitatory and inhibitory GC-PC pathways.

A: Amplitudes of evoked EPSCs (top) and IPSCs (bottom) were measured after correction for the residual current of the preceding current.

B: Short-term dynamics of excitatory (black) and disynaptic inhibitory (blue) inputs onto the PC. Facilitation of excitatory neurotransmission is sustained during the train of seven stimuli. The short-term dynamics at the disynaptic GC-MLI-PC pathway is highly variable, from facilitation to depression, but depression systematically occurs at the end of the stimulation burst.

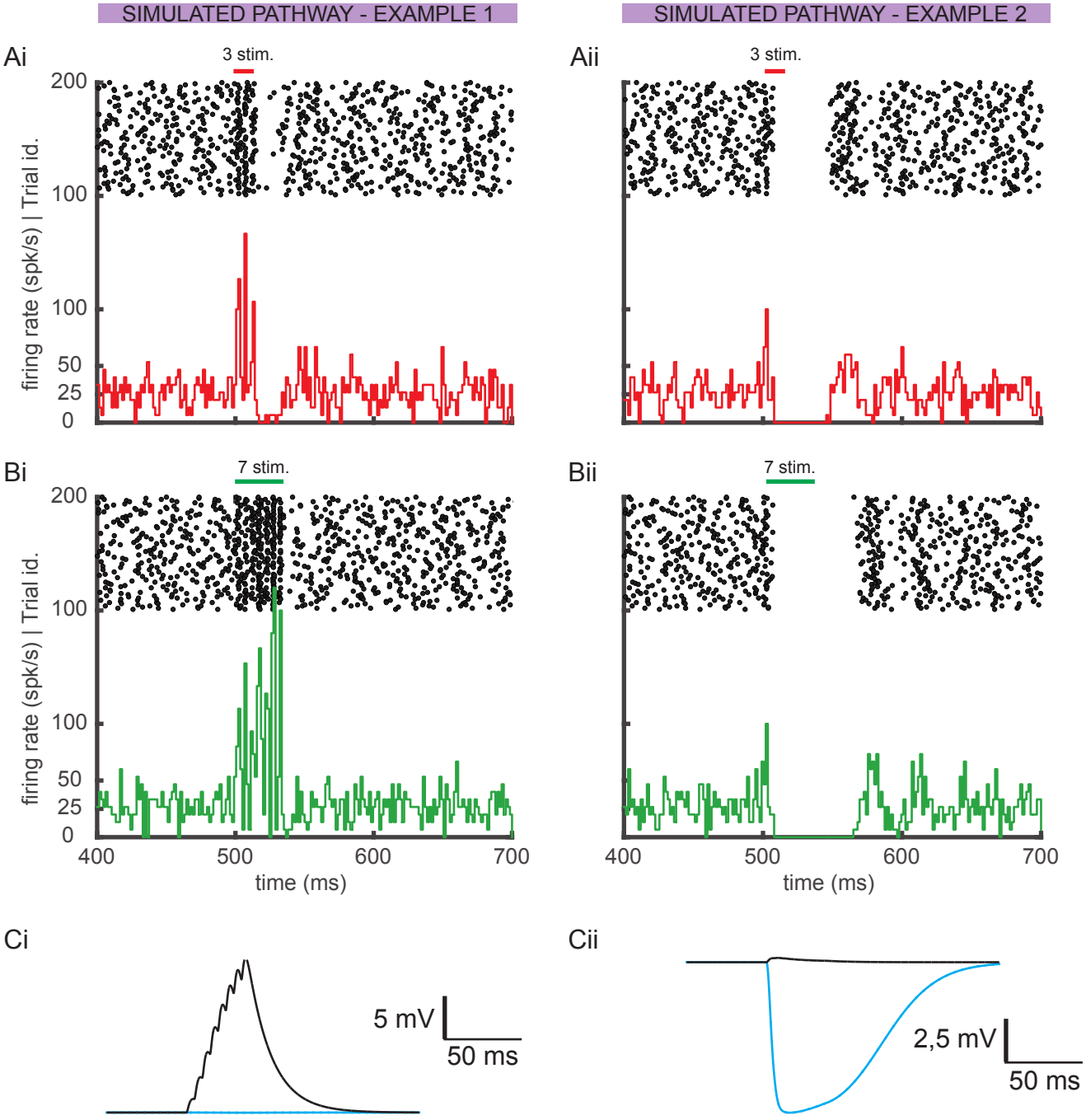

Figure R18: The numerical simulation reproduced experimentally observed Purkinje cell spiking modulations

Data obtained from the simulations of two experimentally recorded PCs (displayed in figure R7). **Ai**, **Bi**, **Ci**: Simulated PC from the acceleration group. **Aii**, **Bii**, **Cii:** Simulated PC from the delay group. **A**, **B**: Raster plot (top) and corresponding mean PSTH (bottom). Simulations could systematically reproduce mean PSTH. **C**: EPSPs (black trace) and IPSPs (blue trace) parameters required to reproduce mean PSTH. **Ci**: EPSPs were strong and facilitating and IPSPs were small and depressing. **Cii**: EPSPs were weak and greatly depressing and IPSPs were strong and facilitating.

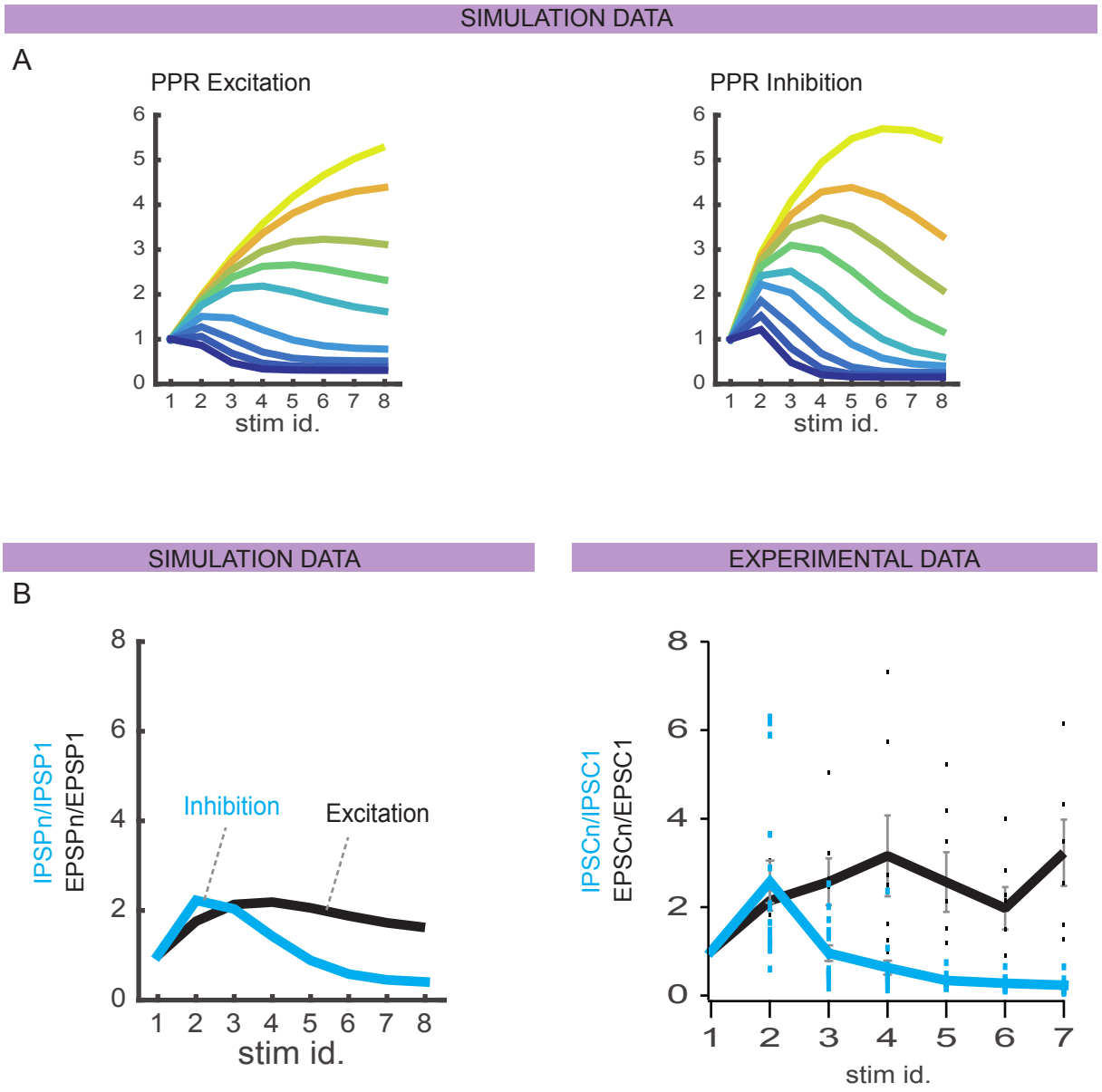

Figure R19: Short-term dynamics of simulated excitatory and inhibitory synapses reproduced experimental data.

A: Calibration of the short-term dynamic for excitation (left) and inhibition (right) in the numerical simulation. The range of short-term dynamics was explored by modifying the synaptic dynamics variable (Ua, see material and methods) while keeping EPSP and IPSP parameters unchanged. The different color lines show simulated data using different synaptic dynamics variable, from depression (bottom) to facilitation (top).
B: EPSP and IPSP short-term dynamics (left) could be tuned to match with the experimental data (right). Left: the two samples are extracted from A (blue).

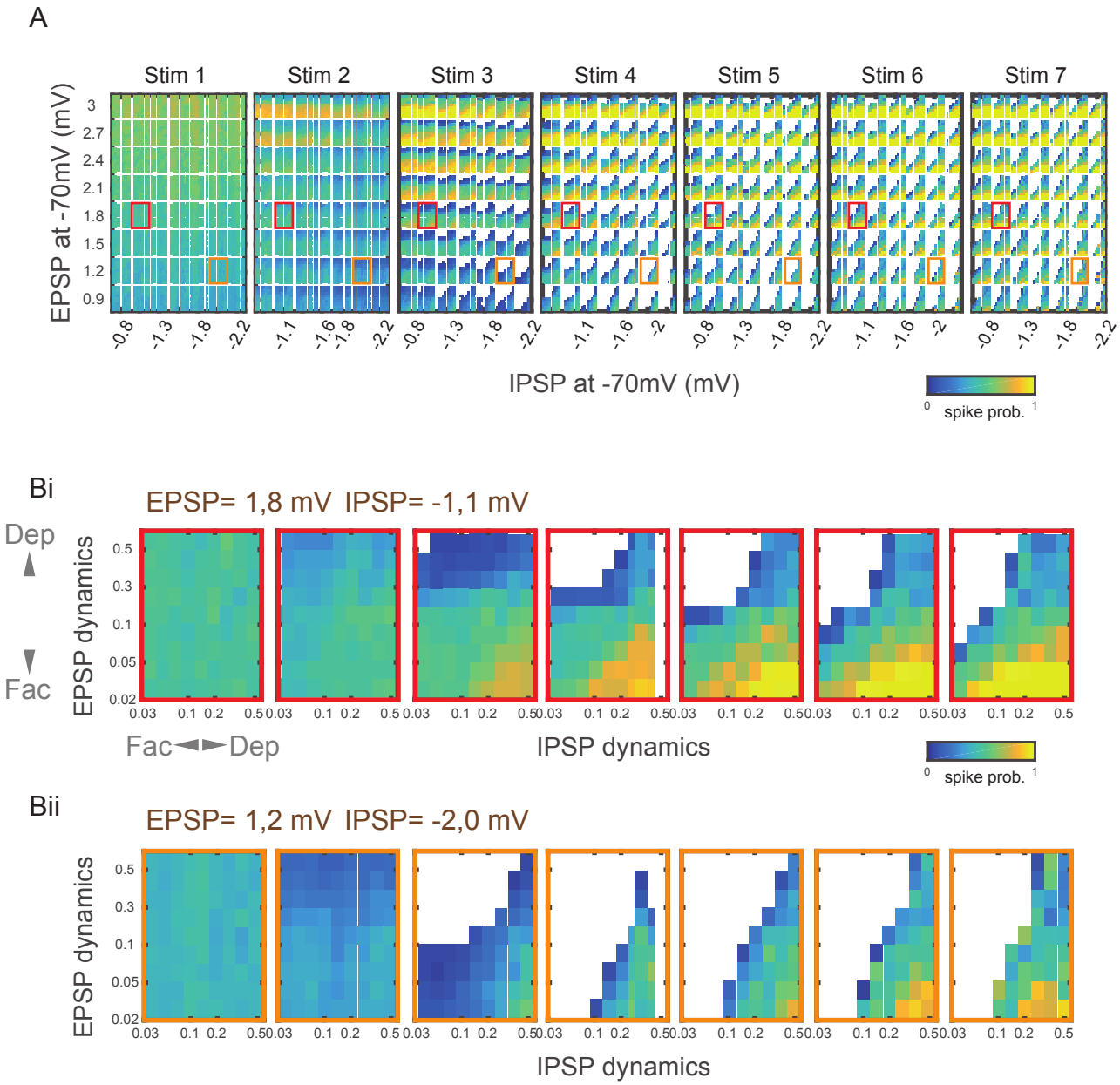

Figure R20: Simulated co-influence of E, I, PPR E and PPR I in PC spike probability.

A: PC spike probability as a function of EPSP and IPSP amplitudes (outer axis) in response to each of the seven GCs stimulus (black subpanels). Blue to yellow scale corresponds to a low to high spike probability. Each subpanel is subdivided into smaller inner squares displaying the PC spike probability as a function of short-term dynamics. EPSPs are depressing from bottom to top. IPSPs are depressing from left to right. Spike probability was measured in a window of 5 ms after the onset of the stimulus. Each of the four parameters can strongly influence PC spike probability.
Bi: Effects of the short-term dynamics of excitation and inhibition onto PC spike probability for a fixed high E/I ratio. Data extracted from A. White inner squares corresponds to a null spike probability. Each small colored inner square correspond to one simulation.
Bii: Same as Bi but for a low E/I ratio.

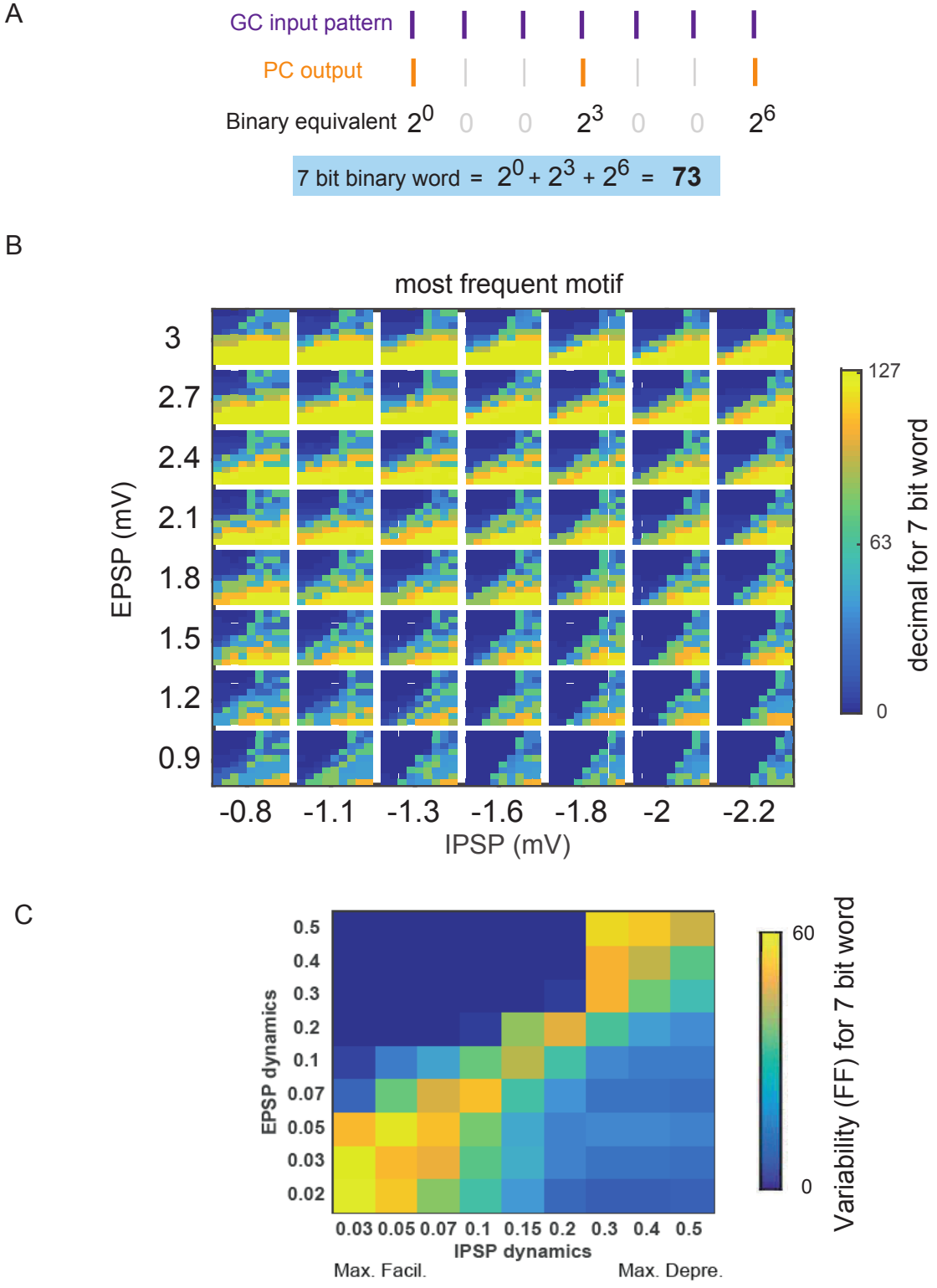

Figure R21: Simulated co-influence of E, I, PPR E and PPR I in PC spike words

A: Conversion of the PC discharge in response to GCs stimulation into spike words. Response to each stimulus was weighted by 2n-1, n being the stimulus number.
B: Most frequent motif as a function of EPSP and IPSP amplitudes (outer axis) in response to seven GCs stimulation. Dark blue indicates a null spike word (no spike/pause). Yellow indicates a full response (7 output spikes). Importantly, small changes in short-term dynamics of excitation and inhibition dramatically modify PC output word.

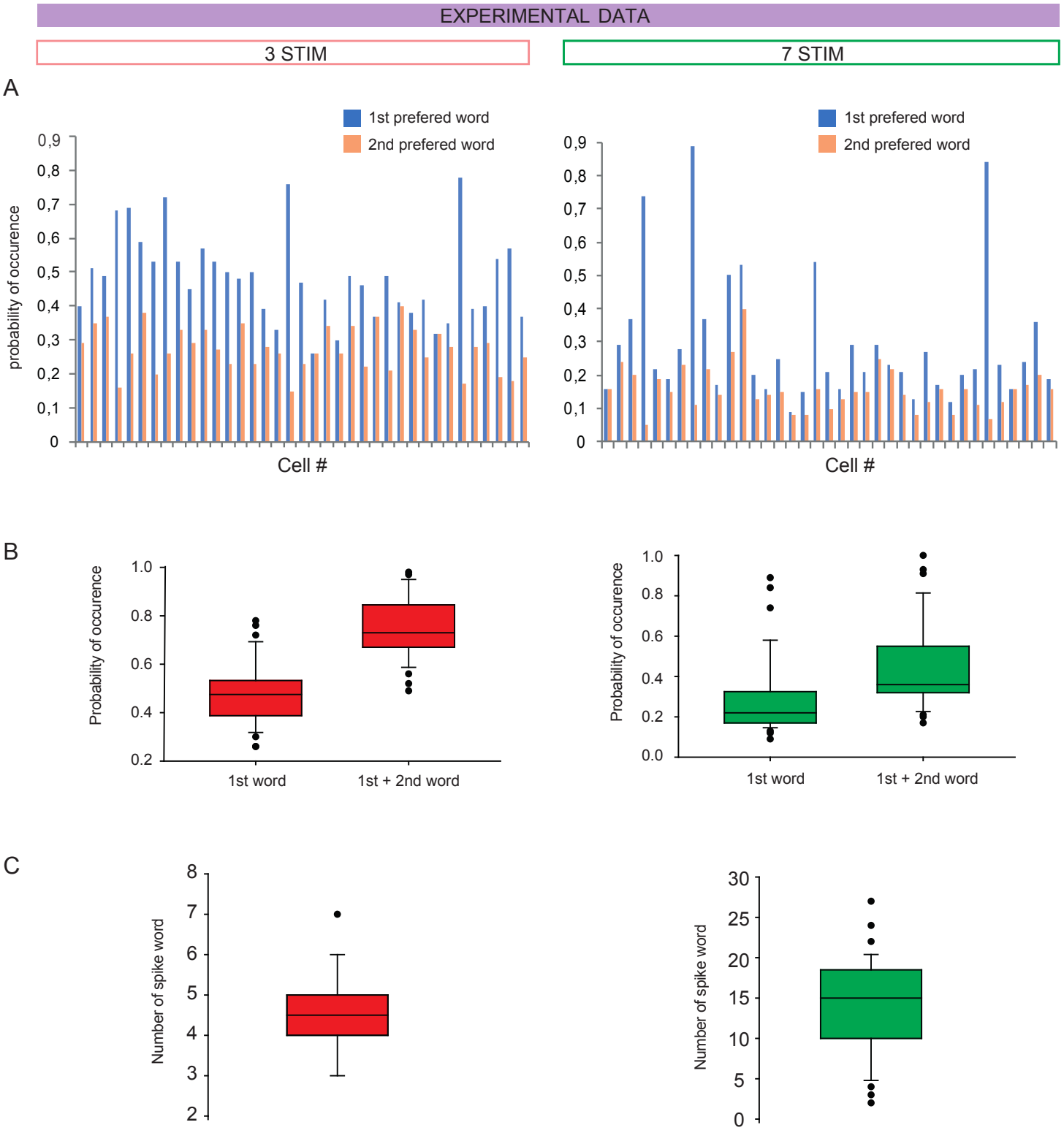

Figure R22. Preferred spike words in experimental recordings.

A: Probability of occurrence of the first and second most frequent PC spike words in response to three (right) and seven (left) GC stimulations.
B: Boxplot showing the mean and variability of the first (left colored box) and second (right colored box) preferred words in response to three (red) or seven (left) GC stimulations.
C: Boxplot showing the mean and variability of the number of words in response to three (red) or seven (left) GC stimulations. The number of motifs increases with the number of stimulations.

DISCUSSION

Our findings revealed that *in vivo* conditions can be partially reproduced in cerebellar acute slices. In addition, we found that subthreshold activations of different groups of GCs modulate PC discharge with a wide diversity of outcomes. Our data showed the importance of excitation for spike transmission and of feed-forward inhibition in shaping PC spike output. Furthermore, we revealed that E/I balance influences but does not predict PC discharge modulation. Finally, we uncovered a huge heterogeneity in short-term dynamics at GC to MLI to PC pathways and demonstrated its key role in determining the modulation of PC discharge.

1. *Critical analysis of the in vitro model used*

To study the modulation of the PC discharge in response to subthreshold GCs inputs, we chose the acute slice model because stimulation and recording electrodes can be precisely positioned and neurons/microcircuits pharmacologically manipulated without interfering with global networks. However, the reduced synaptic connectivity leads to a decrease in synaptic background bombardment (Paré et al., 1998) causing a reduction in: tonic depolarization, membrane conductance (shunt) and membrane potential fluctuations (decreasing input noise). Importantly, although never directly studied yet in the PC, these modified operating conditions have been shown to change the integration mode of synaptic inputs in pyramidal cells, converting them from integrators to resonators in *in-vivo* like conditions (Prescott et al., 2008). The *in vitro* low conductance state therefore potentially leads to an overestimation of the effect of synaptic inputs as well as to a falsely increased reliability of the threshold for spike initiation which would explain the more regular spontaneous firing of PCs observed *in vitro* (Häusser and Clark, 1997) as compared to *in vivo* (Goossens et al., 2001; Shin et al., 2007). As short-lived and/or subtle modulations of the PC discharge could be expected in our study, it was crucial to develop a strategy to minimize this artifact, although the amount of *in vivo* synaptic bombardment or conductance state of PC is not known. By applying a high frequency optogenetic illumination (mimicking patterns of natural mossy fiber inputs) onto acute cerebellar slices of transgenic mice

expressing ChR2 in mossy fibers, we could increase PC discharge irregularity as observed *in vivo.*

One could have considered using dynamic clamp by injecting current through the patch pipette (as in the pyramidal cells study) but our approach instead conferred some invaluable advantages. First, it allows the activation of dendritic conductances producing the shunting effect and increase in membrane noise. Second, we could combine it with non invasive extracellular recordings of PCs. Last, PC discharge irregularity is known to be regulated by both excitatory and inhibitory synaptic inputs (Llinás and Sugimori, 1980; Raman and Bean, 1999) that we could both mimic as barrages and precisely control their amplitude with illumination intensity.

As GCs are activated as patches upon sensory stimulation *in vivo*, we chose to reproduce GC firing patterns by electrically stimulating their somas and not PFs that are likely to arise from sparsely distributed GCs (Kunzle, 1987). Indeed, GCs originating from the same progenitor cells were found to project neighboring PFs while their somas were positioned through the entire depth of the GC layer (Zong et al., 2005; Espinosa and Luo, 2008). It should be acknowledged that the stimulated GCs may differ from the combination of the ones that would have been physiologically activated *in vivo*. Nevertheless, they are likely to be contacted by mossy fibers from the same origin since mossy fibers arising from the spinal cord were shown to innervate the superficial GC layer of the studied anterior vermis while those from the basal pontine nucleus target deep GCs. However, very recent mappings of PF synaptic inputs in crus II of anesthetized mice revealed spatially clustered active PFs (interspaced by about 8.7 µm) in response to sensory stimulation (Wilms et al., 2015). In addition, the authors labeled neighboring GCs and revealed sparsely distributed PFs. Taken together, these findings may rather support the PF stimulation configuration to be better suited for mimicking physiological inputs, although it locally triggers higher depolarization in PC dendrites and glutamate spillover (Marcaggi and Attwell, 2007). It would be actually interesting to investigate whether the same diversity of PC discharge modulations would be obtained if stimulating PFs in our model. Transfecting subsets of mossy fibers could have been a way to generate specific mossy fiber inputs, by for example performing stereotaxic injections of viral constructs carrying ChR2(H134R) in a given precerebellar nucleus.

Using photostimulation, they could have been selectively excited, and their discharge pattern and frequency controlled. However, this approach would not be compatible with our *in vivo*-like model since simultaneous high frequency activation of the two segregated populations of mossy fibers would be required.

2. *Diversity of Purkinje cell discharge following sensory-like inputs*

Although increasing data support a non-uniform information processing at the cerebellar GC to PC pathways (for a review: Cerminara et al., 2015), heterogeneous outcomes in PC discharge have not clearly been demonstrated so far. Here, we provide some evidence that PCs exhibit three types of spiking behaviors in response to GC stimulation, displaying either an increase, a decrease, or both an increase followed by a decrease in simple spikes while only monophasic excitatory responses were observed when blocking inhibitory neurotransmission. Previous *in vitro* studies using subthreshold stimulation of PFs also documented monophasic excitatory and biphasic outputs (Otis et al., 2005; Mittmann et al., 2007), but never in response to the same input pattern. In addition, none to our knowledge have reported purely inhibitory PC spike output in response to GC/PF stimuli, except for one control experiment in the work of Walter and Khodakhah (2006, their figure 7B), which was not further investigated and discussed by the authors. Nevertheless, PC monophasic inhibitory responses were observed when directly stimulating MLIs (Mittmann et al., 2007). Obviously, the fact that most studies were performed with inhibition blocked explained why this has been precluded so far. In addition, the commonly used stimulation of the PFs seemingly activated a mixture of PFs driving excitation and inhibition masking any pure inhibitory effect.

Importantly *in vivo* a wide diversity of sensory-induced changes in PC simple spike responses has been reported, depending on the sensory inputs and the area stimulated. Peripheral tactile stimulation either increases or decreases simple spike

discharge in PCs (Bower and Woolston, 1983; Ekerot and Jörntell, 2001) according to the stimulus location. Conversely, whiskers or perioral stimulation frequently triggered biphasic responses (Bosman et al., 2010; Wilms et al., 2015). The variability in PC response profile is likely to mirror the position of the recorded PC with respect to the active patches of GCs (Valera et al., 2016).

Biphasic responses seemingly arise from the recruitment of both excitation and inhibition by active mossy fibers. Alternatively, in cerebellar cortical zones where receptive fields of the mossy fibers and CFs overlap, biphasic responses could putatively reflect the complex spike pause, although the decrease in spiking turned out to be mostly independent of complex spike occurrence (Bosman et al., 2010), rather supporting the implication of MLIs. Some tri-phasic responses showing a second increase in the simple spike discharge of PCs have also been documented *in vivo* (Bosman et al., 2010; Wilms et al., 2015), which we did not observe. Several putative explanations for this difference can be raised. First, these may arise from simple spike-complex spike interactions that trigger increased post-stimulus frequencies which would correspond to the third component of the tri-phasic response. Yet, CFs were purposely not stimulated in our experiments. Alternatively (or complementary), this could be input specific since recordings in these studies were performed in crus II known to receive direct inputs from the trigeminal nerve and indirect cortico-pontine inputs respectively leading to short and long latency responses (Morissette and Bower, 1996), which is consistent with the double positive peaks of the triphasic response, while GCs in our experiments were synchronously activated with electrical stimulation. Interestingly, subthreshold responses of PCs were recently reported i*n vivo* in response to brief (70 ms) sensory stimulus (airpuffs to the perioral region) (Wilms et al., 2015). Only a few additional and/or omitted spikes were observed (a median of 0.4 additional spikes and 0.5 missed spikes), comparable to what we obtained. Taking together, we could assume that the modulations elicited in our study are observed *in vivo*.

3. *Feed-forward inhibition shapes Purkinje cell output and expands its diversity*

We confirmed the decrease in PC spiking to be mediated by MLIs as previously reported (Smith and Otis, 2005, Mittmann et al., 2007), although a contribution of afterhyperpolarization, i.e. hyperpolarization induced by calcium-activated potassium channels cannot be ruled out in our experiments and would require further investigations.

The observed number of additional spikes when blocking inhibition was in agreement with previous study using similar subthreshold stimulation of a beam of PFs (Mittmann et al., 2005). In our experiments, most of the cells exhibited a decrease in spiking, (preceded or not with a transient increase), which reflects a preponderance of feed-forward inhibition. This is not surprising considering that a single PF is able to elicit a spike in MLIs (Carter and Regehr, 2002; Brenowitz and Regehr, 2007) and that IPSCs triggered by one interneuron strongly shape PC spike output (Haüsser and Clark, 1997; Mittmann et al., 2007). Similarly, feed-forward inhibition was also observed when stimulating a single GC (Barbour, 1993). In addition, the subthreshold level of our stimulation imposes some limitations to the range of excitation and not for the inhibition (only non saturating excitatory responses were selected), which could explain the prevalence of FFI. Lastly, because stimulated GCs were located several tens of micrometers laterally to the recorded PC, GCs ascending axons believed to provide strong excitatory inputs (Sims and Hartell, 2006) were not involved in the effect.

The rapid onset of the inhibition recorded matches with previously reported data (Eccles et al., 1967; Brunel et al., 2004; Mittmann et al., 2005). Through this fast activation of feed-forward inhibition, the time window for spike transmission was limited enforcing precise spike timing in PC output. It is interesting to note that for a few cells, evoked delay in ongoing firing was immediate. This is likely to result from the subthreshold level of excitation in our experimental conditions. It could possibly also arise from the recently discovered instantaneous (non synaptic) ephaptic inhibition provided by the BC pinceau (Blot & Barbour, 2014), which may avert the

transient excitation of PC by suppressing synaptic delay. Alternatively, excitatory GCs to PC synapses could be silenced (Isope and Barbour, 2002).

The parameter contributing the most to the diversity of modulation highlighted in our data was the pause duration and omitted number of spikes, supporting the role of the inhibition in expanding PC output diversity in line with previous experimental and theoretical studies (Haüsser and Clark, 1997; Solinas et al., 2006). It is worth mentioning that feed-forward inhibition onto MLIs is likely to contribute to the spike output variability by regulating feed-forward inhibition onto PCs (Mittmann et al., 2005) and would require further explorations.

4. *Influence of E/I ratios on the cerebellar cortical output*

The balance between excitation and inhibition has been the long-standing focus of interest in physiological neurosciences and was found to be critical in determining the output of many brain structures (for review see Isaacson and Scanziani, 2011) including the auditory cortex (Wehr and Zador, 2003) and the somatosensory cortex (Pouille et al., 2009). In contrast to these, in this thesis we provided evidence for a non unique influence of the E/I ratio on the cerebellar cortical output. This is supported by previous dynamic clamp studies in PCs (Mittmann et al., 2007), where the authors on one hand showed a modification of the PC spike output when balanced LTD of synaptic excitation and inhibition was performed (thereby for a fixed E/I ratio), while on the other hand the extent of the change was found to differ with E/I ratios.

The physiological range of E/I ratios at GC to PC pathways was not known. The only studies exploring E/I focused on its effect onto the PC spike output and were based on simulations (Mittmann et al., 2007; Steuber et al., 2007). Here, our data demonstrate a wide range of naturally occurring E/I ratios (and synaptic strengths) distributed across GC to PC pathways. Although never studied before, this result is expected when considering the synergistic plasticities induced in the

microcircuit (for review see Gao et al., 2012) where the same teaching signal (complex spike) either potentiates excitatory or inhibitory inputs arising from a set of PFs onto the PC, but not both types of inputs (Bell et al., 1997; Han et al., 2000; Jörntell and Ekerot, 2002; Coesmans et al., 2004). Whether such diverse E/I ratios also physiologically exist in the cerebellar posterior lobe and hemispheres remains to be investigated. Besides, it should be mentioned that we may have underestimated E/I ratios owing to space clamp errors (Williams and Mitchell, 2008), but this is unlikely to change the heterogeneity observed.

Importantly, this diversity confirms the predictions from a newly published work performed in the same cortical zone (anterior vermis) that demonstrates heterogeneous connectivity patterns of GCs excitatory inputs onto PCs as well as onto MLIs (Valera et al., 2016). Remarkably, those spatially heterogeneous strengths were conserved across animals and shaped by long-term plasticity induction protocols. In addition, conditioning of simultaneous long-term synaptic plasticity at the GC to PC pathway in acute slices was previously reported to differently alter inhibitory (not excitatory) inputs received by the PC (low-frequency stimulations depressed evoked di-synaptic IPSCs while they were potentiated after PF burst stimulations and evoked EPSCs were potentiated in both conditions) (Smith and Otis, 2005). Lastly, in an independent set of experiments the authors showed that these same protocol increased PC spike following low-frequency stimulations while producing biphasic spike output after PF burst stimulations.

Altogether with our findings, these suggest long-term plasticity as an important trigger in the heterogeneity of modulation of the PCs discharge. Although technically difficult, the combined exploration of the interplay of the three: LTP/LTD, E/I ratio and PC spike output is still missing and will take us one step forward the understanding of the physiological outcomes of cerebellar cortical information processing.

5. *Short-term dynamics of excitation and inhibition determines Purkinje cell discharge*

Despite having being the centre of investigations for years in the cerebral cortex (Markram and Tsodyks, 1996; Galarreta and Hestrin, 1998; Gabernet et al., 2005) or hippocampal areas (Thompson and Gahwiler, 1989; Torborg et al., 2010; Bartley and Dobrunz, 2015), the effect of simultaneous short-term dynamics of excitatory and inhibitory synapses in shaping synaptic efficacy or spike output has not been explored much in the cerebellum. Here, we provide the first investigation of the resulting influence of simultaneous short-term dynamics onto both the E/I ratio and spike output at the granule to PC pathway. The fact that parameters were all explored at the same pathway is a strength in our work (and a prerequisite now) considering the heterogeneous organization of the cerebellar cortex. Our study highlighted the direct influence of short-term dynamics of excitation and inhibition onto the spike probability in PCs and consequently onto the pattern of output spikes produced by the PC.

- **Sustained spike probability and variability of the excitatory driven group**

When exploring STD, we found a facilitation of the excitatory GC to PC pathways in response to high frequency stimulation as widely acknowledged (Dittman et al., 2000; Beierlein et al., 2007; Valera et al., 2012) with a modest and reliable paired-pulse facilitation, in agreement with a previous study using the same stimulation configuration and frequency (Valera et al., 2012). Furthermore, this same study demonstrated that high frequency inputs were accurately transmitted at GC-PC connections, supporting the sustained increased spike probability we observed in PCs. More specifically, these specific synaptic properties of GC-PC connections included a low probability of failure in synaptic transmission (i.e. not releasing any synaptic vesicles) as well as the recruitment of release sites which were quickly replenished during high frequency stimulation preventing vesicular depletion.

Furthermore, those extra release sites required at least one conditioning pulse to be recruited, which would explain the variability we observed from the second pulse.

Considering that short-term dynamics are frequency-dependent, it would be interesting to perform the same set of experiments over the wide range of frequencies that were observed *in vivo*, and confirm predictions from our simulations by performing the same experiments while manipulating short-term dynamics pharmacologically.

- **To shift or not to shift – the input-pattern-dependent short-term dynamics of inhibition as a trigger in the shift**

The shift in spiking behavior in PC responses between short and long bursts of stimulations impressively illustrates how strongly STD can increase PC output diversity and dramatically modify the net effect to its opposite outcome. Interestingly, our data revealed that E/I ratios could be dynamically increased with short-term dynamics and could possibly trigger a shift in the spiking behavior. This contrasts with the decreased or equalized E/I ratio effect of short-term dynamics observed in the cerebral cortex (Galaretta and Hestrin, 1998; Varela et al., 1999; Xue et al., 2014), which is not surprising given the different and specific functions those two structures serve.

Then, how the feed-forward inhibition circuit can dominate over the direct excitatory circuit at the onset of burst stimulation while being dominated at the end of the burst stimulation? In our experiments, the feed-forward inhibitory circuit was dynamically recruited during high frequency stimulation as documented by Bao et al., (2010), and in a more complex and unpredictable way than the direct excitatory circuit. This in part reflects the differences in spike probabilities between the heterogeneous populations of MLIs (Bao et al., 2010). Importantly, as interneurons could be recruited at GC-MLI synapses at the second stimuli, short-term depression of di-synaptic inhibition could be counterbalanced. This would favor a dominance of inhibition over the excitation in response to short burst of stimulation. In addition, the known less reliable high frequency transmission of interneurons could produce some

failure of transmission at GC-MLI synapses and may contribute to prevent from early short-term depression of di-synaptic inhibition.

Although in our study the identity of the MLIs could not be identified, the influential work from Bao and colleagues (2010) allows us to speculate. The authors indeed revealed two mechanisms supporting the shift in spiking behavior observed. First, they showed a powerful difference in synaptic strength of BC - PC synapses and SC-PC synapses, BC-PC synapses being sevenfold stronger. Secondly, they highlighted differential short-term synaptic plasticity of the PF synapses where PF-BC synapses quickly depressed (within tens of milliseconds) while SC-PC facilitates in response to high frequency stimulation (Bao et al., 2010). Therefore, the shift in spiking behavior might be highly dependent on the short-term dynamics of PF-BC. Importantly, these were found to be shaped by presynaptic LTP/LTD mechanisms (Smith and Otis, 2005; Bao et al., 2010), where cAMP-dependent presynaptic LTP is induced in response to high frequency bursts (Salin eta l., 1996; Chen et al., 1997; Smith and Otis, 2005) while LTD is triggered by low frequency stimulation (Smith and Otis, 2005).

Together, the feedforward inhibitory circuit seems to be rearranged/remodeled by modifying the dynamics of synaptic transmission depending on the temporal organization of GCs inputs. Importantly, short-term dynamics seems to act as a gatekeeper, controlling the gain of each of the input spikes, and possibly changing the signal that is transmitted downstream by shifting the integration mode of PCs from integrators to coincident detectors.

6. *Patterns of Purkinje cell spike output: diversity, specificity, significance and readout by DCN*

One very interesting outcome of our work is that although PC output diversity could not be explained by either the E/I ratio or the short-term dynamics of excitation and di-synaptic inhibition at the microcircuit alone, for a given GC stimulation one

reliable (“preferred”) outcome occurs. This strongly suggests that the input-output pattern transformation is not a purely random process but rather regulated.

Apart from gating effects of the feedforward circuit as well as short and long-term activity-dependent processes that dynamically adjust E/I ratios depending on the structure of the input, some other additional mechanisms then seem to be involved and would require further investigations. Heterogeneities of the cerebellar cortex, especially the zebrin II identity, might induce different postsynaptic plasticities (Waldiche et al., 2005; Wang et al., 2011). Similarly, Bergmann glial cells with their close proximity to the dendritic tree of the PC and their role in spillover regulation could be involved. Also, the hyperpolarization-activated current Ih would be a good candidate since it regulates PC responses to inhibitory inputs, hence one could expect its modulation (by for example serotonin (Oldfield et al., 2010; Williams et al., 2002) to contribute to the observed diversity of output patterns between PCs.

It should be noted that full Purkinje cell spike output patterns (where every input spike is transmitted) never occurred in our experiments, which could be simply explained by the subthreshold level of the GCs stimulation used. Additionally, the trial-to-trial output pattern diversity (number of different words) could arise from the stochastic component of vesicular release. Indeed, relatively weak inputs were elicited in our conditions thereby presumably involving a low number of synaptic contacts.

PC output patterns may have a computational/physiological significance only if downstream deep cerebellar nuclei neurons are able to decode them. Then the first important question to address is whether the observed transient modulations of the PC discharge can be discriminated from tonic background activity. This is particularly an arguable point considering both the irregular spontaneous firing of PCs in our experiments (high conductance state) and *in vivo* as well as the subthreshold level of inputs (weak in our case, sparse and/or weak *in vivo*) which, along with the frequency of GC stimulation used, is more prone to trigger modulations of a few inter-spike intervals, largely outnumbered by spontaneous ones. A study reported the existence

of a “couplet” motif (corresponding to the first evoked post-stimulus inter-spike intervals) in response to low frequency PF inputs (~ 1 Hz), which had the characteristic of rarely occurring spontaneously, and could be discriminated from spontaneous firing provided that it was short (5 - 20 ms) (Reusch et al., 2014). In theory, such “couplet” motif could encode both the occurrence and the strength of inputs (Walter and Khodakhah, 2006, 2009). Therefore, it would be interesting to further explore our data (by for example comparing the ISI distributions with the first post-stimulus ISI, or alternatively the evoked pause with the distribution of spontaneous long ISI) to get some insight whether similar discriminative mechanism could occur with high frequency inputs in *in vivo*-like conditions and may favor the readout of output patterns by DCN neurons.

Lastly, supposedly output patterns are “readable”, the next essential question that has long been debated and remains to be solved is whether and how they will impact on DCN neuron firing.

If considering a single PC, this is expected to be severely limited due to the relatively high/modest convergence of PCs onto DCN. Therefore, one valuable related question is how this pattern of activity would be distributed in neighboring ‘on beam’ PCs since they project to the same discrete region in DCN and that synchronization of a few (maybe two) PCs is able to entrain DCN neurons (Person and Raman, 2012). I would speculate that nearby PCs could seemingly produce the same pool of output spike patterns considering all the following. Firstly, on beam PCs receive shared PF inputs (Heck et al., 2007; Wise et al., 2010). Secondly, they most probably belong to the same microzone thereby they share CF inputs arising from the same olivary region. Lastly, nearby PCs presumably share zebrin identity hence express similar protein profiles. Together, as a consequence, induction of synergistic plasticities is likely to be similar, then synaptic weights and short term dynamics of excitation and inhibition (as well as E/I ratio) alike. Lastly, pauses were shown to be synchronized by their associated spikes among nearby PCs (< 100 µm) (Shin and De Schutter, 2006). To confirm/invalidate those predictions, one could perform similar

experiments as we did but using instead simultaneous extracellular recordings of neighboring PCs or multi-electrode recordings of on beam PCs.

7. Conclusions and future perspectives

To conclude, the modulation of the PC discharge by subthreshold GC to PC excitatory inputs and GC to MLI to PC inhibitory inputs brings into play a multitude of interacting cellular and molecular mechanisms. The sign and the time course of input-output transformation will be dictated by the feedforward inhibitory circuit. These will be determined based on the anatomy of the microcircuit (genetically encoded) and its change by long-term synaptic plasticity. The modulation of the PC discharge by high frequency input bursts involved highly dynamic and specific short-term plasticities at the multiple sites of the pathway and most probably will depend on the phase firing cycle of the PC spontaneous activity. Therefore, all of these should be considered to predict how the PC will be modulated under different types of behavior.

In the relatively near future it would be interesting to validate our data in a behavioral context *in vivo*, especially exploring if short-term learning could indeed shift PC spike output. To investigate its relevance, we should consider using a behavioral task that would engage the anterior part of the vermis as we studied. Adaptive locomotor learning could be an option although it remains to be determined which learning paradigm (if any) would be suitable to study and readout any short-term learning (trial-over-trial change) while at the same time not inducing long-term learning.

Lastly, the dream experiment which is technically challenging for now would be to explore how short-term cerebellar learning takes place at the GC to PC pathway in awake behaving animals. Ideally, this could be achieved by performing *in vivo* patch-clamp recordings of PCs while the animal is engaged in adaptive learning in order to directly monitor changes in short-term dynamics at the GC to PC pathway. This dream may come true given that successful patch clamp recordings of cerebellar GCs and mossy fiber boutons were recently obtained in head-fixed mice

while they were walking on a treadmill (Powell et al., 2015). Additionally, the acknowledged targeted patch-clamp recording method applied in Purkinje cells *in vivo* (Kitmaura and Haüsser, 2008) makes it more likely to happen.

BIBLIOGRAPHY

Abitbol K, Acher F, Daniel H (2008) Depression of excitatory transmission at PF-PC synapse by group III metabotropic glutamate receptors is provided exclusively by mGluR4 in the rodent cerebellar cortex. J Neurochem 105:2069–2079.

Aizenman CD, Linden DJ (1999) Regulation of the rebound depolarization and spontaneous firing patterns of deep nuclear neurons in slices of rat cerebellum. J Neurophysiol 82:1697–1709.

Albus JS (1971) A theory of cerebellar function. Math Biosci 10:25–61.

Alcami P, Marty A (2013) Estimating functional connectivity in an electrically coupled interneuron network. Proc Natl Acad Sci U S A 110:E4798–E4807.

Alger BE, Nicoll RA (1980) Spontaneous inhibitory post-synaptic potentials in hippocampus: Mechanism for tonic inhibition. Brain Res 200:195–200.

Alisky JM, Tolbert DL (1997) Quantitative analysis of converging spinal and cuneate mossy fibre afferent projections to the rat cerebellar anterior lobe. Neuroscience 80:373–388.

Andersson G, Oscarsson O (1978) Climbing fiber microzones in cerebellar vermis and their projection to different groups of cells in the lateral vestibular nucleus. Exp Brain Res 32:565–579.

Apps R (1990) Columnar organisation of the inferior olive projection to the posterior lobe of the rat cerebellum. J Comp Neurol 302:236–254.

Apps R, Atkins MJ, Garwicz M (1997) Gating of cutaneous input to cerebellar climbing fibres during a reaching task in the cat. J Physiol.502:203-14.

Apps R, Garwicz M (2000) Precise matching of olivo-cortical divergence and corticonuclear convergence between somatotopically corresponding areas in the medial C1 and medial C3 zones of the paravermal cerebellum. Eur J Neurosci 12:205–214.

Apps R, Garwicz M (2005) Anatomical and physiological foundations of cerebellar information processing. Nat Rev Neurosci 6:297–311.

Apps R, Hawkes R (2009) Cerebellar cortical organization: a one-map hypothesis. Nat Rev Neurosci 10:670–681.

Arenz A, Silver RA, Schaefer AT, Margrie TW (2008) The contribution of single synapses to sensory representation in vivo. Science (80-) 321:977–980.

Armstrong DM, Harvey RJ, Schild RF (1974) Topographical localization in the olivo-cerebellar projection: an electrophysiological study in the cat. J Comp Neurol 154:287–302.

Atkins MJ, Apps R (1997) Somatotopical organisation within the climbing fibre projection to the paramedian lobule and copula pyramidis of the rat cerebellum. J Comp Neurol 389:249–263.

Atluri PP, Regehr WG (1996) Determinants of the Time Course of Facilitation at the Granule Cell to Purkinje Cell Synapse. J Neurosci 16:5661–5671.

Atluri PP, Regehr WG (1998) Delayed release of neurotransmitter from cerebellar granule cells. J Neurosci 18:8214–8227.

Azizi S a, Woodward DJ (1987) Inferior olivary nuclear complex of the rat: morphology and comments on the principles of organization within the olivocerebellar system. J Comp Neurol 263:467–484.

Bao J, Reim K, Sakaba T (2010) Target-dependent feedforward inhibition mediated by short-term synaptic plasticity in the cerebellum. J Neurosci 30:8171–8179.

Barbour B (1993) Synaptic currents evoked in Purkinje cells by stimulating individual granule cells. Neuron 11:759–769.

Barbour B (1994) Prolonged presence of glutamate during excitatory synaptic transmission to

cerebellar Purkinje cells. Neuron 12:1331–1343.

Barmack NH, Yakhnitsa V (2008a) Functions of interneurons in mouse cerebellum. J Neurosci 28:1140–1152.

Barmack NH, Yakhnitsa V (2008b) Distribution of granule cells projecting to focal Purkinje cells in mouse uvula-nodulus. Neuroscience 156:216–221.

Bastian AJ (2006) Learning to predict the future: the cerebellum adapts feedforward movement control. Curr Opin Neurobiol 16:645–649.

Batchelor AM, Garthwaite J (1992) GABA B Receptors in the Parallel Fibre Pathway of Rat Cerebellum. Eur J Neurosci 4:1059–1064.

Batchelor AM, Madge DJ, Garthwaite J (1994) Synaptic activation of metabotropic glutamate receptors in the parallel Fibre-Purkinje cell pathway in rat cerebellar slices. Neuroscience 63:911–915.

Beierlein M, Regehr WG (2006) Local Interneurons Regulate Synaptic Strength by Retrograde Release of Endocannabinoids. J Neurosci 26:9935–9943.

Beitz AJ (1976) The topographical organization of the olivo-dentate and dentato-olivary pathways in the cat. Brain Res 115:311–317.

Bell CC, Grimm RJ (1969) Discharge properties of Purkinje cells recorded on single and double microelectrodes. J Neurophysiol 32:1044–1055.

Bengtsson F, Geborek P, Jörntell H (2013) Cross-correlations between pairs of neurons in cerebellar cortex in vivo. Neural Netw 47:88–94.

Bengtsson F, Jörntell H (2009) Sensory transmission in cerebellar granule cells relies on similarly coded mossy fiber inputs. Proc Natl Acad Sci U S A 106:2389–2394.

Bergles DE, Dzubay JA, Jahr CE, Nicoll RA (1997) Glutamate transporter currents in Bergmann glial cells follow the time course of extrasynaptic glutamate. Neurobiology 94:14821–14825.

Bishop GA (1993) An analysis of HRP-filled basket cell axons in the cat's cerebellum. I. Morphometry and configuration. Anat Embryol (Berl) 188:287–297.

Blackman A V., Abrahamsson T, Costa RP, Lalanne T, Sjöström PJ (2013) Target-cell-specific short-term plasticity in local circuits. Front Synaptic Neurosci 5:1–13.

Blenkinsop TA, Lang EJ (2006) Block of Inferior Olive Gap Junctional Coupling Decreases Purkinje Cell Complex Spike Synchrony and Rhythmicity. J Neurosci 26:1739–1748.

Bloedel JR, Roberts J (1971) Action of Climbing Cortex Fibers of the Cat in Cerebellar. J Neurophysiol 34:17–31.

Blot A, Barbour B (2014) Ultra-rapid axon-axon ephaptic inhibition of cerebellar Purkinje cells by the pinceau. Nat Neurosci 17:289–295.

Boegman RJ, Parent A, Hawkes R (1988) Zonation in the rat cerebellar cortex: patches of high acetylcholinesterase activity in the granular layer are congruent with Purkinje cell compartments. Brain Res 448:237–251.

Bornschein G, Arendt O, Hallermann S, Brachtendorf S, Eilers J, Schmidt H (2013) Paired-pulse facilitation at recurrent Purkinje neuron synapses is independent of calbindin and parvalbumin during high-frequency activation. J Physiol 591:3355–3370.

Bosman LWJ, Koekkoek SKE, Shapiro J, Rijken BFM, Zandstra F, van der Ende B, Owens CB, Potters J-W, de Gruijl JR, Ruigrok TJH, De Zeeuw CI (2010) Encoding of whisker input by cerebellar Purkinje cells. J Physiol 588:3757–3783.

Bower JM (2011) Functional implications of tactile projection patterns to the lateral hemispheres of the

cerebellum of the albino rat: The legacy of Wally Welker. Ann N Y Acad Sci 1225:130–141.

Bower JM, Beermann DH, Gibson JM, Shambes GM, Welker W (1981) Principles of organization of a cerebro-cerebellar circuit. Micromapping the projections from cerebral (SI) to cerebellar (granule cell layer) tactile areas of rats. Brain Behav Evol 18:1–18.

Bower JM, Kassel J (1990) Variability in tactile projection patterns to cerebellar folia crus IIa of the Norway rat. J Comp Neurol 302:768–778.

Bower JM, Woolston DC (1983) Congruence of spatial organization of tactile projections to granule cell and Purkinje cell layers of cerebellar hemispheres of the albino rat: vertical organization of cerebellar cortex. J Neurophysiol 49:745–766.

Braitenberg V (1961) Functional Interpretation of Cerebellar Histology. Nature 190:539–540.

Braitenberg V, Atwood RP (1958) Morphological observations on the cerebellar cortex. J Comp Neurol 109:1–27.

Brenowitz SD, Regehr WG (2007) Reliability and Heterogeneity of Calcium Signaling at Single Presynaptic Boutons of Cerebellar Granule Cells. J Neurosci 27:7888–7898.

Brochu G, Maler L, Hawkes R (1990) Zebrin II: a polypeptide antigen expressed selectively by Purkinje cells reveals compartments in rat and fish cerebellum. J Comp Neurol 291:538–552.

Brown IE, Bower JM (2001) Congruence of mossy fiber and climbing fiber tactile projections in the lateral hemispheres of the rat cerebellum. J Comp Neurol 429:59–70.

Brunel N, Hakim V, Isope P, Nadal J-P, Barbour B (2004) Optimal information storage and the distribution of synaptic weights: perceptron versus Purkinje cell. Neuron 43:745–757.

Buchanan KA, Blackman A V., Moreau AW, Elgar D, Costa RP, Lalanne T, Tudor Jones AA, Oyrer J, Sjöström PJ (2012) Target-Specific Expression of Presynaptic NMDA Receptors in Neocortical Microcircuits. Neuron 75:451–466.

Buisseret-Delmas C, Angaut P (1993) The cerebellar olivo-corticonuclear connections in the rat. Prog Neurobiol 40:63–87.

Caillard O, Moreno H, Schwaller B, Llano I, Celio MR, Marty A (2000) Role of the calcium-binding protein parvalbumin in short-term synaptic plasticity. Proc Natl Acad Sci U S A 97:13372–13377.

Cajal SR (1911) Histologie du système nerveux de l'homme & des vertébrés (Maloine A, ed).

Carter AG, Regehr WG (2000) Prolonged synaptic currents and glutamate spillover at the parallel fiber to stellate cell synapse. J Neurosci 20:4423–4434.

Carter AG, Regehr WG (2002) Quantal events shape cerebellar interneuron firing. Nat Neurosci 5:1309–1318.

Cavelier P, Lohof AM, Lonchamp E, Beekenkamp H, Mariani J, Bossu JL (2008) Participation of low-threshold Ca2+ spike in the Purkinje cells complex spike. Neuroreport 12;19(3):299-303.

Cerminara NL, John A. Rawson, Rawson JA (2004) Evidence that Climbing Fibers Control an Intrinsic Spike Generator in Cerebellar Purkinje Cells. J Neurosci 24:4510–4517.

Cerminara NL, Lang EJ, Sillitoe R V., Apps R (2015) Redefining the cerebellar cortex as an assembly of non-uniform Purkinje cell microcircuits. Nat Rev Neurosci 16:79–93.

Cerminara NL, Rawson JA, Apps R (2010) Electrophysiological characterization of the cerebellum in the arterially perfused hindbrain and upper body of the rat. Cerebellum 9:218–231.

Cesana E, Pietrajtis K, Bidoret C, Isope P, D'Angelo E, Dieudonné S, Forti L (2013) Granule Cell Ascending Axon Excitatory Synapses onto Golgi Cells Implement a Potent Feedback Circuit in the Cerebellar Granular Layer. J Neurosci 33:12430–12446.

Chabrol FP, Arenz A, Wiechert MT, Margrie TW, DiGregorio D a (2015) Synaptic diversity enables temporal coding of coincident multisensory inputs in single neurons. Nat Neurosci.

Chadderton P, Margrie TW, Häusser M (2004) Integration of quanta in cerebellar granule cells during sensory processing. Nature 428:856–860.

Chan-Palay V (1971) The recurrent collaterals of Purkinje cell axons: A correlated study of the rat's cerebellar cortex with electron microscopy and the Golgi method. Zeitschrift für Anat und Entwicklungsgeschichter 134:200–234.

Chance FS, Abbott LF, Reyes AD (2002) Gain modulation from background synaptic input. Neuron 35:773–782.

Chaumont J et al. (2013) Clusters of cerebellar Purkinje cells control their afferent climbing fiber discharge. Proc Natl Acad Sci U S A 110:16223–16228.

Chen S, Augustine GJ, Chadderton P (2016) The cerebellum linearly encodes whisker position during voluntary movement. Elife 5:1–16.

Chiu C-S, Jensen K, Sokolova I, Wang D, Li M, Deshpande P, Davidson N, Mody I, Quick MW, Quake SR, Lester HA (2002) Number, density, and surface/cytoplasmic distribution of GABA transporters at presynaptic structures of knock-in mice carrying GABA transporter subtype 1-green fluorescent protein fusions. J Neurosci 22:10251–10266.

Chung S-H, Kim C-T, Hawkes R (2008) Compartmentation of GABA B receptor2 expression in the mouse cerebellar cortex. Cerebellum 7:295–303.

Chung SH, Marzban H, Hawkes R (2009) Compartmentation of the cerebellar nuclei of the mouse. Neuroscience 161:123–138.

Clark BA, Cull-Candy SG (2002) Activity-dependent recruitment of extrasynaptic NMDA receptor activation at an AMPA receptor-only synapse. J Neurosci 22:4428–4436.

Clarke E, O'Malley CD (1996) The human brain and spinal cord: A historical study illustrated by writings from antiquity to the twentieth century, 2nd ed. Norman Publishing.

Cohen D, Yarom Y (1998) Patches of synchronized activity in the cerebellar cortex evoked by mossy-fiber stimulation: questioning the role of parallel fibers. Proc Natl Acad Sci U S A 95:15032–15036.

Cramer SW, Gao W, Chen G, Ebner TJ (2013) Reevaluation of the beam and radial hypotheses of parallel fiber action in the cerebellar cortex. J Neurosci 33:11412–11424.

Crepel F (1974) Excitatory and inhibitory processes acting upon cerebellar Purkinje cells during maturation in the rat; influence of hypothyroidism. Exp brain Res 20:403–420.

Crepel F (2007) Developmental changes in retrograde messengers involved in depolarization-induced suppression of excitation at parallel fiber-Purkinje cell synapses in rodents. J Neurophysiol 97:824–836.

Crepel F, Daniel H (2007) Developmental Changes in Agonist-Induced Retrograde Signaling at Parallel Fiber Purkinje Cell Synapses: Role of Calcium-Induced Calcium Release. J Neurophysiol 98:2550–2565.

Crepel F, Galante M, Habbas S, McLean H, Daniel H (2011) Role of the vesicular transporter VGLUT3 in retrograde release of glutamate by cerebellar Purkinje cells. J Neurophysiol 105:1023–1032.

Crepel F, Mariani J (1976) Multiple innervation of Purkinje cells by climbing fibers in the cerebellum of the Weaver Mutant Mouse. J Neurobiol 7:579–582.

Crowley JJ, Carter AG, Regehr WG (2007) Fast vesicle replenishment and rapid recovery from desensitization at a single synaptic release site. J Neurosci 27:5448–5460.

D'Angelo E, De Filippi G, Rossi P, Taglietti V (1995) Synaptic excitation of individual rat cerebellar granule cells in situ: evidence for the role of NMDA receptors. J Physiol 484 2:397–413.

D'Angelo E, De Zeeuw CI (2009) Timing and plasticity in the cerebellum: focus on the granular layer. Trends Neurosci 32:30–40.

Davie JT, Clark B a, Hausser M (2008) The Origin of the Complex Spike in Cerebellar Purkinje Cells. J Neurosci 28:7599–7609.

de Solages C, Szapiro G, Brunel N, Hakim V, Isope P, Buisseret P, Rousseau C, Barbour B, Léna C (2008) High-frequency organization and synchrony of activity in the purkinje cell layer of the cerebellum. Neuron 58:775–788.

De Zeeuw CI, Hoogland TM (2015) Reappraisal of Bergmann glial cells as modulators of cerebellar circuit function. Front Cell Neurosci 9:246.

De Zeeuw CI, Koekkoek SK, Wylie DR, Simpson JI (1997a) Association between dendritic lamellar bodies and complex spike synchrony in the olivocerebellar system. J Neurophysiol 77:1747–1758.

De Zeeuw CI, Van Alphen AM, Hawkins RK, Ruigrok TJH (1997b) Climbing fibre collaterals contact neurons in the cerebellar nuclei that provide a GABAergic feedback to the inferior olive. Neuroscience 80:981–986.

Dean I, Robertson SJ, Edwards F a (2003) Serotonin drives a novel GABAergic synaptic current recorded in rat cerebellar purkinje cells: a Lugaro cell to Purkinje cell synapse. J Neurosci 23:4457–4469.

Dean P, Porrill J, Ekerot C-F, Jörntell H (2010) The cerebellar microcircuit as an adaptive filter: experimental and computational evidence. Nat Rev Neurosci 11:30–43.

Dehnes Y, Chaudhry FA, Ullensvang K, Lehre KP, Storm-Mathisen J, Danbolt NC (1998) The glutamate transporter EAAT4 in rat cerebellar Purkinje cells: a glutamate-gated chloride channel concentrated near the synapse in parts of the dendritic membrane facing astroglia. J Neurosci 18:3606–3619.

Destexhe A, Rudolph M, Paré D (2003) The high-conductance state of neocortical neurons in vivo. Nat Rev Neurosci 4:739–751.

Devor A, Yarom Y (2002) Electrotonic coupling in the inferior olivary nucleus revealed by simultaneous double patch recordings. J Neurophysiol 87:3048–3058.

Diana MA, Levenes C, Mackie K, Marty A (2002) Short-term retrograde inhibition of GABAergic synaptic currents in rat Purkinje cells is mediated by endogenous cannabinoids. J Neurosci 22:200–208.

Dieudonne S (2001) Book Review: Serotonergic Neuromodulation in the Cerebellar Cortex: Cellular, Synaptic, and Molecular Basis. Neurosci 7:207–219.

Dieudonné S, Dumoulin A (2000) Serotonin-driven long-range inhibitory connections in the cerebellar cortex. J Neurosci 20:1837–1848.

DiGregorio DA, Nusser Z, Silver RA (2002) Spillover of glutamate onto synaptic AMPA receptors enhances fast transmission at a cerebellar synapse. Neuron 35:521–533.

Dittman JS, Kreitzer AC, Regehr WG (2000) Interplay between facilitation, depression, and residual calcium at three presynaptic terminals. J Neurosci 20:1374–1385.

Dizon MJ, Khodakhah K (2011) The role of interneurons in shaping Purkinje cell responses in the cerebellar cortex. J Neurosci 31:10463–10473.

Dugué GP, Brunel N, Hakim V, Schwartz E, Chat M, Lévesque M, Courtemanche R, Léna C, Dieudonné S (2009) Electrical Coupling Mediates Tunable Low-Frequency Oscillations and

Resonance in the Cerebellar Golgi Cell Network. Neuron 61:126–139.

Duguid IC, Pankratov Y, Moss GWJ, Smart TG (2007) Somatodendritic Release of Glutamate Regulates Synaptic Inhibition in Cerebellar Purkinje Cells via Autocrine mGluR1 Activation. J Neurosci 27:12464–12474.

Duguid IC, Smart TG (2004) Retrograde activation of presynaptic NMDA receptors enhances GABA release at cerebellar interneuron-Purkinje cell synapses. Nat Neurosci 7:525–533.

Dumoulin A, Triller A, Dieudonné S (2001) IPSC kinetics at identified GABAergic and mixed GABAergic and glycinergic synapses onto cerebellar Golgi cells. J Neurosci 21:6045–6057.

Ebner TJ, Bloedel JR (1981) Temporal patterning in simple spike discharge of Purkinje cells and its relationship to climbing fiber activity. J Neurophysiol 45:933–947.

Eccles JC, Ito M, Szentágothai J (1967a) The Cerebellum as a Neuronal Machine. Berlin, Heidelberg: Springer Berlin Heidelberg.

Eccles JC, Sasaki K, Strata P (1967b) Interpretation of the potential fields generated in the cerebellar cortex by a mossy fibre volley. Exp Brain Res 3:58–80.

Edgerton JR, Reinhart PH (2003) Distinct contributions of small and large conductance Ca2+-activated K+ channels to rat Purkinje neuron function. J Physiol 548:53–69.

Egertová M, Elphick MR (2000) Localisation of cannabinoid receptors in the rat brain using antibodies to the intracellular C-terminal tail of CB1. J Comp Neurol 422:159–171.

Ekerot C-F, Jörntell H (2003) Parallel fiber receptive fields: a key to understanding cerebellar operation and learning. Cerebellum 2:101–109.

Ekerot CF, Jörntell H (2001) Parallel fibre receptive fields of Purkinje cells and interneurons are climbing fibre-specific. Eur J Neurosci 13:1303–1310.

Ekerot CF, Larson B (1979) The dorsal spino-olivocerebellar system in the cat. I. Functional organization and termination in the anterior lobe. Exp Brain Res 36:201–217.

Ekerot CF, Larson B (1982) Branching of olivary axons to innervate pairs of sagittal zones in the cerebellar anterior lobe of the cat. Exp brain Res 48:185–198.

Engbers JDT, Anderson D, Asmara H, Rehak R, Mehaffey WH, Hameed S, McKay BE, Kruskic M, Zamponi GW, Turner RW (2012) Intermediate conductance calcium-activated potassium channels modulate summation of parallel fiber input in cerebellar Purkinje cells. Proc Natl Acad Sci U S A 109:2601–2606.

Escobar A, Sampedro ED, Dow RS (1968) Quantitative data on the inferior olivary nucleus in man, cat and vampire bat. J Comp Neurol 132:397–403.

Feng JF, Brown D (1999) Coefficient of variation of interspike intervals greater than 0.5. How and when? Biol Cybern 80:291–297.

Foster KA (2005) The Influence of Multivesicular Release and Postsynaptic Receptor Saturation on Transmission at Granule Cell to Purkinje Cell Synapses. J Neurosci 25:11655–11665.

Fox CA., Barnard JW (1957) A quantitative study of the Purkinje cell dendritic branchlets and their relationship to afferent fibres. J Anat 91:299–313.

Fuhrmann G, Segev I, Markram H, Tsodyks M (2002) Coding of temporal information by activity-dependent synapses. J Neurophysiol 87:140–148.

Gao H, Solages C de, Lena C (2012a) Tetrode recordings in the cerebellar cortex. J Physiol Paris 106:128–136.

Gao Z, van Beugen BJ, De Zeeuw CI (2012b) Distributed synergistic plasticity and cerebellar learning.

Nat Rev Neurosci 13:619–635.

Garwicz M, Andersson G (1992) Spread of synaptic activity along parallel fibres in cat cerebellar anterior lobe. Exp brain Res 88:615–622.

Garwicz M, Apps R, Trott JR (1996) Micro-organization of olivocerebellar and corticonuclear connections of the paravermal cerebellum in the cat. Eur J Neurosci 8:2726–2738.

Garwicz M, Ekerot C-F, Schouenborg J (1992) Distribution of Cutaneous Nociceptive and Tactile Climbing Fibre Input to Sagittal Zones in Cat Cerebellar Anterior Lobe. Eur J Neurosci 4:289–295.

Garwicz M, Ekerot CF (1994) Topographical organization of the cerebellar cortical projection to nucleus interpositus anterior in the cat. J Physiol 474:245–260.

Garwicz M, Jörntell H, Ekerot CF (1998) Cutaneous receptive fields and topography of mossy fibres and climbing fibres projecting to cat cerebellar C3 zone. J Physiol 512:277–293.

Gatzeva-topalova PZ, Warner LR, Pardi A, Carlos M (2011) NIH Public Access. 18:1492–1501.

Gebre SA, Reeber SL, Sillitoe R V. (2012) Parasagittal compartmentation of cerebellar mossy fibers as revealed by the patterned expression of vesicular glutamate transporters VGLUT1 and VGLUT2. Brain Struct Funct 217:165–180.

Giaquinta G, Valle MS, Caserta C, Casabona A, Bosco G, Perciavalle V (2000) Sensory representation of passive movement kinematics by rat's spinocerebellar Purkinje cells. Neurosci Lett 285:41–44.

Glitsch M, Parra P, Llano I (2000) The retrograde inhibition of IPSCs in rat cerebellar purkinje cells is highly sensitive to intracellular Ca2+. Eur J Neurosci 12:987–993.

Goossens J, Daniel H, Rancillac A, van der Steen J, Oberdick J, Crépel F, De Zeeuw CI, Frens MA (2001) Expression of protein kinase C inhibitor blocks cerebellar long-term depression without affecting Purkinje cell excitability in alert mice. J Neurosci 21:5813–5823.

Goto J-I, Inoue T, Kuruma A, Mikoshiba K (2006) Short-term potentiation at the parallel fiber-Purkinje cell synapse. Neurosci Res 55:28–33.

Granit R, Phillips CG (1956) Excitatory and inhibitory processes acting upon individual Purkinje cells of the cerebellum in cats. J Physiol 133:520–547.

Gruol DL, Franklin CL (1987) Morphological and physiological differentiation of Purkinje neurons in cultures of rat cerebellum. J Neurosci 7:1271–1293.

Hansen ST, Meera P, Otis TS, Pulst SM (2013) Changes in Purkinje cell firing and gene expression precede behavioral pathology in a mouse model of SCA2. Hum Mol Genet 22:271–283.

Hartmann MJ, Bower JM (2001) Tactile responses in the granule cell layer of cerebellar folium crus IIa of freely behaving rats. J Neurosci 21:3549–3563.

Harvey RJ, Napper RM (1988) Quantitative study of granule and Purkinje cells in the cerebellar cortex of the rat. J Comp Neurol 274:151–157.

Harvey RJ, Napper RM (1991) Quantitative studies on the mammalian cerebellum. Prog Neurobiol 36:437–463.

Häusser M, Clark BA (1997) Tonic synaptic inhibition modulates neuronal output pattern and spatiotemporal synaptic integration. Neuron 19:665–678.

Hawkes R (1997) An anatomical model of cerebellar modules. Prog Brain Res 114:39–52.

Hawkes R (2014) Purkinje cell stripes and long-term depression at the parallel fiber-Purkinje cell synapse. Front Syst Neurosci 8:41.

Hawkes R, Beierbach E, Tan SS (1999) Granule cell dispersion is restricted across transverse boundaries in mouse chimeras. Eur J Neurosci 11:3800–3808.

Hawkes R, Colonnier M, Leclerc N (1985) Monoclonal antibodies reveal sagittal banding in the rodent cerebellar cortex. Brain Res 333:359–365.

Hawkes R, Leclerc N (1989) Purkinje cell axon collateral distributions reflect the chemical compartmentation of the rat cerebellar cortex. Brain Res 476:279–290.

Heck DH, Thach WT, Keating JG (2007) On-beam synchrony in the cerebellum as the mechanism for the timing and coordination of movement. Proc Natl Acad Sci U S A 104:7658–7663.

Heiney S a, Kim J, Augustine GJ, Medina JF (2014) Precise control of movement kinematics by optogenetic inhibition of Purkinje cell activity. J Neurosci 34:2321–2330.

Hesslow G (1994) Correspondence between climbing fibre input and motor output in eyeblink-related areas in cat cerebellar cortex. J Physiol 476:229–244.

Higley MJ, Contreras D (2006) Balanced Excitation and Inhibition Determine Spike Timing during Frequency Adaptation. J Neurosci 26:448–457.

Hoebeek FE, Stahl JS, van Alphen AM, Schonewille M, Luo C, Rutteman M, van den Maagdenberg AMJM, Molenaar PC, Goossens HHLM, Frens MA, De Zeeuw CI (2005) Increased Noise Level of Purkinje Cell Activities Minimizes Impact of Their Modulation during Sensorimotor Control. Neuron 45:953–965.

Holdefer RN, Miller LE (2009) Dynamic correspondence between Purkinje cell discharge and forelimb muscle activity during reaching. Brain Res 1295:67–75.

Holmes G (1917) The symptoms of acute cerebellar injuries due to gunshot injuries. Brain 40:461–535.

Holmes G (2007) The Croonian Lectures On The Clinical Symptoms Of Cerebellar Disease And Their Interpretation. Lecture I. 1922. Cerebellum 6:142–147; discussion 141.

Holt GR, Softky WR, Koch C, Douglas RJ (1996) Comparison of discharge variability in vitro and in vivo in cat visual cortex neurons. J Neurophysiol 75:1806–1814.

Holtzman T, Rajapaksa T, Mostofi A, Edgley S a (2006) Different responses of rat cerebellar Purkinje cells and Golgi cells evoked by widespread convergent sensory inputs. J Physiol 574:491–507.

Hounsgaard J (1979) Pacemaker properties of mammalian Purkinje cells. Acta Physiol Scand 106:91–92.

Huang CC, Sugino K, Shima Y, Guo C, Bai S, Mensh BD, Nelson SB, Hantman AW (2013) Convergence of pontine and proprioceptive streams onto multimodal cerebellar granule cells. Elife 2013:1972–1974.

Hubbard JI, Stenhouse D, Eccles RM (1967) Origin of synaptic noise. Science 157:330–331.

Hull C, Regehr WG (2012) Identification of an inhibitory circuit that regulates cerebellar Golgi cell activity. Neuron 73:149–158.

Husson F, Lê S, Pagès J (2009) Analyse de données avec R,. Presses Universitaires de Rennes.

Isope P, Barbour B (2002) Properties of unitary granule cell-->Purkinje cell synapses in adult rat cerebellar slices. J Neurosci 22:9668–9678.

Isope P, Murphy TH (2005) Low threshold calcium currents in rat cerebellar Purkinje cell dendritic spines are mediated by T-type calcium channels. J Physiol 562:257–269.

Ito M (1984) The Cerebellum and Neural Control. New York: Raven Press.

Ito M (2001) Cerebellar Long-Term Depression: Characterization, Signal Transduction, and Functional Roles. Physiol Rev 81:1143–1195.

Ito M (2006) Cerebellar circuitry as a neuronal machine. Prog Neurobiol 78:272–303.

Ito M, Kano M (1982) Long-lasting depression of parallel fiber-Purkinje cell transmission induced by conjunctive stimulation of parallel fibers and climbing fibers in the cerebellar cortex. Neurosci Lett 33:253–258.

Iwakura A, Uchigashima M, Miyazaki T, Yamasaki M, Watanabe M (2012) Lack of Molecular-Anatomical Evidence for GABAergic Influence on Axon Initial Segment of Cerebellar Purkinje Cells by the Pinceau Formation. J Neurosci 32:9438–9448.

Jacobson G a, Rokni D, Yarom Y (2008) A model of the olivo-cerebellar system as a temporal pattern generator. Trends Neurosci 31:617–625.

Jaeger D, Bower JM (1994) Prolonged responses in rat cerebellar Purkinje cells following activation of the granule cell layer: an intracellular in vitro and in vivo investigation. Exp brain Res 100:200–214.

Jahnsen H (1986) Electrophysiological characteristics of neurones in the guinea-pig deep cerebellar nuclei in vitro. J Physiol 372:129–147.

Jakab RL, Hámori J (1988) Quantitative morphology and synaptology of cerebellar glomeruli in the rat. Anat Embryol (Berl) 179:81–88.

Jansen J, Brodal A (1940) Experimental studies on the intrinsic fibers of the cerebellum II. The cortico-nuclear projection. J Comp Neurol 73:267–321.

Ji Z, Hawkes R (1994) Topography of purkinje cell compartments and mossy fiber terminal fields in lobules ii and iii of the rat cerebellar cortex: Spinocerebellar and cuneocerebellar projections. Neuroscience 61:935–954.

Jirenhed D-A, Bengtsson F, Jörntell H (2013) Parallel fiber and climbing fiber responses in rat cerebellar cortical neurons in vivo. Front Syst Neurosci 7:16.

Jörntell H, Bengtsson F, Schonewille M, De Zeeuw CI (2010) Cerebellar molecular layer interneurons - computational properties and roles in learning. Trends Neurosci 33:524–532.

Jörntell H, Ekerot C, Garwicz M, Luo XL (2000) Functional organization of climbing fibre projection to the cerebellar anterior lobe of the rat. J Physiol 522 Pt 2:297–309.

Jörntell H, Ekerot C-F (2002) Reciprocal bidirectional plasticity of parallel fiber receptive fields in cerebellar Purkinje cells and their afferent interneurons. Neuron 34:797–806.

Jörntell H, Ekerot C-F (2006) Properties of somatosensory synaptic integration in cerebellar granule cells in vivo. J Neurosci 26:11786–11797.

Jörntell H, Ekerot C-F (2011) Receptive Field Remodeling Induced by Skin Stimulation in Cerebellar Neurons in vivo. Front Neural Circuits 5:3.

Jörntell H, Hansel C (2006) Synaptic Memories Upside Down: Bidirectional Plasticity at Cerebellar Parallel Fiber-Purkinje Cell Synapses. Neuron 52:227–238.

Joseph JW, Shambes GM, Gibson JM, Welker W (1978) Tactile projections to granule cells in caudal vermis of the rat's cerebellum. Brain Behav Evol 15:141–149.

Kandel E, Schwartz J, Jessell T (2000) Principles of Neural Science, 4 edition. McGraw-Hill Medical.

Karavanova I, Vasudevan K, Cheng J, Buonanno A (2007) Novel regional and developmental NMDA receptor expression patterns uncovered in NR2C subunit-beta-galactosidase knock-in mice. Mol Cell Neurosci 34:468–480.

Kassel J, Shambes GM, Welker W (1984) Fractured cutaneous projections to the granule cell layer of the posterior cerebellar hemisphere of the domestic cat. J Comp Neurol 225:458–468.

Katz B, Miledi R (1968) The role of calcium in neuromuscular facilitation. J Physiol 195:481–492.

Kim C-H, Oh S-H, Lee JH, Chang SO, Kim J, Kim SJ (2012) Lobule-specific membrane excitability of cerebellar Purkinje cells. J Physiol 590:273–288.

Kim YS, Shin JH, Hall FS, Linden DJ (2009) Dopamine Signaling Is Required for Depolarization-Induced Slow Current in Cerebellar Purkinje Cells. J Neurosci 29:8530–8538.

King JS, Bishop GA (1982) The synaptic features of horseradish peroxidase-labelled recurrent collaterals in the ganglionic plexus of the cat cerebeliar cortex. J Neurocytol 11:867–880.

Kitamura K, Hausser M (2011) Dendritic Calcium Signaling Triggered by Spontaneous and Sensory-Evoked Climbing Fiber Input to Cerebellar Purkinje Cells In Vivo. J Neurosci 31:10847–10858.

Kitazawa S, Wolpert DM (2005) Rhythmicity, randomness and synchrony in climbing fiber signals. Trends Neurosci 28:611–619.

Konnerth A, Llano I, Armstrong CM (1990) Synaptic currents in cerebellar Purkinje cells. Proc Natl Acad Sci U S A 87:2662–2665.

Korbo L, Andersen BB, Ladefoged O, Møller A (1993) Total numbers of various cell types in rat cerebellar cortex estimated using an unbiased stereological method. Brain Res 609:262–268.

Kreitzer AC, Carter AG, Regehr WG (2002) Inhibition of interneuron firing extends the spread of endocannabinoid signaling in the cerebellum. Neuron 34:787–796.

Kreitzer AC, Regehr WG (2001) Retrograde Inhibition of Presynaptic Calcium Influx by Endogenous Cannabinoids at Excitatory Synapses onto Purkinje Cells. Neuron 29:717–727.

Lainé J, Axelrad H (1998) Lugaro cells target basket and stellate cells in the cerebellar cortex. Neuroreport 9:2399–2403.

Lang EJ (2001) Organization of olivocerebellar activity in the absence of excitatory glutamatergic input. J Neurosci 21:1663–1675.

Lange W (1982) Regional differences in the cytoarchitecture of the cerebellar cortex. In: The Cerebellum - New Vistas. (Palay SL, Chan-Palay V, eds), pp 93–105. Berlin-Heidelberg-New York: Springer-Verlag.

Larramendi LMH, Lemkey-Johnston N (1970) The distribution of recurrent purkinje collateral synapses in the mouse cerebellar cortex: An electron microscopic study. J Comp Neurol 138:451–482.

Larsell O (1952) The morphogenesis and adult pattern of the lobules and fissures of the cerebellum of the white rat. J Comp Neurol 97:281–356.

Larson B, Miller S, Oscarsson O (1969) Termination and functional organization of the dorsolateral spino-olivocerebellar path. J Physiol 203:611–640.

Lee S, Yoon B-E, Berglund K, Oh S-J, Park H, Shin H-S, Augustine GJ, Lee CJ (2010) Channel-Mediated Tonic GABA Release from Glia. Science (80-) 330:790–796.

Lemkey-Johnston N, Larramendi LMH (1968) Types and distribution of synapses upon basket and stellate cells of the mouse cerebellum: An electron microscopic study. J Comp Neurol 134:73–111.

Leznik E, Llinás R (2005) Role of gap junctions in synchronized neuronal oscillations in the inferior olive. J Neurophysiol 94:2447–2456.

Leznik E, Makarenko V, Llinás R (2002) Electrotonically mediated oscillatory patterns in neuronal ensembles: an in vitro voltage-dependent dye-imaging study in the inferior olive. J Neurosci

22:2804–2815.

Liu SJ (2007) Biphasic modulation of GABA release from stellate cells by glutamatergic receptor subtypes. J Neurophysiol 98:550–556.

Llano I, Gerschenfeld HM (1993) Inhibitory synaptic currents in stellate cells of rat cerebellar slices. J Physiol 468:177–200.

Llano I, Leresche N, Marty a (1991) Calcium entry increases the sensitivity of cerebellar Purkinje cells to applied GABA and decreases inhibitory synaptic currents. Neuron 6:565–574.

Llinas R, Baker R, Sotelo C (1974) Electrotonic coupling between neurons in cat inferior olive. J Neurophysiol 37:560–571.

Llinás R, Sugimori M (1980) Electrophysiological properties of in vitro Purkinje cell somata in mammalian cerebellar slices. J Physiol 305:171–195.

Loewenstein Y, Mahon S, Chadderton P, Kitamura K, Sompolinsky H, Yarom Y, Häusser M (2005) Bistability of cerebellar Purkinje cells modulated by sensory stimulation. Nat Neurosci 8:202–211.

Luciani L (1891) Il Cervelletto, nuovi studi di fisiologia normale e patologica. Le Monnier.

Mann-Metzer P, Yarom Y (1999) Electrotonic coupling interacts with intrinsic properties to generate synchronized activity in cerebellar networks of inhibitory interneurons. J Neurosci 19:3298–3306.

Manni E, Petrosini L (2004) A century of cerebellar somatotopy: a debated representation. Nat Rev Neurosci 5:241–249.

Marcaggi P, Attwell D (2005) Endocannabinoid signaling depends on the spatial pattern of synapse activation. Nat Neurosci 8:776–781.

Marcaggi P, Attwell D (2007) Short- and long-term depression of rat cerebellar parallel fibre synaptic transmission mediated by synaptic crosstalk. J Physiol 578:545–550.

Mariño J, Schummers J, Lyon DC, Schwabe L, Beck O, Wiesing P, Obermayer K, Sur M (2005) Invariant computations in local cortical networks with balanced excitation and inhibition. Nat Neurosci 8:194–201.

Markram H, Pikus D, Gupta A, Tsodyks M (1998) Potential for multiple mechanisms, phenomena and algorithms for synaptic plasticity at single synapses. Neuropharmacology 37:489–500.

Marr D (1969) A theory of cerebellar cortex. J Physiol 202:437–470.

Marzban H, Hawkes R (2011) On the architecture of the posterior zone of the cerebellum. Cerebellum 10:422–434.

Mateos JM, Osorio A, Azkue JJ, Benítez R, Elezgarai I, Bilbao A, Díez J, Puente N, Kuhn R, Knöpfel T, Hawkes R, Doñate-Oliver F, Grandes P (2001) Parasagittal compartmentalization of the metabotropic glutamate receptor mGluR1b in the cerebellar cortex. Eur J Anat 5:15–21.

Mathews PJ, Lee KH, Peng Z, Houser CR, Otis TS (2012) Effects of climbing fiber driven inhibition on purkinje neuron spiking. J Neurosci 32:17988–17997.

Matsushita M, Wang CL (1987) Projection pattern of vestibulocerebellar fibers in the anterior vermis of the cat: an anterograde wheat germ agglutinin-horseradish peroxidase study. Neurosci Lett 74:25–30.

McCormick BA, Pape HC (1990) Noradrenergic and serotonergic modulation of a hyperpolarization-activated cation current in thalamic relay neurons. 840:319–342.

McKay BE, Engbers JDT, Mehaffey WH, Gordon GRJ, Molineux ML, Bains JS, Turner RW (2007) Climbing Fiber Discharge Regulates Cerebellar Functions by Controlling the Intrinsic Characteristics of Purkinje Cell Output. :2590–2604.

McKay BE, Turner RW (2005) Physiological and morphological development of the rat cerebellar Purkinje cell. J Physiol 567:829–850.

Middleton SJ, Racca C, Cunningham MO, Traub RD, Monyer H, Knöpfel T, Schofield IS, Jenkins A, Whittington MA (2008) High-Frequency Network Oscillations in Cerebellar Cortex. Neuron 58:763–774.

Midtgaard J (1992) Stellate cell inhibition of Purkinje cells in the turtle cerebellum in vitro. J Physiol 457:355–367.

Mintz IM, Sabatini BL, Regehr WG (1995) Calcium control of transmitter release at a cerebellar synapse. Neuron 15:675–688.

Mitchell SJ, Silver R a (2000) Glutamate spillover suppresses inhibition by activating presynaptic mGluRs. Nature 404:498–502.

Mitchell SJ, Silver RA (2003) Shunting Inhibition Modulates Neuronal Gain during Synaptic Excitation. Neuron 38:433–445.

Mittmann W, Häusser M (2007) Linking synaptic plasticity and spike output at excitatory and inhibitory synapses onto cerebellar Purkinje cells. J Neurosci 27:5559–5570.

Mittmann W, Koch U, Häusser M (2005) Feed-forward inhibition shapes the spike output of cerebellar Purkinje cells. J Physiol 563:369–378.

Miyashita Y, Nagao S (1984) Analysis of signal content of Purkinje cell responses to optokinetic stimuli in the rabbit cerebellar flocculus by selective lesions of brainstem pathways. Neurosci Res 1:223–241.

Mouginot D, Bossu JL, Gähwiler BH (1997) Low-threshold Ca2+ currents in dendritic recordings from Purkinje cells in rat cerebellar slice cultures. J Neurosci 17:160–170.

Mukamel E, Nimmerjahn A, Schnitzer M (2009) Automated analysis of cellular signals from large-scale calcium imaging data. Neuron 63:747–760.

Müller T, Möller T, Neuhaus J, Kettenmann H (1996) Electrical coupling among Bergmann glial cells and its modulation by glutamate receptor activation. Glia 17:274–284.

Nahir B, Jahr CE (2013) Activation of Extrasynaptic NMDARs at Individual Parallel Fiber-Molecular Layer Interneuron Synapses in Cerebellum. J Neurosci 33:16323–16333.

Nam SC, Hockberger PE (1997) Analysis of spontaneous electrical activity in cerebellar Purkinje cells acutely isolated from postnatal rats. J Neurobiol 33:18–32.

Napper RM, Harvey RJ (1988a) Quantitative study of the Purkinje cell dendritic spines in the rat cerebellum. J Comp Neurol 274:158–167.

Napper RM, Harvey RJ (1988b) Number of parallel fiber synapses on an individual Purkinje cell in the cerebellum of the rat. J Comp Neurol 274:168–177.

Nunzi MG, Shigemoto R, Mugnaini E (2002) Differential expression of calretinin and metabotropic glutamate receptor mGluR1?? defines subsets of unipolar brush cells in mouse cerebellum. J Comp Neurol 451:189–199.

O'Donoghue DL, King JS, Bishop GA (1989) Physiological and anatomical studies of the interactions between Purkinje cells and basket cells in the cat's cerebellar cortex: evidence for a unitary relationship. J Neurosci 9:2141–2150.

Odeh F (2005) Pontine Maps Linking Somatosensory and Cerebellar Cortices Are in Register with Climbing Fiber Somatotopy. J Neurosci 25:5680–5690.

Oldfield CS, Marty A, Stell BM (2010) Interneurons of the cerebellar cortex toggle Purkinje cells between up and down states. Proc Natl Acad Sci U S A 107:13153–13158.

Oostland M, van Hooft JA (2013) The role of serotonin in cerebellar development. Neuroscience 248:201–212.

Orduz D, Llano I (2007) Recurrent axon collaterals underlie facilitating synapses between cerebellar Purkinje cells. Proc Natl Acad Sci U S A 104:17831–17836.

Oscarsson O (1968) Termination and functional organization of the ventral spino-olivocerebellar path. J Physiol 196:453–478.

Oscarsson O (1979) Functional units of the cerebellum - sagittal zones and microzones. Trends Neurosci 2:144–145.

Ozden I, Sullivan MR, Lee HM, Wang SS-H (2009) Reliable coding emerges from coactivation of climbing fibers in microbands of cerebellar Purkinje neurons. J Neurosci 29:10463–10473.

Pakhotin P, Verkhratsky A (2005) Electrical synapses between Bergmann glial cells and Purkinje neurones in rat cerebellar slices. Mol Cell Neurosci 28:79–84.

Palay SL, Chan-Palay V (1974) Cerebellar Cortex. Berlin, Heidelberg: Springer Berlin Heidelberg.

Palkovits M, Magyar P, Szentágothai J (1971) Quantitative histological analysis of the cerebellar cortex in the cat. Brain Res 32:1–13.

Palkovits M, Mezey E, Hámori J, Szentágothai J (1977) Quantitative histological analysis of the cerebellar nuclei in the cat. I. Numerical data on cells and on synapses. Exp Brain Res 28-28:189–209.

Paré D, Shink E, Gaudreau H, Destexhe A, Lang EJ (1998) Impact of spontaneous synaptic activity on the resting properties of cat neocortical pyramidal neurons In vivo. J Neurophysiol 79:1450–1460.

Pedarzani P, Mosbacher J, Rivard a, Cingolani L a, Oliver D, Stocker M, Adelman JP, Fakler B (2001) Control of electrical activity in central neurons by modulating the gating of small conductance Ca2+-activated K+ channels. J Biol Chem 276:9762–9769.

Pennartz CM, Bierlaagh M a, Geurtsen a M (1997) Cellular mechanisms underlying spontaneous firing in rat suprachiasmatic nucleus: involvement of a slowly inactivating component of sodium current. J Neurophysiol 78:1811–1825.

Perkel DJ, Hestrin S, Sah P, Nicoll RA (1990) Excitatory synaptic currents in Purkinje cells. Proc Biol Sci 241:116–121.

Person AL, Raman IM (2012a) Synchrony and neural coding in cerebellar circuits. Front Neural Circuits 6:97.

Person AL, Raman IM (2012b) Purkinje neuron synchrony elicits time-locked spiking in the cerebellar nuclei. Nature 481:502–505.

Pichitpornchai C, Rawson J a, Rees S (1994) Morphology of parallel fibres in the cerebellar cortex of the rat: an experimental light and electron microscopic study with biocytin. J Comp Neurol 342:206–220.

Pijpers A, Apps R, Pardoe J, Voogd J, Ruigrok TJH (2006) Precise spatial relationships between mossy fibers and climbing fibers in rat cerebellar cortical zones. J Neurosci 26:12067–12080.

Pijpers A, Voogd J, Ruigrok TJH (2005) Topography of olivo-cortico-nuclear modules in the intermediate cerebellum of the rat. J Comp Neurol 492:193–213.

Popa LS, Hewitt a. L, Ebner TJ (2012) Predictive and Feedback Performance Errors Are Signaled in the Simple Spike Discharge of Individual Purkinje Cells. J Neurosci 32:15345–15358.

Pouille F, Scanziani M (2004) Routing of spike series by dynamic circuits in the hippocampus. Nature 429:717–723.

Pouzat C, Hestrin S (1997) Developmental regulation of basket/stellate cell-->Purkinje cell synapses in the cerebellum. J Neurosci 17:9104–9112.

Powell K, Mathy A, Duguid I, Häusser M (2015) Synaptic representation of locomotion in single cerebellar granule cells. Elife 4:1–18.

Prescott SA, Ratté S, De Koninck Y, Sejnowski TJ (2008) Pyramidal neurons switch from integrators in vitro to resonators under in vivo-like conditions. J Neurophysiol 100:3030-42.

Pugh JR, Jahr CE (2011) Axonal GABAA Receptors Increase Cerebellar Granule Cell Excitability and Synaptic Activity. J Neurosci 31:565–574.

Quy PN, Fujita H, Sakamoto Y, Na J, Sugihara I (2011) Projection patterns of single mossy fiber axons originating from the dorsal column nuclei mapped on the aldolase C compartments in the rat cerebellar cortex. J Comp Neurol 519:874–899.

Raman IM, Bean BP (1997) Resurgent sodium current and action potential formation in dissociated cerebellar Purkinje neurons. J Neurosci 17:4517–4526.

Raman IM, Bean BP (1999) Ionic currents underlying spontaneous action potentials in isolated cerebellar Purkinje neurons. J Neurosci 19:1663–1674.

Ramos C, Chardonnet S, Marchand CH, Decottignies P, Ango F, Daniel H, Le Maréchal P (2012) Native presynaptic metabotropic glutamate receptor 4 (mGluR4) interacts with exocytosis proteins in rat cerebellum. J Biol Chem 287:20176–20186.

Rancz E a, Ishikawa T, Duguid I, Chadderton P, Mahon S, Häusser M (2007) High-fidelity transmission of sensory information by single cerebellar mossy fibre boutons. Nature 450:1245–1248.

Reeber SL, Arancillo M, Sillitoe R V. (2014) Bergmann Glia are Patterned into Topographic Molecular Zones in the Developing and Adult Mouse Cerebellum. The Cerebellum:1–12.

Reichenbach A, Siegel A, Rickmann M, Wolff JR, Noone D, Robinson SR (1995) Distribution of Bergmann glial somata and processes: implications for function. J für Hirnforsch 36:509–517.

Rieke F, Bialek W, Warland D, de Ruyter van Steveninck R (1999) Spikes: Exploring the Neural Code (Computational Neuroscience). MIT Press (MA).

Rieubland S, Roth A, Häusser M (2014) Structured connectivity in cerebellar inhibitory networks. Neuron 81:913–929.

Riquelme R, Miralles CP, De Blas AL (2002) Bergmann glia GABA(A) receptors concentrate on the glial processes that wrap inhibitory synapses. J Neurosci 22:10720–10730.

Roitman A V. (2005) Position, Direction of Movement, and Speed Tuning of Cerebellar Purkinje Cells during Circular Manual Tracking in Monkey. J Neurosci 25:9244–9257.

Rokni D, Llinas R, Yarom Y (2007) Stars and stripes in the cerebellar cortex: a voltage sensitive dye study. Front Syst Neurosci 1:1.

Rokni D, Tal Z, Byk H, Yarom Y (2009) Regularity, variability and bi-stability in the activity of cerebellar purkinje cells. Front Cell Neurosci 3:12.

Rokni D, Yarom Y (2009) State-dependence of climbing fiber-driven calcium transients in Purkinje cells. Neuroscience 162:694–701.

Rolando L (1809) Saggio Sopra la Vera Struttura Del Cervello Dell'uomo e Degli Animali Sopra le Funzioni del Sistema Nervoso. (Sassari, Stamperia di S S R M Privil).

Rossi DJ, Hamann M (1998) Spillover-mediated transmission at inhibitory synapses promoted by high affinity alpha6 subunit GABA(A) receptors and glomerular geometry. Neuron 20:783–795.

Ruigrok TJ, Osse RJ, Voogd J (1992) Organization of inferior olivary projections to the flocculus and ventral paraflocculus of the rat cerebellum. J Comp Neurol 316:129–150.

Ruigrok TJ, Voogd J (2000) Organization of projections from the inferior olive to the cerebellar nuclei in the rat. J Comp Neurol 426:209–228.

Ruigrok TJH (2003) Collateralization of climbing and mossy fibers projecting to the nodulus and flocculus of the rat cerebellum. J Comp Neurol 466:278–298.

Sahin M, Hockfield S (1990) Molecular identification of the Lugaro cell in the cat cerebellar cortex. J Comp Neurol 301:575–584.

Santamaria F, Jaeger D, De Schutter E, Bower JM (2002) Modulatory effects of parallel fiber and molecular layer interneuron synaptic activity on Purkinje cell responses to ascending segment input: A modeling study. J Comput Neurosci 13:217–235.

Santamaria F, Tripp PG, Bower JM (2007) Feedforward inhibition controls the spread of granule cell-induced Purkinje cell activity in the cerebellar cortex. J Neurophysiol 97:248–263.

Sarna JR, Marzban H, Watanabe M, Hawkes R (2006) Complementary stripes of phospholipase Cbeta3 and Cbeta4 expression by Purkinje cell subsets in the mouse cerebellum. J Comp Neurol 496:303–313.

Satake S, Saitow F, Yamada J, Konishi S (2000) Synaptic activation of AMPA receptors inhibits GABA release from cerebellar interneurons. Nat Neurosci 3:551–558.

Saviane C, Silver RA (2006) Fast vesicle reloading and a large pool sustain high bandwidth transmission at a central synapse. Nature 439:983–987.

Sawtell NB (2010) Multimodal integration in granule cells as a basis for associative plasticity and sensory prediction in a cerebellum-like circuit. Neuron 66:573–584.

Schmidt H, Brachtendorf S, Arendt O, Hallermann S, Ishiyama S, Bornschein G, Gall D, Schiffmann SN, Heckmann M, Eilers J (2013) Nanodomain coupling at an excitatory cortical synapse. Curr Biol 23:244–249.

Schmolesky MT, Weber JT, De Zeeuw CI, Hansel C (2002) The making of a complex spike: ionic composition and plasticity. Ann N Y Acad Sci 978:359–390.

Schnitzler A, Gross J (2005) Normal and pathological oscillatory communication in the brain. Nat Rev Neurosci 6:285–296.

Schnoebel R, Wolff M, Peters SC, Bräu ME, Scholz A, Hempelmann G, Olschewski H, Olschewski A (2005) Ketamine impairs excitability in superficial dorsal horn neurones by blocking sodium and voltage-gated potassium currents. Br J Pharmacol 146:826–833.

Schonewille M, Khosrovani S, Winkelman BHJ, Hoebeek FE, De Jeu MTG, Larsen IM, Van der Burg J, Schmolesky MT, Frens MA, De Zeeuw CI (2006) Purkinje cells in awake behaving animals operate at the upstate membrane potential. Nat Neurosci 9:459–461; author reply 461.

Schultz SR, Kitamura K, Post-Uiterweer A, Krupic J, Hausser M (2009) Spatial Pattern Coding of Sensory Information by Climbing Fiber-Evoked Calcium Signals in Networks of Neighboring Cerebellar Purkinje Cells. J Neurosci 29:8005–8015.

Schwartz EJ, Rothman JS, Dugue GP, Diana M, Rousseau C, Silver RA, Dieudonne S (2012) NMDA Receptors with Incomplete Mg2+ Block Enable Low-Frequency Transmission through the Cerebellar Cortex. J Neurosci 32:6878–6893.

Schweighofer N, Doya K, Kuroda S (2004) Cerebellar aminergic neuromodulation: Towards a functional understanding. Brain Res Rev 44:103–116.

Serapide MF, Pantó MR, Parenti R, Zappalá A, Cicirata F (2001) Multiple zonal projections of the basilar pontine nuclei to the cerebellar cortex of the rat. J Comp Neurol 430:471–484.

Shakkottai VG, do Carmo Costa M, Dell'orco JM, Sankaranarayanan A, Wulff H, Paulson HL (2011) Early changes in cerebellar physiology accompany motor dysfunction in the polyglutamine disease spinocerebellar ataxia type 3. J Neurosci 31:13002–13014.

Shakkottai VG, Paulson HL (2009) Physiologic alterations in ataxia: channeling changes into novel therapies. Arch Neurol 66:1196–1201.

Shambes GM, Beermann DH, Welker W (1978a) Multiple tactile areas in cerebellar cortex: another patchy cutaneous projection to granule cell columns in rats. Brain Res 157:123–128.

Shambes GM, Gibson JM, Welker W (1978b) Fractured somatotopy in granule cell tactile areas of rat cerebellar hemispheres revealed by micromapping. Brain Behav Evol 15:94–140.

Shepherd GMG, Raastad M, Andersen P (2002) General and variable features of varicosity spacing along unmyelinated axons in the hippocampus and cerebellum. 99.

Shin S-L, De Schutter E (2006) Dynamic Synchronization of Purkinje Cell Simple Spikes. J Neurophysiol 96:3485–3491.

Shin S-L, Hoebeek FE, Schonewille M, De Zeeuw CI, Aertsen A, De Schutter E (2007) Regular patterns in cerebellar Purkinje cell simple spike trains. PLoS One 2:e485.

Shinoda Y, Sugihara I, Wu HS, Sugiuchi Y (2000) The entire trajectory of single climbing and mossy fibers in the cerebellar nuclei and cortex. Prog Brain Res 124:173–186.

Shinomoto S et al. (2009) Relating neuronal firing patterns to functional differentiation of cerebral cortex. PLoS Comput Biol 5:e1000433.

Sillitoe R V., Chung S-H, Fritschy J-M, Hoy M, Hawkes R (2008) Golgi Cell Dendrites Are Restricted by Purkinje Cell Stripe Boundaries in the Adult Mouse Cerebellar Cortex. J Neurosci 28:2820–2826.

Sillitoe R V., Marzban H, Larouche M, Zahedi S, Affanni J, Hawkes R (2004) Conservation of the architecture of the anterior lobe vermis of the cerebellum across mammalian species. Prog Brain Res 148:283–297.

Sillitoe R V, Hawkes R (2002) Whole-mount immunohistochemistry: a high-throughput screen for patterning defects in the mouse cerebellum. J Histochem Cytochem 50:235–244.

Silver RA, Traynelis SF, Cull-Candy SG (1992) Rapid-time-course miniature and evoked excitatory currents at cerebellar synapses in situ. Nature 355:163–166.

Simat M, Parpan F, Fritschy J-M (2007) Heterogeneity of glycinergic and gabaergic interneurons in the granule cell layer of mouse cerebellum. J Comp Neurol 500:71–83.

Sims RE, Hartell NA (2005) Differences in transmission properties and susceptibility to long-term depression reveal functional specialization of ascending axon and parallel fiber synapses to Purkinje cells. J Neurosci 25:3246–3257.

Spencer RMC (2003) Disrupted Timing of Discontinuous But Not Continuous Movements by Cerebellar Lesions. Science (80-) 300:1437–1439.

Steuber V, Mittmann W, Hoebeek FE, Silver RA, De Zeeuw CI, Häusser M, De Schutter E (2007) Cerebellar LTD and pattern recognition by Purkinje cells. Neuron 54:121–136.

Sugihara I, Ebata S, Shinoda Y (2004) Functional Compartmentalization in the Flocculus and the Ventral Dentate and Dorsal Group y Nuclei: An Analysis of Single Olivocerebellar Axonal Morphology. J Comp Neurol 470:113–133.

Sugihara I, Fujita H, Na J, Quy PN, Li B-Y, Ikeda D (2009) Projection of reconstructed single Purkinje cell axons in relation to the cortical and nuclear aldolase C compartments of the rat cerebellum. J Comp Neurol 512:282–304.

Sugihara I, Quy P (2007) Identification of aldolase C compartments in the mouse cerebellar cortex by olivocerebellar labeling. J Comp Neurol 1092:1076–1092.

Sugihara I, Shinoda Y (2004) Molecular, topographic, and functional organization of the cerebellar cortex: a study with combined aldolase C and olivocerebellar labeling. J Neurosci 24:8771–8785.

Sugihara I, Wu H, Shinoda Y (1996) Morphology of axon collaterals of single climbing fibers in the deep cerebellar nuclei of the rat. Neurosci Lett 217:33–36.

Sugihara I, Wu HS, Shinoda Y (1999) Morphology of single olivocerebellar axons labeled with biotinylated dextran amine in the rat. J Comp Neurol 414:131–148.

Sugihara I, Wu HS, Shinoda Y (2001) The entire trajectories of single olivocerebellar axons in the cerebellar cortex and their contribution to Cerebellar compartmentalization. J Neurosci 21:7715–7723.

Sultan F (2001) Distribution of mossy fibre rosettes in the cerebellum of cat and mice: evidence for a parasagittal organization at the single fibre level. Eur J Neurosci 13:2123–2130.

Sultan F, Bower JM (1998) Quantitative Golgi Study of the Rat Cerebellar Molecular Layer Interneurons. 373:353–373.

Szapiro G, Barbour B (2007) Multiple climbing fibers signal to molecular layer interneurons exclusively via glutamate spillover. Nat Neurosci 10:735–742.

Taber KH, Strick PL, Hurley RA (2005) Rabies and the cerebellum: new methods for tracing circuits in the brain. J Neuropsychiatry Clin Neurosci 17:133–139.

Tal Z, Chorev E, Yarom Y (2008) State-dependent modification of complex spike waveforms in the cerebellar cortex. Cerebellum 7:577–582.

Tan J, Gerrits NM, Nanhoe R, Simpson JI, Voogd J (1995) Zonal organization of the climbing fiber projection to the flocculus and nodulus of the rabbit: a combined axonal tracing and acetylcholinesterase histochemical study. J Comp Neurol 356:23–50.

Taube AG (2010) Communication: Constrained search formulation of the ground state energy as a functional of an idempotent one-matrix. J Chem Phys 133.

Thach T, Keating G, Thach WT, Goodkin HP, Keating JG (1992) The cerebellum and the adaptive coordination of movement. Annu Rev Neurosci 15:403–442.

Trott R, Armstrong DM (1987) The cerebellar corticonuclear projection from lobule Vb/c of the cat anterior lobe: a combined electrophysiological and autoradiographic study - I. Projections from the intermediate region. Exp Brain Res 66:318–338.

Tsodyks M, Goettingen D-, Markram H (1998) Neural Networks with Dynamic Synapses. 835:821–835.

Tsutsumi S, Yamazaki M, Miyazaki T, Watanabe M, Sakimura K, Kano M, Kitamura K (2015) Structure-Function Relationships between Aldolase C/Zebrin II Expression and Complex Spike Synchrony in the Cerebellum. J Neurosci 35:843–852.

Valera AM, Binda F, Pawlowski SA, Dupont J-L, Casella J-F, Rothstein JD, Poulain B, Isope P (2016) Stereotyped spatial patterns of functional synaptic connectivity in the cerebellar cortex. Elife 5:1–22.

Valera AM, Doussau F, Poulain B, Barbour B, Isope P (2012) Adaptation of granule cell to Purkinje cell synapses to high-frequency transmission. J Neurosci 32:3267–3280.

Valle MS, Bosco G, Poppele R (2000) Information processing in the spinocerebellar system. Neuroreport 11:4075–4079.

van Kan PL, Gibson AR, Houk JC (1993) Movement-related inputs to intermediate cerebellum of the

monkey. J Neurophysiol 69:74–94.

Vervaeke K, Lorincz A, Gleeson P, Farinella M, Nusser Z, Silver RA (2010) Rapid Desynchronization of an Electrically Coupled Interneuron Network with Sparse Excitatory Synaptic Input. Neuron 67:435–451.

Veys K, Snyders D, De Schutter E (2013) Kv3.3b expression defines the shape of the complex spike in the Purkinje cell. Front Cell Neurosci 7:205.

Vincent P, Armstrong CM, Marty A (1992) Inhibitory synaptic currents in rat cerebellar Purkinje cells: modulation by postsynaptic depolarization. J Physiol 456:453–471.

Vincent P, Marty A (1996) Fluctuations of inhibitory postsynaptic currents in Purkinje cells from rat cerebellar slices. J Physiol 494:183–199.

Voogd J (1967) Comparative aspects of the structure and fibre connexions of the mammalian cerebellum. Prog Brain Res 25:94–134.

Voogd J (1969) The importance of fiber connections in the comparative anatomy of the mammalian cerebellum. In: Neurobiology of cerebellar evolution and development (Llinás R, ed), pp 493–514. Chicago: American medical association.

Voogd J (2011) Cerebellar zones: a personal history. Cerebellum 10:334–350.

Voogd J, Glickstein M (1998) The anatomy of the cerebellum. Trends Neurosci 21:370–375.

Voogd J, Pardoe J, Ruigrok TJH, Apps R (2003) The distribution of climbing and mossy fiber collateral branches from the copula pyramidis and the paramedian lobule: congruence of climbing fiber cortical zones and the pattern of zebrin banding within the rat cerebellum. J Neurosci 23:4645–4656.

Voogd J, Ruigrok TJH (2004) The organization of the corticonuclear and olivocerebellar climbing fiber projections to the rat cerebellar vermis: The congruence of projection zones and the zebrin pattern. J Neurocytol 33:5–21.

Wada N, Kishimoto Y, Watanabe D, Kano M, Hirano T, Funabiki K, Nakanishi S (2007) Conditioned eyeblink learning is formed and stored without cerebellar granule cell transmission. Proc Natl Acad Sci U S A 104:16690–16695.

Wadiche JI, Jahr CE (2005) Patterned expression of Purkinje cell glutamate transporters controls synaptic plasticity. Nat Neurosci 8:1329–1334.

Wall MJ (2002) Furosemide reveals heterogeneous GABA(A) receptor expression at adult rat Golgi cell to granule cell synapses. Neuropharmacology 43:737–749.

Walter JT, Alviña K, Womack MD, Chevez C, Khodakhah K (2006) Decreases in the precision of Purkinje cell pacemaking cause cerebellar dysfunction and ataxia. Nat Neurosci 9:389–397.

Walter JT, Khodakhah K (2006) The linear computational algorithm of cerebellar Purkinje cells. J Neurosci 26:12861–12872.

Wang F, Xu Q, Wang W, Takano T, Nedergaard M (2012) Bergmann glia modulate cerebellar Purkinje cell bistability via Ca2+-dependent K+ uptake. Proc Natl Acad Sci 109:7911–7916.

Wang H, Peca J, Matsuzaki M, Matsuzaki K, Noguchi J, Qiu L, Wang D, Zhang F, Boyden E, Deisseroth K, Kasai H, Hall WC, Feng G, Augustine GJ (2007) High-speed mapping of synaptic connectivity using photostimulation in Channelrhodopsin-2 transgenic mice. Proc Natl Acad Sci U S A 104:8143–8148.

Wang X, Chen G, Gao W, Ebner TJ (2011) Parasagittally aligned, mGluR1-dependent patches are evoked at long latencies by parallel fiber stimulation in the mouse cerebellar cortex in vivo. J Neurophysiol 105:1732–1746.

Warnaar P, Couto J, Negrello M, Junker M, Smilgin A, Ignashchenkova A, Giugliano M, Thier P, De Schutter E (2015) Duration of Purkinje cell complex spikes increases with their firing frequency. Front Cell Neurosci 9:1–16.

Watanabe M, Kano M (2011) Climbing fiber synapse elimination in cerebellar Purkinje cells. Eur J Neurosci 34:1697–1710.

Watanabe S, Takagi H, Miyasho T, Inoue M, Kirino Y, Kudo Y, Miyakawa H (1998) Differential roles of two types of voltage-gated Ca2+ channels in the dendrites of rat cerebellar Purkinje neurons. Brain Res 791:43–55.

Williams SR, Christensen SR, Stuart GJ, Häusser M (2002) Membrane potential bistability is controlled by the hyperpolarization-activated current I(H) in rat cerebellar Purkinje neurons in vitro. J Physiol 539:469–483.

Wise AK, Cerminara NL, Marple-Horvat DE, Apps R (2010) Mechanisms of synchronous activity in cerebellar Purkinje cells. J Physiol 588:2373–2390.

Witter L, De Zeeuw CI (2015) Regional functionality of the cerebellum. Curr Opin Neurobiol 33:150–155.

Wolpert DM, Miall RC, Kawato M (1998) Internal models in the cerebellum. Trends Cogn Sci 2:338–347.

Womack MD, Khodakhah K (2002) Characterization of large conductance Ca2+-activated K+ channels in cerebellar Purkinje neurons. Eur J Neurosci 16:1214–1222.

Womack MD, Khodakhah K (2003) Somatic and dendritic small-conductance calcium-activated potassium channels regulate the output of cerebellar Purkinje neurons. J Neurosci 23:2600–2607.

Woody CD, Swartz BE, Gruen E (1978) Effects of acetylcholine and cyclic GMP on input resistance of cortical neurons in awake cats. Brain Res 158:373–395.

Wu HS, Sugihara I, Shinoda Y (1999) Projection patterns of single mossy fibers originating from the lateral reticular nucleus in the rat cerebellar cortex and nuclei. J Comp Neurol 411:97–118.

Wulff P, Schonewille M, Renzi M, Viltono L, Sassoè-Pognetto M, Badura A, Gao Z, Hoebeek FE, van Dorp S, Wisden W, Farrant M, De Zeeuw CI (2009) Synaptic inhibition of Purkinje cells mediates consolidation of vestibulo-cerebellar motor learning. Nat Neurosci 12:1042–1049.

Xiao J, Cerminara NL, Kotsurovskyy Y, Aoki H, Burroughs A, Wise AK, Luo Y, Marshall SP, Sugihara I, Apps R, Lang EJ (2014) Systematic regional variations in purkinje cell spiking patterns. PLoS One 9:e105633.

Xu-Friedman M a, Regehr WG (2003) Ultrastructural contributions to desensitization at cerebellar mossy fiber to granule cell synapses. J Neurosci 23:2182–2192.

Xu-Friedman MA, Harris KM, Regehr WG (2001) Three-dimensional comparison of ultrastructural characteristics at depressing and facilitating synapses onto cerebellar Purkinje cells. J Neurosci 21:6666–6672.

Yartsev MM, Givon-Mayo R, Maller M, Donchin O (2009) Pausing purkinje cells in the cerebellum of the awake cat. Front Syst Neurosci 3:2.

Yatim N, Billig I, Compoint C, Buisseret P, Buisseret-Delmas C (1996) Trigeminocerebellar and trigemino-olivary projections in rats. Neurosci Res 25:267–283.

Yoon B-E, Jo S, Woo J, Lee J-H, Kim T, Kim D, Lee CJ (2011) The amount of astrocytic GABA positively correlates with the degree of tonic inhibition in hippocampal CA1 and cerebellum. Mol Brain 4:42.

Yoon B-E, Woo J, Chun Y-E, Chun H, Jo S, Bae JY, An H, Min JO, Oh S-J, Han K-S, Kim HY, Kim T,

Kim YS, Bae YC, Lee CJ (2014) Glial GABA, synthesized by monoamine oxidase B, mediates tonic inhibition. J Physiol 592:4951–4968.

Zhou H, Lin Z, Voges K, Ju C, Gao Z, Bosman LW, Ruigrok TJ, Hoebeek FE, De Zeeuw CI, Schonewille M (2014) Cerebellar modules operate at different frequencies. Elife 3:e02536.

Zhou H, Voges K, Lin Z, Ju C, Schonewille M (2015) Differential Purkinje cell simple spike activity and pausing behavior related to cerebellar modules. J Neurophysiol:jn.00925.2014.

Zhou ZS, Zhao ZQ (2000) Ketamine blockage of both tetrodotoxin (TTX)-sensitive and TTX-resistant sodium channels of rat dorsal root ganglion neurons. Brain Res Bull 52:427–433.

Zhu L, Lovinger D, Delpire E (2005) Cortical neurons lacking KCC2 expression show impaired regulation of intracellular chloride. J Neurophysiol 93:1557–1568.

APPENDIX

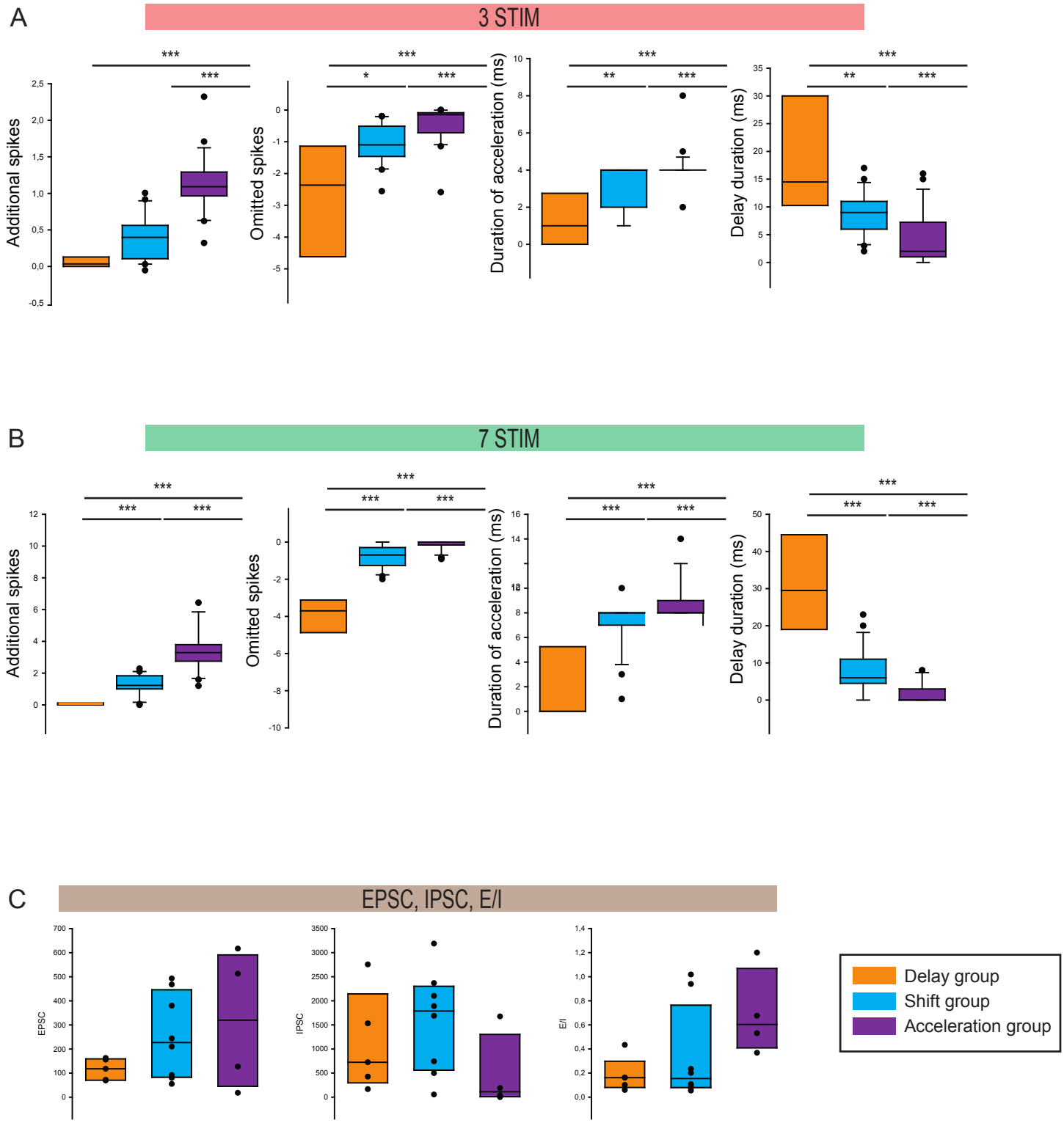

Annex. Characteristics of the three groups of behavior identified in the granule cell-Purkinje cell pathway - Time course of Purkinje cellsmodulation and synaptic parameters.

Oral communications

- Grangeray A, Kumar A, Isope P. Subthreshold Information Decoding at the Cerebellar Granule Cell to Purkinje Cell Synapse (2015) Biennal meeting of the French Neuroscience Society, Montpellier, France.

- Grangeray A, Isope P. Subthreshold Information Decoding at the Cerebellar Granule Cell to Purkinje Cell Synapse (2014) FENS Forum of Neuroscience, Milan, Italy.

- Grangeray A, Isope P. Subthreshold Information Decoding at the Cerebellar Granule Cell to Purkinje Cell Synapse (2014) International society for *Cerebellar* Research congress, Rome, Italy.

Publications

- Grangeray A, Kumar A, Isope P. Short-term dynamics of excitation and inhibition balance determines Purkinje cell spike output (under preparation).

- Grangeray A, Dorgans K, Roux S and Bossu JL. The Purkinje cell as an integrative machine (2016) in Essentials of Cerebellum and Cerebellar Disorders. Springer ed.

- Licitra F, Laredj L, Grangeray A, Stefely J, Schlagowski AI, Reutenauer L, Messadeq N, Zoll J, Pierrel F, Pagliarini D, Isope P and Puccio H. Loss of Adck3 leads to Purkinje cells dysfunction, skeletal muscle defect and Coenzyme Q_9 deficiency, recapitulating the physiopathology of human ARCA2. (submitted) J Clin Invest.

- Grangeray Vilmint A., Lelièvre V. (2012) The medial migratory stream: A new turn in postnatal neurogenesis. Cell Adhesion and Migration 6: 1-3.

1. *Contexte*

Le cervelet est impliqué dans le contrôle et l'apprentissage moteur des mouvements complexes. Lors de l'exécution d'un mouvement volontaire, une copie efférente de la commande motrice en provenance du cortex moteur vers les muscles est reçue par le cervelet, ainsi que l'ensemble des informations somato-sensorielles, auditives, visuelles, vestibulaires et proprioceptives de l'organisme. À partir de l'intégration de ces signaux, le cervelet prédit le retour sensoriel, et ajuste finement chaque étape du programme moteur. Une erreur entre la prédiction et le retour sensoriel du mouvement effectué conduit à une correction et à des mécanismes d'apprentissage dans le cortex cérébelleux. De nombreuses données suggèrent que la connexion entre les cellules des grains et les cellules de Purkinje du cortex cérébelleux est un site majeur de traitement et de stockage d'information lors des apprentissages moteur. Des mécanismes de plasticité à long terme ont été mis en évidence et corrélés à certains types d'apprentissages/taches/comportements. Les informations contextuelles sont encodées par la voie fibres moussues – cellules des grains – cellules de Purkinje. Les axones des cellules des grains contactent les cellules de Purkinje par une connexion monosynaptique excitatrice et font également synapse sur des interneurones de la couche moléculaire qui inhibent les cellules de Purkinje. Cette inhibition en partie antérograde et disynaptique a pour conséquence de moduler l'excitation de la cellule de Purkinje. La cellule de Purkinje est spontanément active en l'absence d'entrées synaptiques, et des expériences *in vivo* ont montré que sa décharge est modulée par des entrées sensori-motrices. L'intégration des informations traitées dans le cortex cérébelleux semble donc se manifester par la modulation du patron de décharge des cellules de Purkinje.

Les cellules de Purkinje sont l'unique sortie du cortex cérébelleux, et inhibent les neurones des noyaux profonds, seules sorties du cervelet.

Une telle organisation suggère un rôle déterminant de l'intégration et du codage de l'information par les cellules de Purkinje dans le signal de sortie du cervelet et le

contrôle moteur. Des études ont par ailleurs montré une altération de la décharge des cellules de Purkinje chez des souris ataxiques qui présentent des problèmes de coordination motrice.

2. *Objectifs*

La cellule de Purkinje étant spontanément active, des petites entrées ne déclenchant pas directement de potentiel d'action (entrées sous seuils) peuvent potentiellement modifier sa décharge. Ma thèse a pour objectif d'étudier l'impact d'entrées sous-seuils, en provenance d'un groupe de cellules des grains et l'influence des interneurones inhibiteurs sur le patron de décharge des cellules de Purkinje.

3. *Résultats*

- **Reproduction de l'irrégularité des cellules de Purkinje dans un modèle de tranches agues**

Nous avons utilisé un modèle de tranches aigues de cervelet afin de permettre une maîtrise des paramètres d'entrée (entrées sous seuils) et de mesure du signal de sortie (enregistrement d'une cellule de Purkinje unique et connectée au groupe de grains actifs). La cellule de Purkinje *in vivo* reçoit un bombardement synaptique d'en moyenne 170000 entrées, excitatrices et inhibitrices, distribuées sur l'ensemble de son arbre dendritique Cependant, contrairement aux données *in vivo*, des études *in vitro* révèlent une décharge beaucoup plus régulière des cellules de Purkinje du fait de la diminution du nombre d'entrées en tranches aigues. Cette baisse d'activité du réseau peut potentiellement modifier l'état de conductance des cellules de Purkinje et donc leurs propriétés d'intégration.

J'ai ainsi consacré la première partie de ma thèse au développement et à la validation d'une stratégie pour compenser ce phénomène. Une première approche pharmacologique basée sur l'utilisation du furosémide, un bloqueur de l'inhibition tonique des cellules des grains, s'est avérée peu concluante, sans modification de la

décharge des cellules de Purkinje. Dans une seconde approche, nous avons voulu mimer ce bombardement synaptique sur l'arbre dendritique des cellules de Purkinje. Nous avons pour cela utilisé une lignée de souris transgénique (L7-ChR2-YFP) récemment caractérisée dans l'équipe. Cette lignée de souris exprime spécifiquement dans les cellules de Purkinje la channelrhodopsine 2 (ChR2), une protéine photoactivable dépolarisante/excitatrice, dont l'activation mime une entrée synaptique. Nous avons donc réalisé des protocoles de photostimulation optogénétique sur des tranches de cervelet de ces souris et avons observé une augmentation significative de l'irrégularité de la décharge des cellules de Purkinje ainsi qu'une augmentation de la conductance membranaire. Cette stratégie probante ne permet toutefois pas de mimer le bombardement synaptique inhibiteur.

Nous avons donc appliqué des protocoles de photostimulation optogénétique similaires sur une autre lignée de souris transgénique (Thy1-ChR2-YFP) qui exprime la ChR2 dans les fibres moussues. Les fibres moussues excitant les cellules des grains, cette approche génère potentiellement un bruit excitateur et inhibiteur sur les cellules de Purkinje connectées. Nous avons pu générer des protocoles capables d'augmenter l'irrégularité des cellules de Purkinje.

- **Modulation de la décharge des cellules de Purkinje par des entrées sous-seuils des cellules des grains**

Dans ce modèle d'étude développé, notre objectif a été d'étudier et de décrire l'influence d'entrées sous-seuils provenant des cellules des grains sur la décharge de la cellule de Purkinje. *In vivo*, les cellules des grains déchargent à très faible fréquence au repos et sont capables de produire des bouffées de potentiels d'action (« burst ») à haute fréquence lors d'entrées sensorielles. Par des techniques d'électrophysiologie, nous avons reproduit ces patrons de décharge en stimulant électriquement les somas des cellules des grains et avons enregistré en extracellulaire la décharge d'une cellule de Purkinje connectée. Afin d'étudier les entrées qui ont été sélectionnées au cours de la vie de l'animal, nous avons bloqué pharmacologiquement les mécanismes de plasticité à long terme pouvant être induits par nos protocoles de stimulation.

Nous avons ainsi étudié l'influence des entrées sous-seuils provenant d'un petit groupe de cellules des grains sur le patron de décharge des cellules de Purkinje. Nous avons observé aussi bien une accélération ou un retard dans le temps de survenue du potentiel d'action suivant de la cellule de Purkinje. Deux hypothèses pourraient expliquer le retard observé. La première implique des interneurones inhibiteurs actifs, la seconde suggère une phase d'hyperpolarisation induite par des canaux potassiques activés par le calcium (« afterhyperpolarisation »). Afin de tester notre première hypothèse, nous avons bloqué la neurotransmission inhibitrice par l'application de picrotoxine (un antagoniste des récepteurs GABAA) et observé une suppression totale de l'effet de retard confirmant alors l'implication des interneurones dans la modulation observée.

- **Impact de la balance excitation/inhibition et des plasticités à court terme**

Nous avons ensuite étudié l'effet du nombre de potentiels d'action (1, 3 ou 7) dans le train de stimulation des cellules des grains sur la décharge des cellules de Purkinje. Nos résultats montrent une très grande diversité de l'effet net, suggérant une intégration différente des séquences excitation-inhibition selon les synapses cellules des grains-cellules de Purkinje.

Ce résultat pouvant être potentiellement la résultante d'une balance excitation/inhibition différente, nous avons choisi de réaliser une autre série d'expériences dans laquelle les enregistrements extracellulaires sont suivis de l'enregistrement des courants excitateurs et inhibiteurs de la cellule de Purkinje par la technique de patch clamp en voltage imposé. Nos résultats montrent que le ratio entre les entrées excitatrices et inhibitrices ne permet pas de prédire l'influence des cellules des grains sur la cellule de Purkinje.

Les paramètres pouvant expliquer la modulation de la décharge de la cellule de Purkinje étant très nombreux (fréquence et régularité de la décharge spontanée des cellules de Purkinje, plasticités à court terme...), nous avons utilisé une analyse en composante principale, un outil de statistique exploratoire. Cette approche nous a permis d'extraire 3 groupes de comportement des cellules de Purkinje au sein

desquels le fonctionnement des connexions cellules des grains-cellules de Purkinje semble similaire. De manière surprenante, un des 3 groupes présente des balances excitation/inhibition très disparates. Ce groupe a la particularité de présenter une inversion de l'effet net de la modulation entre 3 et 7 stimulations, résultant potentiellement du jeu de plasticités synaptiques. En effet, il a été montré chez le rat, que les entrées excitatrices à la synapse cellules des grains-cellules de Purkinje facilitent lors de stimulation en bursts alors qu'à l'inverse les entrées inhibitrices à la synapse interneurones-cellules de Purkinje déprime. Aucune étude à notre connaissance ne s'est intéressée à la résultante de ces deux plasticités opposées sur la cellule de Purkinje. Nous avons donc mesuré la modification de l'amplitude des courants inhibiteurs au cours de trains de 7 stimulations, et avons observé une dépression systématique de l'inhibition à partir de la 3ème stimulation.

Ces résultats suggèrent que les bursts courts favoriseraient l'inhibition tandis que les bursts longs conduiraient à un effet net excitateur.

Dans le but d'étudier comment ces plasticités à court terme influencent le signal de sortie de la cellule de Purkinje, nous avons développé un modèle mathématique, en collaboration avec l'équipe du Dr. Arvind Kumar de l'Institut royal de technologie de Stockholm (KTH).

Par cette approche, nous avons d'une part validé nos résultats expérimentaux, et d'autre part montré que la dynamique des plasticités à court terme est une des variables les plus influentes dans le contrôle de la décharge des cellules de Purkinje.

4. *Conclusion*

Nous avons montré l'influence d'entrées sous seuils d'un petit groupe de grains sur l'organisation temporelle de la décharge des cellules de Purkinje.

Nous avons mis en évidence une forte hétérogénéité de l'effet net sur le signal de sortie du cortex cérébelleux.

La diversité observée au sein d'une population de connexions cellules des grains-cellules de Purkinje semble régis par une interaction complexe de plusieurs paramètres comme la structure du patron d'entrées (nombre, fréquence), la balance excitation-inhibition et la résultante des plasticités à court termes.

Le modèle de simulation que nous avons développé suggère un rôle prépondérant des plasticités à court terme dans la diversité de modulation à la connexion cellules des grains-cellules de Purkinje. La variation de ce paramètre dans les gammes physiologiques offre la plus large gamme dynamique de réponses. Quel est l'impact de la modulation de la décharge des cellules de Purkinje mis en évidence par nos recherches sur les neurones des noyaux profonds, neurones de sorties du cervelet ? Est-ce que la modulation d'une seule cellule de Purkinje peut influencer le signal de sortie ou une synchronisation de plusieurs cellules de Purkinje est nécessaire pour qu'une modulation soit « lisible » par les neurones des noyaux profonds ? … Ce sont tout autant de questions qui s'ouvrent concernant le décodage de cette modulation de la décharge des cellules de Purkinje par les neurones des noyaux profonds.

UNIVERSITÉ DE STRASBOURG

École Doctorale des Sciences de la Vie et de la Santé STRASBOURG

Anaïs GRANGERAY-VILMINT

Modulation of cerebellar Purkinje cell discharge by subthreshold granule cell inputs

Résumé

La décharge des cellules de Purkinje (CP), neurone de sortie du cortex cérebelleux, joue un rôle majeur dans le contrôle moteur. Les CP reçoivent des entrées excitatrices provenant des cellules des grains (CG), lesquelles génèrent également une inhibition antérograde sur les CP via l'activation d'interneurones de la couche moléculaire (IN). Lors de ma thèse, j'ai étudié l'influence simultanée de la balance excitation-inhibition (E/I) et des plasticités à court terme aux synapses CG-IN-CP sur la décharge des CP, par des techniques d'électrophysiologie, d'optogénétique et de simulation. Ces travaux démontrent l'existence d'une hétérogénéité d'E/I dans le cortex cérébelleux ainsi qu'une grande diversité de modulation des CP en réponse à la stimulation de CG. Le nombre de stimulation des CG influence fortement la direction et l'intensité de la modulation observée. Enfin, la combinaison de plasticités à court terme et d'E/I génère dans la décharge des CP des motifs de réponses complexes mais reproductibles, ayant sans doute un rôle essentiel dans l'encodage sensoriel.

Mots clés : Cellule de Purkinje, cellule des grains, cervelet, électrophysiologie in vitro, potentiel d'action, codage neuronal, balance excitation-inhibition, plasticités synaptiques à court terme, neurosciences.

Summary

Rate and temporal coding in Purkinje cells (PC), the sole output of the cerebellar cortex, play a major role in motor control. PC receives excitatory inputs from granule cells (GC) which also provide feedforward inhibition on PC through the activation of molecular layer interneurons (MLI). In this thesis, I studied the influence of the combined action of excitation/inhibition (E/I) balance and short-term plasticity of GC-MLI-PC synapses on PC discharge, by using electrophysiological recordings, optogenetic stimulation and modelling. This work demonstrates that E/I balances are not equalized in the cerebellar cortex and showed a wide distribution of PC discharge modulation in response to GC inputs, from an increase to a shutdown of the discharge. The number of stims in GC bursts strongly controls the strength and sign of PC modulation. Lastly, the interplay between short-term plasticity and E/I balance implements complex but reproducible output patterns of PC responses to GC inputs that should play a key role in stimulus encoding by the cerebellar cortex.

Keywords : Purkinje cell, granule cell, cerebellum, in vitro electrophysiology, spike, feedforward inhibition, neural coding, excitation-inhibition balance, short-term synaptic plasticity, neuroscience.